The Dissertation Committee for Dong Hyun Kim certifies that this is the approved version of the following dissertation:

Reliability Study of SnPb and SnAg Solder Joints in PBGA Packages

Committee:

Tess J. Moon, Co-Supervisor

Glenn Y. Masada, Co-Supervisor

Eric P. Fahrenthold

Paul S. Ho

David P. Morton

RELIABILITY STUDY OF SnPb AND SnAg SOLDER JOINTS IN PBGA PACKAGES

by

DONG HYUN KIM, B.S.; M.E.

DISSERTATION

Presented to the Faculty of the Graduate School of

The University of Texas at Austin

in Partial Fulfillment

of the Requirements

for the Degree of

DOCTOR OF PHILOSOPHY

The University of Texas at Austin

December 2007

Dedication

To my parents:

Father Suk Kee Kim, Mother Young Hwa Chung.

Acknowledgements

First I would like to give my special gratitude to my supervising professors, Drs. Glenn Y. Masada and Tess J. Moon, for teachings and trainings. They taught me a lot more than academic matters. Also, I would like to thank my PhD committee, Dr. Eric P. Fahrenthold, Dr. Paul S. Ho, and Dr. David P. Morton, for their encouragements and academic advices. I would like to thank Andrew Mawer, Dr. Thomas Koschmieder and Billy Oyler in Freescale for technical support. Also, I'd like to thank UT lab collaborators, Changyoung Park, Budi Hadisujoto, Praveen Bhagavathula, Jose Marcio Filho, Bernardo Cuogo, and Daniel Santos, for helping me with data collection and analysis. The financial support of National Science Foundation and Texas Higher Education Coordinating Board Advanced Technology Program is greatly appreciated. My fellow students and Dr. Young Hoon Han in ME Department and my co-workers in Cisco Systems have encouraged me to carry out this research. Most of all, I would like to give my special acknowledgement to my respectful parents, Suk Kee Kim and Young Hwa Chung. Without their support, endless encouragement and love, I would never obtain my PhD degree. Also, I'd like to express my special love to my wife, Joo Hee Park, for her long support as a student's wife, and to my joyful sons, Samuel Kim and Paul Kim. Finally I want to honor God, Jesus Christ, for allowing me this special period in my life and blessing me and my family. I will not worry for the rest of my life since He is always with me.

<December 7, 2007>

RELIABILITY STUDY OF SnPb AND SnAg SOLDER JOINTS IN PBGA PACKAGES

Publication No._____

Dong Hyun Kim, Ph.D.

The University of Texas at Austin, 2007

Co-Supervisors: Tess J. Moon and Glenn Y. Masada

This study investigates the reliability of SnPb and SnAg solder joints in semiconductor packages subjected to thermal cycling. More specifically, solder joint crack growth and life are experimentally measured, and FEM models are run to explain the test results. Ultimately a life-prediction model is proposed for both SnPb and SnAg solder joint packages. Motorola 357-plastic ball grid array packages on printed wiring boards were thermal cycled with the following test parameters: SnPb and SnAg solders, three post-process conditions (aged, air-cooled and quenched), four package layouts on the printed circuit boards (single-dense, single-sparse, double-alternating, and double-dense), three accelerated thermal cycling protocols (0°C to 100°C, -40°C to 125°C, and -55°C to 125°C), and tests run at Motorola and the University of Texas. At predetermined thermal

cycles, packages were removed from the environmental chambers, dye-penetrated, packages removed to expose the solder joints, and optical images taken. Images were processed to measure crack area, shape, orientation and length to show crack growth. Selected joints were sectioned and polished to investigate microstructure and failure modes. Selected boards were connected to an ANATECH event detector to monitor life from joint failures. FEM crack initiation and propagation models were developed to better understand failure mechanisms.

Major experimental results are: 1) SnPb joints have about 50% faster crack growth rates than SnAg joints, subsequently SnPb joints have half the life of SnAg joints, 2) air-cooled and quenched packages had similar failure characteristics, but aged SnPb joints had lower life and aged SnAg joints had significantly longer life than the comparable nonaged joints, 3) double-dense package layout significantly decreased life (by 75%) over the other package layouts, which were similar to each other, 4) the test results at the two locations (UT and Motorola) were similar for SnPb solder joints, but significantly different for SnAg solder joints, and 5) the largest cracks occurred at the corners of joints just under the die edge. Major FEM simulation results are: 1) the crack initiation life of SnAg joints is approximately 100% longer than SnPb joints, 2) shear load is a major cause of crack growth, but the contribution of tensile load increases as the cracks grow, 3) primary cracks at the board interface appear to reduce the propagation rate of the primary crack on the package interface, 4) secondary cracks are suppressed when compressive stresses prevent voids from nucleating,

5) the double-dense configuration shows no PWB warping due to symmetry, and its stresses are larger than for the other package layouts, and (6) the stresses and strains for single-dense, single-sparse, and double-alternating package layouts are similar because the stresses/strains are dominated by local effects due to the CTE mismatch between the die and board.

Based upon the experimental results and FEM simulations, a life-prediction model based upon a severity metric was proposed. The metric estimates damage to the solder joints and links material properties and parameters associated with package layout and thermal test conditions to the time-dependent creep, time-independent plastic deformation, and a time-dependent and geometric effective stress of the solder. The severity metric predicted life very well for most of the data tested and was more accurate than the industry-standard life-prediction models for SnPb solder joints.

Table of Contents

List of Tables

List of Figures

CHAPTER 1

Introduction and Background

1.1. RELIABILITY OF SEMICONDUCTOR PACKAGES

Semiconductor packaging enables silicon-level interconnects to be joined to the motherboard by providing the medium for electrical bridges or interconnections, as well as the mechanical support and protection of the electronic circuitry. As integration levels in semiconductors increase, packages get denser, forcing smaller pitches on peripherally-leaded integrated circuit packages. Demands for increased input-output and electrical performance in denser chips have prompted creative advanced package designs, e.g., solder-bumped flip-chip technology, plastic ball grid array (PBGA) technology, and chip-scale packaging (CSP) [1] (see Figure 1.1 for examples). Solder still provides the electrical, thermal and mechanical connections; hence, solder joint reliability is one of the most critical issues in the development of these technologies [1, 2].

Semiconductor packages are exposed to various environments, such as temperature, humidity, dust, shock and vibration, which contribute to failures as shown in Figure 1.2 [3]. Temperature is the major cause of failure by inducing thermal stress in the solder joints under normal operating conditions due to the differences in the coefficients-of-thermal expansion (CTE) between the chip and

board. Currently, accelerated thermal cycling (ATC) tests are run to evaluate solder joint reliability, to minimize time-to-market, and to satisfy customer expectation of long term reliability by inducing thermal stress levels higher than those experienced in normal operating conditions.

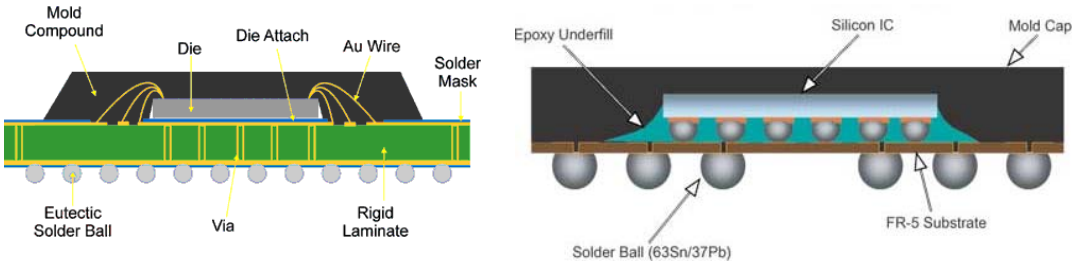

(a) (b)

Figure 1.1. Area-type packages (a) wire-bond PBGA (b) flip chip CSP [2]

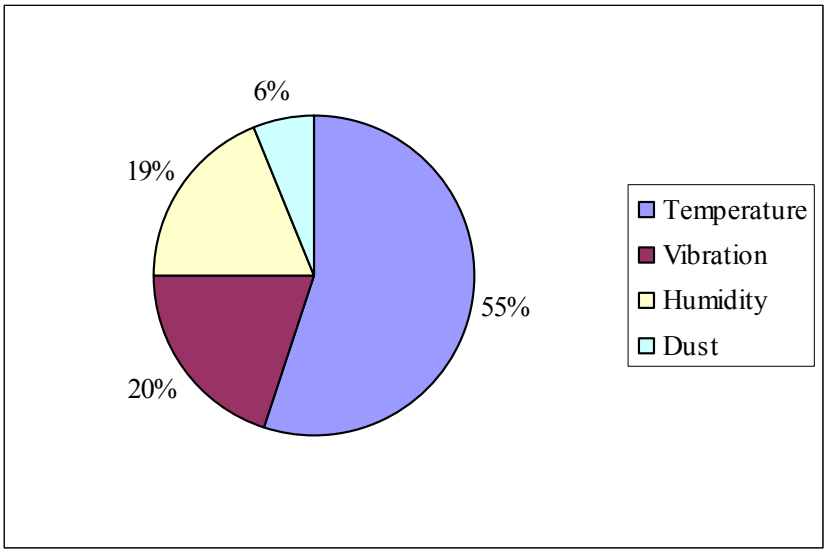

Figure 1.2. Causes of failures in electronic packages [3]

1.2. ISSUES IN SOLDER JOINT RELIABILITY

Solder joints creep at room temperature due to the low melting temperature of solder (i.e., 183°C for eutectic tin-lead solder). Therefore, thermal stresses in solder joints relax by creep under thermal cycling, and the solder microstructure evolves under cycling [4]. The grains grow in size over some period as the structure reduces its internal energy, then voids start to nucleate at the grain boundaries and grow by thermal diffusion. Micro-cracks are formed when two neighboring voids coalesce. Finally, the macro-cracks propagate through the solder joints. Since the macro-crack propagation takes up approximately 80-90% of the life of solder joints, the major failure mechanism is crack propagation [4]. Thus, the reliability of solder joints primarily depends on how to resist or delay crack propagation. It is important to investigate crack characteristics and crack growth to assess reliable solder joint designs [5-6].

Eutectic tin lead solder (63%Sn37%Pb) has been used in electronics packaging for well over 50 years because of its low melting temperature, excellent wetting on copper, high ductility, etc. [7, 8]. Its properties are tabulated in Appendix A. However, due to environmental concerns of lead, the electronics industry is looking for a reliable lead-free solder [9]. The European Union (EU) will ban the use of lead-based solders within the present decade, and Japan has enacted an "Electronics Recycle Law" that requires manufacturers to collect and recycle their own products [10]. EU will implement the ROHS (Restriction Of the use of certain Hazardous Substances in electrical and electronic equipment) directive that bans, effective July 1, 2006, lead (Pb), mercury (Hg), cadmium

(Cd), hexavalent chromium (Cr^{6+}) and two flame retardants (PBB—polybrominated biphenyls and PBDE—polybrominated diphenys ethers) in printed circuit boards (PCBs). Products that do not comply will be removed from the EU market [11].

As a result these legislations, various lead-free alloys, such as eutectic tin-silver (96.5%Sn3.5%Ag), tin-silver-copper (96%Sn3.5%Ag0.5%Cu—SAC), tin-silver-bismuth (6.5%Sn3.5%AgBi), and tin-copper (99.3%Sn0.7%Cu), have been studied extensively to replace Sn-Pb eutectic solder [12, 13]. The properties of eutectic and SAC alloys are tabulated in Appendix A. Therefore, the evaluation of lead-free solder reliability and the adaptability to the current manufacturing facilities and processing are critical issues in the semiconductor industry. In this study, eutectic SnAg solder (96.5%Sn3.5%Ag) is chosen as a lead-free solder, and its reliability is compared with conventional SnPb solder (62%Sn36%Pb2%Ag).

1.3. OBJECTIVES OF THIS RESEARCH

The major objectives of this research are to: 1) develop an integrated, experimentally-verified, life-prediction model that includes material and structural parameters and that is based upon the prototypic packaging system, plastic ball-grid arrays, and 2) evaluate the reliability of semiconductor packages with SnPb versus SnAg solder under three different post-process conditions: air-cooled, ice-quenched and aged at 150ºC (for SnPb) or 160ºC (for SnAg) for 1000hrs. To

achieve these objectives, this study undertakes extensive experimental and analytical studies.

The organization of the dissertation is as follows: 1) Introduction to reliability measurements and models (Ch.1); 2) Experimental methods and results (Ch.2-4), 3) Crack model development (Ch. 5-6) and 4) Life results and life prediction (Ch. 7). The contents of each chapter are as follows.

Chapter 1, "Introduction and Background", introduces the reliability issues of solder joints in semiconductor packages and previous research on solder joint reliability are described, and the objectives of this research are outlined. Previous work and existing life-prediction models are also discussed.

Chapter 2, "Testing and Measurement", introduces the experimental rationale, the test specimen, facilities, and design of experiments.

Chapter 3, "Microstructural Analysis of Solder Joint Failure", visually examines the microstructural evolution and failure path analysis in SnPb and SnAg solder joints for the three different post-process conditions. Using standard sectioning techniques and photomicrography, the crack failure modes and propagation paths are investigated. Additional test results are provided to explain the longer life of aged versus air-cooled SnAg solder joints.

Chapter 4, "Crack Evolution: Crack Shape, Orientation, Area and Length", presents the results of the experimental study of crack growth in SnPb and SnAg solder joints for different number of thermal cycles using dye penetration techniques. Crack characteristics, such as shape, size, orientation, area and length, are described.

Chapter 5, “Crack Initiation Modeling and Analysis”, presents crack initiation models for SnPb and SnAg solder joints under different post-process conditions using finite element method (FEM) techniques.

Chapter 6, “Crack Propagation Modeling and Analysis”, runs a detailed experimental investigation of crack propagation in solder joints located under the die periphery. Using FEM techniques and fracture mechanics methods, crack growth models are formulated for SnPb and SnAg solder joints, and crack propagation analysis, such as interaction between multiple cracks in a joint, is implemented.

Chapter 7, “ATC Life Tests and Life Prediction Modeling”, presents a novel life prediction model that is based upon a severity metric. The metric estimates damage to the solder joints and links material properties and parameters associated with package layout (SD and DD only) and thermal test conditions to the time-dependent creep, time-independent plastic deformation, and a time-dependent and geometric effective stress of the solder. Finite element analysis is performed to analyze the effects of test conditions and package layouts on joint reliability. The severity model predictions are compared to experimental data.

Chapter 8, “Conclusions and Recommendations”, summarizes observations from the experimental and analytical studies and presents conclusions. Recommended future work is also included.

1.4. BACKGROUND

Studies abound on various investigations of SnPb solder joints, and as expected, studies on lead-free solders have increased rapidly in the last few years. Previous relevant studies in the literature are presented below in the same order as the topics presented in this dissertation, namely the experimental studies and modeling efforts.

1.4.1. Experiments: Microstructural Evolution

Several studies compare eutectic 96.5%Sn3.5%Ag and 63%Sn37%Pb solders and their various alloys, the most popular being SnAgCu (SAC). Takemoto et al. [14] reported that eutectic SnAg solder has better thermal fatigue resistance than eutectic SnPb solder because the SnAg microstructure is more stable and less sensitive to strain-rate. Glazer [15] reported the same conclusion as Takemoto, but attributed the improvement to the lack of microstructural coarsening in eutectic SnAg solder. Schubert et al. [16] pointed out that 95.5%Sn3.8%Ag0.7%Cu solders are more creep-resistant at low stresses (<20MPa), but less creep-resistant at high stresses (>20MPa) than eutectic SnPb solders. Kim and Elenius [17] used sectioning to measure crack lengths at the outermost corner joints of 96%Sn3.5%Ag0.5%Cu and eutectic SnPb solder joints in chip-scale packages under 1-hour thermal cycling from –40°C to 125°C for 1220 cycles. They found that 96%Sn3.5%Ag0.5%Cu solder joints have approximately 50% lower crack growth rates than eutectic SnPb solder joints.

Grivas et al. [18] studied the deformation kinetics of eutectic SnPb solder with an initial grain size range of 5.5 μm to 9.9 μm over a range of temperatures from 0-160°C and strain rates from 2.66×10^{-5} to 1.33×10^{-2} s^{-1}. They found that eutectic SnPb solder deforms by two parallel mechanisms: superplastic deformation (grain boundary sliding) and conventional plastic deformation (dislocation), and that grain size affects the former deformation rate, but not the latter. Eutectic SnPb solder joints have ductile lead phase particles that are highly soluble in tin matrix and have a large volume fraction near 30%. On the other hand, eutectic SnAg solder joints have small, hard, finely dispersed Ag_3Sn particles that are insoluble in a tin matrix and comprise a mere 4% of the volume fraction**.** Therefore, the amount of silver that precipitates out of the tin matrix is limited by the insolubility of silver in tin, so further growth of Ag_3Sn is limited [19]. Choi et al. [20] ran liquid-to-liquid thermal shock cycles from –40°C to 125°C, with 20-minute dwell times at each temperature for eutectic SnAg solder. Their microstructural study revealed no grain coarsening and cracks propagated along the grain boundaries of the β-Sn phase.

1.4.2. Experiments: Crack Propagation and Life Studies

Since solder joints in semiconductor packages fail mainly by crack propagation, many experimental crack studies of solder joints have been reported. Logsdon et al. [21] explored SnPb material fracture mechanics parameters, such as stress intensity factor and strain energy release rate, and Fatigue Crack Growth Rate (FCGR) under isothermal fatigue tests. They found that the fracture

toughness of eutectic SnPb solder is greater at –55°C than at room temperature. Transgranular fracture was found at –55°C, while intergranular fracture was found at room temperature. They pointed out that creep deformation effects could not be introduced into the FCGR tests, since the solder crack tip is blunted by the effects of creep. Guo and Conrad [22, 23] observed the evolution of crack area to develop a fatigue crack growth model as a function of plastic work per cycle. Using notched-solder joints and measuring crack length and crack area, they found that: 1) crack area increases proportionally to crack length and 2) fatigue life can be evaluated by crack area growth rate. Darveaux [24] studied crack propagation of solder joints by correlating crack growth rates with strain energy density per cycle. He measured crack length in solder joints using dye-penetration technique and estimated crack area from the crack length. He achieved better correlation between crack growth rates and strain energy densities per cycle by separating joint life into two periods: crack initiation and crack propagation. He observed primary and secondary cracks in the solder joints, and developed a life prediction model based on strain energy density per cycle. Lau et al. [25] observed the growth of inner and outer cracks at the corner solder joints using a sectioning technique and developed crack propagation rates of solder joints in wafer-level chip-scale packages. Satoh et al. [26] observed crack propagation of high lead (5%Sn95%Pb) and eutectic SnPb solder under thermal cycling conditions of -55°C to 150°C and suggested that cracks propagate in a direction along the package center to the joint center. Hu [27] developed an empirical crack

propagation rate for high lead (10%Sn90%Pb) solder joints with different strain ranges under thermal cycling at 40°C to 140°C.

Many crack studies have been done to find fracture mechanics parameters, such as stress intensity factor, for formulating crack growth rate. Most focused on crack size and growth, but not on crack geometry, and little attention has been given to multiple cracks in solder joints.

There have been several experimental studies showing the increased reliability of lead-free solder joints. Syed [28] assembled 256 I/O PBGA packages (27x27mm, 1.27mm pitch, 10x10mm die) on 1.6mm-thick, OSP-finish (Organic Solder Protect) FR-4 boards. He found that 95.9%Sn3.4%Ag0.7%Cu joints have 46% longer mean cycle-to-failure than eutectic SnPb joints under -40-125°C, 1-hr ATC cycle testing. Farooq et al. [29] used 937 I/O CBGA packages (32.5x32.5mm, 1.27mm pitch) assembled on 1.83mm-thick, OSP finish FR4 test boards. They found 95.5%Sn3.8%Ag0.7%Cu joints had 77% longer cycle-to-failure at 0-100°C, 30-min cycles than conventional mixed SnPb solder joints with 90%Pb10%Sn balls joined to eutectic SnPb screened solder on the test board pads. Mawer and Levis [30] assembled 324 I/O PBGA packages (23x23mm, 1mm pitch, 10x10mm die) on 0.79mm-thick, ENIG-finish (Electroless Ni/Immersion Au) test boards and compared the reliability of 62%Sn36%Pb2%Ag solder joints with eutectic SnAg solder joints. They found that SnAg joints had at least twice the life of SnPbAg joints under two thermal cycling conditions, -40 to 125°C, 1-hr cycle and -50 to 150°C, 78-min cycle. INEMI (International Electronics Manufacturing Initiative) studied reliability of

lead-free solder joints on CBGA and Micro BGA [31]. They showed 95.5%Sn3.4%Ag0.7%Cu joints, assembled on 93mil-thick, electrolytic Ni-Au finish test board, have 2.2 times longer cycle-to-failure than eutectic SnPb joints under 0-100°C, 30-min cycle, and they concluded that lead-free solder joints have longer fatigue life than conventional eutectic SnPb joints.

1.4.3. Experiments: Post-Process and Package Layout Studies

The engineering properties of a material are determined by its chemical composition and current microstructure. Meanwhile, microstructure is determined by the chemical composition and the processing the material has been subjected to [32]. Likewise, the extent of resistance to crack growth depends on solder composition and microstructure. The desired microstructure can be obtained through post-process heat treatment by reheating the material to some temperature below its melting temperature. Therefore, many experimental studies have been done to find the effects of post-process heat treatment, but most have been conducted on SnPb solder, not on SnAg solder joints.

Mei et al. [33] studied the effects on fatigue life of eutectic SnPb solder joints of three different heat treatments: 1) air-cooled, 2) quenched to 0°C by immediate immersion into ice water, and 3) furnace-cooled by keeping the boards inside the furnace for 30 minutes after the furnace power was turned off. The joints were subsequently tested at 20°C and 65°C with strain rates of 10^{-4} s^{-1}. Tests showed that quenched joints had twice the life of aged joints due to their refined microstructures. Shine et al. [34] reported that coarse-grained solders

cause matrix creep that originates from dislocation generated within grains, resulting in faster failure in fatigue. Pang et al. [35] studied the aging effects on fatigue life of eutectic SnPb solder. For joints exposed to thermal cycling aging for 1000 cycles (56-minute cycle from -40°C to 125°C) after exposure to reflow temperature, they found that the microstructure coarsened due to aging and the fatigue life of aged solder joints was reduced by a factor of six than non-aged solder joints. Miyazawa and Ariga [36] investigated hardness of eutectic SnPb and SnAg solders for aged and air-cooled conditions. They showed that aging lowered the hardness of both solder alloys; hardness of the SnPb solder decreased from 20 HV to 13 HV in 10 hours, while hardness of the SnAg solder decreased from 27HV to 18HV in approximately 1000 hours. They also claimed that the age-softening in SnAg solder was caused by recrystallization and coarsening of eutectic microstructures, while in SnPb solder age-softening was caused by the transformation from a non-equilibrium to an equilibrium state.

Package reliability may also be based upon the package layout on the PWB, which include packages on both sides of the board, package spacing on a single side of the board, etc. These parameters alter the stiffness of the board assembly. Katchmar et al. [37] examined PWB layout, package design and processing factors on the fatigue life of solder joints. They assembled four 313 I/O PBGA packages (35x35mm body, 12.5x12.5mm die) as single-sided on different locations of 1.7mm thick, HASL-finish (Hot Air Solder) test boards; two packages placed near the corners of board and the other two in the center of board. They concluded that PBGA package location on PWB does not affect

fatigue life but that local stiffening effects due to the CTE mismatch between the die and board to impact fatigue life of solder joints. Logterman et al. [38] investigated solder joint reliability of 256 I/O BGA and 48 I/O CSP packages, which were assembled on 32mil-thick, 6-layer boards as single-sided and double-sided with different package-to-package spacings (0.1", 0.15", and 2.5"). The packages were thermal-cycled for 3500 cycles at 0-100°C, 30-min ATC cycling. Double-sided 256 I/O BGAs started to fail at 974 cycles, but no failures were observed in single-sided or double-sided 48 I/O CSP and single-sided 256 I/O BGAs. Also, failure analysis using dye penetration techniques showed more joint failures occurred along the package edges with tightest package-to-package spacing, 0.1", indicating a possible degradation of solder joint reliability under tighter package-to-package spacing. Ghaffarian [39] investigated reliability in CSP for single-sided and double-sided assemblies. He observed an approximately 50% reduction in solder joint life for various CSPs, such as 232 I/O CSPs with 0.5mm pitch, 176 I/O CSPs with 0.8mm pitch, and 144 I/O CSPs with 0.8mm pitch. He attributed such reduction in fatigue life to localized stiffness changes due to the second package, and solder joint height changes resulting from the second reflow. Ahn et al. [40] compared package warpage in double-sided with single-sided boards. They mentioned that stress in the solder joint is relieved by flexing the board, but the restricted board flexing for double-sided mounting caused larger stress in the solder joints. They found that package warpage of double-sided boards is reduced by half, less than 10 microns, than single-sided boards.

In this study, four different package layouts are tested to determine spacing effects on the reliability of solder joints.

1.4.4. Modeling: Crack Initiation (Damage Mechanics)

Damage mechanics introduces a quantity "damage" that is characterized as a function of stress and strain to indicate load history to a local region. It can be used to estimate/ predict the initial crack formation as well as the crack path [41]. This method, however, requires extensive computation time. Therefore, damage mechanics is often used just to predict the initial crack formation, but previous work focuses on SnPb solder, and little exists for SnAg solders. Wong and Helling [5, 6] developed a mechanistic life prediction model based on the microstructure failure process, e.g. voiding and grain coarsening of eutectic SnPb solder. He commented that the mechanism-based life model justified extrapolating of the test results to operational conditions beyond those tested in the laboratory. Pan [42] developed a mechanistic energy-based model using a critical accumulated strain energy density for eutectic SnPb solder. He simulated crack initiation and growth by removing elements from his finite element method solder joint model when they reached the threshold strain energy density value, 4.55 MPa/mm^3, for eutectic SnPb solder. Vianco et al. [43] used damage mechanics to simulate coarsening of eutectic tin-lead solder joint. He chose lead phase size as a damage indicator. He found the solder joints fails when the lead phase size reaches a threshold value of 9 microns.

1.4.5. Modeling: Crack Propagation (Fracture Mechanics)

Fracture mechanics uses energy release rate instead of stress and strain to describe crack growth rate. It is useful to evaluate crack propagation rates and paths, but an initial crack must be hypothesized [41]. Again, most of the literature focused on SnPb solders. Lau [44] initiated life prediction of solder joints using finite element method (FEM). He embedded different sized cracks into an FEM solder joint model and calculated energy release rates to predict solder joint life. Lau and Lee [45] also developed a crack propagation model in wafer-level chip scale packages using a calculated stress intensity factor as well as the measured inner and outer cracks in solder joints. Pidaparti et al. [46] analyzed crack propagation for life prediction using FEM; he found that crack propagation life is approximately 4 times higher than the crack initiation life. Ju et al. [41] used a fracture-mechanics-based technique for life prediction of eutectic SnPb solder joint.

1.4.6. Modeling: Life-Prediction

A number of analytic life-prediction models have been proposed for solder joint fatigue. The Coffin-Manson model was developed to predict life from strain distribution in solder joints [47, 48]. It is empirically based and widely used due to ease of use. The most popular Coffin-Manson-type power-law models are strain-based for low cycle fatigue and use a single damage parameter such as inelastic strain (see below):

$$N\left(\Delta\varepsilon_p\right)^n = Const. \tag{1.1}$$

where N is the life in cycles, $\Delta\varepsilon_p$ is plastic strain range, n is an empirical constant.

Since the Coffin-Manson model has no parameters for temperature-dependent properties of solder and time-dependent creep, Engelmaier [49] proposed a life-prediction model for eutectic SnPb solder joints by including parameters such as empirical effects of package type, mean test temperatures, dwell times, coefficients of thermal expansion (CTE) and solder joint geometry (see below).

$$N = \frac{1}{2}\left[\frac{2\varepsilon_f'}{\Delta D}\right]^{\frac{-1}{C}} \tag{1.2}$$

$$C = -0.442 - 6\times10^{-4} T_{SJ} + 1.74\times10^{-2} \ln\left(1 + \frac{360}{t_D}\right) \tag{1.3}$$

where N is the life in cycles, ε_f' is fatigue ductility coefficient (0.325 for eutectic SnPb solder), T_{SJ} cycles is mean cyclic solder joint temperature [^{o}C], t_D is half-cycle dwell time in minutes, and ΔD is cyclic fatigue damage that is a function of strain.

$$\Delta D = \left[\frac{FL_D\Delta(\alpha\Delta T)}{h}\right] \tag{1.4}$$

where F is an empirical coefficient, L_D is the distance from the neutral [mm], α is CTEs (Coefficients of Thermal Expansion) of die and PCB, ΔT is temperature difference between maximum temperature and minimum temperature [^{o}C],

$\Delta(\alpha\Delta T)$ is absolute cyclic thermal expansion mismatch between die and PCB, and h is solder joint height [mm].

Norris and Landzberg [50] developed an empirical life-prediction model for eutectic SnPb solder joints that accounts for different levels of creep, temperature-dependent properties of solder. The model calculates an acceleration factor, which is the ratio of lifecycles in use condition to lifecycles in test condition to estimate useable life (see below).

$$AF = \frac{N_o}{N_t} = \left(\frac{f_o}{f_t}\right)^{\frac{1}{3}} \left(\frac{\Delta T_t}{\Delta T_o}\right)^2 \exp\left[1414\left(\frac{1}{T_{\max,o}} - \frac{1}{T_{\max,t}}\right)\right] \tag{1.5}$$

where f is frequency cycles per day, ΔT is temperature range, subscript "*o*" and "*t*" stands for testing and operating conditions, T_{max} is the maximum temperature [K], and T_{min} is the minimum temperature [K].

1.5. OBJECTIVES OF THIS RESEARCH—RESTATED/EXPANDED

Summarizing Section 1.3, the major objectives of this research are to: 1) develop an integrated, experimentally-verified life-prediction model and 2) evaluate the reliability of semiconductor packages with SnPb and SnAg solders under different post-process heat treatment, thermal loading and package layouts. Specifically the parameters of this study are:

Solder type: SnPb: 62%Sn36%Pb2%Ag

SnAg: 96.5%Sn3.5%Ag

Post-process heat treatment:

Air-cooled

Quenched to 0°C

Aged at 150 °C (SnPb) and 160 °C (SnAg) for 1008 hours

Thermal loading—accelerated thermal cycling (ATC) test protocols:

0 °C to 100 °C, 30-minute cycles

-40 °C to 125 °C, 1-hour cycles

-55 °C to 125 °C, 10-minute cycles

Package Layouts (package layout on PWB defined in Chapter 2):

Single (sided)-sparse—SS

Single (sided)-dense—SD

Double (sided)-alternating—DA

Double (sided)- dense—DD

Extensive experimental testing and analytical modeling were conducted to support the objectives. The approaches and methodologies used in this work are summarized below for the experimental and modeling efforts.

1.5.1. Experiments: Microstructural Evolution

Due to the extensive literature on microstructural evolution of SnPb solders, this section of the research will focus exclusively on PBGA packages with eutectic SnAg solder that have been post-processed by air-cooling or aging at 160°C for 1008 hours and exposed to 0 -100 °C ATC test cycles. Six packages, chosen at 0, 6K, 12K, 18K, and 24K cycles were mounted, ground, polished and etched to reveal the microstructures of the solder joints located under the die.

Photographs of selected joints were taken and the microstructure evolution and comparisons are discussed in Chapter 3.

1.5.2. Experiments: Crack Propagation

Results from an extensive experimental study of crack growth in SnPb (62%Sn36%Pb2%Ag) and eutectic SnAg solder joints for three different post-process heat treatment conditions and exposure to 0-100 ^{o}C ATC testing is reported using dye penetration techniques. Cracks are characterized by their shape, size, orientation, length, and the location of the joint in the package. Primary and secondary crack growths were measured both on the package and board interfaces of the solder joints in the boundary region (See Figure 2.2, Chapter 2). These results are provided in Chapters 4 and 5.

1.5.3. Experiments: Life

Experimental life data is presented in Chapter 7 for 1) SnPb and SnAg solder air-cooled packages exposed to two different ATC tests (0 -100 ^{o}C and -40 - 125 ^{o}C) and four different package layouts, 2) SnPb and SnAg solder air-cooled packages exposed to the liquid-liquid shock thermal cycle (-55-125 ^{o}C) for the single-dense package layout configuration, 3) SnPb and SnAg solder packages exposed to 0-100^{o}C ATC test cycles for three different post-process heat treatment conditions. Failure was monitored by an event detector.

1.5.4. Modeling

Crack Initiation Model

Using finite element techniques and damage mechanics methods, crack initiation models for SnPb and SnAg solders were developed in Chapter 5 to integrate the progression of grain growth and the formation and growth of voids, micro-cracks and macrocracks. Governing constitutive models for each phase of crack growth and threshold values governing transitions between phases is presented in Chapter 5. The micro-models describing the crack initiation mechanisms are coupled to joint sub-models and global board-level models. Simulation results for crack initiation on the joints located under the die corners are shown.

Crack Propagation Model

Using finite element techniques and fracture mechanics methods, crack growth models are formulated in Chapter 6for SnPb and SnAg solder joints based upon energy release rates. The global board-level and solder joint sub-models are coupled to compute stress intensity factors and energy release rates. Simulations for crack growth are shown and compared with independent data. The effects on energy release rates resulting from multiple cracks (primary and secondary cracks at the package interface, primary cracks at the board interface) and board warpage are simulated and discussed.

Life-Prediction Model

A severity metric is proposed in Chpater 7 as a life-prediction measure that links material properties, parameters associated with post-process heat treatment, package-on-board configuration, and thermal cycling conditions to the time-dependent creep, plastic deformation and a geometric effective stress in solder joints. Experimental life data from this study and from external sources are compared with life predicted by the severity metric.

CHAPTER 2

Testing and Measurement

The electronics packaging experimental program was designed in collaboration with Motorola (now Freescale Semiconductor, Inc., 6501 William Cannon Drive West, Austin Quality Laboratory, Austin TX 78735) using prototypic plastic ball grid array packages (PBGA) mounted onto specially designed printed wiring boards. The key experimental variables were related to the test vehicle (solder type, packing density and package layout, post-process heat treatment) and test conditions and environment (accelerated thermal cycle, testing facility). The key observations and data collected were related to joint life, crack properties, and microstructural evolution.

2.1. TEST VEHICLES: PACKAGES & BOARDS

2.1.1. Motorola Package

The Motorola 357-PBGA package was used. The daisy-chained 357-joint (19x19) array has 1.27mm pitch and solder-mask-defined Cu pads with electrolytic NiAu finish on the package-side and Cu pads with Hot Air Solder Level (HASL) finish on the board-side. The solder mask openings at the package and board interfaces are 560 μm and 584 μm, respectively. The edge of the 10x10mm die is bounded by joints N7-N13 and G7-G13 (see Figures 2.1 and 2.2).

Joint Regions

A previous report on the data [51] suggested that crack measurement results were symmetric in the package and that the joints on the die periphery (see Fig 2.2) had the largest crack areas, particularly those three adjacent joints at each of the four corners. As a result, package joints were assembled into and studied in six regional groups covering 155 of the total 357 solder joints. The six regions are described below, in the order of predicted failure.

1) Boundary Region (shaded red, Fig 2.2)

These 24 joints lie immediately inside the die periphery and were expected to experience the greatest shear due to the thermal expansion mismatch between the die (10x10x0.35mm—2.62ppm/K) and PWB (115x200x1.57mm—16ppm/K). The boundary region is a square strip of length 8.9 mm. Boundary Joints: G7-13, M7, L7, K7, I7, H7, M13, L13, K13, I13, H13, N7-13

2) Inner Boundary Region (shaded orange, Fig 2.2)

These 16 joints that lie along the interior boundary of the die periphery may also experience high shear stresses. This region is a square strip of length 7.62 mm.

Inner Boundary Joints: H8-H12, I8, K8, L8, I12, K12, L12, M8-M12

3) Outer Boundary Region (shaded purple, Fig 2.2)

These 32 joints lie along the exterior boundary of the die periphery and form a square strip of length 12.7 mm.

Outer Boundary Joints: F6-14, G6, G14, H6, H14, I6, I14, K6, K14, L6, L14, M6, M14, P6-14

4) Inside Region (shaded light green, Fig 2.2)

These nine inner-most joints lie under the center of the die (and hence package) and form a square region of length 5.1 mm.

Inside joints: J9-J11, K9-K11, L9-11

5) S-Outside Region (S refers to a **s**ection outside of the die region)

These 32 "corner" joints lie outside the die region and along the package diagonal region. The length of this 6x6 square section is 8.9 mm.

S-Outside Joints: N15-18, P15-18, R13-18, T13-18, U13-18, V13-18

6) Outside Region

These 42 "remote" joints lie outside the die region and constitute all joints in quadrant III not covered by any of the other regions. The length of this 10x10 square section is 14 mm.

Outside Joints: K15-19, L15-19, M15-19, N19, P19, R10-12, R19, T10-12, T19, U10-12, U19, V10-12, V19, W10-18

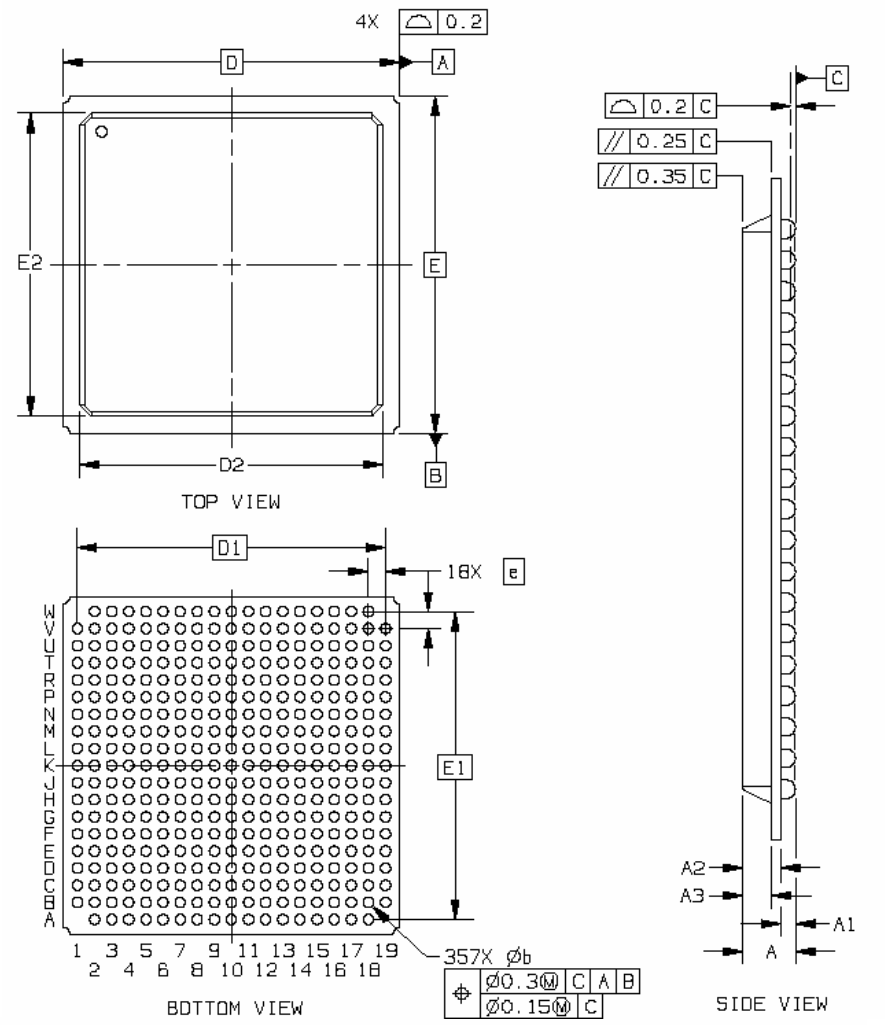

1. Dimensioning and tolerancing per ASME Y14.5 M-1994
2. Dimension b is the maximum solder ball diameter measured parallel to Datum C

	Min. (mm)	Max. (mm)		Min. (mm)	Max. (mm)
A	-	2.05	D1	22.86 BSC	
A1	0.50	0.70	D2	22.40	22.60
A2	0.95	1.35	e	1.27 BSC	
A3	0.70	0.90	E	25.00 BSC	
b	0.60	0.90	E1	22.86 BSC	
D	25.00 BSC		E2	22.40	22.60

Figure 2.1. Motorola 357-PBGA package [52]

Note: BSC, 'BASIC', represents theoretical exact dimension or dimension target.

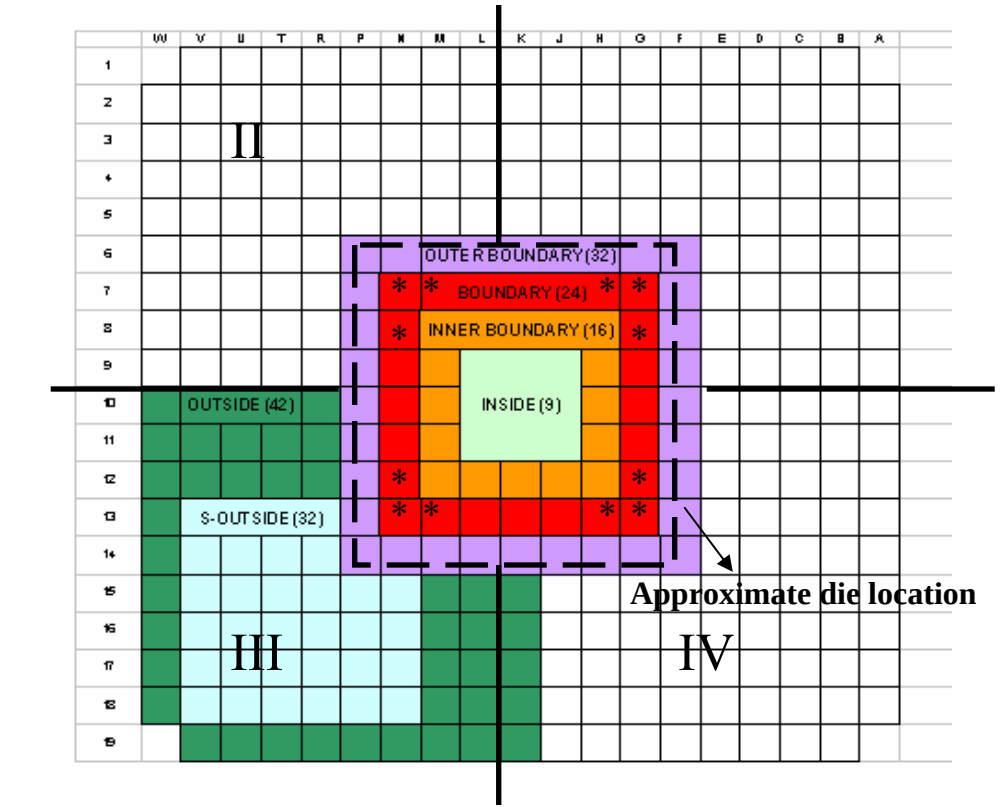

Figure 2.2. Six joint regions and four quadrants of the 357-PBGA package (* joints with largest cracks)

2.1.2. 357 Longhorn Board

The printed wiring test board (PWB) was designed by Motorola to accommodate 15 packages (3x5 matrix) on the top and bottom, as configured in Figure 2.3. The test board is 0.062" thick, made of FR-406 epoxy/glass material with a glass transition temperature of 170°C, and has two dummy inner layers for stiffness and two outer layers for routing. The outer layers have 1/2 oz (0.0007") rolled Cu foil plus approximately 0.001" thick electroplated Cu, and the inner layers have 1 oz. (0.0014") Cu without plating.

The Longhorn boards have electrical connection tabs for continuous monitoring of electrical continuity (as defined by IPC-9701 [53]). Some populated boards were monitored for the joint life study. Other boards were cut apart along pre-slotted lines into five strips (strips A-E, see Fig 2.4) and thermally cycled for the crack and microstructural evaluation studies—the packages in the strip A were electrically monitored for continuity but those in strips B-E were not electrically monitored.

The material properties of the board are listed in Appendix A.

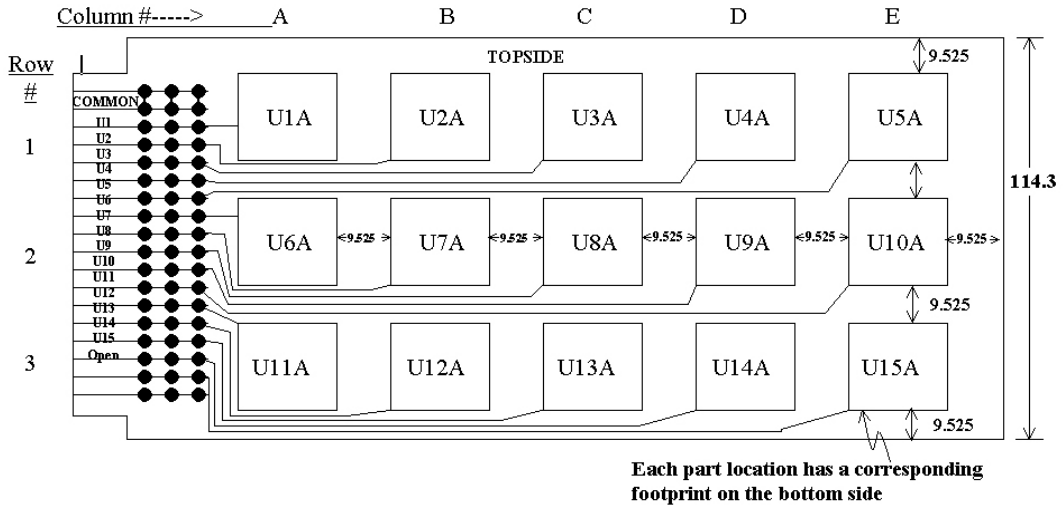

TOP SIDE

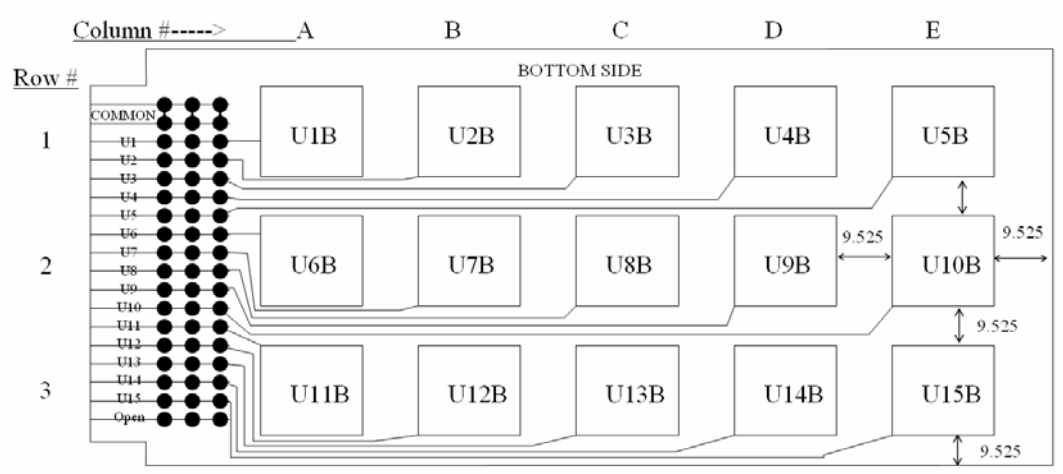

BACK SIDE (from Top view)

Figure 2.3. Longhorn board assembly layout (unslotted) [52]

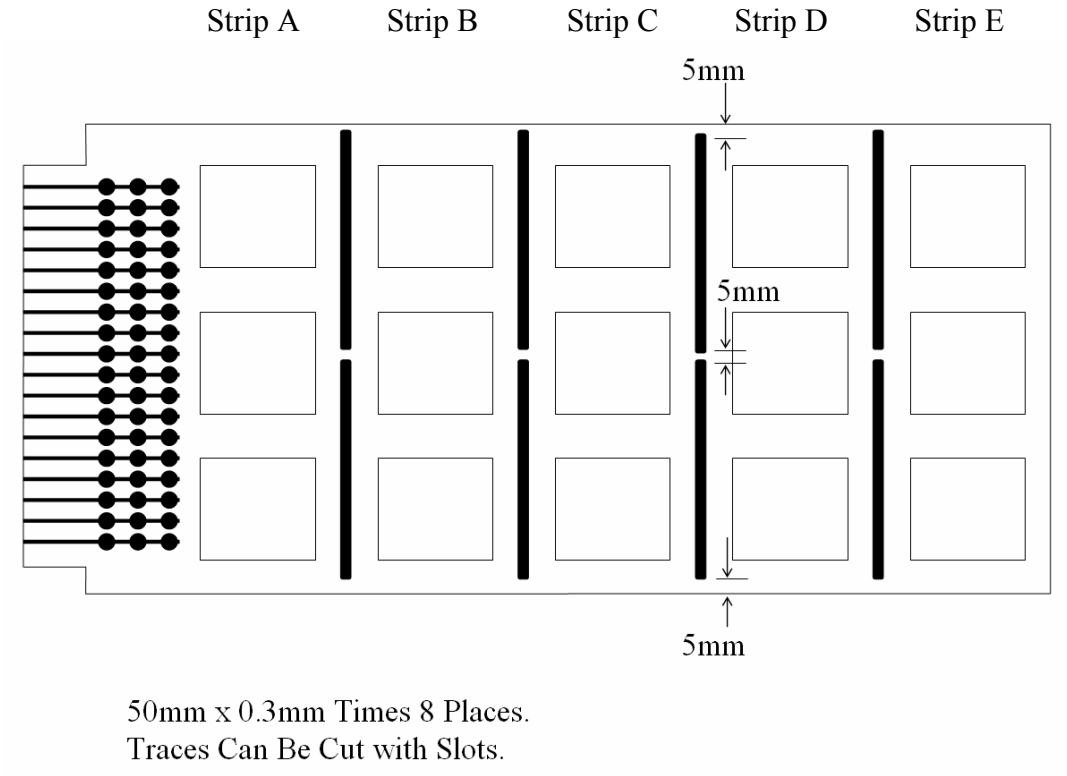

Figure 2.4. Longhorn board assembly layout (slotted) showing five strips and packages on strips designated as top/middle/bottom [52]

2.1.3. Assembly and Reflow Profiles

All boards were assembled and processed in February, 2000 at Motorola's Customer Applications Support Section, Ed Bluestein Facility in Austin, TX. Solder paste was printed using a 6mil thick stencil (1:1 aperture size). Eutectic 63%Sn37%Pb and 95.5%Sn3.8%Ag0.7%Cu solder pastes were printed and later reflowed with the 62%Sn36%Pb2%Ag and eutectic 96.5%Sn3.5%Ag solder spheres, respectively. After paste printing, the Longhorn test boards were visually

inspected for missing solder paste and paste bridging between neighboring PCB lands.

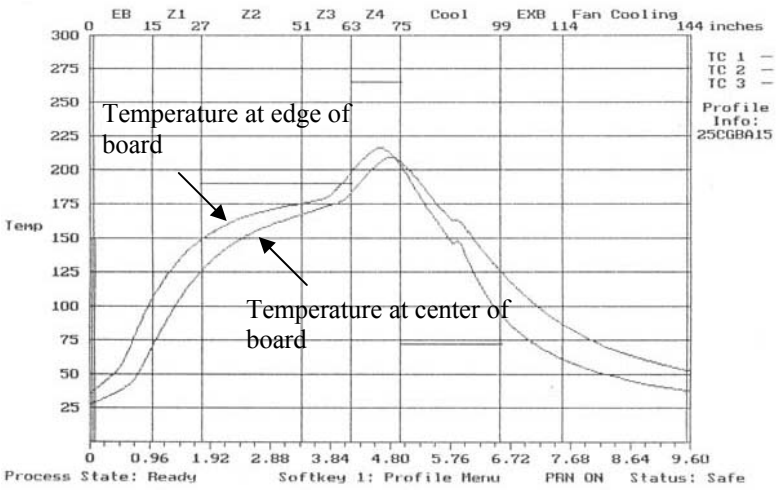

(a)

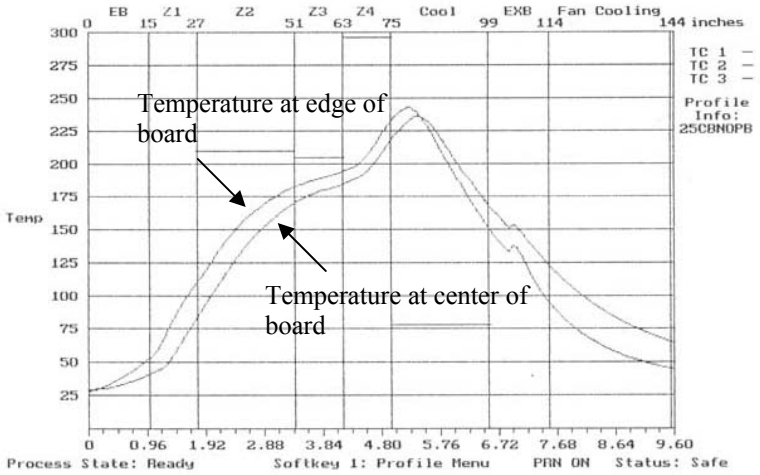

(b)

Figure 2.5. Longhorn board assembly reflow profile (a) SnPb profile (b) SnAg profile [52]

Using a pick-and-place machine, the 357 PBGAs were placed on the PCB, and the assembled boards were put in a RTC Model EFC 615 forced convection reflow furnace. The SnPb and SnAg solder spheres and pastes were reflowed with peak temperatures of 216C and 243C, respectively. Figure 2.5 shows the reflow profiles used. For double-sided package layouts, after the top side of the Longhorn 357 board assembly was completed, the board was flipped over and the process repeated—solder paste printing, visual inspection, placement of 357 PBGAs, and solder reflow. The assembled boards were inspected using an x-ray machine to check for open solder joints or bridging between neighboring joints.

2.2. TEST MATRIX AND VARIABLES

2.2.1. Test-Vehicle related Variables

Solder Balls and Paste

SnPb solder: spheres (62%Sn36%Pb2%Ag) and paste (63%Sn37%Pb)

SnAg solder: spheres (96.5%Sn3.5%Ag) and paste (95.5%Sn3.8%Ag0.7%Cu)

The solder pastes had the following specifications:

Manufacturer:	Kester Type R2444 NC	Indium Corporation
Alloy:	63%Sn37%Pb	95.5%Sn3.8%Ag0.7%Cu
Mesh:	-325+500	-325+500
Visc. Kcops:	1000+/-10%	Metal: 89.3%
PO#:	PNXG0830	
Lot#:	9102071	
DOM:	10/7/99	12/01/99

In this study, reference to SnPb joints denotes joints formed from solder spheres (62%Sn36%Pb2%Ag) and paste (63%Sn37%Pb), and reference to SnAg joints denotes joints formed from solder spheres (96.5%Sn3.5%Ag) and paste (95.5%Sn3.8%Ag0.7%Cu). In the modeling efforts, material properties for 62%Sn36%Pb2%Ag were used for SnPb and properties for 96.5%Sn3.5%Ag were used for SnAg. The material properties are listed in Appendix A.

Packing Density and Arrangements: Package Layout

In order to study the effects, if any, of packing density and the spatial distribution of packages upon board warpage and corresponding reduction in joint life, four different package layouts, shown in Figure 2.6 were tested (air-cooled post-process only)

1) Single-Dense (SD)

These boards were fully populated with 15 packages on the front, "A"-side of the PWB: packages U1A-U15A. Due to the relatively high packing density on a single side, these boards were expected to demonstrate the highest levels of out-of-plane warpage.

1) Double-Dense (DD)

The boards were fully populated with 15 packages (30 packages total) in both the front, "A"- and back "B"- sides of the PWB: packages U1A-U15A, U1B-U15B. Due to their symmetry about the board mid-plane, these boards were expected to demonstrate the least, indeed negligible, out-of-plane warpage.

2) Double-Alternating (DA)

The boards were partially populated with nine and six packages in the front "A"-and back "B"-sides, respectively, of the PWB: front-side packages column A (U1A, U6A, U11A), column C (U3A, U8A, U13A), and column E (U5A, U10A, U15A)—backside packages, column B (U2B, U7B, U12B), and column D (U4B, U9B, U14B). Due to the alternating arrangement of packages, the boards were expected to potentially warp locally (over the length scale of the package) but not to warp globally (over length scale of the board).

3) Single-Sparse (SS)

The boards were the least populated boards with only 6 packages on the front "A"-side of the PWB: packages, column A (U1A, U11A), column C (U3A, U13A), and column E (U5A, U15A). Due to the sparse packing, these boards were expected to demonstrate lower levels of global, out-of-plane warpage than the SD PWBs.

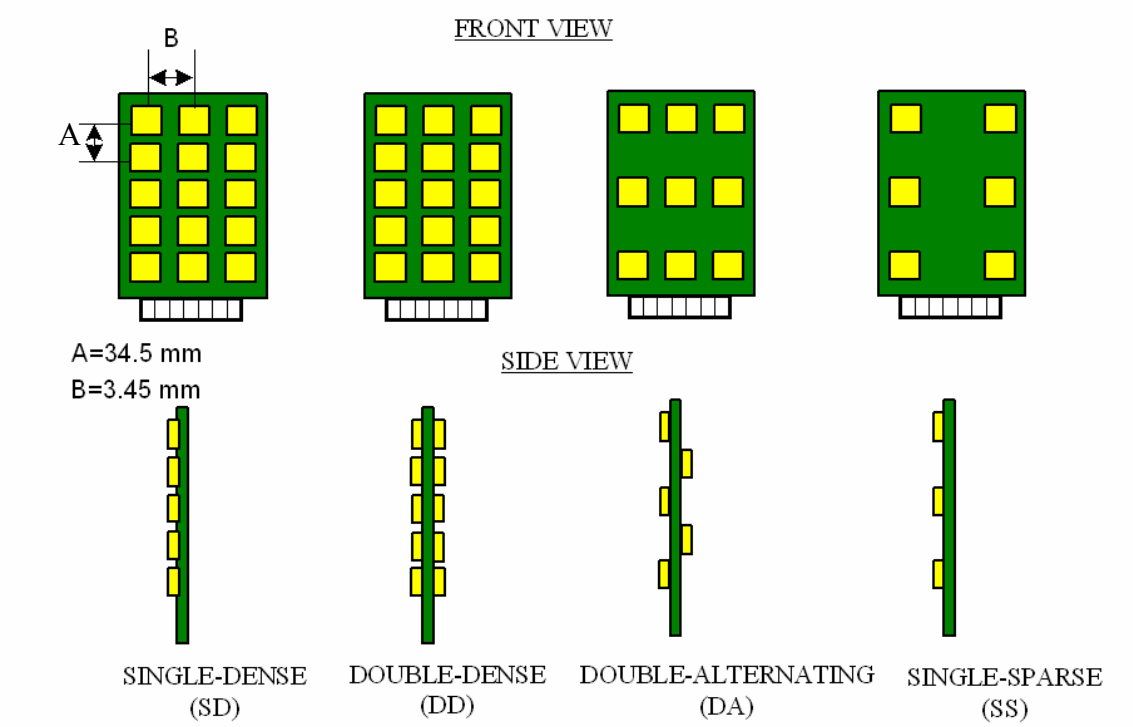

Figure 2.6. Four package layouts

Post-process Heat Treatment

The board assemblies were exposed to three post-process conditions before accelerated thermal cycle (ATC) testing in order to study the effectiveness of heat treatment in extending the life of solder joints: Upon exiting the solder reflow furnace, boards were either 1) air cooled to room temperature, or 2) quenched to 0^{o}C by submerging them into an ice water bath, or 3) aged for 1008 hours at 150±5 ^{o}C (~0.9 in homologous temperature) for SnPb boards and at 160±5 ^{o}C (~0.9 in homologous temperature) for SnAg boards. The air-cooled and quenched heat treatments were done at Motorola's Ed Bluestein facility

immediately following the assembly and reflow. The aging heat treatment was done at the University of Texas Pickle Research Center.

2.2.2. Test-Environment related Variables

Accelerated Thermal Cycling Test (ATC) Protocols

The boards were thermally-cycled using three different accelerated thermal cycle (ATC) test protocols:

1) "Nominal": 0-100 ^{o}C

As shown in Figure 2.7, this 30-minute cycle has 10-minute ramps and 5-minute dwells at 0 and 100^{o}C. It is one of the standard ATC protocols in the electronics packaging industry (IPC-9701 [53]).

2) "Severe": -40-125 ^{o}C

As shown in Figure 2.7, the 1-hour cycle has 15-minute ramps and 15-minute dwells at -40 and 125^{o}C. It is also one of the standard ATC protocols in the electronics packaging industry for qualifying electrical components for severe environments, e.g. "under the hood" in the automotive industry.

3) "Liquid-Liquid Thermal Shock" (LLTS): -55-125 ^{o}C

As shown in Figure 2.7, this 10-minute cycle has ~1-minute ramp and ~4-minute dwells at -55^{o}C (in liquid perfluorocarbon) and 125^{o}C (in liquid perfluorocarbon) per JEDEC standard, JESD22-A106B [54]. This aggressive protocol is used to shorten qualification times, but may (and probably does) change failure mechanisms.

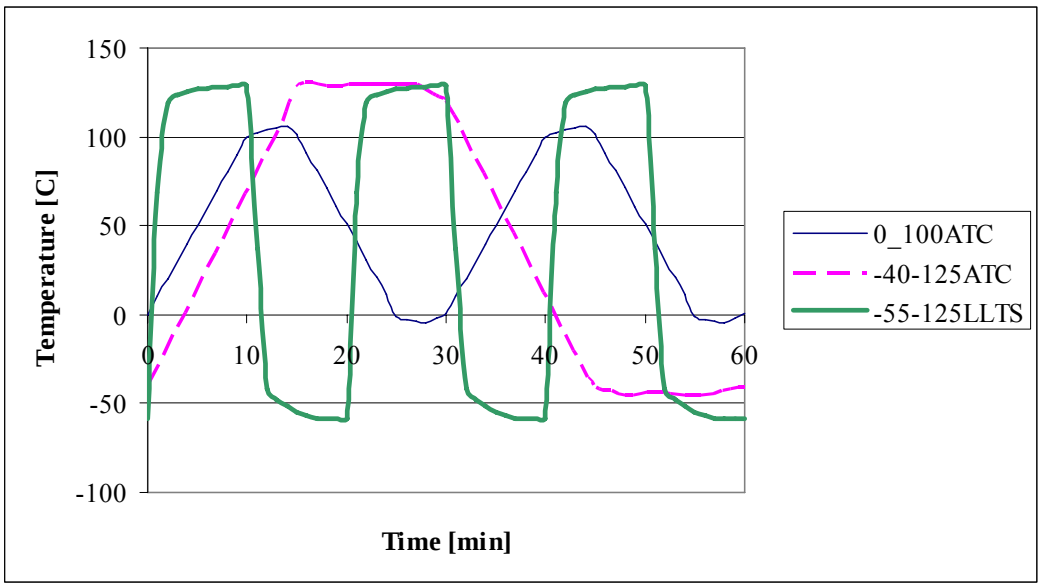

Figure 2.7. Temperature profiles of -40°C to 125°C, 0°C to 100°C and -55°C to 125°C accelerated thermal cycles (measured from the top surface of 357 PBGA package, typically U8B or U8A)

Test Location and Monitoring

Thermal testing and electrical continuity monitoring of the assembled 357-PBGA boards were done at the University of Texas Pickle Research Center and at Motorola's Ed Bluestein facility based upon equipment availability/capability at the two facilities as noted below.

University of Texas Pickle Research Center (UT)

Two Blue M ETC -09DH-G environmental chambers

Tandem-compressors, -73 to 190^{o}C, at 15^{o}C/minute

Precision oven

Room temperature to 50^{o}C

Fisher Scientific oven

Constant temperature heating

256-channel ANATECH event detector (on loan from Motorola)

The UT chambers were only capable of running the 0 to 100^{o}C ATC test.

Motorola Ed Bluestein Facility

Full complement of environmental chambers using liquid nitrogen for cooling

Full complement of ovens

Full complement of ANATECH event detectors

The Motorola environmental chambers were capable of all three ATC testing protocols used in this study.

The microstructural and crack evolution results presented in this work are from boards cycled at UT only. The life results are from boards cycled at UT and Motorola (see Test Matrix below).

2.2.3. Test Matrix

A total of 60 Longhorn boards were thermally tested as follows:

24 boards at UT (6 unslotted, 18 slotted)

SnPb, SnAg solders

All single dense (SD) package layout

Air-cooled, quenched, aged post-process

Nominal ATC test: 0 to 100^{o}C

Packages from unmonitored (not electrically monitored), slotted boards were used for crack propagation and microstructural evolution studies. Packages from unslotted and monitored slotted (three packages in A strips) boards were used for the life study.

36 boards at Motorola (all unslotted): All packages were used in the life study.

SnPb, SnAg solders

Single sparse (SS), single dense (SD), double dense (DD), double alternating (DA)

Nominal (0 to 100^{o}C), severe (-40 to 125^{o}C), and liquid-liquid shock (-55 to 125^{o}C)

Summary:

The experimental program had five principal test variables:

1) Solder Balls/Paste
   - SnPb (62%Sn36%Pb2%Ag)/(63%Sn37%Pb)
   - SnAg (96.5%Sn3.5%Ag)/ (95.5%Sn3.8%Ag0.7%Cu)
2) Package layouts
   - Single-sided, sparsely-populated (SS)

- Single-sided, densely-populated (SD)
- Double-sided, densely-populated (DD)
- Double-sided, alternating-populated (DA)

3) Post-process heat treatments
   - Air-cooled (< 1hr)
   - Quenched to 0^{o}C (<1 min)
   - Aged at 150 ^{o}C (SnPb) or 160 ^{o}C (SnAg) for 1008 hrs
4) Accelerated thermal cycle test protocols
   - Nominal, 0-100C, 30-min cycles
   - Severe, -40-125C, 1-hour cycles
   - Liquid-liquid shock, -55-125C, 10-min cycles
5) Test location
   - UT, PRC (Pickle Research Campus), Burnet Street, Austin, TX 78712
   - Motorola, Semiconductor Products Sector, Ed Bluestein Street, Austin, Texas USA 78721

A condensed summary of how the five principal test variables were configured is shown in Table 2.1. Detailed test matrices "Longhorn 357 PBGA Test Build Matrix" and "Longhorn 357 PBGA Test Build Matrix (Listed Build Order)" are given in Appendix B. The former matrix is listed by board numbers (separated by UT and Motorola), and the latter list is by solder type. Then both matrices list by package layout.

The test matrix was not fully populated due to:

1) resource constraints (time, money, personnel)
2) exploratory nature of certain parameter ranges (significance of effects not certain a priori)
3) testing facility availability

(two ATC tests—severe and liquid-liquid shock—were only available at Motorola).

Table 2.1. Test matrix (condensed version)

	SnPb			SnAg		
Thermal condition	Quenched	Air-cooled	Aged	Quenched	Air-cooled	Aged
0-100°C	**Single-dense***	**Single-dense**** Single-sparse Double-alt Double-dense	**Single-dense***	**Single-dense***	**Single-dense**** Single-sparse Double-alt Double-dense	**Single-dense***
-40-125°C		**Single-dense** Single-sparse Double-alt Double-dense			**Single-dense** Single-sparse Double-alt Double-dense	
-55-125°C		**Single-dense**			**Single-dense**	

Note: * Test run in UT, ** Test run in UT and Motorola, Other test run in Motorola

2.2.4. Nomenclature

Due to the large number of experimental parameters—solder type, package layout, post-process condition, ATC test, and test location—a descriptive nomenclature was developed for this study as follows:

LOCA-B-C-D-E-F-G-H-I-J

Where LOCA MOT or UT board number A=1-26

B	Package number (U1A-U15A)	
C	Solder type	SPA=SnPb, SA=SnAg
D	Postprocess	AG=aged, A=air-cooled, Q=quenched
E*+	Number of thermal cycles in K cycles	
F*+	Joint location in package	1-19 row number A-W column number
G+	Package interface	PI=package interface BI=board interface
H*	Lateral location in joint cross section	C=center TC=toward package center AC=away from package center
I*	Location	CL=centerline
J*	Magnification	500X, 1000X

Note: * denotes information used in microstructural studies

+ denotes information used in crack evolution studies (dye penetration)

Examples:

UT5-U15A-SA-A (this version usually used for life monitoring study)

Board UT5, package U15A, SnAg solder, air-cooled post process

UT14-U1A-SA-AG-15-N7-PI (this version usually used in crack evolution-dye penetration study)

Board UT14, package U1A, SnAg solder, aged post process, 15K thermal cycles, joint N7, dye penetration on package interface

UT13-U13A-SPA-Q-0-G5-AC-CL-500X (this version usually used in microstructural evolution study)

Board UT13, package U13A, SnPb solder, quenched post process, 0K thermal cycles, joint G5, microstructural picture away from the package center in the centerline of that section, picture taken at 500X

2.3. OBSERVATIONS AND DATA COLLECTION

This study involves a series of parallel experiments to measure and observe

1) microstructural evolution (phase size and distribution, crack propagation path) in solder joints and their respective interfaces/interphases with the package and boards;
2) crack propagation rates (crack sizes) and orientations (crack shape and direction) of the solder joints;
3) joint life as defined by the number of thermal cycles experienced before specific, repeatable electrical failure.

To experimentally assess the evolution of microstructural and crack properties in solder joints with the number of thermal cycles, SnPb and SnAg PBGA packages were nominally removed from the environmental chambers every 2K

and 3K cycles, respectively. At those cycle times (called read-points) two sets of two strips (each with three packages—see Figure 2.4) for each of the three post-process heat treatments (total of six strips or 18 packages per set) were removed—one set of six strips for the microstructural study and one set of six strips for the crack propagation study. Non-monitored strips (B-E strips) were removed from the environmental chamber first. Then monitored strips (A strips) and/or strips from unslotted (monitored) boards were removed if the packages had already failed. If the packages had not already failed, the monitored strips or boards were dye-penetrated then put back into the environmental chamber. At the time of failure, these strips were cut out of the boards for microstructural or crack property measurements, as appropriate. The remaining unfailed strips were rewired to allow continued electrical continuity monitoring for the joint life study.

Deviations from the nominal strip removal times were due to human error. The exact removal times were:

SnPb: 0K, 2K, 4K, 6K, 8K, 10K, 13K (aged)/15K (air)/14K (quenched), 16K

SnAg: 0K, 3K, 6K, 9K, 12K, 15K, 18K, 21K, 24K, 27K, 30K(quenched)

The following describes the data collection techniques used in the microstructural and crack studies.

2.3.1. Measurement and Assessment of Microstructural Evolution

Microstructural Sectioning Technique

The microstructural evolution study focuses on solder joints in row 7 (see Figure 2.2, Chapter 2) of the 357-PBGA package. These joints are under the die edge (boundary region) and show the largest cracks of any region in the package. The microstructural sectioning protocol consisted of 1) cutting the package assembly (package and PWB) out of the strip; 2) grinding the package assembly using a Streuers Rotopol-15 polishing machine with 80 and 180-grit silicon carbide paper to get close to row 7 and then sequentially using 1200, 2400, and 4000-grit paper to get closer to row 7 and to remove major scratches; 3) hand-polishing the joint cross-sections sequentially with 3 μm, 1 μm, and 0.05 μm diamond suspensions; 4) etching the polished specimen to reveal grain features with a chemical solution of 20 ml of HCl and 80 ml of H_20 for 20 seconds; 5) taking pictures and measuring dimensions of the microstructural features using a Nikon Optiphot 200 Optical microscope. A Hitachi S4500II scanning electron microscope (SEM) and a Joel JSM-5610 SEM and Oxford INCA 200 Energy Dispersive Spectrometer (EDS) were used for material composition analysis.

2.3.2. Measurement and Assessment of Crack Propagation Rates and Orientations

The dye-penetration technique is widely used to reveal the crack geometry and orientation at the interfaces of the solder joint with the package (package-side) and the PWB (board-side).

Dye-penetration Technique for Crack Study

The dye-penetration protocol consisted of the following steps: 1) soak the strip in isopropyl alcohol for 48 hours; 2) clean strip with compressed air; 3) apply red dye along the edges of the packages (capillary action will let the dye penetrate into the cracks); 4) place strip in a vacuum chamber for two minutes; 5) place the strip in an oven at 125oC for 20 minutes, and 6) carefully pry the packages from the PWB by flexing the board. Since the solder joints do not always break at the interface of interest (typically the interface between the package and the solder joint), it was necessary to shear some joints off manually. Initially, a programmed shear force tool was used but at room temperature the sheared area smeared very easily, as shown in Figure 2.8a, thus obscuring the red dye from view. Instead, liquid nitrogen was 'poured' on the joint to make it brittle and a shear tool, in this case the end of a tweezer, easily removed the joint from the interface with no smearing as shown in Figure 2.8b. Once the joints were removed, the interfaces were photographed under 100X magnification using a Nikon Optiphot 200 microscope or Fujix HC-300Z digital camera. The photo was image processed to provide better contrast, crack boundaries manually traced in Photoshop Version 5.5, and crack areas measured (in terms of % of total joint interface area) using Scion Image Beta Version 4.0.2 (see Figure 2.8c) [55]. Note, in this study manually tracing the outline of the crack to compute crack area was very time-consuming. Alternatively, Dareveaux [56] proposed a crack area computation based upon measuring crack lengths and assuming a concave-shaped

geometry—a comparison of measured crack areas and areas computed using his method is presented in Appendix C.

(a) (b) (c)

Figure 2.8. Dye-penetrated crack in solder joint (a) smeared joint, (b) after image processing (dark area represents crack), (c) in Scion Image

Crack Orientation

Measurement of crack length depended on the direction of propagation (orientation). Instead of computing maximum stresses and strains from detailed finite element analysis to estimate crack orientation, three approaches were proposed. The first is based purely on geometry: the crack is assumed to propagate along the line joining the centers of the package and of the joint. This angle is used by most researchers [56] because it is easy to compute and is referred to as the geometric angle in this study. The second approach uses data generated from the crack areas measured by dye-penetration described above. The experimental angle at which the crack is assumed to propagate is along the line

joining the center of the package and the centroid of the measured crack area. The third approach, to be discussed in more detail in Chapter 4, Section 4.1.3, uses finite element analysis and the computed the creep energy density area during the early stages of thermal cycling. Comparisons of the angles resulting from applying these three approaches are discussed in detail in Chapter 4, Section 4.1.3.

2.3.3. Measurement and Assessment of Joint Life

Accelerated thermal cycling (ATC) tests are testing protocols used to predict the reliability of electronic packages (joint life) by exposing the packages to thermal conditions that are estimated to be more severe than normal operating conditions. The packages are monitored to determine electrical continuity. Once continuity is lost (package/joint failure), the life cycle at failure is used in a Weibull chart to estimate life cycles under normal operating conditions. The electrical continuity checking method and an industry-standard failure criterion are discussed below.

It was found that the industry-standard failure criterion was valid for packages with SnPb solder, but predicted unrealistic short lives for packages with SnAg solder. Alternative failure detection criteria are proposed and discussed in Chapter 7 and Appendix D.

ATC Testing

To ensure the validity of the ATC test protocol, temperatures from two thermocouples in the environmental chamber were recorded on a PC using LabVIEW software. One thermocouple is placed in the air of the chamber and the other is taped on top of a dummy package. The UT chambers and data acquisition system are shown in Figure 2.9.

Figure 2.9. Blue M ETC-09DH-G Environmental Chambers and ANATECH event detector at the UT Pickle Research Center

Failure Detection Method of the Event Detector

Electrical failure of the 357-PBGA package (hence, solder joint failure) during the ATC testing is monitored by a 256-channel Analysis Tech Event

Detector/Datalog (Anatech), which measures the resistances of the daisy-chained packages on the PWB. Electrical connectors on the Longhorn boards are set into ribbon connectors on a card carrier that connect the carrier to the event detector—every channel of the ribbon cable is associated with a specific package on a board. The event detector is connected to a PC for data monitoring and storage. The resistance of a 357-PBGA package is nominally 1.5Ω. The Anatech checks resistances every 10 seconds (each check is called a poll)—in the 'nominal' 30-minute 0 to 100^{o}C ATC test, each channel (package) is polled 180 times. An 'event' (potential package failure) is detected whenever a resistance measurement exceeds 300Ω (set by user) and the event detector records the channel number and thermal cycle number that the event occurred (note does not record the resistance value) in a data file. When 10 events (total of 10 polls with resistance measurements exceeding 300Ω) have been detected on a channel, the Anatech stops recording more events for that channel on the dat. file. Note, however that whenever a new data file is initiated, as occurs when the chamber is restarted after a repair, the Anatech starts monitoring the channels again with no prior knowledge or history of what happened before—in other words, the Anatech resets itself to start anew. A package failure is confirmed by removing the board from the environmental chamber and manually measuring the resistance across the package with an ohmmeter.

Industry-Standard Failure Criterion

The industry-standard failure criterion (IPC-SM-785) defines package failure as "the first interruption of electrical continuity that is confirmed by nine additional interruptions within an additional 10% of the cyclic life" [57]. For example, failure at 5000 cycles occurs if the first event occurred at cycle 5000 and nine additional events occurred within the next 500 cycles.

Proposed Alternative Failure Detection Criterion for SnAg Solder

Ideally, package failures occurring during ATC testing are detected by the event detector and confirmed with subsequent manual high resistance measurements. For packages with SnPb solder joints, this was the case. However, for packages with SnAg solder joints, early failures detected by the event detector using the industry-standard failure criterion were not confirmed by high resistance values nor were they consistent with crack area measurements. It appears that the industry-standard failure criterion must be modified for packages with SnAg solder. Appendix D describes in detail, the failure detection methodology of the event detector and the industry-standard failure criterion, discusses early false failures, proposes and compares alternative failure criteria with data, and discusses the rationale for choosing an alternative failure criterion for packages with SnAg solder joints.

Life Study Matrix

Table 2.2 summarizes the 24 test cases used in the life study. Test parameters include solder type, post-processing, ATC test, package layout and testing location. The results of this joint life test are given and discussed in Chapter 7.

Table 2.2. Life study test conditions with different solders, ATC tests, number of packages, package layout, and post-process heat treatment

Test Case	Solder Type	ATC Tests, °C	No. of Failed Packages	Package Layout	Post-Process
1*	SnPb	0-100	24	SD	Aged
2*	SnPb	0-100	23	SD	Air
3*	SnPb	0-100	24	SD	Quench
4	SnPb	0-100	26	SD	Air
5	SnPb	-40-125	29	SD	Air
6	SnPb	-55-125	13	SD	Air
7	SnPb	0-100	18	SS	Air
8	SnPb	-40-125	18	SS	Air
9	SnPb	0-100	13	DA	Air
10	SnPb	-40-125	13	DA	Air
11	SnPb	0-100	14	DD	Air
12	SnPb	-40-125	15	DD	Air
13*	SnAg	0-100	12	SD	Aged
14*	SnAg	0-100	11	SD	Air
15*	SnAg	0-100	24	SD	Quench
16	SnAg	0-100	25	SD	Air
17	SnAg	-40-125	26	SD	Air
18	SnAg	-55-125	13	SD	Air
19	SnAg	0-100	15	SS	Air
20	SnAg	-40-125	14	SS	Air
21	SnAg	0-100	14	DA	Air
22	SnAg	-40-125	11	DA	Air
23	SnAg	0-100	15	DD	Air
24	SnAg	-40-125	15	DD	Air

Note: *tests run in UT, and others at Motorola

2.4. SUMMARY OF CHAPTER

This chapter described in detail the test packages and boards, test equipment and protocols, test matrices, design and process parameter variables and conditions, and the evaluation criteria. The experiments were comprehensive and designed to determine effects of the design and processing parameters on life, microstructural changes and crack evolution while the test specimen underwent accelerated thermal cycling tests.

CHAPTER 3

Microstructural Analysis of Solder Joint Failure

The detailed experimental accelerated thermal cycling test (ATC) life and crack area results will be presented in Chapters 7 and 4, respectively, but two observations from these results are listed below.

- SnAg solder joints have twice the life of their SnPb counterparts.
- Aged SnAg solder joints have more than 70% longer life than the quenched and air-cooled SnAg solder joints

To explain these results, this chapter investigates microstructural differences and evolution using sectioning techniques for the 357-PBGA packages that were exposed to three different post-process heat treatments and thermal-cycled at the 0-100^{o}C ATC test. Sectioned joint pictures show crack path patterns that may explain differences in life. For aged SnAg solders, the long aging time allowed resin cracks to initiate in the substrate and test board thereby reducing the stresses on the solder joints and artificially increasing their thermal cycling life.

3.1. INTRODUCTION: HEAT TREATMENT

Most engineering metals, whether ferrous or non-ferrous, are used as alloys for additional strength, and the effects of alloying cannot be discussed without reference to heat treatment. Improved strength or ductility of alloys can

be achieved by reheating the unstable alloy to some temperature below the melting temperature [32]. Using this principle, post-process heat treatment could be introduced to the solder joints in semiconductor packages. However, solder joints are manufactured as-cast because of 1) the economic imbalance between the cost associated with heat treatment and the anticipated improvement in reliability for SnAg solder and 2) the detrimental aging effect on the reliability of eutectic SnPb solders [33, 34].

For solder joints in semiconductor packages, differences in the coefficients of thermal expansion of the different materials in the electronic assembly and a changing thermal environment are known to be major factors for inducing strains. Cracks form and propagate due to thermal fatigue, and this propagation is reported to be the primary failure mechanism in solder joints [4]. The type of solder mostly affects the crack propagation rates, but further resistance to the crack propagation can be achieved by tailoring microstructures via post-processing. ATC test results to be presented in Chapter 7 showed that the quenched and air-cooled (non-aged) SnPb packages have a 1.1-1.15 AF (Acceleration Factor: ratio of lifecycles in use condition to lifecycles in test condition) over the life of aged SnPb packages. However, the aged SnAg packages have approximately a 1.7 AF over the life of non-aged SnAg packages—opposite to the results of the SnPb joints. A microstructural failure analysis is presented to explain these results.

3.2. INITIAL MICROSTRUCTURE (NO THERMAL CYCLING)

3.2.1. SnPb Solder Joints

Figure 3.1 shows typical examples of the initial microstructures (0K cycles) taken from the upper right-side area of SnPb joints for the three different post-process conditions. Aged SnPb joints show large lead-rich phases (black region) of about 4μm (STD=0.62-0.68, n≥20) in size in the tin matrix (white region), while the air/quenched joints show small and more uniformly scattered lead-rich phases of 0.6-0.8μm (STD=0.16-0.43, n≥20) size due to rapid cooling rates. Table 3.1 shows the mean and standard deviation of measured lead phase sizes in SnPb joints G7 and N7 (corner joints in the Boundary Region just under the package die—see Figure 2.2—for sample sizes greater than 20). Aging induces lead to diffuse out of the tin phase and results in a larger lead phase [58].

Table 3.1. Phase size of lead (μm) in SnPb solder joints at time=0 for different post-processing conditions (see Appendix E for phase size data at different cycles)

Aged				Air				Quench			
Joint G7 n ≥ 20		Joint N7 n ≥ 20		Joint G7 n ≥ 20		Joint N7 n ≥ 20		Joint G7 n ≥ 20		Joint N7 n ≥ 20	
Avg.	σ	Avg.	σ	Avg.	σ	Avg.	σ	Avg.	σ	Avg.	σ
3.55	0.62	4.63	0.68	0.72	0.27	1.15	0.16	0.81	0.18	1.28	0.43

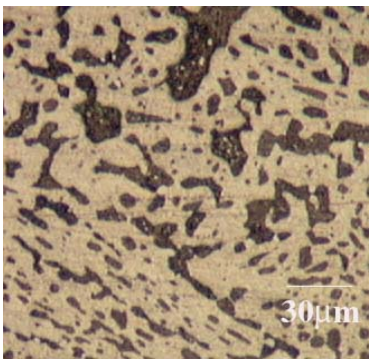

(a) UT1-U15A-SPA-AG-0-G7-PI-AC-400X

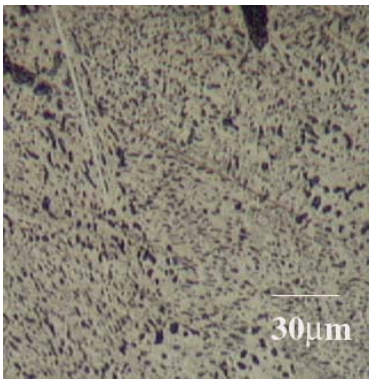

(b) UT5-U15A-SPA-A-0-G7-PI-AC-400X

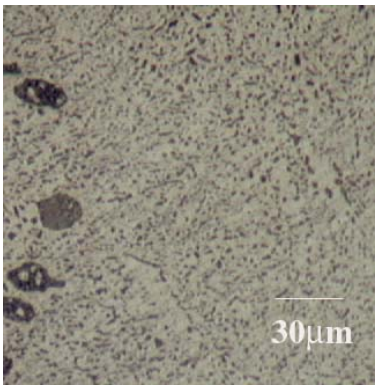

(c) UT10-U15A-SPA-Q-0-G7-PI-AC-400X

Figure 3.1. Initial microstructure of SnPb solder joints (Dark=Lead Phase, Light=Tin Phase) [x400 optical microscope] (a) aged, (b) air-cooled, (c) quenched

The lead phase sizes between air and quenched joints are similar because the cooling rates for both were similar due to the small solder joint volumes. These observations are consistent with measurements in the literature [18]. The aged joint has a coarse microstructure, so it tends to deform more by dislocation than by grain sliding, resulting in earlier failure than air-cooled or quenched joints. The smaller lead phase sizes in the air-cooled and quenched SnPb solder joints are expected to distribute stress more uniformly in the joint and, hence, increase fatigue life compared to aged SnPb joints [32, 33].

3.2.2. SnAg Solder Joints

SnPb solder joints have ductile lead phase particles, which are highly soluble in tin matrix and have a volume fraction of ~30% [19]. Meanwhile, SnAg solder joints have small and hard dispersed Ag_2Sn particles and the volume fraction is less than 3% [19]. Figure 3.2 shows the initial microstructures at the upper right-side area in the SnAg joints. The microstructure consists of primary Sn phase (light) surrounded by Sn-Ag eutectic structures (dark). Compared to air-cooled and quenched microstructures, the SnAg eutectic structure for the aged joint has smaller, globular Ag_2Sn particles, compared to the larger, rod-like Ag_2Sn particles in non-aged SnAg joints. These observations are consistent with the literature [20], and the globular shapes of Ag_2Sn particles in aged SnAg joints show the effects of a long thermal diffusion process.

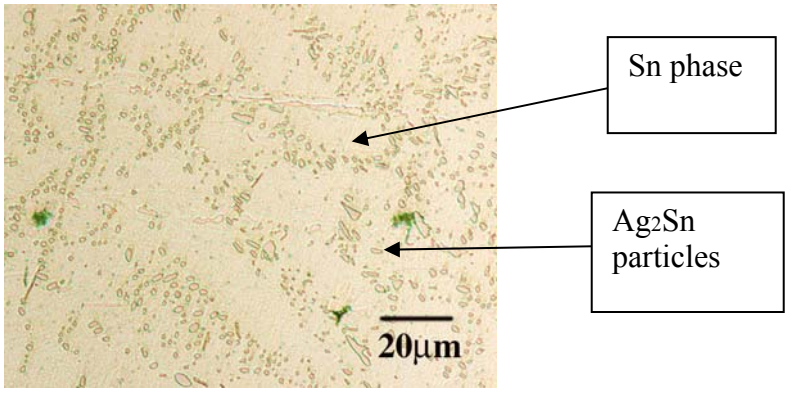

(a) UT14-U15A-SA-AG-0-G7-PI-AC-400X

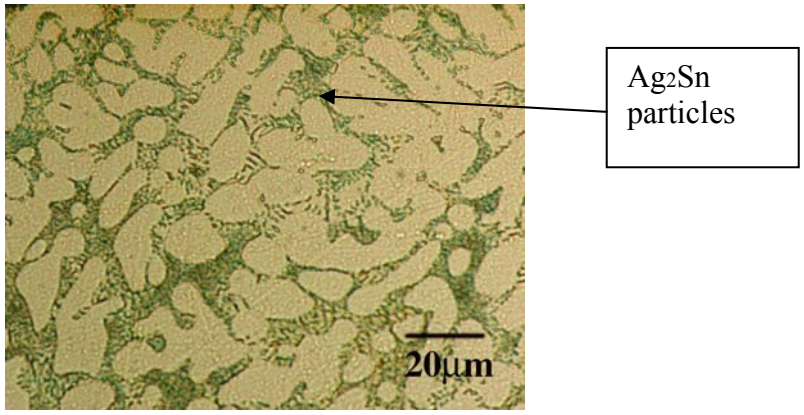

(b) UT18-U15A-SA-A-0-G7-PI-AC-400X

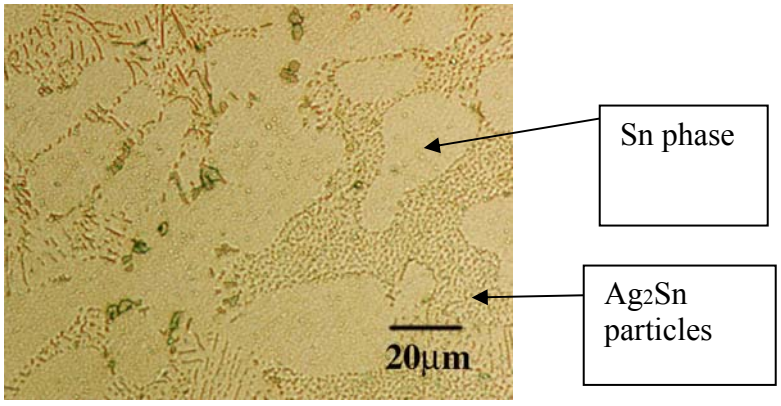

(c) UT23-U15A-SA-Q-0-G7-PI-AC-400X

Figure 3.2. Initial microstructure of SnAg solder joints [x400 optical microscope] (a) aged, (b) air-cooled, (c) quenched

SEM micrographs in Figure 3.3 show similar initial structures.

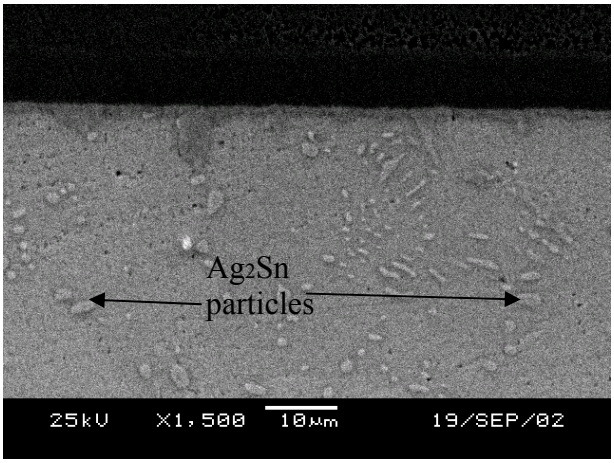

(a) UT14-U15A-SA-AG-0-N7-PI-C-1500X

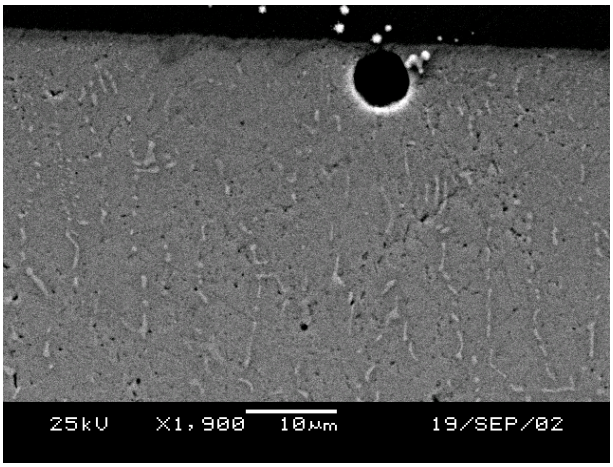

(b) UT18-U15A-SA-A-0-G7-PI-C-1900X

Figure 3.3. Initial microstructure of SnAg solder joints [SEM] (a) aged (b) air-cooled

3.3. FAILURE MODE ANALYSIS

3.3.1. SnPb Solder Joints

ATC test results showed that the non-aged SnPb packages have a 1.1-1.15 AF (Acceleration Factor) over the life of aged SnPb packages To investigate failure mode, selected six SnPb joints, cycled at 10K (three are shown in Figure 3.4), were polished and etched to reveal microstructures at the crack front (which moved from right to left). For 1008-hour aged joints, a CuNiSn intermetallic layer about 9μm thick formed during the long aging process and 10K thermal cycles. The tin phase near the joint interface was diffused towards the joint interface to form the intermetallic layer, resulting in an underlying long layer of lead-rich phase. No CuNiSn intermetallic layer was observed at the package interface in the air-cooled and quenched packages until 14K cycles, when a layer 1-2μm thick developed, albeit in close proximity to the intermetallic layer. No measurement of intermetalic layer thickness was made after 14K cycles. Intergranular failure in the solder was observed in all six sectioned quenched, air-cooled and aged SnPb joints.

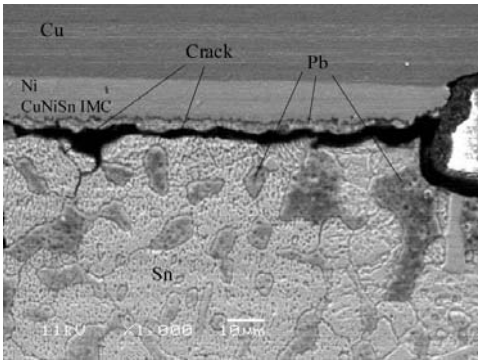

(a) UT2-U2A-SPA-AG-10-N7-PI-AC-1000X

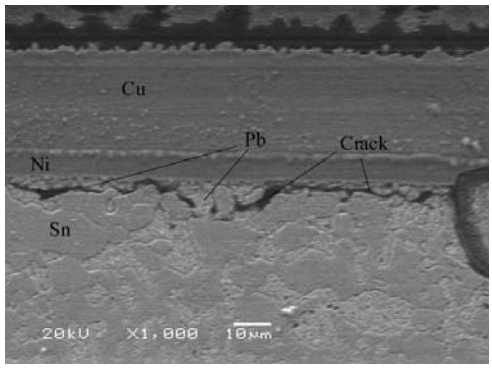

(b) UT6-U2A-SPA-A-10-N7-PI-AC-1000X

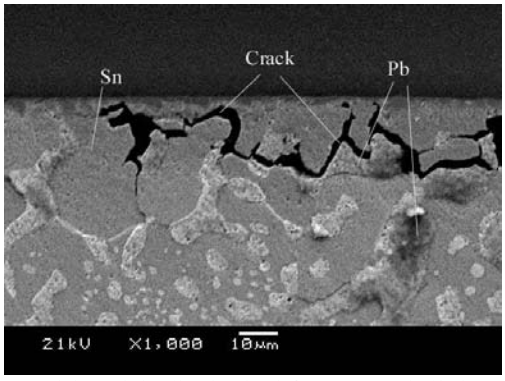

(c) UT11-U1A-SPA-Q-14-R7-PI-AC-1000X

Figure 3.4. Microstructures in upper right-side area of SnPb joints at nominal 10K cycles [x1000 SEM] (Dark=Lead phase, Light=Tin phase) (a) aged, 10K cycles, (b) air-cooled, 10K cycles, (c) quenched, 14K cycles

3.3.2. SnAg Solder Joints

Selected SnAg joints, cycled to 21K, were polished and etched to show the microstructure at the crack front (moving right to left) in Figure 3.5. For aged, air-cooled and quenched SnAg joints, coarse Ag_2Sn particles were found to reside within or at the grain boundary. The microstructure pictures show intergranular failures, and most of the grain boundaries around the crack fronts were revealed in the etched air-cooled and quenched SnAg joints, while few grain boundaries were revealed in aged SnAg joints. More microstructural pictures for SnAg aged and air-cooled joints can be found in Appendix E.

Again, albeit in close proximity to the intermetallic layer, SnAg joints failed by intergranular fracture. In the air-cooled and quenched SnAg joints, failure occurred well within the solder; however, in the aged SnAg joints, failure occurred along the Ni-solder interface/interphase which may have been depleted of Sn as the intermetallic layer grows with time.

The preliminary microstructural observations between aged and non-aged SnAg packages did not reveal anything substantive to explain the longer life of aged SnAg solders. It was decided to expand the investigation into 1) hardness of the solder joints that could explain the more ductile behavior of aged joints and 2) possible laminate cracking outside of solder joints that could induce stress relieving of solder joints and inducing longer fatigue life.

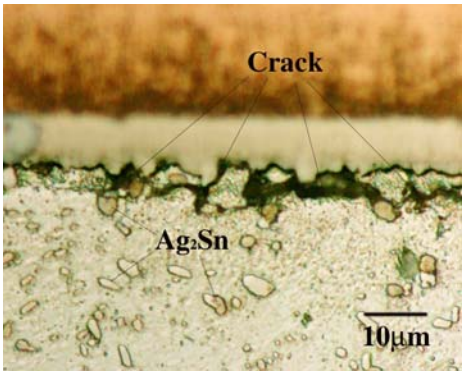

(a) UT15-U6A-SA-AG-21-H7-PI-AC-1000X

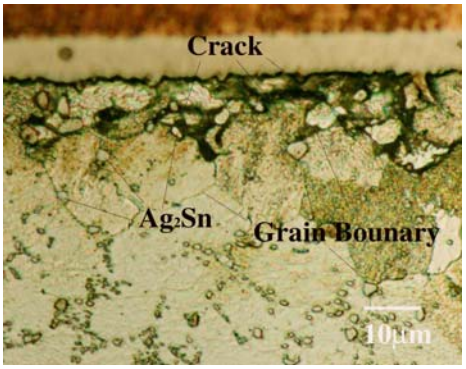

(b) UT19-U6A-SA-A-21-F7-PI-AC-1000X

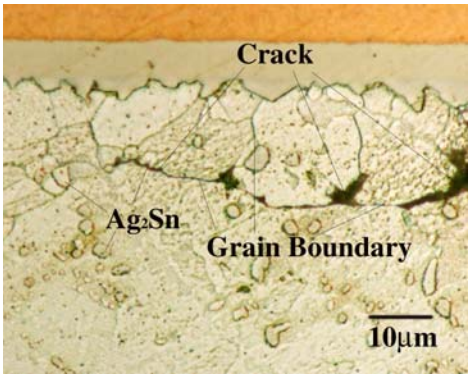

(c) UT23-U6A-SA-Q-21-K7-PI-AC-1000X

Figure 3.5. Microstructures of upper right-side area of SnAg joints at 21K cycles [x1000 optical microscope] (a) aged (b) air-cooled, (c) quenched

3.3.3. Endicott Laboratory Testing

The analysis discussed above did not clearly indicate why aged SnAg solders had longer cycle life than air-cooled SnAg solder joints. To further investigate this result, six SnAg samples, listed in Table 3.2, were analyzed by Endicott Interconnect Technology Laboratory (EIT) of Endicott, NY, a leading electronic interconnect solutions firm.

Table 3.2. Test matrix for microstructural testing at Endicott Interconnect Technology: SnAg aged and air-cooled solder joints

Solder	Post-Process	Board	Package	No. Cycle
SnAg	Aged	UT15	U4A	6K
		UT14	U3A	9K
		UT15	U2A	15K
	Air-Cooled	UT19	U4A	6K
		UT18	U3A	9K
		UT19	U2A	15K

1) Preliminary Analysis

Specimen were repolished to remove oxidation and the following preliminary observations taken:

Backscattered SEM Images revealed cracks on UT19-U2A-SA-A-15-H7 (SnAg, air-cooled, 15K cycles).

Figure 3.6 shows cracks at all four corners of joint H7.

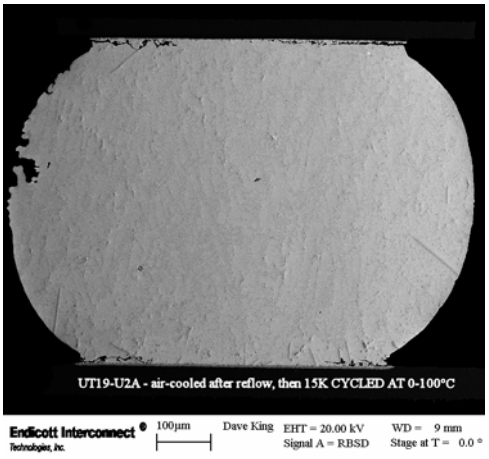

Figure 3.6. SEM image showing cracks in joint H7 of UT19-U2A-SA-A-15-H7

Figure 3.7 shows the crack at the upper left corner of the joint. The recognized phases are marked: fine precipitants are mostly Ag_2Sn, but some Cu_6Sn_5 are present; the large flake (needle) is Ag_2Sn; the intermetallic is Ni-Sn, with some Cu substitution.

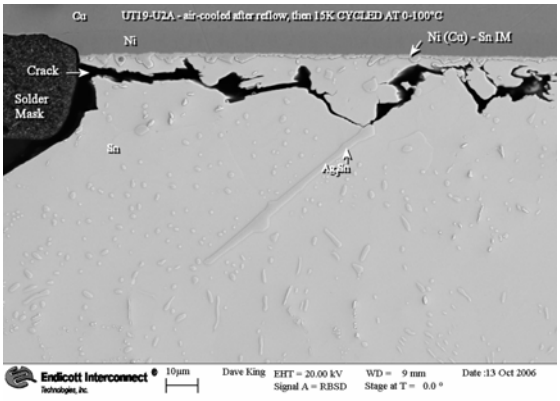

Figure 3.7. SEM image of upper left corner crack in joint H7 of UT19-U2A-SA-A-15-H7 (Note: Ag_2Sn intermetallic flake (needle))

Figure 3.8 shows the crack at the lower left corner of the joint.

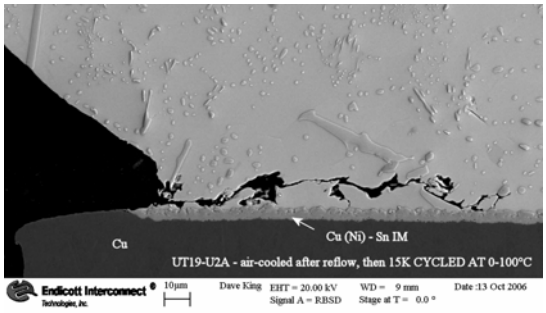

Figure 3.8. SEM image of lower left corner crack in joint H7 of UT19-U2A-SA-A-15-H7 (Note: upper left—Ag_2Sn intermetallic flake (needle))

Backscattered SEM Images to reveal cracks on UT15-U2A-SA-AG-15 (SnAg, aged, 15K cycles).

Figure 3.9 shows a large solidification shrinkage void at the right center and a very thick Cu-Sn intermetalic layer along the card side (bottom).

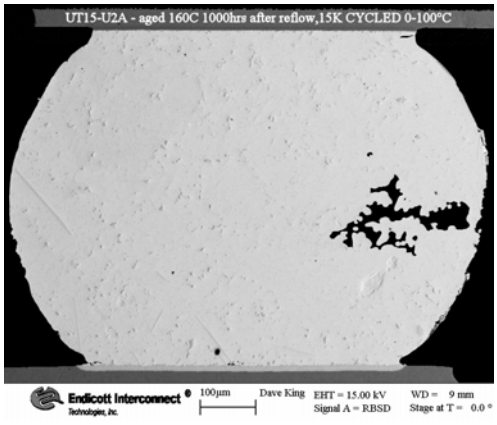

Figure 3.9. SEM image of joint G7 of UT15-U2A-SA-AG-15-G7

Figure 3.10 shows the thick intermetallic Cu6Sn5 layer and intermetallic particles.

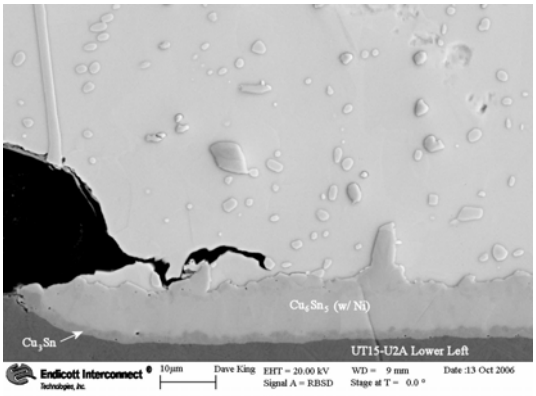

Figure 3.10. SEM image of lower left corner of joint G7 of UT15-U2A-SA-AG-15-G7 (Note: upper left—Ag_2Sn intermetallic flake (needle))

Cross polarized images to determine the differences in grain structures:

All joints were single crystal for UT19-U2A-SA-A-15 (SnAg, air-cooled, 15K cycles) and UT15-U4A-SA-AG-6 (SnAg, aged, 6K cycles). Except for those joints shown below, the solder joints on the remaining four specimen were a single crystal. In summary, the grain structures were not significantly different to explain the life differences between aged and air-cooled SnAg solder joints.

(a) UT19-U4A-SA-A-6-D7

(b) UT19-U4A-SA-A-6-A7

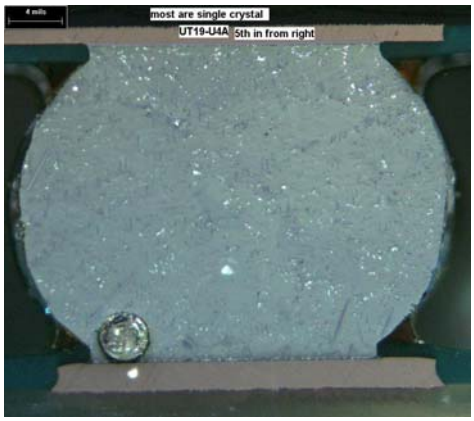

(c) UT19-U4A-SA-A-6-E7 (single crystal)

Note void in the lower left corner.

Figure 3.11. Grain structure for UT19-U41-SA-A-6 (SnAg, air-cooled, 6K cycles)

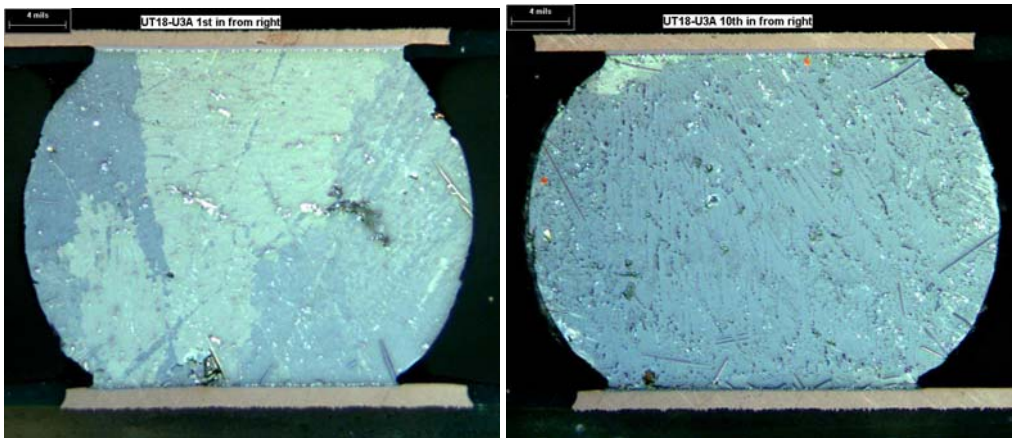

(a) UT18-U3A-SA-A-9-A7 (b) UT18-U3A-SA-A-9-J7

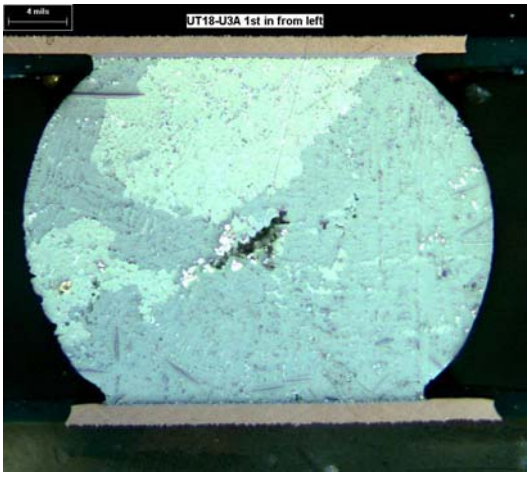

(c) UT18-U3A-SA-A-9-W7

Figure 3.12. Grain structure for UT18-U3A-SA-A-9 (SnAg, air-cooled, 9K cycles) (Shades show different crystallic orientation.)

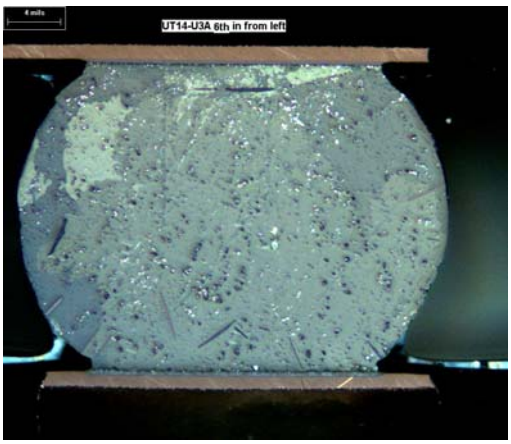

(a) UT14-U3A-SA-AG-9-P7

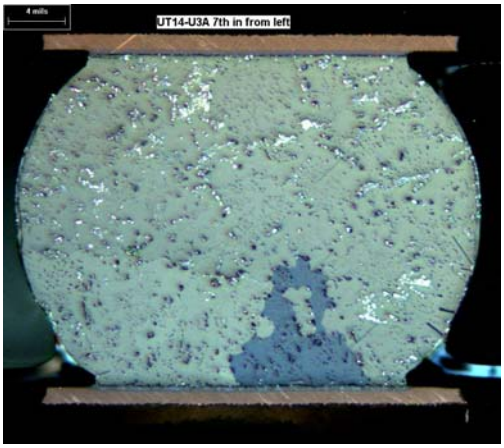

(b) UT14-U3A-SA-AG-9-N7

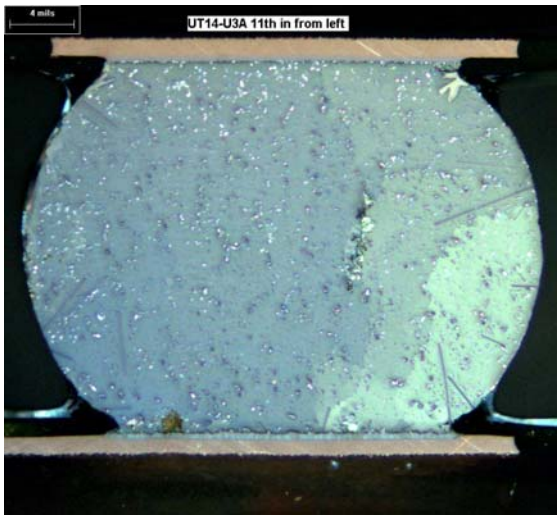

(c) UT14-U3A-SA-AG-9-J7

Figure 3.13. Grain structure for UT14-U3A-SA-AG-9 (SnAg, aged, 9K cycles) (Shades show different crystallic orientation.)

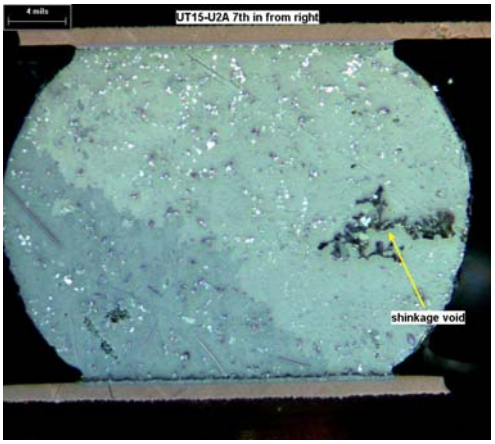

(a) UT15-U2A-SA-AG-15-G7

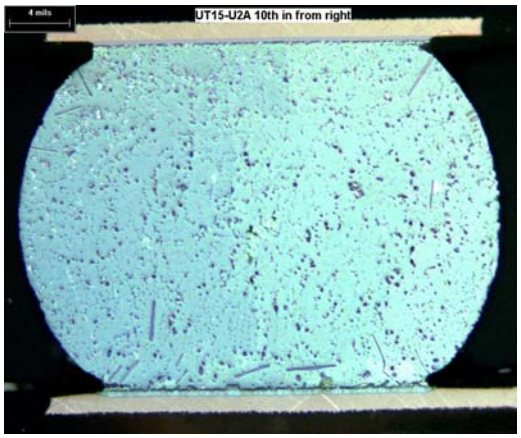

(b) UT15-U2A-SA-AG-15-J7

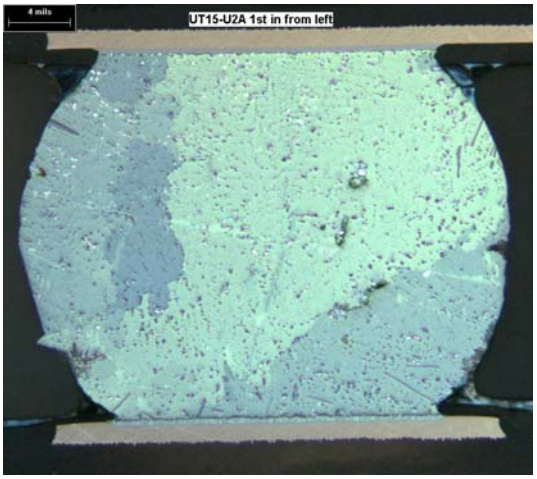

(c) UT15-U2A-SA-AG-15-W7

Figure 3.14. Grain structure for UT15-U2A-SA-AG-15 (SnAg, aged, 15K cycles) (Shades show different crystallic orientation.)

2) Age-Softening Study

Age-hardening strengthens nonferrous metals through heat treatment [59]. This process consists of two steps: first, an unstable condition is produced in the

alloy structure through the formation of a supersaturated solid solution by quenching the alloy; second, a certain degree of precipitation of the supersaturated phase imparts the increased hardness and strength to the metal by aging under the melting temperature. During this aging, a metastable precipitate forms within the crystal structure of the solvent, and, if over-aged, conversion of the precipitate from the metastable form to its own equilibrium crystal structure. The precipitation stage represents the actual precipitation-hardening reactions, and the latter over-aging stage causes age-softening. If the temperature is too high, or the over-aging time is too long, the latter stage may prevail. The aged SnAg joints went through 160^{o}C (~0.9 melting temperature) for 1008hrs, and it is expected that the hardness decreased and the solder joint softened, thereby increasing life cycles. This was verified from Knoop microhardness [60] measurements were run on selected joints in the six test packages previously listed in Table 3.4.

Figure 3.15 shows a typical Knoop hardness indent with a 25 gram load on a joint in package UT15-U2A-SA-AG-15-G7. Table 3.1 shows the measured Knoop hardnesses for the joints. The measurements show that while the aged SnAg joints are slightly softer than the air-cooled SnAg joints, the differences are not significant. Therefore, it is believed that the improved cycle-life of aged SnAg joints over air-cooled SnAg joints is not attributed to the softening effect of aged SnAg joints.

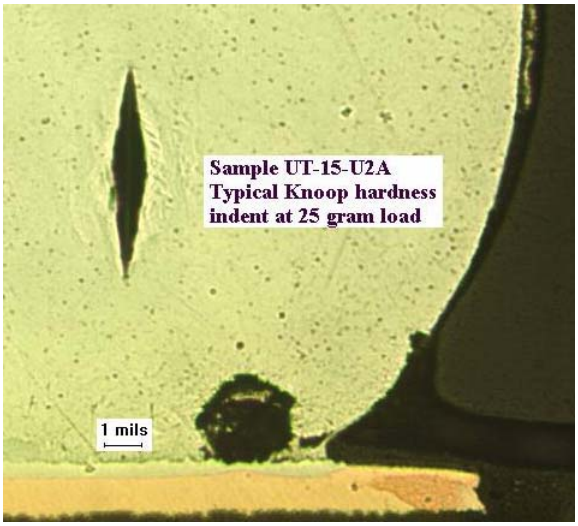

Figure 3.15. Knoop hardness indent at 25 gram load on sample joint on package UT15-U2A-SA-AG-15-G7

Table 3.3. Knoop hardness measurement (25gram) for air-cooled and aged SnAg joints

Trial	Air-Cooled			Aged		
	UT19-U4A	UT18-U3A	UT19-U2A	UT15-U4A	UT14-U3A	UT15-U2A
1	17	16	17	15	16	14
2	16	16	18	14	14	15
3	16	16	17	15	16	15
AVG	16.6 (n=9)			14.9 (n=9)		
STD	0.73			0.78		

3) Laminate cracking

Since the Knoop hardness results of the aged SnAg joints were only 10% lower than the air-cooled SnAg joints, further observations were run to determine

the aging effect on SnAg joints. Based upon the Endicott Lab's evaluators' experiences, two possibilities were identified:

a) cracks exist between the die and substrate and/or

b) cracks exist in test board or package substrate

In either case, the thermal stresses in the solder joints would be reduced, explaining longer joint life under thermal cycling conditions. The results of the investigation follow.

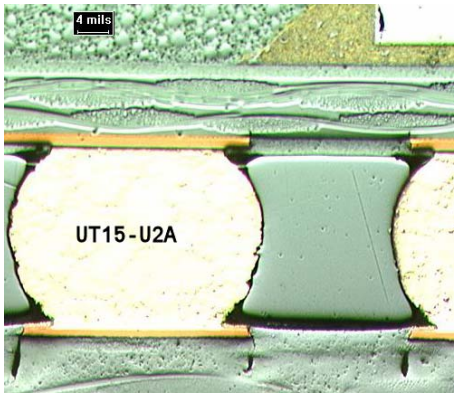

(a)

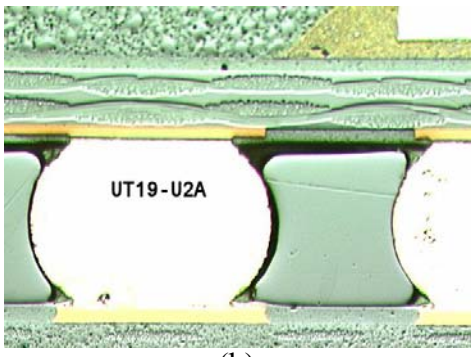

(b)

Figure 3.16. Laminate resin crack in (a) aged SnAg joint (UT15-U2A-SA-AG-15-G7) and resin cracks in solder mask and epoxy resin into glass weave (UT15-U2A-SA-AG-15-G7) and (b) no crack in air-cooled SnAg joint (UT19-U2A-SA-A-15)

Observation from aged sample (UT15-U2A-SA-AG-15-G7)

- The corners of both substrate and test board pads have resin cracks through the solder mask and epoxy resin, into the glass weave (and further into the test board side). Notice the wide cracks in the test board resin revealed by light optics in Figure 3.16 (a).
- Similar resin cracking was found in another aged sample, UT14-U3A-SA-AG-9-J7, which had 9K cycles.
- No cracks were found in the die attach area between the die and package substrate.
- No overmold debonding was found.
- Samples (board and package) were aged at 160°C for 1000 hours, and the glass transition temperature of the board is 170°C. The PCB resin degraded due to exposure to the high temperature and long aging period. For lead-free solder, new PCB material, such as polyimide, are now being used to accommodate the high temperature.

Observation from air-cooled sample (UT19-U2A)

- No laminate cracking was found in UT19-U2A, which was exposed to 15K cycles, 0 to 100°C ATC in Figure 3.16 (b)
- No cracks were found in die attach area between the die and package substrate
- No overmold debonding was found

UT18-U3A, which had 9K cycles, also had no resin cracking.

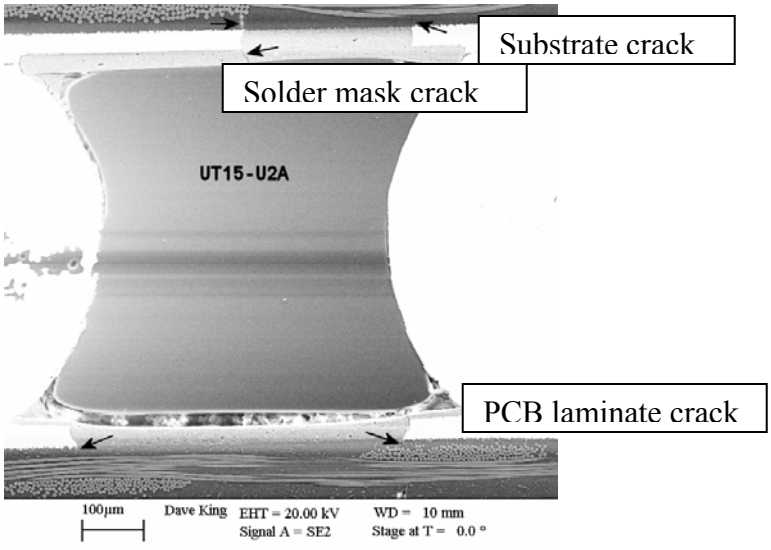

Figure 3.17. Substrate cracks and test board cracks in aged SnAg joint pads (UT15-U2A-SA-AG-15)

Summary

- The reasons for the marked improved life of aged SnAg joints were investigated. The age-softening effect (ductility) was investigated using the Knoop hardness measurement. No significant differences in hardness were found between measurements of aged and air-cooled SnAg joints.
- In Figure 3.17, cracks at the corners of the PBGA ball pads on the package propagated to the glass cloth. The cracks passed through both the package-side and board-side solder mask. Finally a large, wide resin crack propagated

(white spot) into the resin at the right, even below the glass cloth in the PCB. In summary, laminate cracks were found in the package substrate and test board in aged SnAg joints but not in the air-cooled SnAg joints. It is hypothesized that the cracks were created due to the embrittling effects of the long aging (1008hr at 160^{o}C) on the epoxy resins.

- No cracks were found between the die and substrate or die and overmold in both aged and air-cooled SnAg joints, suggesting the rootcause of extended life is the PCB laminate crack.
- The cracks in the laminate packages of aged SnAg joints, generally identified as pad cratering, which are commonly believed to relieve the strain and stress on the solder joints, artificially increasing the cycle life under ATC testing.

3.4. MICROSTRUCTURAL STUDY SUMMARY

SnPb Solder Joints

- Compared to non-aged SnPb joints, aged SnPb solder joints exhibited a coarser microstructure, tending to deform more by dislocation than by grain sliding, resulting in earlier failure. Initially, aged SnPb joints showed large lead-rich phases of about 4μm (STD=0.62-0.68, n≥20) in size in the tin matrix, while the air/quenched joints showed smaller and more uniformly scattered lead-rich phases of 0.6-0.8μm (STD=0.16-0.43, n≥20) in size.
- For aged SnPb joints, a CuNiSn intermetallic layer about 9μm (STD=0.6) thick formed during aging and early thermal cycling. The tin phase near

the joint interface was consumed to form the intermetallic layer, resulting in a long layer of lead-rich phase. No CuNiSn intermetallic layer was observed at the package interface in the air-cooled and quenched SnPb packages until 14K cycles, when a layer 1-2μm thick developed (no additional measurements done beyond 14K cycles). Intergranular failure within the solder was observed in all sectioned quenched, air-cooled and aged SnPb joints and propagated through the interphase lying between the lead-rich and tin-rich phases. For aged SnPb joints, straight cracks propagated along the layer of lead-rich phase. For air-cooled and quenched SnPb joints the crack path was more tortuous, i.e. longer and coarser.

SnAg Solder Joints

- Initially, SnAg solder joint microstructure consisted of primary Sn phase surrounded by Sn-Ag eutectic structures, and the aged joints showed smaller, globular Ag_2Sn particles (effect reflectin the long thermal diffusion process), compared to the rod-like Ag_2Sn particles in the non-aged joints.
- At 21K cycles for the 0-100^{o}C ATC test conditions, coarse Ag_2Sn particles were found to reside within or at the grain boundaries for all SnAg joints. Microstructural pictures revealed grain boundaries in the etched air-cooled and quenched SnAg joints, while few, if any, grain boundaries were revealed in aged SnAg joints. Preliminary microstructural observations between aged and non-aged SnAg packages

did not reveal anything substantive to explain the longer life of aged SnAg solders.

- Knoop microhardness measurements showed that aged SnAg joints were 10% softer than the non-aged SnAg joints, but the differences were not significant based upon the Endicott Lab's evaluators' judgments.
- Laminate cracks were found in the package substrate and test board in aged SnAg joints only. The laminate cracks were most likely created by the embrittling effect of the long aging (1008hr at 160^{o}C) on the epoxy resins. These cracks, so called pad cratering, were believed to relieve the strain and stress on the aged SnAg solder joints thereby prolonging life in ATC testing.

CHAPTER 4

Crack Evolution: Crack Shape, Orientation, Area, & Length

This chapter presents the results of an extensive experimental study of crack growth in SnPb and SnAg solder joints exposed to the 0-100^{o}C ATC test at UT. Using standard dye penetration techniques, crack shape, size, orientation, area and length are computed from optical images and using image processing techniques. The effects of solder type and post-processing are reported. Please note that the aged SnAg data presented throughout this dissertation reflects the effects of cracks found in the microstructural investigation presented in Chapter 3, Section 3.3.3.

4.1. SOLDER CRACK MEASUREMENTS

Experimental data on crack properties presented below were collected at different thermal cycle times (nominally every 2K cycles for SnPb and 3K for SnAg) using dye penetration techniques for specimen run only at UT and only using the single-dense package layout and the 0-100^{o}C ATC test cycle.

4.1.1. Previously Reported Crack Area Data

Due to the large expense of collecting data, of the total 357 solder joints on a package, only a subset of 155 joints (die area and fourth quadrant of the

package), previously shown in Chapter 2 (Figure 2.2) and repeated here in Figure 4.1, was selected for study. These joints include:

- Inside region (9 joints)
- Inner boundary region (16 joints)
- Boundary region (24 joints)

  The boundary region is underneath the silicon die edges (die area bounded by solder joints, N7-N13 and G7-G13), and the solder joints in this region are expected to show the largest cracks.
- Subsection of outside region (32 joints)
- Outer boundary region (32 joints)
- Outside region (42 joints)

Over 4100 SnPb and 4800 SnAg solder joints were analyzed. The dye penetration protocol, optical image picture-taking, and subsequent image processing was summarized in Section 2.3.2 of Chapter 2 and in an earlier M.S. Thesis by Changyoung Park [51]. That reference also contains the raw data on crack area and length evolution measurements, comparison of solder type and post-processing, statistical megthods, data analysis, and detailed evaluation of the package regions and package joints exhibiting the largest cracks. The main result from that report are:

- The boundary region had the largest mean crack areas compared to the other five regions, and the data from that region was statistically significant compared to the other five regions for SnPb joints after 2K cycles. For example, Table 4.1 shows the statistical results for multiple comparisons

using the student t-test of the means of % crack area in the six regions for quenched SnPb packages [51]; air-cooled and aged packages showed similar results.

Table 4.1. Mulitiple comparisons of student t-test of the mean of % crack area in the six regions for quenched SnPb packages (bold indicates pairs which are statistically significantly different from each other) [51]

Mean Dif	SnPb-Quench-Top chips - Boundary Region						
Std Err Dif							
Lower CL Dif Upper CL Dif	BD 2K	BD 4K	BD 6K	BD 8K	BD 10K	BD 14K	BD 16K
Inner BD 2K to 16K, respectively	0.3 4.0 -7.5 8.1	-5.5 4.7 -14.7 3.8	**-8.7** **4.0** **-16.5** **-0.9**	**-12.8** **4.0** **-20.6** **-5.0**	-3.9 4.0 -11.7 3.9	**-13.7** **4.0** **-21.6** **-5.9**	**-8.2** **4.0** **-16.0** **-0.3**
S-out side 2K to 16K, respectively	-1.0 3.4 -7.7 5.7	**-10.7** **3.8** **-18.2** **-3.3**	**-13.9** **3.4** **-20.6** **-7.3**	**-17.3** **3.3** **-23.9** **-10.8**	**-24.9** **3.3** **-31.4** **-18.3**	**-11.1** **3.3** **-17.6** **-4.5**	3.6 3.3 -3.0 10.1
Outer BD 2K to 16K, respectively	-2.9 3.4 -9.6 3.8	**-10.6** **4.1** **-18.6** **-2.6**	**-17.0** **3.4** **-23.7** **-10.3**	**-22.6** **3.3** **-29.2** **-16.1**	**-24.0** **3.3** **-30.5** **-17.5**	**-20.3** **3.3** **-26.9** **-13.8**	**-8.0** **3.3** **-14.5** **-1.5**
Inside 2K to 16K, respectively	-3.3 4.8 -12.8 6.1	**-14.1** **5.1** **-24.1** **-4.0**	**-14.7** **4.8** **-24.2** **-5.3**	**-25.9** **4.8** **-35.4** **-16.5**	**-19.7** **4.8** **-29.2** **-10.3**	**-21.7** **4.8** **-31.1** **-12.2**	**-23.4** **4.8** **-32.8** **-13.9**
Out side 2K to 16K, respectively	-2.9 3.2 -9.2 3.4	**-15.9** **3.7** **-23.1** **-8.7**	**-21.7** **3.2** **-27.9** **-15.5**	**-29.2** **3.2** **-35.5** **-22.9**	**-37.7** **3.2** **-43.9** **-31.5**	**-36.6** **3.2** **-42.8** **-30.3**	**-24.9** **3.2** **-31.2** **-18.7**

1. Mean difference: mean in column – mean in row
2. Standard error of the difference between two means
   (Pooled variance/equivalent degree of freedom)
3. Lower 95% confidence interval of the difference (= Mean – $t_{0.95/2}$·Standard error)
4. Upper 95% confidence interval of the difference (= Mean + $t_{0.95/2}$·Standard error)

- Similarly, the boundary region had the largest mean crack areas compared to the other five regions for SnAg solder joints, but the data from that region was not as statistically significant compared to the other five regions as it was for SnPb. For example, Table 4.2 shows the statistical results for multiple comparisons using the student t-test of the means of % crack area in the six regions for quenched SnAg packages [51]; air-cooled and aged packages showed similar results. Notice that there are more comparison pairs whose data is not statistically different.
- The three adjacent joints at each of the four corners of the boundary area (joints under the corners of the die) show the largest mean crack areas.

Since the solder joints in the boundary region had the largest measured cracks of any region, unless specifically denoted, the experimental crack data presented below focuses only on the 24 solder joints in the boundary region (N7-13, G7-13, M7, M13, L7, L13, K7, K13, J7, J13, H7, H13), as shown in Figure 4.1.

Table 4.2. Mulitiple comparisons of student t-test of the mean of % crack area in the six regions for quenched SnAg packages (bold indicates pairs which are statistically significantly different from each other) [51]

Mean Dif Std Err Dif Lower CL Dif Upper CL Dif	SnAg-Quench-Top chips - Boundary Region									
	BD 3K	BD 6K	BD 9K	BD 12K	BD 15K	BD 18K	BD 21K	BD 24K	BD 27K	BD 30K
Inner BD 3K to 30K, respectively	-4.2 5.3 -14.7 6.3	-0.6 5.3 -11.1 9.9	**-13.7** **5.3** **-24.2** **-3.2**	3.6 5.3 -6.9 14.1	-6.8 5.3 -17.3 3.7	-1.3 5.3 -11.8 9.1	**-10.7** **5.3** **-21.1** **-0.2**	**-16.8** **5.3** **-27.3** **-6.3**	-6.1 5.4 -16.7 4.5	**-14.1** **5.3** **-24.6** **-3.6**
S-out side 3K to 30K, respectively	-7.3 4.5 -16.2 1.6	-7.7 4.5 -16.5 1.0	**-9.7** **4.5** **-18.5** **-0.9**	-1.1 4.5 -9.9 7.6	**-12.3** **4.5** **-21.2** **-3.5**	**-9.9** **4.5** **-18.7** **-1.2**	**-14.1** **4.5** **-22.9** **-5.3**	**-17.5** **4.5** **-26.3** **-8.7**	**-13.7** **4.5** **-22.6** **-4.8**	**-22.1** **4.5** **-30.9** **-13.3**
Outer BD 3K to 30K, respectively	-6.8 4.5 -15.6 2.0	**-11.0** **4.5** **-19.8** **-2.1**	**-14.8** **4.5** **-23.5** **-6.0**	-3.9 4.5 -12.8 5.0	**-15.0** **4.5** **-23.8** **-6.1**	**-13.0** **4.5** **-21.8** **-4.3**	**-21.3** **4.5** **-30.1** **-12.6**	**-18.6** **4.5** **-27.3** **-9.8**	**-13.4** **4.5** **-22.3** **-4.5**	**-15.8** **4.5** **-24.6** **-7.0**
Inside 3K to 30K, respectively	-4.5 6.5 -17.2 8.2	0.3 6.5 -12.4 13.0	**-16.4** **6.5** **-29.1** **-3.7**	2.8 6.5 -9.9 15.5	-7.5 6.5 -20.2 5.2	-12.1 6.5 -24.8 0.6	**-24.5** **6.5** **-37.2** **-11.8**	**-17.0** **6.5** **-29.7** **-4.3**	**-27.3** **6.5** **-40.1** **-14.6**	-4.5 6.5 -17.2 8.2
Out side 3K to 30K, respectively	-7.3 4.3 -15.6 1.1	**-12.3** **4.3** **-20.6** **-3.9**	**-17.5** **4.2** **-25.8** **-9.2**	-4.2 4.3 -12.6 4.1	**-19.6** **4.3** **-28.0** **-11.2**	**-18.7** **4.2** **-27.0** **-10.4**	**-27.3** **4.3** **-35.6** **-18.9**	**-25.6** **4.3** **-34.0** **-17.3**	**-23.9** **4.3** **-32.4** **-15.4**	**-31.7** **4.2** **-40.1** **-23.4**

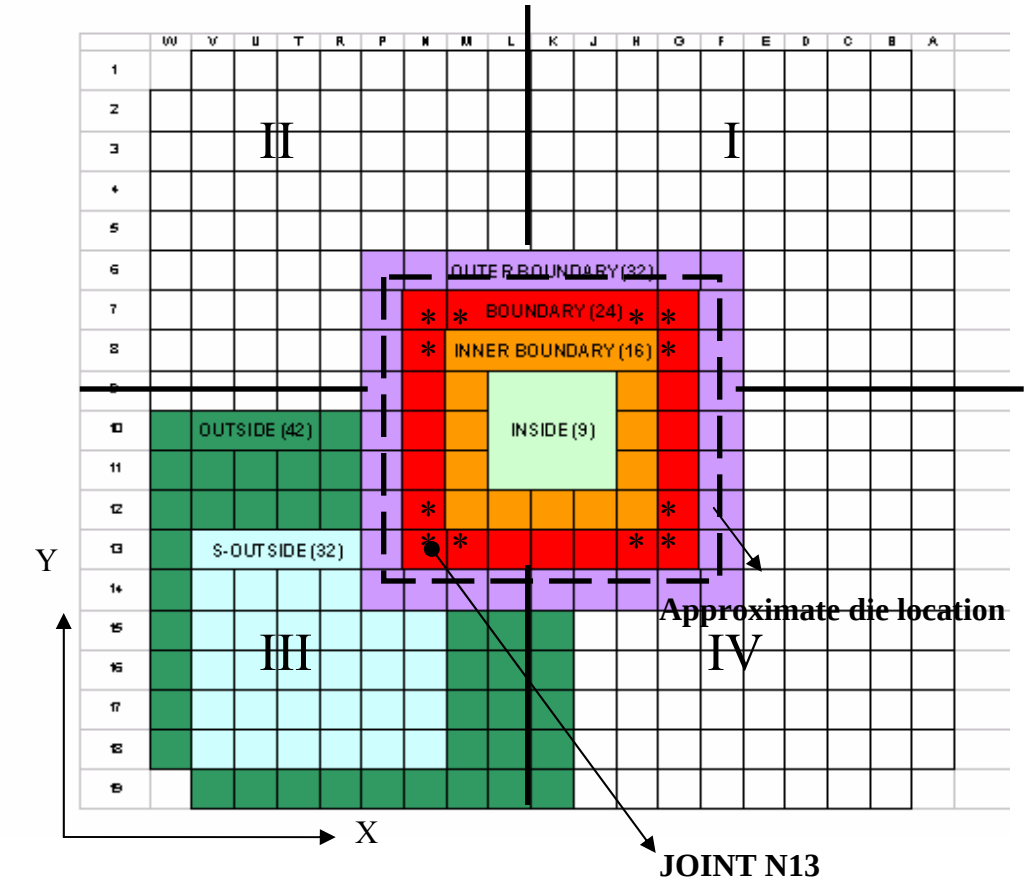

Figure 4.1. Six joint regions and four quadrants of the 357-PBGA package (* joints with largest cracks)

4.1.2. Crack shape

The dye penetration study revealed that cracks grew in concave-shaped (horse-shoe) fronts for all joints, except for aged SnPb joints, whose crack fronts grew in a diametrically-linear front (see Figure 4.2). Figure 4.2 shows dye-penetrated cracks in the solder joints that were 10K thermal-cycled under 0-100^{o}C

ATC test condition. The crack front of aged SnPb solder joint, which has no secondary crack, grows into a diametrically-linear front, while the crack of air-cooled solder joint, which has secondary crack, looks concave-shaped (horse-shoe).

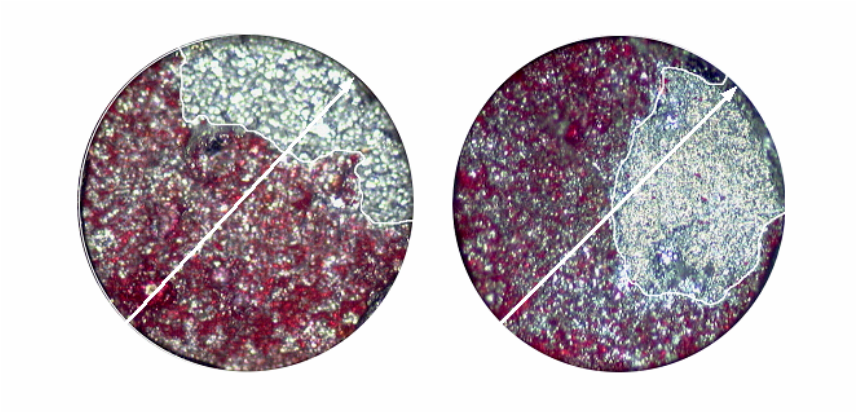

Figure 4.2. Crack shape and crack front of joint N13 at 10K for aged SnPb (left, UT3-U2A-SPA-AG-10-N13-P-PI) and air-cooled SnPb (right, UT7-U2A-SPA-A-10-N13-P-PI). Arrow shows direction of FEM-estimated crack orientation angle. (dark areas represent cracks)

4.1.3. Crack Orientation Angle

The length of a crack depends on the angle of propagation, therefore it was necessary to determine this orientation angle. Two possible crack propagation (orientation) angles were previously discussed in Chapter 2, Section 2.3.2: geometric (package to joint centers) and experimental angles (joint center to crack area centroid). The proposed third angle uses the angle from the joint center to the

centroid of the FEM-computed creep energy density area, which is assumed to be a measure of damage because solder joints accumulate damage by creep.

The FEM analysis uses a global and sub-modeling technique to reduce computational time and achieve economic meshing. First, the global model, representing a ¼ package assembly, was constructed of 56348 8-node continuum solid elements. A total of 100 joints (81 full joints, 18 half joints, 1 quarter joint) were modeled--each full joint was constructed of 24 elements (see the detailed joint geometry in Figure 5.3(b) in Chapter 5). Two symmetric planes, 1-2 and 2-3 were used to represent the ¼ package assembly. Figure 4.3 shows the geometry of the ¼-package and the FEM model (see Figure 2.1 in Chapter 2 for the package geometry details).

The sub-model represents the solder joints (5 full joints, 2 half joints) in Figure 4.3(a) under the die periphery, and each joint with a refined meshing scheme to generate the creep energy density (creep energy devided by volume) in the joint interface. Figure 4.4 shows three solder joints (G12, G13, H13) from the sub-model, and each joint was constructed of 1024 8-node continuum solid elements.

Thermal cycles of 0-100^{o}C are simulated in the global model, and the displacement history is generated from the common nodes of the global and sub-models. The displacements are then imposed on the sub-model along with the thermal cycles. Finally the sub-model calculates the creep energy density in each first layer of elements in each solder joint.. Here, the solder joints are modeled as visco-plastic, and other structures are modeled as elastic (see in Appendix A).

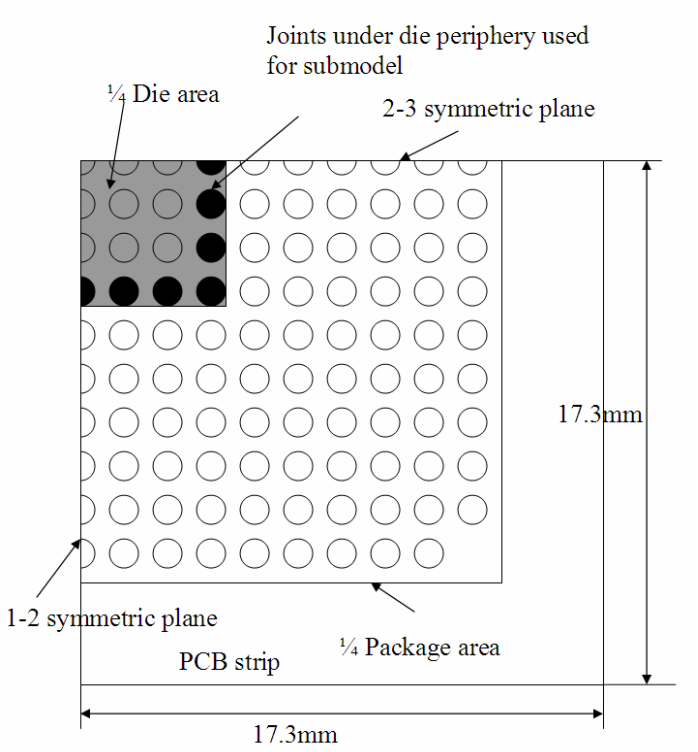
Joints under die periphery used
for submodel
¼ Die area
2-3 symmetric plane
17.3mm
1-2 symmetric plane
¼ Package area
PCB strip
17.3mm

(a)

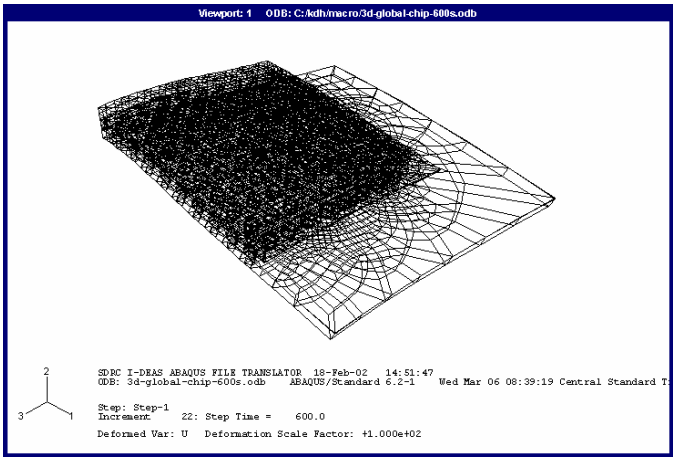
Viewport: 1 ODB: C:/kdh/macro/3d-global-chip-600s.odb
SDRC I-DEAS ABAQUS FILE TRANSLATOR 18-Feb-02 14:51:47
ODB: 3d-global-chip-600s.odb ABAQUS/Standard 6.2-1 Wed Mar 06 08:39:19 Central Standard T
Step: Step-1
Increment 22: Step Time = 600.0
Deformed Var: U Deformation Scale Factor: +1.000e+02

(b)

Figure 4.3. ¼-package geometry (top view) and the corresponding FEM model

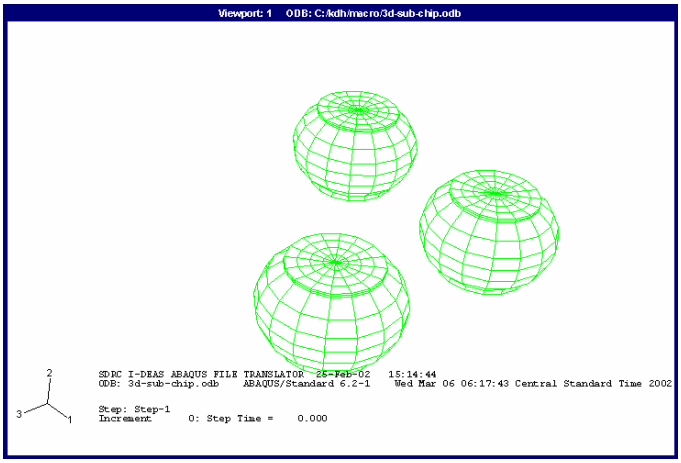

Figure 4.4. FEM solder joint sub-models, representing joints G12, G13, H13

The detailed constitutive equations used to model the creep behavior of SnPb and SnAg solder joints are discussed in Chapter 5. Three 0-100^{o}C ATC thermal cycles were simulated to compute stress, strain and dissipated creep energy density distributions in the joints. Three cycles were used because the stress and strain hysteresis loop after three thermal cycles is representative of the stress state of solder joints [24].

Once simulated, the area in a joint having dissipated creep energy densities in a certain range was assumed to represent the probable future crack area. In Figure 4.5, the dark areas of a sample G12 joint represent the areas with creep energy densities in five ranges. For example, for the range of dissipated

creep energy densities between 0.65MPa and 0.78MPa, the dark area is 2% of the total area. Using the centroid of this area, the orientation angle is 65° relative to the joint center. By expanding the energy density into larger ranges, it was found that the orientation angle tended toward a constant of 29°, as shown in Figure 4.5—this angle will be called the FEM-estimated crack orientation angle. While the discussion above focused only on joint G12, the other joints showed the same convergence to one angle as the energy density ranges increased.

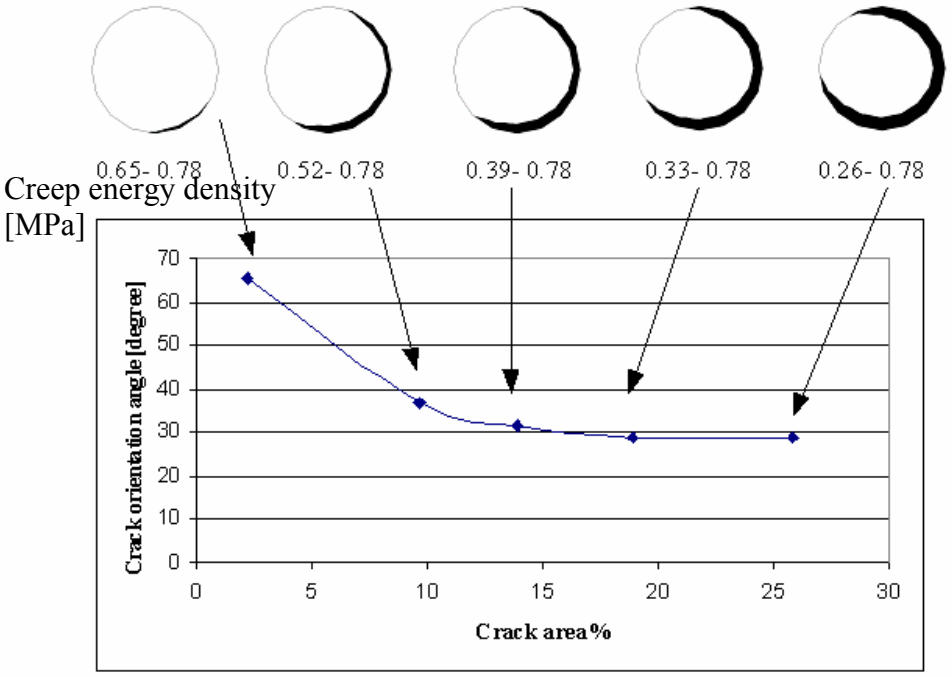

Figure 4.5. Estimated crack orientation angle based upon ranges of dissipated creep energy density areas for sample G12 joint in the top package of a strip

Table 4.3 shows the results of applying the three orientation angle criteria: 1) geometric angle—package center to joint centers, 2) experimental angle—joint center to the crack area centroid—for the 24 joints in the boundary region (see Fig. 2.2 for joint location) and 3) the estimated angle using the FEM model—joint center to the creep energy density centroid. Note due to symmetry of the FEM model and package only ¼ of the angles were actually computed. The experimental angle was computed using crack data from 4K and 10K cycles for SnPb and 6K and 24K cycles for SnAg, since data from earlier cycles showed too little crack areas or multiple crack areas. Appendix F contains the experimental data used in Table 4.3.

The FEM-estimated and geometric crack angles are within $\pm 5^{o}$ of each other. The experimental data has large standard deviations, but half of the experimental mean angles are within $\pm 15^{o}$ of the geometric/FEM-estimated angles. Based upon these results, the FEM-estimated orientation angles are used to compute the crack length. As demonstrated by the large standard deviations, the experimental orientation analges had too much scatter to use for this study.

Table 4.3. Experimental, FEM-estimated, and geometrical crack orientation angles of joints in the boundary region

Joint Loc.	Experimental, deg.		FEM-estimated deg.	Geometric deg.
	N	Mean (Std)		
G7	75	-31 (39)	-43	-45
G8	73	-59 (42)	-29	-34
G9	75	-30 (52)	-15	-18
G10	75	-9 (49)	0	0
G11	76	-12 (50)	15	18
G12	72	34 (40)	29	34
G13	74	22 (32)	43	45
H7	75	-73 (42)	-59	-56
H13	76	69 (46)	59	56
J7	73	-65 (62)	-74	-72
J13	74	67 (58)	74	72
K7	72	-79 (56)	-90	-90
K13	75	56 (67)	90	90
L7	74	-91 (54)	-106	-108
L13	75	110 (53)	106	108
M7	74	-112 (42)	-121	-124
M13	75	125 (33)	121	124
N7	74	-131 (41)	-137	-135
N8	74	-121 (31)	-151	-146
N9	76	-131 (42)	-165	-162
N10	76	142 (45)	180	180
N11	73	113 (55)	165	162
N12	73	123 (32)	151	146
N13	75	125 (40)	137	135

4.1.4. Crack Area

The crack area data presented here focuses only on the 24 joints under the die edge in the boundary region (see Figure 4.1) since this region had the largest crack areas. The data represents seven read-point cycles and three post-process conditions, with each read-point having up to 72 (24 joints x 3) data points from three packages. Again, these results are for the 0-100^{o}C ATC test and UT test location. Tables 4.4 and 4.5 show the number of joints and the mean and standard deviation of % crack area at each read-point cycle for SnPb and SnAg packages, respectively. The % crack area is based upon a reference area with nominal diameter of 560μm. The raw data were presented in an earlier M.S. thesis by Changyoung Park (see Table A in Appendix A [51]).

As expected, the mean % crack area of SnPb and SnAg joints increases with cycles for all aging conditions, and the mean % crack areas of SnPb joints are larger than those of SnAg joints in all cycles (about 10-27% larger at 6K cycles and 50%-300% larger at 15K). Note that for SnAg joints, the crack areas of the non-aged joints are approximately 50% larger than the aged joints.

The data was analyzed using the paired student t-test with the null hypothesis that the variances of the two data sets (assumed to be distributed normally) are equal and alternative hypothesis that the variances are different. Here the p-values—the probability of obtaining a result at least as extreme as a given data point under the null hypothesis—was calculated to determine whether the null hypothesis was true (if $p \geq 0.05$) or rejected (if $p < 0.05$) in favor of the alternative hypothesis that the two data sets are indeed statistically significantly

different from each other. These are the underlying hypotheses throughout this dissertation. The paired student t-test results (with 95% confidence level) in Table 4.6 show that for SnPb solder, the mean % crack area among the three post-process conditions are not statistically different for most of cycles, except at 2K cycles for aged and non-aged joints and at 10K cycles for aged and quenched joints. For SnAg solder, the mean % crack area of aged joints are statistically different from the non-aged joints at all cycles, and the air-cooled joints are only statistically different from quenched joints at 15K, 21K, 24K cycles.

Table 4.4. Mean % crack area (nominal joint diameter=560 μm) in SnPb aged, air-cooled, and quenched joints: boundary region, 0-100^{o}C ATC, single-dense, UT-cycled samples

Cycles	Aged			Air-cooled			Quenched		
	N	Mean	StD	N	Mean	StD	N	Mean	StD
2K	71	4.7	4.5	61	7.0	3.9	70	7.0	3.4
4K	71	20.8	14.0	72	22.2	8.3	64	22.8	9.1
6K	71	33.8	19.6	72	35.1	12.0	72	34.9	10.6
8K	68	51.1	22.7	72	50.9	14.9	72	49.8	11.2
10K	68	57.6	24.0	72	58.3	13.2	72	63.9	13.2
*13K	72	68.0	21.7	72	73.9	14.7	72	76.0	12.4
16K	72	69.9	20.2	72	82.0	12.7	72	81.2	13.0

Note: 13K applied to aged joints, 14K applied to quenched joints, 15K applied to air-cool joints

Table 4.5. Mean % crack area (nominal joint diameter=560 μm) in SnAg aged, air-cooled, and quenched joints: boundary region, 0-100°C ATC, single-dense, UT-cycled samples

Cycles	Aged			Air-cooled			Quenched		
	N	Mean	StD	N	Mean	StD	N	Mean	StD
3K	72	3.9	4.7	72	11.3	7.4	71	12.1	8.4
6K	72	8.9	9.1	70	25.7	13.5	70	24.7	12.4
9K	68	17.7	11.3	72	35.0	13.4	72	35.3	18.2
12K	69	19.2	14.8	72	41.0	18.9	72	44.6	18.7
15K	71	24.1	14.8	71	50.5	16.1	71	43.5	17.8
18K	23	27.4	15.9	24	53.6	15.3	24	52.3	18.8
21K	24	23.7	14.0	24	50.5	21.9	24	66.2	14.0
24K	24	37.8	15.0	24	56.7	18.6	24	70.5	16.1
27K				24	64.8	12.8	23	68.8	19.3
30K							24	73.9	22.3

Table 4.6. Paired student t-test results (95% confidence level) for crack area using data of Tables 4.4 - 4.5. AG=Aged, A=Air-cooled, Q=Quenched (bold indicates pairs which are statistically significantly different from each other)

SnPb Joints				SnAg Joints			
Cycle No.	AG & A	AG & Q	Q & A	Cycle No.	AG & A	AG & Q	Q & A
2K	**1.0**	**1.1**	-1.3	3K	**5.1**	**5.8**	-1.6
4K	-2.2	-1.7	-3.0	6K	**12.8**	**11.8**	-2.9
6K	-3.5	-3.7	-4.6	9K	**12.4**	**12.7**	-4.5
8K	-5.4	-4.2	-4.4	12K	**15.9**	**19.6**	-2.1
10K	-5.1	**0.4**	-0.1	15K	**20.9**	**13.9**	**1.5**
				18K	**16.4**	**15.0**	-8.3
				21K	**17.0**	**32.7**	**5.8**
				24K	**9.3**	**23.1**	**4.2**

4.1.5. Crack Length

Using the FEM-estimated crack orientation angles determined in Section 4.1.2, crack lengths of joints in the boundary region were measured for 0-100^{o}C ATC, single-dense package layout and UT location.

Tables 4.7 and 4.8 show the number of joints and the mean and standard deviations of crack length (% of joint diameter= 560μm) for each read-point for SnPb and SnAg joints, respectively. As expected, the mean % crack length increases with cycles for all aging conditions, and lengths of SnPb joints are larger than SnAg joints at all cycles (about 7-26% larger at 6K cycles and 84%-260% larger at 16K). The paired student t-test results in Table 4.9 show that for SnPb joints, the mean % crack length of non-aged joints are statistically different from the aged joints only at 8K and 10K cycles, and air-cooled joints are not different from quenched joints at all cycles. For SnAg solder, the mean % crack lengths of aged and non-aged joints are statistically different at all cycles, and the air-cooled joints are statistically different from quenched joints only at 15K cycles. The raw data used in this crack length investigation is given in Appendix G.

Table 4.7. Mean % crack length (nominal joint diameter= 560μm) in SnPb aged, air-cooled, and quenched joints: boundary region, 0-100^{o}C ATC, single-dense, UT-cycled samples

Cycles	Aged			Air-cooled			Quenched		
	N	Mean	STD	N	Mean	STD	N	Mean	STD
2K	71	4.4	5.6	61	5.8	4.4	70	4.7	3.7
4K	71	18.7	14.1	72	15.2	8.2	64	16.4	8.4
6K	71	29.2	19.3	72	26.0	11.7	72	25.3	10.3
8K	68	49.4	24.1	72	38.5	16.5	72	37.6	10.9
10K	68	56.5	25.8	72	46.3	14.2	72	50.2	12.4
*13K	72	64.7	24.2	72	63.7	17.8	72	64.0	15.0
16K	72	67.4	22.3	72	74.2	18.6	72	72.1	18.7

* 13K applied to aged joints, 14K applied to quenched joints, 15K applied to air-cool joints

Table 4.8. Mean % crack length (nominal joint diameter=560μm) in SnAg aged, air-cooled, and quenched joints: boundary region, 0-100°C ATC, single-dense, UT-cycled samples

Cycles	Aged			Air-cooled			Quenched		
	N	Mean	STD	N	Mean	STD	N	Mean	STD
3K	72	3.0	4.7	72	6.6	7.3	70	6.5	7.3
6K	72	5.9	7.4	70	18.7	13.2	70	18.0	12.0
9K	68	14.1	12.4	72	24.3	13.5	72	27.7	18.1
12K	69	15.1	15.5	72	28.6	16.9	72	33.6	20.0
15K	71	18.6	14.7	71	40.3	16.6	71	32.7	18.8
18K	23	21.2	16.0	24	41.8	17.2	24	42.7	18.2
21K	24	19.2	14.2	24	43.0	20.8	24	52.5	14.0
24K	24	28.6	14.7	24	50.2	20.1	24	58.1	18.3
27K				24	51.9	14.9	23	58.9	19.0
30K							24	67.8	23.1

Table 4.9. Student t-test (95% confidence level) results for crack length using data of Tables 4.7-4.8 AG=Aged, A=Air-cooled, Q=Quenched (bold indicates pairs which are statistically significantly different from each other)

SnPb Joints				SnAg Joints			
Cycle No.	AG & A	AG & Q	Q & A	Cycle No.	AG & A	AG & Q	Q & A
2K	-0.2	-1.3	-0.5	3K	**1.3**	**1.3**	-2.1
4K	-0.02	-1.4	-2.4	6K	**9.0**	**8.3**	-3.0
6K	-1.5	-0.8	-4.0	9K	**5.2**	**8.6**	-1.5
8K	**4.9**	**5.8**	-4.9	12K	**7.6**	**12.6**	-0.7
10K	**4.1**	**0.2**	-2.1	15K	**16.1**	**8.5**	**2.0**
				18K	**10.5**	**11.4**	-9.0
				21K	**14.1**	**23.6**	-0.08
				24K	**11.2**	**19.2**	-2.3

Note: AG=Aged, A=Air-cooled, Q=Quenched, bold shows statistically significant)

4.2. CRACK AREA VS. LENGTH

4.2.1. Crack Shape and Implications

It was observed that the crack fronts of the aged SnPb joints were rather straight, while the crack fronts in the non-aged SnPb and all SnAg joints were concave as shown in Figure 4.2, and it was postulated that the differences are attributed to the presence/lack of secondary cracks. If the crack shape is concave, one could have a large crack area but a proportionally smaller crack length, as determined by the crack orientation angle. The discussion below compares area and length to see it one correlates better with solder joint life.

Figure 4.2 shows aged and air-cooled SnPb joint images, located at the same location on their respective packages at 10K cycles, and the FEM-estimated crack orientation direction represented by the white arrow. These two joints had similar mean % crack areas of 70% and 64%, for aged and air-cooled, respectively, for a difference of 6%. In contrast, the mean % crack lengths are 64% and 46%, respectively, for a much larger difference of 18%. This difference in percentage raises the question—is crack propagation better described by crack length or crack area?

Figure 4.6 shows a graphical comparison between the mean % crack area and mean % crack length using the data presented in Tables 4.4-4.5 and 4.7-4.8. The trends are similar, but the mean % crack area is always larger than the mean % crack length. The differences between crack area and length in aged SnPb joints are much smaller than in non-aged joints because of its different crack

shape. For example, at 10 K cycles, the difference in area and length in aged SnPb joints is 1.1%, and the differences are 12% and 13% for SnPb air-cooled and quenched joints, respectively. For SnAg joints, the crack shapes are similar (i.e. concave), so the differences between means of % crack area and length are expected to be large and at 24K cycles are 9.2%, 6.5%, and 12.4%, respectively, for aged, air-cooled and quenched joints.

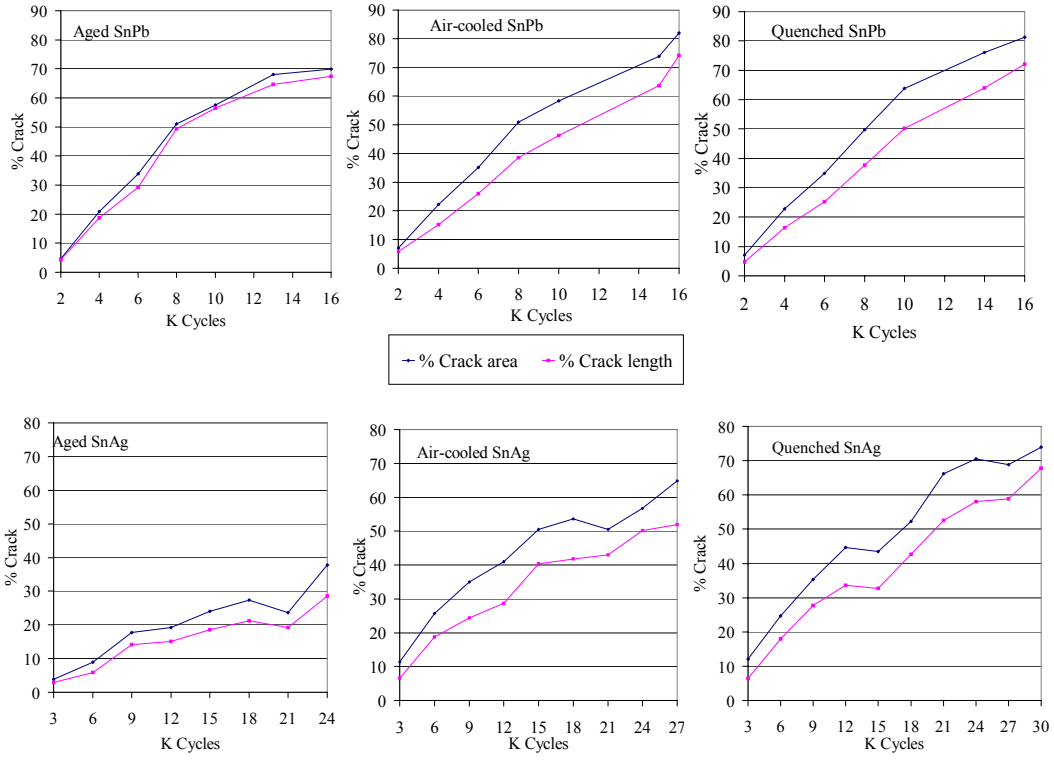

Figure 4.6. Mean % crack area and mean % crack length of SnPb and SnAg joints: boundary region, 0-100^{o}C ATC, singe-dense, UT (data from Tables 4.4-4.5, 4.7-4.8)

4.2.2. Crack Propagation Data Analysis

Figure 4.7a shows the comparisons among the mean % crack area of the SnPb joints in the boundary region for the three post-process conditions, 0-100^{o}C ATC, single-dense, and UT location. While differences are small up to 8K cycles, the quenched joints appear to have larger areas than the other two conditions at larger cycles.

According to experimental life results for SnPb solder (presented in chapter 7), the order of failure was aged, quenched, and then air-cooled. The % crack area data from Figure 4.7a at 10K cycles (chosen because the mean life of SnAg solder joints was between 10-13K cycles) could be interpreted as inferring failure in the following order—quenched, air-cooled, and aged. In constrast, at the same 10K cycles, the mean % crack length of the SnPb joints in Figure 4.7b infers the order of failure as aged, quenched, then air-cooled—this matches the experimental failure sequence. For SnAg joints, the order of life interpreted from both the % crack area and % crack length plots at 21K cycles is same as the experimental results—quenched, air-cooled, then aged.

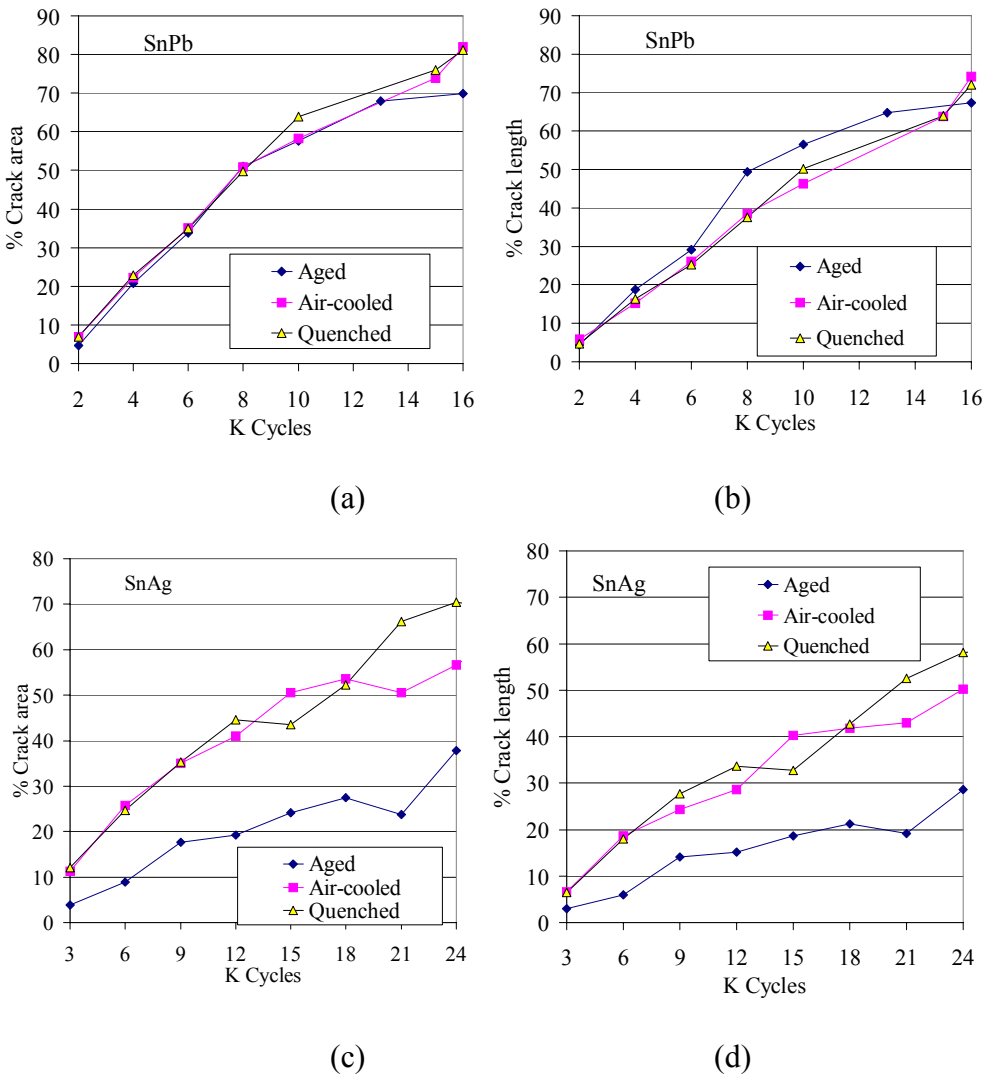

Figure 4.7. Measured mean %crack area and mean %crack length for SnPb and SnAg solder joints for three post-process conditions: boundary region, 0-100°C ATC, single-dense, UT (a) SnPb % crack area (b) SnPb % crack length (c) SnAg % crack area (d) SnAg % crack length

To confirm if % crack length provides a better estimate of life than % crack area, the Student t-tests were compared on both data sets. Table 4.6 showed the t-test results of SnPb joints using % crack area—statistically significant differences occur only at two cycles—at 2K cycles, between aged and non-aged joints, and at 10K cycles, between aged and quenched joints. There are no statistically significant differences between aged and non-aged joints at the other read-point cycles—inferring that it is not possible to differentiate differences in mean % crack areas among the three aging conditions. Table 4.9 showed the t-test results of SnPb joints using mean % crack length—aged joints are statistically different from non-aged joints at 8K and 10K cycles.

For SnAg solder, % crack area in Table 4.6 shows air-cooled joints are statistically different from quenched joints at 21K and 24K cycles, while from Table 4.9 using % crack length, air-cooled joints are not different from quenched joints.

4.3. SUMMARY

357-PBGA packages on PWBs were thermally cycled to evaluate solder crack growth (area, length), dye-penetrated and the crack areas, angles, and lengths measured. The data showed the following observations for 0-100^{o}C ATC testing of single-dense boards at UT and focusing only on solder joints in the boundary region:

- SnPb solder joints had about twice the crack growth rates compared to SnAg joints, reflecting shorter life.

- Air-cooled and quenched solder joints had similar crack growth characteristics, independent of solder type.
- Aged SnAg joints had much smaller growth rates (as much as 50% less) than non-aged SnAg joints.
- Experimental crack orientation angles, measured from the joint center to the centroid of the measured crack areas, had similar trends as the geometric and FEM-estimated angles, but with large standard deviations and only about half of the angles agreed to within $\pm 15^{o}$ of the other two angle measures.
- Crack shapes were concave in all SnPb and SnAg solder joints except for aged SnPb joints which exhibited straight crack fronts.
- For aged SnPb joints, the % crack length appeared to better predict joint life than % crack area.

CHAPTER 5

Crack Initiation Modeling and Analysis

This chapter presents crack initiation modeling and analysis using experimental data and finite element models for SnPb and SnAg solder joints under different post-process conditions. The crack initiation model is composed of three models: a global (package assembly) model, a solder joint model, and a microstructural micro model. The global model, which includes the PBGA package, solder joints, and board, estimates the warping/ deformation of the card assembly and computes the displacements under thermal cycling conditions. The joint model, representing joint G13 located under die periphery, takes these displacements and temperature as inputs and computes stresses and strains in the solder joint. Then, the microstructural micro model computes the phase growth, void nucleation and growth, and microcracking governing crack initiation. These models provide insights into observed and measured crack data on the effects of variables such as joint location in the package, crack location in the solder joint, and number of thermal cycles on crack initiation.

5.1. INITIAL CRACKS: EXPERIMENTAL DATA

This section presents the observed and measured data on joint cracks during the early stages of thermal cycling. Optical microscope and SEM images

of cracks in joints thermal cycled for 2K-3K cycles were taken at the four corners of selected joints as illustrated in Figure 5.1a. Figure 5.1b shows an example of a SEM image of a primary crack at the lower left-side of the board interface of a 2K-cycled aged SnPb joint (UT3-U5A-SPA-AG-2-G7-BI-TC-700X). Polished images showed that primary cracks at the package interface were the largest of four cracks, followed in order of size by primary cracks at the board interface, and secondary cracks at the package and board interfaces.

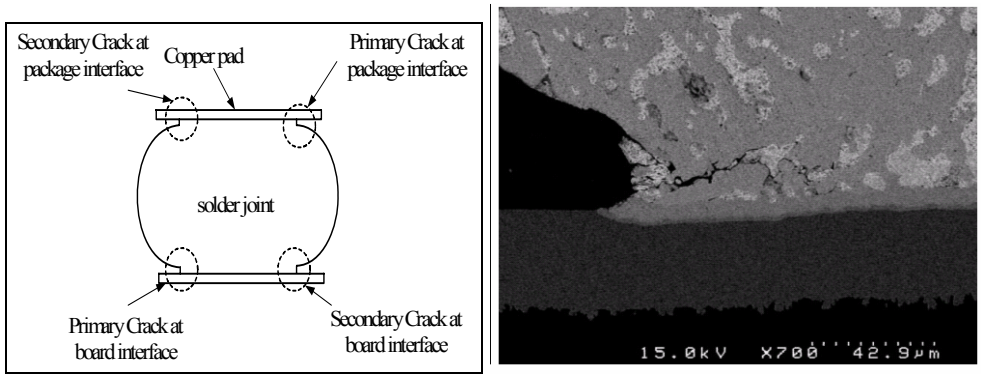

(a) (b)

Figure 5.1. Crack locations in SnPb and SnAg joints (a) four crack locations in a joint (b) primary crack at board interface at 2K-cycled aged SnPb joints [×700 SEM] (UT3-U5A-SPA-AG-2-G7-BI-TC-700X)

The experimental data presented below is limited to tests done on single-dense boards, 0-100°C ATC testing at UT and for the joints in the boundary region. Moreover, in order to focus on the joints with the largest cracks, only the crack data associated with the upper standard deviation is used—refer to Tables

G.1 and G.3 for SnPb and Tables G.2 andG.4 for SnAg in Appendix G (see data in bold)—only those data in the upper standard deviation, are represented here.

The mean % crack length (% of attachment diameter of 560 μm at the package interface and 584 μm at the board interface), standard deviation and sample size for SnPb and SnAg solder joints with different post-processing and cycled at 2K and 3K thermal cycles, respectively, are listed in Table 5.1, and the following results are summarized.

- Primary Cracks (P) at Package Interface (PI)

The mean % primary crack lengths in SnAg joints at 3K cycles for air-cooled, 19.9%, and quenched, 18.2%, were about 1.3-2 times larger than in SnPb joints at 2K cycles 13.5% and 9.7%, respectively. The mean lengths for aged SnPb cracks, 15.5%, at 2K cycles were 1.3 times larger than aged SnAg cracks, 11.9%, at 3K cycles. Among the SnPb joints, the aged joints had the largest mean % crack length, 15.5%, 13.5% and 9.7% for aged, air-cooled and quenched, respectively, while the aged cracks were the smallest among SnAg joints, 11.9%, 19.9% and 18.2% for aged, air-cooled and quenched, respectively.

- Secondary Cracks (S) at Package Interface (PI)

Among the SnPb joints, only the air-cooled joints showed secondary cracks at the board interface at 1.9% at 2K cycles. Among the SnAg joints, the air-cooled and quenched joints, 1.7% and 2.5%, respectively, at 3K cycles were more than five times larger than the aged joints at 0.3%.

- Primary Cracks (P) at Board Interface (BI)

Primary cracks at the board interface were much more significant in SnAg solder joints that in SnPb joints when compared with primary cracks at the package interface. Among the SnPb joints at 2K cycles, the aged, air-cooled, and quenched joints had primary crack lengths at the board interface that were 2.8%, 1.4%, and 0.7% (which were 18%, 10% and 7%, respectively, of the larger primary crack lengths at the package interface). Among the SnAg joints at 3K cycles, the aged, air-cooled, and quenched joints had primary cracks at the board interface that were 4.3%, 13.1%, and 6.4%, respectively (which were 36%, 66% and 35%, respectively, of the larger primary crack lengths at the package interface).

- Secondary Cracks (S) at Board Interface (BI)

Among the SnPb joints, only the air-cooled joints showed secondary cracks at the board interface at 0.3% at 2K cycles. All SnAg joints showed small secondary cracks of between 0.1% and 0.9% at 3K cycles.

Table 5.1. Mean % crack length in SnPb and SnAg solder joints in the upper standard deviation in the boundary region (Std. Deviation): 0-100°C ATC, UT (nominal diameter: 560 μm-PI and 584 μm-BI)

			SnPb 2K cycles		SnAg 3K cycles	
			Sample size	Mean (STD)	Sample size	Mean (STD)
Aged joints	PI	P	10	15.5 (4.2)	12	11.9 (3.3)
		S	10	0 (0)	12	0.3 (1.0)
	BI	P	10	2.8 (4.5)	10	4.3 (5.3)
		S	10	0.3 (1.1)	10	0.3 (1.1)
Air-cooled joints	PI	P	4*	13.5 (1.5)	10	19.9 (4.6)
		S	4*	1.9 (1.5)	10	1.7 (3.3)
	BI	P	1*	1.4 (N/A)	9	13.1 (8.9)
		S	1*	0 (N/A)	9	0.9 (1.9)
Quench joints	PI	P	16	9.7 (1.3)	11	18.2 (6.0)
		S	16	0 (0)	11	2.5 (3.4)
	BI	P	5	0.7 (1.5)	10	6.4 (3.0)
		S	5	0.0 (0)	10	0.1 (0.3)

Note: PI (BI)=package (board) interface and P (S)=primary (secondary) crack * Only a few joints were available due to the entire Cu pad being pulled off when removing joints from the board and package interfaces

The data presented here will be used to compare with FEM model predictions of crack initiation. The model development follows.

5.2. FLOWCHART OF CRACK INITIATION ANALYSIS

This section briefly explains how the crack initiation analysis is accomplished by coupling three FEM models. The global model computes the package assembly warping due to the CTE mismatch between the die and the PWB under thermal cycling. The resulting displacements together with temperature changes are imposed on the solder joint model, causing thermal stress and strain in the joints. Concurrently, forces from the joint model resulting from the package assembly deflections are fed back to the global model. Finally, a micro model takes the stress and strain data and evaluates the microstructure evolution, which includes phase coarsening, void nucleation, void growth and micro cracking. The changes in grain sizes in the micro-model are fed back to the joint model to reflect the stress and strain in the SnPb joint constitutive model (see Eq. 5.1).

Figure 5.2 shows the flowchart of the coupling of the global, joint and micro-models for SnPb and SnAg solder joints. The output of the micro-model is the crack location and microcracking. The following sections describe the three models.

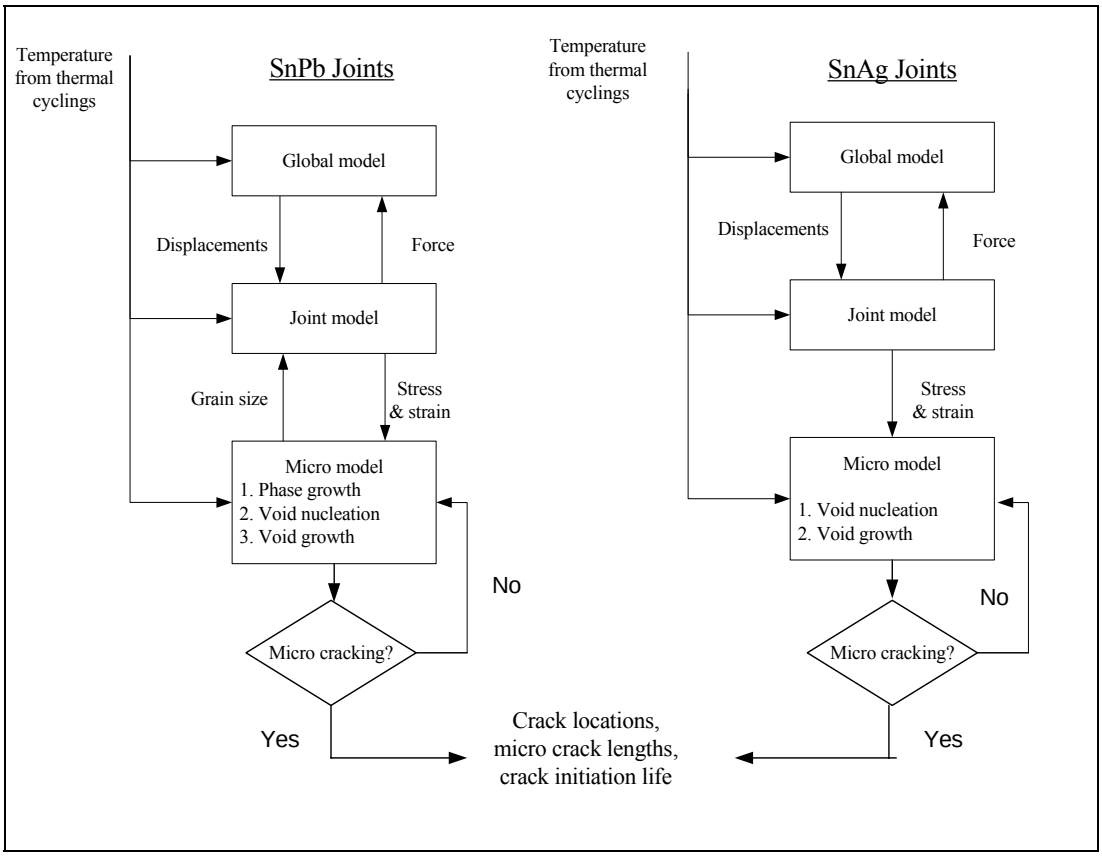

Figure 5.2. Flowchart showing the coupling of the global, joint and micro-models for crack initiation analysis of SnPb and SnAg solder joints

5.3. GLOBAL MODEL: PACKAGE ASSEMBLY WARPING

The joints at the four corners of the boundary region in the 357-PBGA showed the largest crack areas [51]. Therefore, a two-dimensional, 9-joint FEM global model was built by cross-sectioning the package along its principal diagonal direction, as shown in Figure 5.3(a). Starting from the package outside,

the nine joints modeled are B18, C17, D16, E15, F14, G13, H12, J11, and K10 (see fourth quadrant of Figure 2.2 in Chapter 2). Figure 5.3(b) shows the joint dimension. The left edge of the global model was constrained to apply a symmetry condition as shown in Figure 5.3(c), and the material properties are listed in Appendix A.

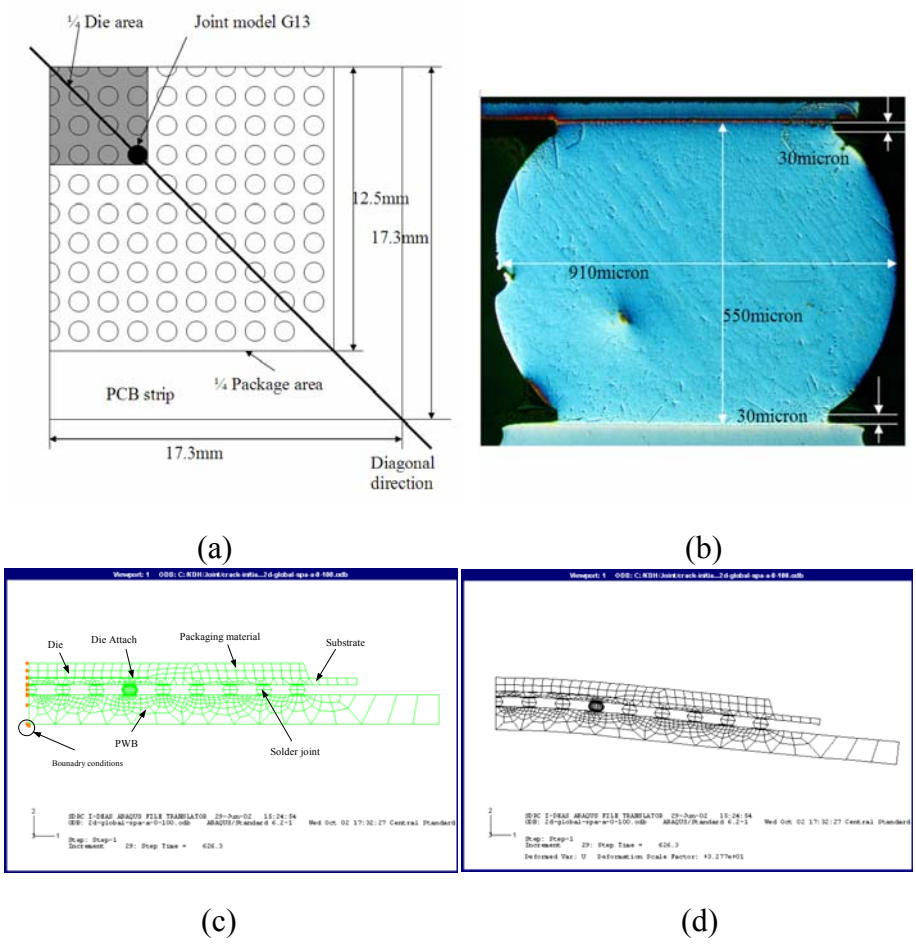

Figure 5.3. FEM model of 357 PBGA (a) top view of ¼ package assembly and the cross-sectioning diagonal direction (b) joint dimensions (UT19-U4A-SA-A-6-G8-100X) (c) stress-free state at 100°C (d) deformation at 0°C, after being held at 100°C

Two-dimensional, 4-node plain strain elements were generated for the die (13 elements), die attach (13 elements), PWB (405 elements), substrate (131 elements), and packaging material (54 elements), and two-dimensional, 4 node plain stress elements were generated for the solder joints (242 elements). A total of 858 elements and 923 nodes were created. Please see Section 2.1.1 in Chapter 2 for detailed package dimensions. Figure 5.3(d) shows the deformation of the assembly package as it cooled to 0°C from its stress-free state at 100°C.

5.4. JOINT MODEL: STRESS-STRAIN

The solder joint model is chosen as joint G13 of the global model. The joint G13 under the die periphery is chosen as the joint model since it has largest stress and strain due to thermal CTE mismatch between die and PCB. Therefore, the joint G13 model interacts with the global model under thermal cycling as part of global model, and it takes displacement and temperature as inputs, computes joint stress and strain, and outputs these values to the micro model. Then, the micro model which is embedded into the joint model simulates crack initiation process and calculates microcracking. The corner joint (G13) at the die edge, 4th joint from the symmetry plane, was meshed with refinement (182 elements) to simulate crack initiation process.

Based upon measurements [58] one layer of 8μm thick Cu6Sn5 and 8μm thick CuNiSn intermetallic layers were included in the FEM model of the aged SnPb joint, and 8μm thick Cu6Sn5 intermetallic layer included for aged SnAg

joint. Each intermetallic layer was constructed of 15 two-dimensional, 4-node plain stress elements. Here, the CuNiSn intermetallic layer was placed in the package interface between Cu pad and joint and the Cu6Sn5 intermetallic layer was placed in the board interface between Cu pad and joint.

5.5. MICRO-MODEL: CRACK INITIATION

Cracks in solder joints initiate by void growth. Since SnPb joints creep by grain boundary sliding and dislocation, each contribution to void growth should be evaluated separately. Also, aging creates coarsened microstructures which cause higher dislocation-induced creep and results in faster void growth and larger cracks. Therefore, the model for SnPb joints must include the microstructure coarsening process and take into account the effects of grain size on stress and strain. In contrast to SnPb joints, SnAg joints deform by dislocation creep and have stable Ag_2Sn particles dispersed in a tin matrix. Therefore, SnAg joints were characterized as a dispersion-hardened alloy [61] and modeled from void nucleation to void growth, skipping the coarsening process. The increased ductility for aged joints was included to distinguish aged from non-aged joints.

5.5.1. Micro-Model: SnPb

Constitutive behavior of SnPb joints

The constitutive equation for creep deformation in SnPb solder is represented as the sum of two parallel mechanisms, grain boundary sliding and dislocation [62], by

$$\dot{\gamma}^{cr} = \frac{C_2}{T}\frac{\tau^{n_2}}{d^p}\exp\left(\frac{-\Delta H_2}{RT}\right) + \frac{C_3}{T}\tau^{n_3}\exp\left(\frac{-\Delta H_3}{RT}\right) \quad (5.1)$$

where $\dot{\gamma}^{cr}$ is shear creep strain rate [s^{-1}], τ is shear stress [MPa], T is temperature [K], C_2= 1.39x10^{-6}, C_3= 2.38x10^{-3}, n_2=1.96, n_3=7.1, p=1.8, ΔH_2=46 [kJ/mol], ΔH_3= 77.6 [kJ/mol], R = 8.314 [J / K mol], and d is a mean phase size (grain size) [m] [62]. Eq. (5.1) shows that SnPb joints with smaller phase sizes have larger grain boundary sliding-induced creep strains, while SnPb joints with larger phase sizes have larger dislocation-induced creep strains. The large phase size creates a higher resistance to grain boundary sliding and results in higher stress.

Coarsening model

For eutectic SnPb solder, the coarsening of the lead-rich phase has been recognized, and it is driven by the elevated temperature (static coarsening) and the applied strain energy (dynamic coarsening) [63]. The coarsening model proposed by P.T. Vianco et al. [43] is used, and their approach for determining fitting constants in the model was followed. Phase boundary mobility, Fick's 1st law [64], was used to model the evolution of the Pb-phase size as

$$\frac{d\lambda}{dt} = M\frac{A_1}{\lambda^p} \quad (5.2)$$

where λ is the mean lead phase diameter and M is the mobility of lead phase boundary that can be expressed as

$$M = \frac{D}{RT} \quad (5.3)$$

where $D = D_v(v_x + v_0)$ is diffusivity, v_x is dynamic vacancy concentration, and v_0 is static vacancy concentration. Since dynamic vacancy concentration, v_x, is proportional to creep strain rate, it can be represented as

$$\dot{v}_x = A_3 \dot{\varepsilon}^{cr} \tag{5.4}$$

where $\dot{\varepsilon}^{cr}$ is the creep strain rate and A_3 is a fitting constant. Static vacancy concentration, v_0, can be represented as

$$v_0 = \exp\left(\frac{-\Delta H_f}{RT}\right) \tag{5.5}$$

The diffusion coefficient, D_v, can be represented as

$$D_v = D_0 \exp\left(\frac{-\Delta H_m}{RT}\right)$$

where D_0 = 9.7 cm^2/sec and ΔH_m is vacancy motion activation energy = 15.7 kcal/mol, and ΔH_f is the vacancy formation activation energy = 11.8 kcal/mol [65]. From Eqs. (5.2) and (5.3), the growth rate of lead-rich phase size becomes

$$\frac{d\lambda}{dt} = \frac{D_v(v_0 + v_x)}{RT}\frac{A_1}{\lambda^p} = A_2\frac{(v_0 + v_x)}{\lambda^p} \tag{5.6}$$

Inserting Eq. (5.3) into Eq. (5.2), the growth rate of lead-rich phase size can be divided into two terms, static coarsening and dynamic coarsening, as follows.

$$\frac{d\lambda}{dt} = A_2\frac{v_0}{\lambda^p} + A_2A_3\frac{\dot{\varepsilon}^{cr}}{\lambda^p} \tag{5.7}$$

To determine A_2, the empirical static coarsening equation from the static aging test of lead-rich phase was introduced. It can be represented by

$$\lambda - \lambda_0 = At^n \exp\left(\frac{-\Delta H}{RT}\right) \tag{5.8}$$

where A = 0.075, $_{\Delta H}$ = 23.5 kJ/mol, and n = 0.256 [62].

Differentiating Eq. (5.8) with respect to time and making it equal to the static coarsening part of Eq. (5.7), the constant A_2 in Eq. (5.7) can be determined as follows.

$$A_2 v_0 = 1.03\times10^{-5}\exp\left(\frac{-11081}{T}\right) \tag{5.9}$$

Inserting Eq. (5.5) into Eq. (5.9), A_2 becomes

$$A_2 = 1.03\times10^{-5}\exp\left(\frac{-5121}{T}\right) \tag{5.10}$$

By replacing λ by $\lambda-\lambda_0$ in Eq. (5.7), the growth rate of lead-rich phase size becomes

$$\frac{d\lambda}{dt} = \frac{1.03\times10^{-5}\exp(-11081/T)}{(\lambda-\lambda_0)^{2.9}} + A_3\frac{1.03\times10^{-5}\exp(-5121/T)\dot{\varepsilon}^{cr}}{(\lambda-\lambda_0)^{2.9}} \tag{5.11}$$

where A_3 was approximated as 4.1×10^{-3} from the measured lead phase particles of air-cooled SnPb joints at 2K cycles, and λo, the measured initial lead phase sizes, which are 0.6 μm and 4.0 μm for air-cooled and aged joints, respectively, from a previously reported M.S. thesis by Praveen Bhagavathula [58].

Void nucleation and growth

The microstructure evolution of SnPb solder joints begins at microstructure coarsening under thermal cycling, and then voids start to grow when the microstructures coarsen enough to nucleate voids. For solder joints with small sized second phase particles (such as Pb), stress concentrated around the particles is relaxed rapidly due to the local diffusion creep around them. Therefore, for SnPb joints to nucleate voids, the lead phase particles must become

large enough to overcome the local diffusion and create voids. A Needleman-Rice parameter [66, 67] was introduced to determine the critical particle size that provides an appropriate diffusion length, where stress concentrations are relaxed rapidly. Lead phase particles below this length are not likely to nucleate voids, and the critical particle size can be represented as

$$\Lambda = A_4 \left[\frac{\Omega \delta D_{gb} \sigma}{kT\dot{\varepsilon}} \right]^{1/3} \tag{5.12}$$

where σ is Von Mises stress [MPa], $\dot{\varepsilon}$ is creep strain rate [1/sec], D_{gb} is grain boundary diffusivity =100exp(−57000/RT) [mm^2/sec] [18], δ is grain boundary thickness=5.8×10^{-7} [mm], Ω is atomic volume=2.71×10^{-20} [mm^3] [5], k =1.38×10^{-20} [Nmm/K], A_4=2. The form of Eq. (5.12) is rationalized in terms of localized Coble creep [68]. Once voids are nucleated, they reach the critical size rapidly due to local grain boundary diffusion, and the critical void size can be assumed as [69]

$$\rho = \frac{2\gamma}{\sigma_h} \tag{5.13}$$

where ρ is the radius of the void embryo, γ is the solder surface energy, and σ_h is the positive hydrostatic stress. Therefore, for voids to nucleate, two conditions should be satisfied: 1) a second phase particle must be larger than the critical size defined by Eq. (5.12), and 2) the hydrostatic stress must be positive.

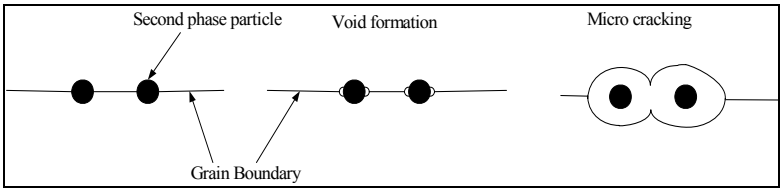

Figure 5.4. Voiding process

Figure 5.4 shows a schematic of void nucleation and growth for creeping materials with second phase particles in the grain boundary. Since stress is concentrated at the apices of the lead phase particles, voids start to nucleate and grow until they merge with each other. Once voids are nucleated, the rate of void volume increase for creeping materials is proportional to creep strain rate and void volume [70], and an experimental formulation can be represented by

$$\frac{dv}{dt} = Cv\frac{d\varepsilon^{cr}}{dt} \tag{5.14}$$

where C is a fitting constant, and ν is void volume. For SnPb solder, creep mechanisms from grain boundary sliding and dislocation contribute to the growth rate of the void radius and can be described as [5-6]

$$\dot{\rho} = B_2\rho\dot{\varepsilon}_{gbs} + B_3\rho\dot{\varepsilon}_{dc} \tag{5.15}$$

where ρ is a void radius, $\dot{\varepsilon}_{gbs}$ is the grain boundary sliding-induced creep strain rate, $\dot{\varepsilon}_{dc}$ is the dislocation-induced creep strain rate, and B_2 and B_3 are fitting constants, chosen as approximately 0.2 and 3.3, respectively, from the measured cracks at 2K cycles. The values of B_2 and B_3 were chosen to match the simulated

and measured primary crack sizes at the package interface for air-cooled and aged SnPb solder joints, shown in Table 5.1.

Since lead phase particles in SnPb joints reside at the junctions of the tin matrix boundary, the void interspacing distance can be represented by the phase size as

$$a \approx 2d - \lambda \tag{5.16}$$

where d is mean phase size and λ is lead phase size. When the void radius reaches half the void interspacing distance, two neighboring voids merge, and a micro crack is formed.

5.5.2. Micro-Model: SnAg

Constitutive behavior of SnAg joints

The constitutive equation for the creep deformation of SnAg solder can be represented as dislocation creep [71] by

$$\dot{\varepsilon}^{cr} = D_1[\sinh(D_3\sigma)]^{D_2} \exp\left(\frac{-D_4}{RT}\right) \tag{5.17}$$

where $\dot{\varepsilon}^{cr}$ is creep strain rate [s^{-1}], D_1=178.6 [s^{-1}], D_2 =4.75, D_3 =0.115 [MPa^{-1}], and D_4 =57.1 [KJ/mol].

Void nucleation and growth

As in SnPb joints, a Needleman-Rice parameter was introduced to determine the critical particle size that provides an appropriate diffusion length. However, for SnAg joints, since lattice diffusion through the matrix is rate controlling, Eq. (5.12) was expressed as [68]

$$\Lambda = \left[\frac{\Omega D_L \sigma}{\pi k T \dot{\varepsilon}} \right]^{1/3} \tag{5.18}$$

where σ is Von Mises stress [MPa], $\dot{\varepsilon}$ is creep strain rate [1/sec], D_L is lattice diffusivity, 0.71exp(−55100/RT)[mm^2/sec] [72]. The form of Eq. (5.18) is rationalized in terms of localized Nabarro-Herring creep in the vicinity of the particles [73]. Since Ag_2Sn particles are dispersed in tin matrix for SnAg joints, void nucleation rate is needed to determine void interspacing distance. When the two conditions of critical particle size and positive hydrostatic stress, described in the previous SnPb section, are satisfied, voids start to nucleate at the following rate [74].

$$N = p\varepsilon^{cr} \tag{5.19}$$

where N is a number of voids per unit area, ε^{cr} is a creep strain, and p is a proportionality factor having the dimension [m^{-2}], and can be approximated from strain to failure. The empirical relation for creeping materials was represented by [75]

$$\varepsilon_f = 1250 p^{-0.4} \tag{5.20}$$

where ε_f is strain to failure, which is accumulated strain when fracture occurs. According to the literature [14], the strain to failure of air-cooled SnAg solder is 27.4%, while SnAg solder aged at 393 K for 500 hours is 36.3%, indicating that aged SnAg is tougher. Therefore, using Eq. (5.19), the proportionality factors, p, of air-cooled and aged SnAg joints can be approximated as 1.45×10^9 and 0.71×10^9 [m^{-2}], respectively. The values used for quenched are the assumed to be same as

for air-cooled based upon experimental results of crack growth and life. Assuming voids are nucleated uniformly, the number of voids can be described by

$$N = \frac{1}{a^2} \tag{5.21}$$

where $a = \sqrt{(1/N)}$ is the void spacing distance. The growth of void radius can be represented by

$$\dot{\rho} = B_4 \rho \dot{\varepsilon}^{cr} \tag{5.22}$$

where ρ is void radius, $\dot{\varepsilon}^{cr}$ is creep strain rate, and a fitting constant, B_4, was approximated as 0.11 from the measured cracks at 3K cycles. B_4 was chosen after 3K cycles to match the simulated and measured primary crack sizes at the package interface of air-cooled and aged SnAg solder joints, as listed in Table 5.1.

5.5.3. FEM Implementation of Micro-Model

The micro-model was embedded using a user-subroutine function USDFLD in ABAQUS 6.2-1 [76]. Since the SnPb joints coarsen, the stress changes caused by phase size changes need to be updated. Therefore, the micro-model of SnPb joints interacts with the joint model. For SnPb joints, the coarsening model of lead phase particles, Eq. (5.11), is active from the beginning of thermal cycling. At the same time a void nucleation model, Eq. (5.12), remains active until it determines void nucleation. Once voids are nucleated, the void growth model, Eq. (5.15), becomes active, and voids start to grow until neighboring voids merge. When microcracks form in the elements located in the solder joint, those elements do not carry load and their Young's modulus is set to

zero. For SnAg joints, the micro model starts from the void nucleation model, Eq. (5.18). Once voids nucleate, the void nucleation rate, Eq. (5.19), is active, and the void growth model, Eq. (5.22), is active at the same time until microcracking occurs. At the end of the simulation, crack location, size and the number of cycles spent for the crack initiation process are generated as outputs. Here, a user-subroutine function CREEP describes the constitutive behavior of SnPb joints, while a built-in hyperbolic creep function is used for SnAg joints.

The micro model is embedded into integration point of every element of the joint model (corner joint, G13), and it takes stress and strain from the joint model as inputs together with temperature and calculates the time when microcracking occurs as the output. Therefore, the micro model predicts crack initiation location in the joint model, using user-subroutine function USDFLD. Table 5.2 and Table 5.3 show criterion/ critical values and initial conditions in the micro-model process for aged and air-cooled SnPb and SnAg joints, respectively.

Table 5.2. Micro-model process and criteria, initial conditions, critical values for aged and air-cooled SnPb joints

Process	Governing Equations	Initial conditions	Critical values /Criterion*
Phase growth	Eq(5.11)	Air-cooled joint: 0.6micron+ Aged joint: 4.0micron+	Air-cooled joint: 1.3 micron Aged joint: 4.0 micron
Void nucleation	Eq(5.12)	NA	Eq(5.12) < lead-phase size Positive hydrostatic stress
Void growth	Eq.(5.15)	0.5micron^	NA
Micro cracking	Eq.(5.16)	NA	Half of void interspacing distance defined by Eq.(5.16) = void radius Void radius = 4.9micron for air-cooled joint, 7 micron for aged joint

+[58], ^[77], *calculated from FEM simulations

Table 5.3. Micro-model process and criteria, initial conditions, critical values for aged and air-cooled SnAg joints

Process	Governing Equations	Initial conditions	Critical values /Criterion*
Void nucleation	Eq(5.18)	NA	Eq(5.18) < Ag2Sn particle size Positive hydrostatic stress
Void growth	Eq.(5.22)	0.5micron+	NA
Micro cracking	Eq.(5.16)	NA	Half of voids interspacing distance by Eq.(5.16) = void radius Void radius = 3.2micron for air-cooled joint, 4.2 micron for aged joint

+[77], *calculated from FEM simulations

5.6. CRACK INITIATION: FEM SIMULATION RESULTS

Continuous thermal cycles of the 0-100°C ATC test protocol were imposed on the SnPb global, joint, and mico-models. As shown in Figure 5.5a for air-cooled joint G13, the lead phase particle grew from the initial size, 0.6 μm (based on microstructural results Chapter 3, Section 3.2), to 1.3 μm at around 1070 cycles, then microcracking occurred at the void radius, 4.9 μm. For aged joint G13 simulations showed the 4 μm sized lead phase particles did not grow because they were initially stabilized from aging. Figure 5.5b shows the distribution of different lead phase particles on corner joint G13 at 2K cycles, and it shows that the particles located in the package and board interfaces coarsen more than at the other regions of the joint, and the right corner of the package interface has the most significant growth.

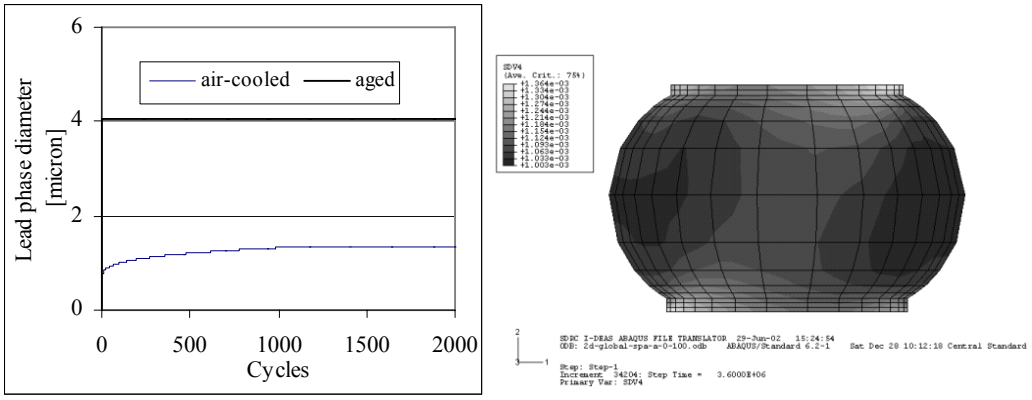

(a) (b)

Figure 5.5. Calculated lead phase particle growth in SnPb joint G13 under 0-100°C ATC thermal cycling (a) air-cooled versus aged and (b) air-cooled SnPb joint at 2K cycles

Since primary cracks at the package interface are the largest, the following discussion on crack initiation simulations focuses on those cracks. Figure 5.6 shows the void nucleation and radius growth in the six elements located at the right corner of the package interface of joint G13 (see red-colored box in Figure 5.6) for aged and air-cooled SnPb and SnAg solders.

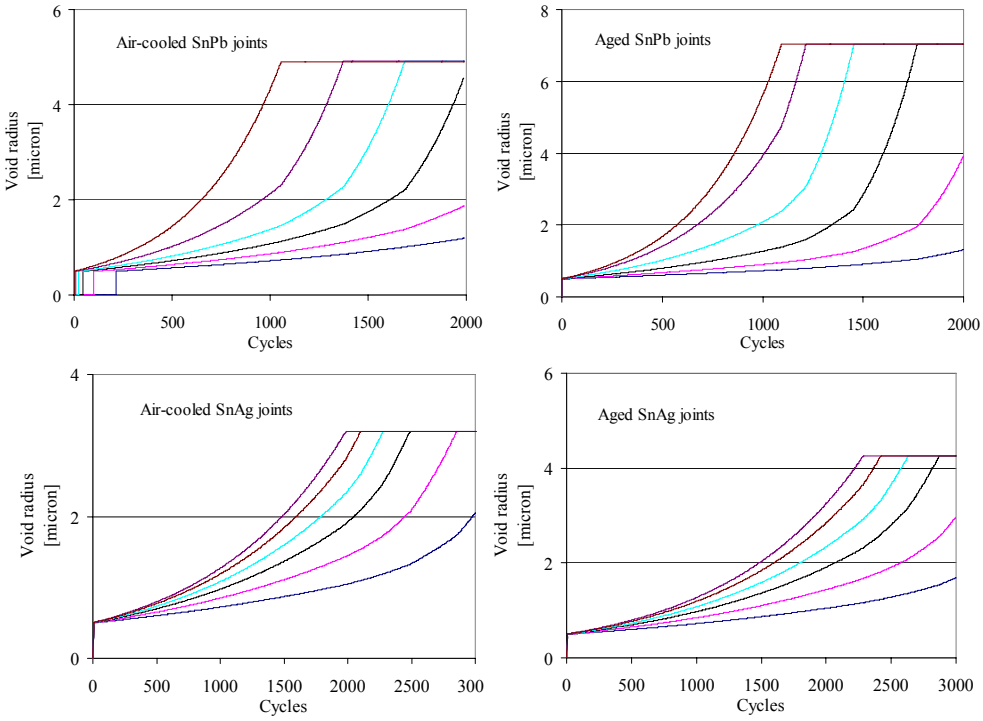

Figure 5.6. Calculated void growth in the right corner of the package interface in corner joint G13 for SnPb and SnAg joints

Here, the measured initial particle size is 0.6 μm and 1.5 μm for SnPb and SnAg joints, respectively, and the initial void radius was assumed to be 0.5 μm [77] since voids nucleate in the tin matrix for both solder joints. For air-cooled SnPb joints, voids in the six elements nucleated at different cycles of 1, 7, 22, 46, 101, and 215 cycles, respectively. Recall from Section 5.3.1. that for solder joints to nucleate voids, the particles must become large enough to overcome the local diffusion and create voids. In other joints such as aged SnPb joints and air-cooled and aged SnAg joints, initial particle size are already large enough to nucleate voids. For air-cooled SnPb, the first three elements located from the surface,

reached a critical void radius size of 4.9 μm at 1070, 1385, 1700 cycles, respectively, when micro cracking began.

For aged SnPb solder joints, void growth rate increased as the void radius increased. In contrast to air-cooled joints, the voids of aged SnPb joints started to nucleate from the 1st-cycle because the initial lead phase particles of 4 μm was large enough to nucleate voids. Four elements at the right corner of the package interface reach a critical size, 7μm, at different cycles, 1111, 1230, 1467, and 1782 cycles, respectively. The aged joint spent 1467 cycles in microcracking the first three elements, while for air-cooled joints, 1700 cycles was needed (16% longer).

For air-cooled SnAg joints, the voids starts to nucleate from the 1st-cycle, and voids in the five elements reach a critical size of 3.2 μm at 2009, 2116, 2296, 2516, 2870 cycles, respectively, when micro cracking started. For aged SnAg joints, four elements reach a critical size, 4.2 μm, at 2301, 2439, 2652, 2886 cycles, respectively. In constrast to SnPb joints, the aged SnAg joint had 40% smaller cracks than the air-cooled joint. SnAg joints do not show microcracking until 2K cycles, while SnPb joints have microcracking around 1K cycles. The simulation results show that the crack initiation life, which is defined as the time when two neighboring cavities are linked together [4] for air-cooled and aged SnPb and SnAg joints are 1070, 1111, 2009, and 2301 cycles, respectively.

Table 5.4 shows the simulated cycles-to-void nucleation and cycles-to-micro-cracking for aged and air-cooled SnPb and SnAg solder joints. Since

primary cracks in the package interface are the largest, these crack initiation simulation results are calculated for that crack.

Table 5.4. Calculated cycles-to-void nucleation and to micro-cracking for aged and air-cooled SnPb and SnAg solder joints

	Cycles-to-	Element 1	Element 2	Element 3	Element 4	Element 5	Element 6
SnPb air-cooled	Void nucleation	1	7	22	46	101	215
	Microcracking	1070	1385	1700	NA	NA	NA
SnPb Aged	Void nucleation	1	1	1	1	1	1
	Microcracking	1111	1230	1467	1782	NA	NA
SnAg air-cooled	Void nucleation	1	1	1	1	1	1
	Microcracking	2009	2116	2296	2516	2870	NA
SnAg Aged	Void nucleation	1	1	1	1	1	1
	Microcracking	2301	2439	2652	2886	NA	NA

Here, simulation stopped at 2K cycles for SnPb joints and 3K cycles for SnAg joints. NA represents the element did not reach microcracking during simulation.

The crack initiation life of an aged joint is about 4% and 15% longer than the air-cooled joint for SnPb and SnAg joints, respectively. Also, the crack initiation life of SnAg joints is about 100% longer than SnPb joints. Table 5.5 lists the simulated crack initiation life for SnAg and SnPb joints.

Table 5.5. Calculated simulated crack initiation life-cycles for 0-100ºC ATC assumed for primary crack at package interface (see Table 5.4, Element 1)

SnPb		SnAg	
Aged	Air-cooled	Aged	Air-cooled
1111	1070	2009	2301

Note that during the above simulations, other cracks such as primary cracks at the board interface or secondary cracks were computed at the same time, however they were not looked at because the major crack is the primary crack at the package interface.

Figure 5.7 shows the void distribution in joint G13, where the white colored area represents nucleated voids and the black colored area no voids. The joints have void distributions concentrated at the right corner of the package interface and the left corner of the board interface. Aged SnPb joints have larger lead phase sizes thereby larger areas of void distribution than air-cooled SnPb joints. Air-cooled SnAg joints have larger void distributed areas than the aged joints because the void nucleation rate is higher.

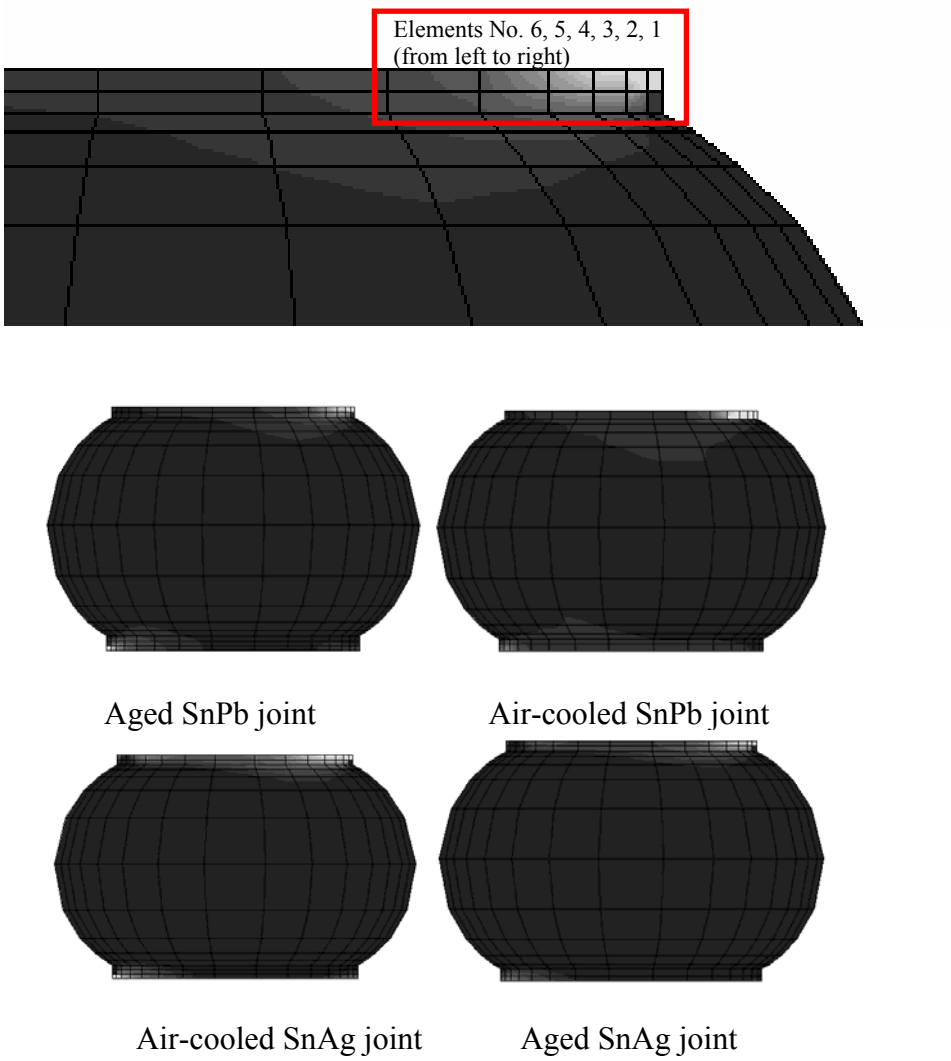

Figure 5.7. Calculated void distributions in joint G13 of SnPb (2K cycles) and SnAg (3K cycles) at 0-100°C ATC thermal cycles

Table 5.6. Mean % crack length in joint G13 omparison of simulated and experimental (Table 5.1) (data beyond two standard deviations above the mean) (Std. Deviation): 0-100°C ATC, UT (nominal diameter: 560 μm-PI and 584 μm-BI)

Postprocess			SnPb 2K cycles		SnAg 3K cycles	
			experiment	simulation	experiment	simulation
Aged	PI	P	15.5 (4.2)	15.8	11.9 (3.3)	16.9
		S	0	0	0.3 (1.0)	0.5
	BI	P	2.8 (4.5)	0.5	4.3 (5.3)	0.6
		S	0.3 (1.1)	0.2	0.3 (1.1)	0
Air-cool	PI	P	13.5 (1.5)	11.6	19.9 (4.6)	25.1
		S	1.9 (1.5)	0.3	1.7 (3.3)	0.6
	BI	P	1.4	3.4	13.1 (8.9)	3.7
		S	0	0.4	0.9 (1.9)	0.6

Note: PI (BI)=package (board) interface and P (S)=primary (secondary) crack

Simulated crack length results from the micro-model in Table 5.6.were compared with experimental data (sample from upper standard deviation) of Table 5.1. The simulation results do show primary and secondary cracks at the package and board interfaces and are qualitatively consistent with the experimental data.

5.6.1. Crack Initiation in Aged SnPb Joints: Secondary Cracks at Package Interface

Experimental data showed secondary cracks at the package interface of SnPb and SnAg joints except for aged SnPb joints. To investigate this anomaly, the stress components at the left corner of package interface were analyzed. In order to nucleate voids, the hydrostatic stress must be positive at the nucleation sites. For aged SnPb solder joints, Figures 5.8 (a) and (b) show the Mises stress and hydrostatic stress profiles under one thermal cycle (0-100°C ATC) at the location of the primary crack at the package interface at the right corner, where voids nucleate, and at the location of the missing secondary crack at the package interface in the left corner, where voids did not nucleate, respectively. At the right corner, a large positive hydrostatic stress exists when the Mises stress is maximum, while at the left corner there is a compressive stress. In contrast, for air-cooled SnPb solder joints, a positive hydrostatic stress forms when the Mises stress is maximum in the left corner of the package interface as shown in Figure 5.9c, so voids nucleate. Thus, for aged SnPb joints, voids do not nucleate at the left corner of package interface, and there is no secondary cracks at the package interface due to the compressive stress. Aged SnPb joints had a 9μm thick CuNiSn intermetallic layer (IMC) at the package interface (see Chapter 3) due to long aging process. This IMC layer shifted the crack initiation point of the secondary crack at the package interface down to the end of solder mask end and thereby resulted in a compressive stress that inhibited void initiation.

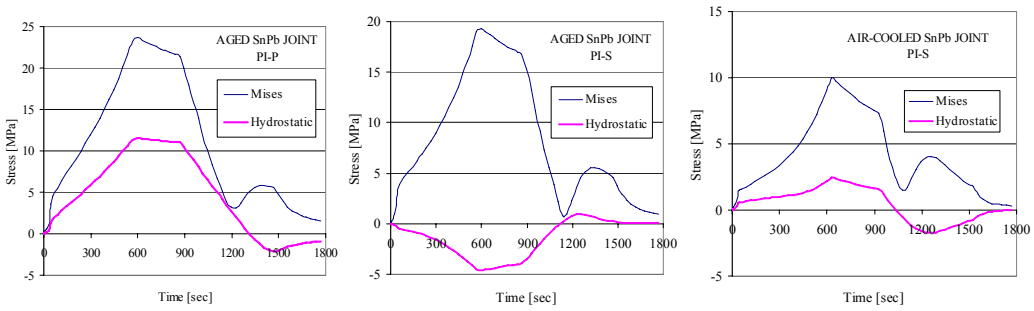

(a) (b) (c)

Figure 5.8. Mises and hydrostatic stresses in SnPb joint G13 at the package interface (calculated at element 1 in Figure 5.7), 0-100°C ATC (a) right-corneraged (b) left-corner aged and (c) left-corner air-cooled

5.7. SUMMARY

Mechanistic models of SnPb and SnAg solder joints in 357-PBGA packages were developed to simulate the crack initiation process using FEM techniques. First, dye penetration crack length measurements for the largest cracks in the boundary region were tabulated for aged and air-cooled SnPb and SnAg solder joint G13 at the package and board interfaces. Data on the primary and secondary cracks at the four corners of the joint G13 were given when exposed to 0-100°C ATC thermal cycling. Then three FEM models were described: global model of the package assembly, joint model for stress/strain, and a micro-model to describe crack initiation. Detailed governing equations were given for the SnPb joints to model coarsening, voiding and micro-cracking, and for the SnAg joints, from voiding to micro cracking. Critical values describing the transition from one stage to the next were given. The FEM simulation results

qualitatively matched the experimental data. The results from this chapter are the following.

Based upon experimental data:

- Cracks propagated through the package and board interfaces of joints, and the primary cracks at the package interface showed the largest growth followed by the primary cracks at the board interface.
- There were no secondary cracks observed at the package interface of aged SnPb joints.

Based upon FEM simulations:

- Simulation showed lead phase particles of aged SnPb joints did not grow, while in air-cooled joints they grew from 0.6 μm to 1.3 μm until microcracking occurred. The voids of air-cooled SnPb joints did not nucleate until the lead phase particles became large enough to cause void nucleation. Once voids nucleated, the growth rates increased as void size increased.
- Voids are distributed at the joint interfaces, and no voids nucleated in the other areas.
- Aged SnPb joints had larger cracks because of larger dislocation creep caused by larger phase sizes than air-cooled SnPb joints (4μm versus 0.6-0.8μm)
- Secondary cracks were suppressed at the package interface of aged SnPb joints because compressive stresses prevented voids from nucleating.

- The void nucleation rate of aged SnAg joints was slower than in air-cooled joints due to higher strain to failure, and the time spent for microcracking in aged SnAg joints was 15% longer than in air-cooled SnAg joints.
- The crack initiation life in SnAg joints was approximately 100% longer than in SnPb joints.

CHAPTER 6

Crack Propagation Modeling and Analysis

This chapter presents crack propagation modeling and analysis using experimental data and models based upon finite element techniques and fracture mechanics approaches for SnPb and SnAg solder joints under different post-process conditions. The crack propagation model has two models: a global model and a joint model. Like the global model used for the crack initiation simulation, the global model represents the entire package assembly including PBGA die, solder joints, and board. Experimentally-measured cracks are embedded into the global model as cracks propagate, and the global model computes the displacements sent to the joint model. A crack embedded joint model takes these displacements as input together with temperature and computes energy release rate and stress intensity factor. The crack propagation model provides insights into observed and measured crack data on crack evolution with number of thermal cycles, and the effects of multiple cracks in a joint and assumed boundary conditions on energy release rates and stress intensity factors.

6.1. CRACK PROPAGATION: EXPERIMENTAL DATA

The experimental data presented in this chapter is limited to tests done on single-dense boards, 0-100°C ATC testing at UT and for the joints in the

boundary region. Moreover, in order to focus on the joints with the largest cracks, only the crack data associated with the upper standard deviation (data beyond two standard deviations above the mean) is represented here—refer to Tables 6.1 and 6.2 for SnPb and SnAg solder, respectively (raw data can be found in Appendix G, Tables G.1-G.2 for SnPb and Tables G.3-G.4 for SnAg. See data in bold).

Figure 6.1 shows the evolution of mean % crack length (% of attachment diameter of 560 μm at the package interface (PI) and 584 μm at the board interface (BI)) with number of thermal cycles in SnPb and SnAg joints with different post-process conditions. The mean % crack length, standard deviation and sample size of the selected data are shown in Tables 6.1-6.2. Here, air-cooled joints were selected to represent non-aged joints since measured cracks in air-cooled and quenched joints were similar and not statistically different from each other [51]. The full data set used in these plots and tables are given in Appendix G.

In reviewing the data, it is important to note that the data was generated from different packages, therefore, some % crack length data decreased with increased cycle number. That is, at each read-point cycle, uniquely specified packages were removed from the environmental chamber and destructive crack measurements taken at the University of Texas using the dye-penetration protocol that was outlined in Chapter 2. Here, data at different cycle times represent measurements from different packages. The results are discussed below.

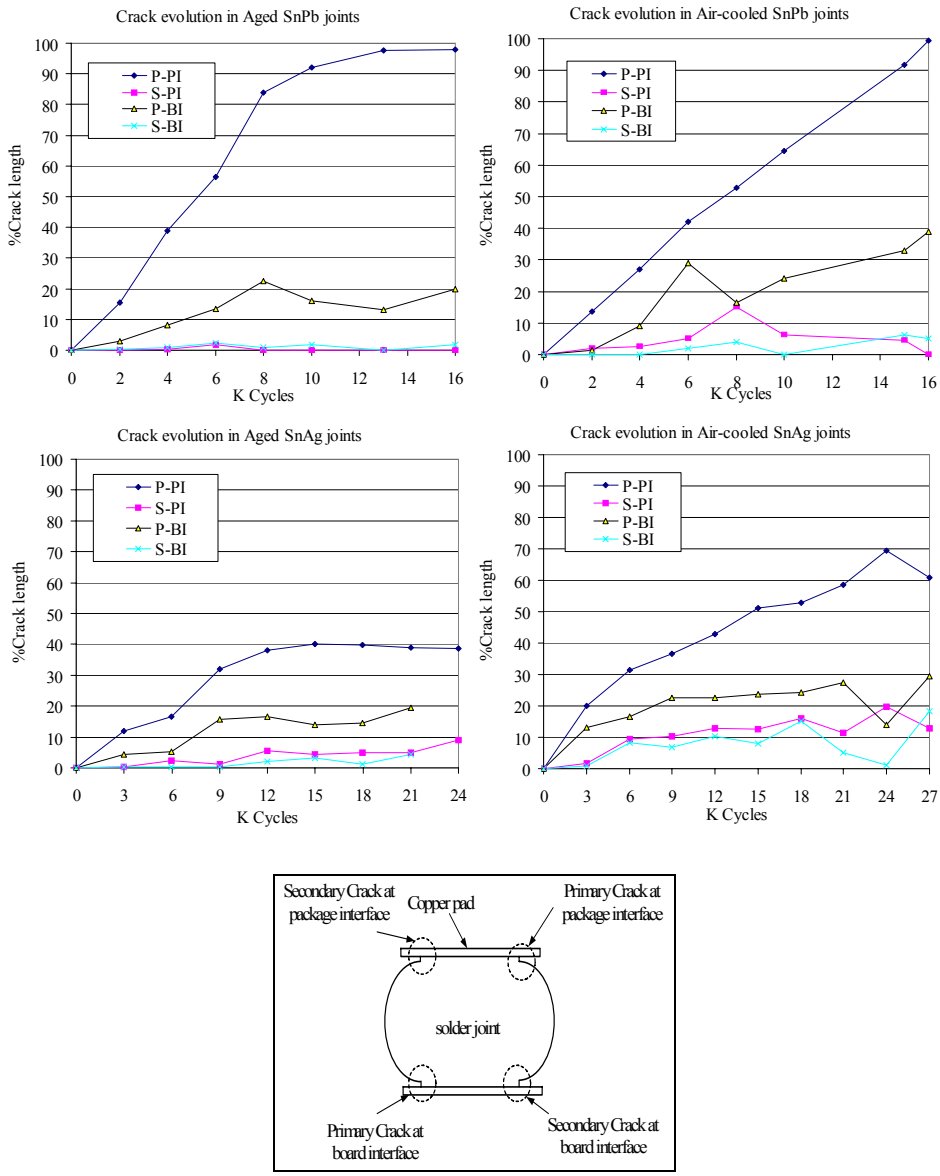

Figure 6.1. Experimentally measured evolution of mean % crack length in aged and non-aged SnPb and SnAg joints for data two standard deviations above the mean in the boundary region, 0-100°C ATC, UT cycling (nominal joint diameter: PI-560 μm, BI-584 μm) Note: PI (BI)=package (board) interface and P (S)=primary (secondary) crack. Joint represents G13 (joint4 in Figure 6.2(a)).

Table 6.1. Experimentally measured evolution of mean % crack length in aged and air-cooled SnPb joints for data two standard deviations above the mean in the boundary region, 0-100°C ATC, UT cycling (nominal joint diameter: PI, 560 μm; BI, 584 μm)

Number of Cycles	Aged SnPb joints						Air-cooled SnPb joints					
	PI			BI			PI			BI		
	N	P-PI	S-PI	N	P-BI	S-BI	N	P-PI	S-PI	N	P-BI	S-BI
2K	10	15.5 (4.2)	0 (0)	10	2.8 (4.5)	0.3 (1.1)	4	13.5 (1.5)	1.9 (1.5)	1	1.4	0
4K	13	38.9 (7.4)	0.2 (0.7)	13	8.1 (10.8)	0.9 (3.3)	6	26.9 (2.5)	2.5 (2.5)	4	8.9 (3.5)	1.0 (0)
6K	13	56.4 (7.6)	1.6 (3.0)	13	13.5 (11.1)	2.4 (4.5)	6	42.1 (4.6)	5.1 (4.3)	6	28.9 (16)	1.9 (3.8)
8K	10	83.9 (11.2)	0 (0)	10	22.6 (10.9)	0.9 (3.0)	7	52.8 (6.6)	15.0 (10.2)	6	16.5 (10.2)	4.0 (5.7)
10K	12	92.0 (7.4)	0.1 (0.3)	12	16.0 (18.6)	1.6 (3.0)	6	64.4 (7.4)	6.2 (4.4)	4	24.1 (6.1)	0 (0)
13K*/15 K**	13	97.6 (3.3)	0 (0)	13	13.2 (11.8)	0 (0)	4	91.8 (15)	4.6*** (9.3)	3	33.0 (17.7)	6.3 (5.7)
16K	14	97.8 (2.6)	0 (0)	11	19.9 (28.7)	1.8 (6.0)	9	99.3 (0.4)	0*** (0)	9	38.8 (20.5)	5.0 (4.8)

PI (BI)=package (board) interface and P (S)=primary (secondary) crack
Note: *aged joints ** air-cooled joints *** three out of four secondary cracks merged with primary crack ****all secondary cracks merged with primary crack

Table 6.2. Experimentally measured evolution of mean % crack length in aged and air-cooled SnAg joints for data two standard deviations above the mean in the boundary region, 0-100°C ATC, UT cycling (nominal joint diameter: PI, 560 μm; BI, 584 μm)

Number of Cycles	Aged SnAg joints						Air-cooled SnAg joints					
	PI			BI			PI			BI		
	N	P-PI	S-PI	N	P-BI	S-BI	N	P-PI	S-PI	N	P-BI	S-BI
3K	12	11.9 (3.3)	0.3 (1.0)	10	4.3 (5.3)	0.3 (1.1)	10	19.9 (4.6)	1.7 (3.3)	9	13.1 (8.9)	0.9 (1.9)
6K	14	16.4 (4.7)	2.2 (3.1)	14	5.3 (6.7)	0.4 (1.6)	8	31.5 (4.5)	9.6 (7.1)	8	16.5 (9.6)	8.2 (7.1)
9K	15	32.0 (6.7)	1.0 (1.9)	13	15.6 (10)	0.2 (1.1)	13	36.7 (5.8)	10.3 (6.8)	13	22.4 (8.7)	6.9 (7.5)
12K	11	38.0 (8.0)	5.6 (4.7)	10	16.7 (8.4)	2.1 (3.3)	11	43.0 (7.0)	12.9 (7.5)	10	22.4 (8.3)	10.2 (7.6)
15K	13	40.1 (7.1)	4.4 (7.1)	12	13.9 (15.9)	3.0 (6.3)	15	51.2 (10.8)	12.5 (8.6)	13	23.7 (9.9)	7.9 (8.2)
18K	4	39.8 (0.2)	4.8 (7.9)	4	14.6 (17.5)	1.2 (2.5)	4	52.9 (9.0)	16.0 (11.2)	4	24.3 (7.2)	15.2 (10.2)
21K	4	38.9 (4.0)	4.9 (9.9)	4	19.4 (13.7)	4.2 (8.5)	5	58.6 (10.5)	11.4 (12.3)	5	27.4 (12.4)	5.1 (6.1)
24K	4	38.7 (11.4)	9.0 (15.3)		N/A	N/A	3	69.3 (26.3)	19.8 (19.6)	3	13.9 (10.6)	1.1 (1.9)
27K	No data available						4	60.8 (3.2)	12.9 (8.2)	4	29.4 (9.2)	18.3 (12.1)

PI (BI)=package (board) interface and P (S)=primary (secondary) crack

Aged SnPb joints

For aged SnPb joints, the primary crack at the package interface grew approximately at a constant rate of 10%/K cycles until 8K cycles (84% length), then the rate decreased to ~3%/K cycles to 13K cycles (98% length) when the growth rate dropped to zero after 13K cycles. The primary crack at the board interface grew almost linearly to 20% length at 8K cycles and remained relatively constant thereafter. There were virtually no secondary cracks at the package interface, while the secondary crack at the board interface grew very slowly to approximately 2% at 16K cycles. Up to 10K cycles, the ratio of the crack lengths at the board to package interfaces averaged 21% (18%, 21%, 24%, 27%, and 17% at 2K, 4K, 6K, 8K, and 10K cycles, respectively), with some variability.

Air-cooled SnPb joints

For air-cooled SnPb joints, the primary crack at the package interface grew almost linearly at 6%/K cycles to 100% length at 16K cycles, and the secondary crack grew to less than 20% length during the 15K cycles. Note the secondary crack at 16K cycles was recorded as 0% because it had merged with the primary crack. Also note that except for 8K cycles, the secondary crack measurements were below 10%. The primary crack at the board interface increased to 30% length at 6K cycles and slowly increased to about 40% at 16K cycles—twice the length of the aged SnPb solder data at 16K. The secondary crack length at the board interface was <6%, but more than twice the length of the aged value. Comparing aged versus air-cooled data, notice that at 10K cycles, the

air-cooled joint showed 71% crack length, while the aged joint showed 92% crack length. Up to 10K cycles, the ratio of board to package interface crack lengths averaged 36% (10%, 33%, 69%, 32%, and 37% at 2K, 4K, 6K, 8K, and 10K cycles, respectively), but with substantial variability.

Aged SnAg joints

For air-cooled and aged SnAg joints, the primary and secondary cracks were found at the package and board interfaces. For aged SnAg joints, the primary crack at the package interface grew almost constantly at a rate of 2.7%/K cycles to a 40% length at 15K cycles, then the length remained relatively constant thereafter. The secondary crack at the package interface grew to 9% length at 24K cycles at a rate of approximately 0.4%/K cycles. The primary crack at the board interface grew to 15% length until 9K cycles, then remained relatively constant thereafter, while the secondary crack at the board interface grew very slowly to approximately 4% length at 21K cycles. The 24K cycle data at the board interface were not available because the joint pads ripped off the boards while removing the joints from the board. Up to 21K cycles, the ratio of board to package interface crack lengths averaged 40% (36%, 32%, 49%, 44%, 35%, 37%, and 50% at 3K, 6K, 9K, 8K, 12K, 15K, 18K, and 21K cycles, respectively), with less variability than seen for the air-cooled SnPb joints.

Air-cooled SnAg joints

For air-cooled SnAg joints, the primary and secondary cracks at the package interface grew almost linearly at 2.4%/K cycles between 3K (19.9%) and 24K (69.3%) cycles and 0.14%/K cycles between 6K (9.6%) and 27K (12.9%) cycles, respectively. At the board interface the primary crack grew to approximately 27% length at 21K cycles, and the secondary crack grew to 18% at 27K cycles. Up to 21K cycles, the ratio of the crack lengths at the board to package interfaces averaged 53% (69%, 52%, 61%, 52%, 46%, 46%, and 47% at 3K, 6K ,9K, 8K, 12K, 15K, 18K, and 21K cycles, respectively).

In contrast to the SnPb results, aged SnAg joints had approximately 50% smaller crack growth rates than air-cooled joints. As explained in Chapter 3, a plausible reason for the much smaller crack rates of aged SnAg solder joints (thereby longer life) was the existence of resin cracks in the substrate and test board that increased compliance of the board assembly.

SnPb versus SnAg Solder Joints

The experimental data shows that the crack growth rate is much slower for SnAg solder joints than SnPb joints. For example, for air-cooled joints at 6K (15K) cycles, the primary crack lengths at the package interface are 42% (91.8%) and 31.5% (51.2%) for SnPb and SnAg solder joints, respectively. The data shows that the ratio of the primary cracks at the board interface compared to the primary cracks at the package interfaces is almost 50% larger for SnAg solder joints than for SnPb joints. For example, for air-cooled SnPb joints up to 10K

cycles and SnAg joints up to 21K cycles, the mean ratios are 36% and 53%, respectively. Also the ratio of the secondary cracks compared to the primary cracks at the package interface is larger for SnAg solder joints than for SnPb joints at all thermal cycles. For example, for air-cooled joints at 6K cycles, the ratios are 12% and 30% for SnPb and SnAg joints, respectively.

The data presented in this section will be used for crack propagation predictions using FEM modeling. The FEM models are described in the following sections.

6.2. FEM CRACK PROPAGATION ANALYSIS

In this section, the FEM models are described and simulation results are presented to describe the effects of the multiple cracks in the joint on board warping, energy release rates and stress intensity factors are shown to better understand the crack propagation results.

6.2.1. FEM Models: Global and Joint

For crack propagation simulations, only global and joint FEM models were developed. The micro-model of Chapter 5, Section 5.3 was not used—instead, the measured mean %crack lengths from the experimental data were embedded into the joint model.

Global model

The global model in Figure 6.2(a) is the same model described in Chapter 5, Section 5.4, but the number of elements increased to a total of 3112 2D-plane strain elements and 3272 nodes. This increase of number of elements was needed to embed the measured cracks to the solder joints in the global model and to compute proper boundary conditions to be imposed on the joint model.

The joints represented in the global model are: inside region (joint1-K10, joint2-J11), inner boundary region (joint3-H12), boundary region (joint4-G13), outer boundary region (joint5-F14) and subsection of the outside region (joints 6-E15, 7-D16, 8-C17, 9-B18). Mean measured cracks (see Table 3.4—3.6, 3.14—16 in Changyoung Park's Master thesis [51]) were embedded into the model by removing the corresponding elements. Figure 6.3 shows FEM models showing removed elements to assure proper boundary conditions are imposed on the joint model. The removed elements in the joints represent cracks (from measured crack data) in SnPb aged joints.

Joint model

As shown in Figure 6.2(b), the displacement boundary conditions computed from the global model were applied to the nodes surrounding the solder joint, and temperature changes were applied uniformly to all nodes of the joint model. The joint model used here is different than the joint model used in Chapter 5 and is therefore referred to as the sub-model in this chapter. While the joint model is part of global model in Chapter 5 and, consequently, interacts with

the global model, here the joint sub-model takes displacement as input from the global model but does not feedback forces to the global model.

A single joint sub-model for joint 4-G13 was constructed of a total 2527 8-node plain strain elements and 7722 nodes. The surfaces along which the crack propagated are specified by SLAVE nodes and MASTER elements to define the separated surfaces and model two crack surfaces [76]. Measured cracks in Table 6.1 and 6.2 including primary and secondary cracks in both package and board interfaces were embedded into the model by removing the corresponding elements. Figure 6.2(b) shows the single joint sub-model used. Here, the corner joint in boundary region (G13, see Fig 2.2) was chosen since it has the largest crack propagation rate.

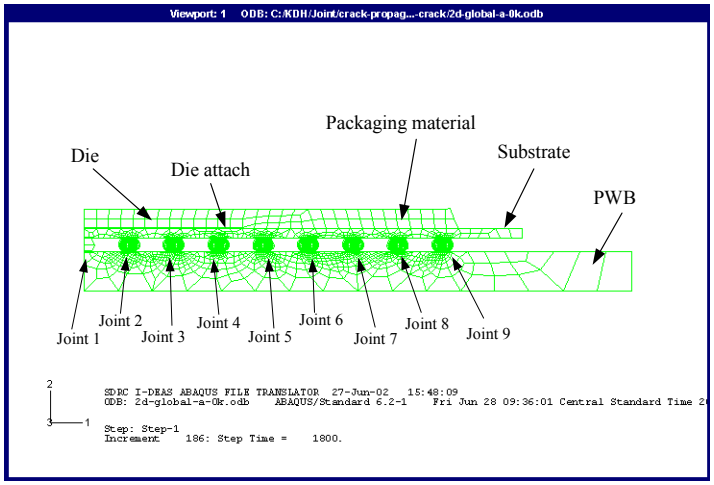

(a)

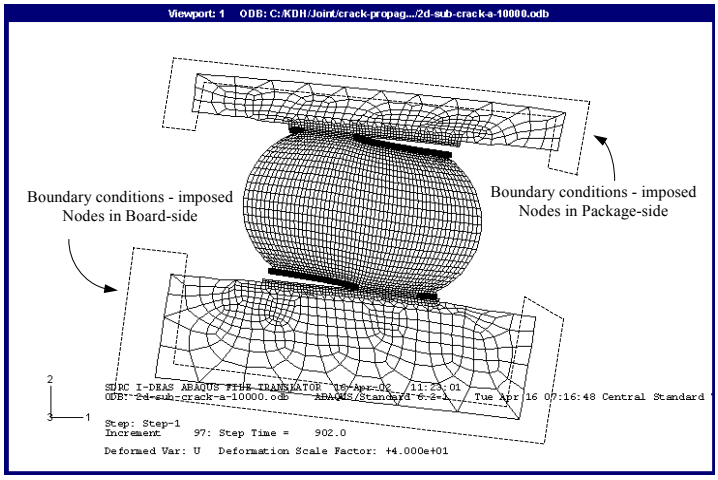

(b)

Figure 6.2. FEM models for crack propagation (a) global model, (b) joint sub-model

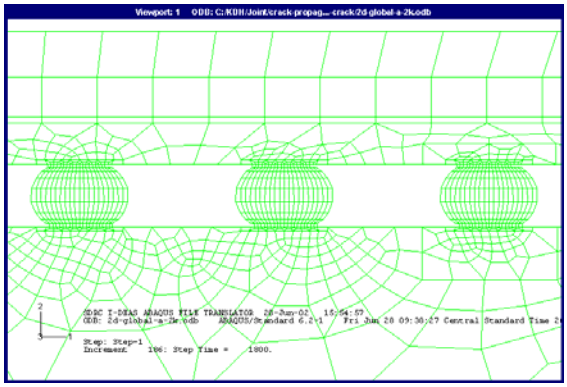

2K cycles

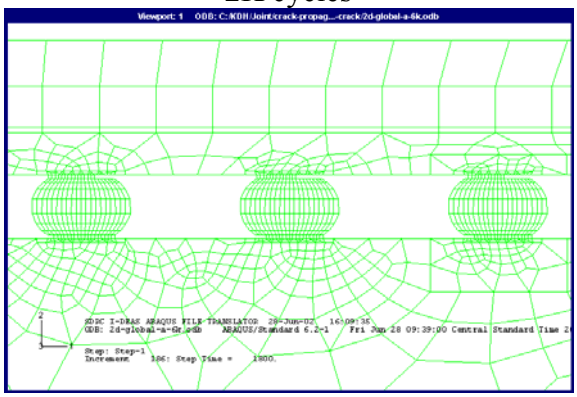

6K cycles

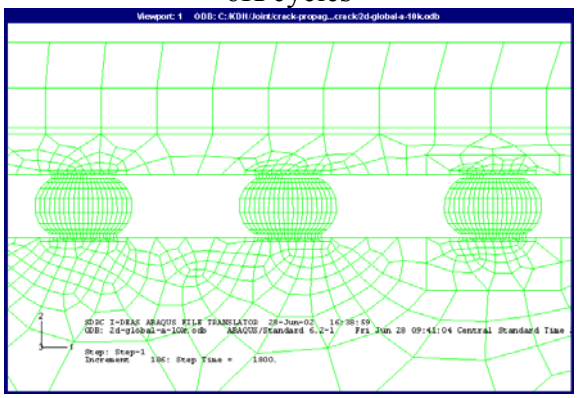

10K cycles

Figure 6.3. FEM crack propagation model showing removed elements in joints to represent cracks (from measured crack data) in SnPb aged joints 3, 4, 5 in the global model

The global and joint sub-models were used in several simulation studies to determine the effects of assumed boundary conditions (PWB warping) and crack locations on crack growth (energy release rates, stress intensity factors) as described below.

6.2.2. FEM Simulation: PWB Warping

As cracks grow, joint compliance increases and the amount of PWB warping decreases. The elements corresponding to the crack in each of the nine joints of the global model were removed from the global model as shown in Figure 6.3 and the changes in PWB warping were simulated. This was done for air-cooled SnPb solder joints to illustrate the effects of joint cracks on the compliance of the board assembly.

Figure 6.4 shows PWB displacements from the nodes located at the bottom of the PWB for the air-cooled SnPb joints in the 1-direction (longitudinal) and 2-direction (transverse) for different number of cycles (see Figure 6.2(a)). As expected, the longitudinal displacements measured from the neutral point (symmetry plane in Figure 6.2(a)) do not change for different cycles. However, the transverse displacements changed (decreased) by about 4 μm at the end of PWB due to lower stiffness compared to the deflection with no cracks. The joint sub-model was therefore run for the crack propagation study with these changing displacements at its boundaries.

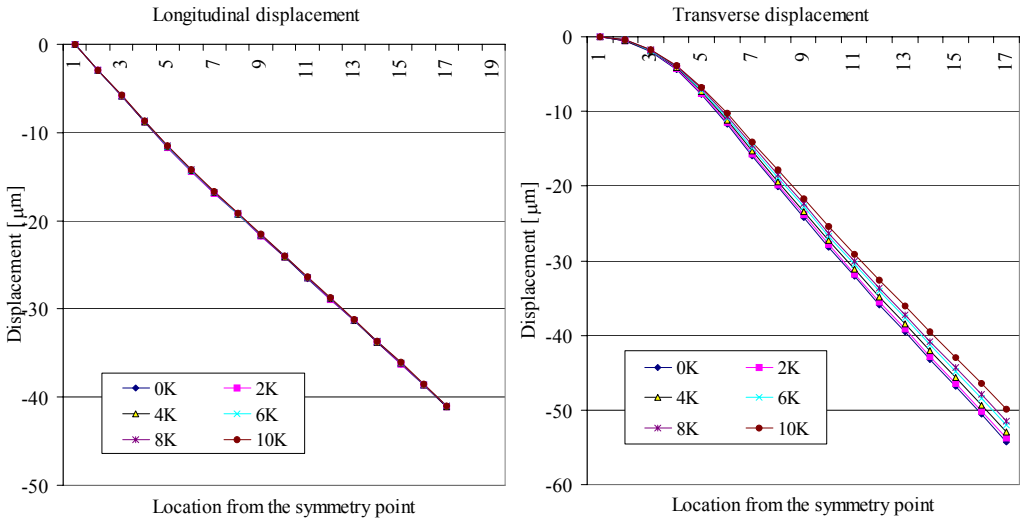

Figure 6.4. Simulated FEM PWB deformation (μm) in air-cooled SnPb joints at 0°C when subject to the 0-100°C ATC cycle

6.2.3. FEM Simulation: Crack Analysis in a Joint—Energy Release Rates and Stress Intensity Factors

The joint sub-model was used to calculate the energy release rates and stress intensity factors.

Energy release rate: J-integral

The crack propagation rate is a function of energy release rate [78], so the energy release rate at the crack tip was calculated from the joint model in Figure 6.2(b), where the measured mean % crack lengths from the experimental data for the primary and secondary cracks on the package and board interfaces were used. Using Paris' law [78], the crack propagation rate is related to the energy release rate as,

$$\frac{da}{dN} = C(\Delta J)^m \ [\mu m / cycle] \tag{6.1}$$

where ΔJ = Jmax - Jmin is the difference in energy release rate in a cycle [N / m]. The energy release rate, J, reaches maximum at the low temperature 0°C, since stress increases from its stress-free state at 100°C, and J reaches a minimum (≈0) when the temperature goes back to 100°C, its stress-free state. Therefore, the values in Figure 6.5 represent Jmax.

The energy release rate can be derived from the J-integral as

$$J = -\int_{\Gamma}\left(Wn_x - T_i\frac{\partial u_i}{\partial x}\right)ds \tag{6.2}$$

where W is the strain energy density, n_x is the x component of the unit vector normal to the contour, T_i is the traction, u_i is the displacement in the x or y direction, and Γ is the integration contour. The energy release rates of the primary cracks for joint4-G13 at the package interface, the largest of all cracks, were calculated in ABAQUS plotted for SnPb and SnAg joints. The assumed phase sizes were 9.5 micron and 4.5micron for aged and air-cooled SnPb joints, respectively.

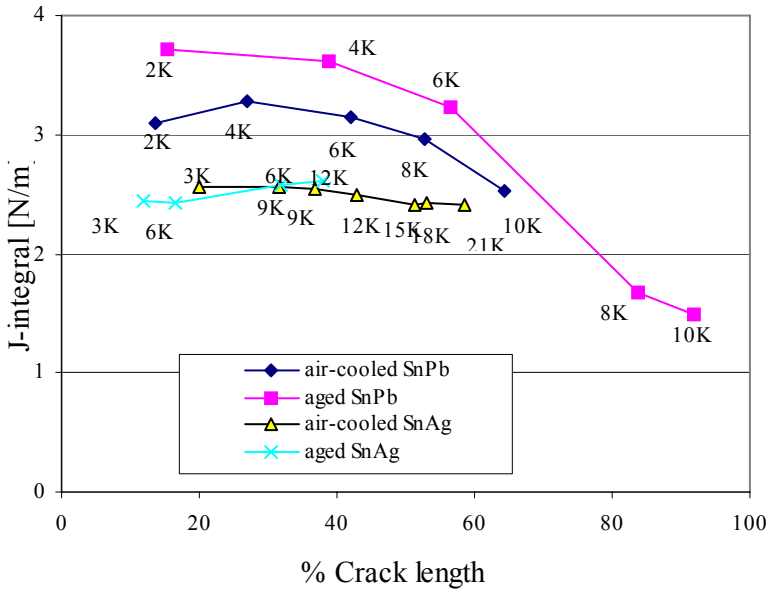

Figure 6.5. ABAQUS calculated energy release rates for joint4-G13 in SnPb and SnAg solders subjected to 0-100°C ATC test

Notice that although at 2K cycles, the crack lengths are similar for aged and air-cooled SnPb solder, the energy release rate is different because of the differences in phase sizes. Also notice that although the air-cooled joints show only 65% crack at 10K and its life is only about 12K cycles, the plot does not take into account that there is a secondary crack growth that merges at the end.

Note for the aged SnAg case, the cracks do not grow significantly after 12K cycles (see 15K, 18K, 21K, 24K data in Table 6.2). Note that the energy release rate is same for SnAg joints because the constitutive equation (see Eq.

5.17 in Chapter 5) for SnAg joints has no parameter that differentiates air-cooled joints from aged joints.

Figure 6.5 shows energy release rates for different % crack lengths in SnPb and SnAg joints. Aged SnPb joints have approximately 30% larger energy release rates than air-cooled joints–hence a faster crack growth. The rate decreases rapidly after 60% crack length, which is consistent with Figure 6.1 which shows crack growth rate decreasing after 8K cycles. For air-cooled SnPb joints, the energy release rate decreases after about 30% crack length, but the decrease is less than that for aged joints because the air-cooled primary crack merged with the secondary crack before the energy release rate decreased further—this is expected to occur between 10K and 15K cycles from life data. While intermediate crack data was not available, but at 15K cycles crack data confirmed the merged cracks. Therefore, the primary crack at the package interface of the air-cooled joint keeps growing at approximately at the same rate as shown in Figure 6.1. The energy release rates of SnAg joints are smaller and remain relatively constant, and the smaller rates result in slower crack growths as shown in Figure 6.1.

It was found that the energy relase rate is sensitive not only to solder type and aging but also to number of thermal cycles. Number of themal cycles changes the joint crack size and, consequently the joint compliance.

Table 6.3. Mean % crack length in aged and air-cooled SnPb joint 4-G13 and energy release rate, 0-100°C ATC, UT (nominal diameter: 560 μm-PI and 584 μm-BI). Mean % crack length data from Table 6.1.

No. cycles	Aged SnPb joint		Air-cooled SnPb joint	
	% Crack length P-PI	Jmax [N/m]	% Crack length P-PI	Jmax [N/m]
2k	15.5	3.7	13.5	3.1
4k	38.9	3.7	26.9	3.1
6k	56.4	3.6	42.1	3.3
8k	83.9	3.2	52.8	3.2
10k	92.0	1.7	64.4	3.1

PI =package interface and P =primary crack

Table 6.4. Mean % crack length in aged and air-cooled SnAg joint 4-G13 and energy release rate, 0-100°C ATC, UT (nominal diameter: 560 μm-PI and 584 μm-BI). Mean % crack length data from Table 6.2.

No. cycles	Aged SnAg joint		Air-cooled SnAg joint	
	% Crack length P-PI	Jmax [N/m]	% Crack length P-PI	Jmax [N/m]
3K	11.9	2.4	19.9	2.6
6K	16.4	2.4	31.5	2.6
9K	32.0	2.4	36.7	2.6
12K	38.0	2.6	43.0	2.5
15K			51.2	2.5
18K			52.9	2.4
21K			58.6	2.4

PI =package interface and P =primary crack

Table 6.5. Estimated constants in crack propagation rates of SnPb and SnAg joints defined by Paris' Law (Equation 6.1) derived from joint sub-model

	SnPb/Aged	SnPb/Air-cooled	SnAg/Aged	SnAg/Air-cooled
C	0.0155	0.0105	0.00134	0.00232
M	1.1	1.1	1.9	1.9

Using the measured % crack length and the calculated energy release rate from the joint sub-model, the crack propagation constants in Paris's law (Eq. 6.1) were computed using regression in Microsoft Excel and tabulated in Table 6.5. Here, m was assumed to be constant for solder, and C was curve-fit using a least-mean-squares algorithm to the plot of J integral and crack growth rate and derived to satisfy different crack propagation rates for different post-process conditions.

Table 6.5 shows the differences in crack growth rate parameters (thereby crack growth) between SnPb and SnAg joints and also between aged and air-cooled joints (for 357-PBGA and 0-100^{o}C ATC). For SnPb joints, aged joints have faster crack growth rate, while air-cooled joints have faster growth rate for SnAg joints. Here, the slower crack growth rate in aged SnAg joints is suspected to have been due to resin cracks (see section Chapter 3). Also the exponent, m, of SnAg joints is larger than for SnPb, which means the crack growth rate of SnAg joint is more crack-sensitive (less tough) than SnPb joints. Therefore, SnAg life

SnAg joints under the 0-100^{o}C tests is longer than SnPb joints as the cracks propagate slower, albeit are more to external loading.

Stress intensity factor

Stress intensity factors were used to analyze the relative contribution of each loading mode—tensile (Mode 1) or shear (Mode 2)—to the joint crack propagation. Recall from the previous section, the J-integral method was used as a quantitative means to compare crack propagation rates between solders and aging conditions. In this section, the stress intensity factor is introduced as a qualitative means for comparing load-mode analysis.

As the test vehicles are thermally cycled, the solder joints have two different loading modes—Mode 1 and 2. Since solder joints typically fail due to the CTE mismatch between the die and the board, Mode 2 or the shear load is dominant. However, as cracks propagate, the relative contributions from the two loading modes to crack growth evolve. Stress intensity factors at the crack tip were computed to illustrate how the loading modes change for different crack sizes, and they are defined as [78]

$$K_i = \sigma_i \sqrt{\pi a} \tag{6.3}$$

where σ_i is the stress in the i-direction and a is crack length.

Figure 6.6 shows the evolution of stress intensity factors for K1 (tensile load), K2 (shear load), and effective K, $\sqrt{K_1^2 + K_2^2}$ as computed by ABAQUS in

SnPb and SnAg joints. These calculated stress intensity factors are listed in Tables 6.6 and 6.7 for SnPb and SnAg, respectively.

As cracks grow, the energy release rate decreases due to lower joint compliance (shown in Figure 6.5). Likewise, the K2 stress intensity factor for the shear mode decreases and the effective stress intensity factor decreases. However, the simulated data shows that the contribution of tensile load generally increases as cracks grow. For air-cooled SnPb joints, the shear load is dominant at the beginning of crack growth, but as cracks grow the tensile mode increases while the shear mode decreases–converging at ~65% crack length. Similar trends were observed from air-cooled and aged SnAg joints. These observations imply cracks initiate and propagate mainly due to shear stress caused by the CTE mismatch between die and PCB, but as cracks grow in size, the effect of tensile stress on crack propagation increases. The stress intensity factor K2 in aged SnPb joints decreases from 3.2 to 1.7 MPa$\sqrt{mm}$ because the crack length of 92% reduces the amount of shear stress in the joint. K1 is also decreases from 6.2 (crack length 56%) to 5.2 (crack length 92%).

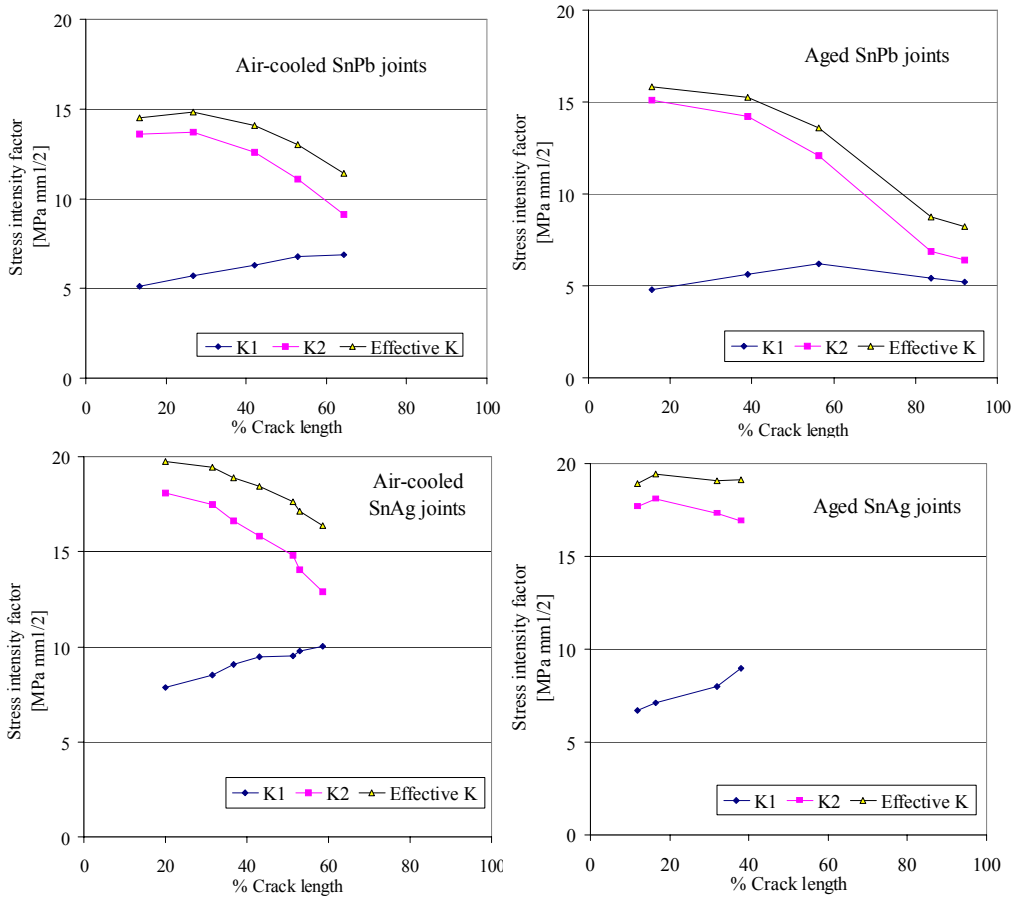

Figure 6.6. ABAQUS-calculated simulated FEM stress intensity factor versus % crack length for SnPb and SnAg joint4-G13 subjected to 0-100°C ATC

Table 6.6. ABAQUS-calculated mean % crack length in aged and air-cooled SnPb G13 joint and stress intensity factors K1 under tensile load, K2 under shear load, and Keff, effective stress intensity factor, units: MPa$\sqrt{mm}$ for 0-100°C ATC, UT (nominal diameter: 560 μm-PI). Mean % crack length data from Table 6.1.

	Aged SnPb joint				Air-cooled SnPb joint			
No. cycles	% Crack P-PI	K1	K2	Keff	% Crack P-PI	K1	K2	Keff
2k	15.5	4.8	15.1	15.8	13.5	5.1	13.6	14.5
4k	38.9	5.6	14.2	15.3	26.9	5.7	13.7	14.8
6k	56.4	6.2	12.1	13.6	42.1	6.3	12.6	14.1
8k	83.9	5.4	6.9	8.8	52.8	6.8	11.1	13.0
10k	92.0	5.2	6.4	8.2	64.4	6.9	9.1	11.4

PI =package interface and P =primary crack

Table 6.7. ABAQUS-calculated mean % crack length in aged and air-cooled SnAg G13 joint and stress intensity factors K1 under tensile load, K2 under shear load, and Keff, effective stress intensity factor, units: MPa$\sqrt{mm}$ for 0-100°C ATC, UT (nominal diameter: 560 μm-PI). Mean % crack length data from Table 6.2.

	Aged SnAg joint				Air-cooled SnAg joint			
No. cycles	% Crack P-PI	K1	K2	Keff	% Crack P-PI	K1	K2	Keff
3K	11.9	6.7	17.7	18.9	19.9	7.9	18.1	19.7
6K	16.4	7.1	18.1	19.4	31.5	8.5	17.5	19.5
9K	32.0	8.0	17.3	19.1	36.7	9.1	16.6	18.9
12K	38.0	9.0	16.9	19.1	43.0	9.5	15.8	18.4
15K					51.2	9.5	14.8	17.6
18K					52.9	9.8	14.1	17.1
21K					58.6	10.0	12.9	16.4

PI =package interface and P =primary crack

Based upon the results given above, the FEM models were run to investigate the effects of secondary cracks in a joint and the displacement boundary conditions imposed on a joint.

Effects of secondary crack

Experimental data in Figure 6.1 show that solder joints fail mainly due to the growth of the primary crack at the package interface, whether secondary cracks exist or not. At first glance, the effects of secondary cracks at the package interface seem negligible since they grow to at most 20%. However, recall that aged SnPb joints had demonstrated secondary cracks and the growth rates of the primary cracks at the package interface decreased significantly after 8K cycles. Figure 6.7 shows dye-penetrated images of the primary cracks in corner joint G7 for different number of thermal cycles. The images show the primary crack growth rate decreases at ~80% crack length when there is no secondary crack as in aged SnPb, however, the rate is rather constant during a joint life when there are secondary cracks as in air-cooled SnPb joints. This is because the secondary cracks merge with the primary cracks and, consequently, the primary crack grows rather linearly with cycles. This explains why the effects of secondary cracks need attention.

To investigate the effects of secondary cracks on joint life, FEM simulations were run for aged SnPb joints with and without secondary cracks

embedded. Here, life was calculated and compared based on crack propagation life from an initial 15.5% to final 100% primary crack length.

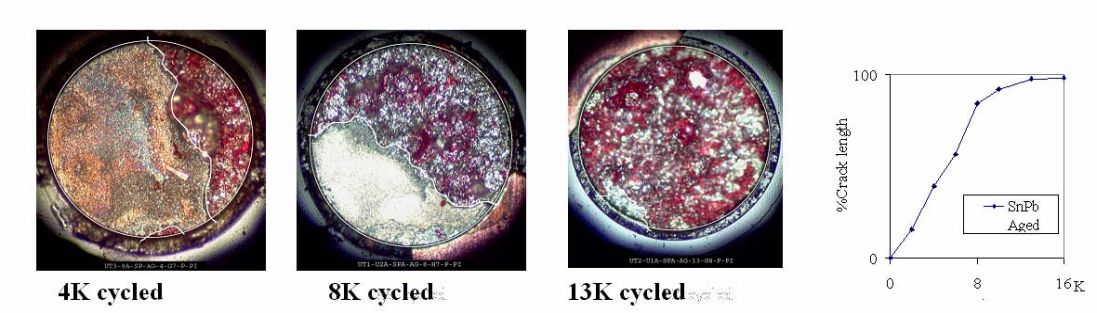

(a)

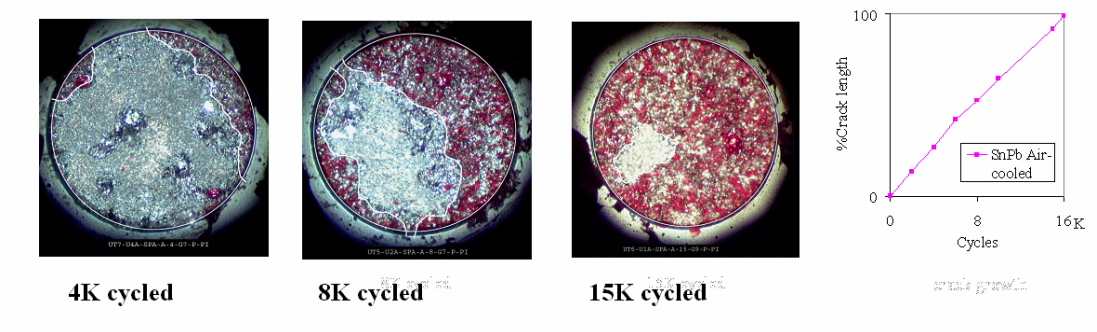

(b)

Figure 6.7. Dye-penetrated pictures for crack growth and plot of primary crack at the package interface of SnPb joint G13 subjected to 0-100°C ATC test cycles (a) aged SnPb (b) air-cooled SnPb (dark areas represent cracks)

Figure 6.8 shows the energy release rates for joints with and without secondary cracks. For aged SnPb joint with secondary crack, the energy release rates were calculated up to 85% crack length since the secondary crack (15% length) merged with the primary crack. Using the crack growth model in Equation

(6.1) and corresponding constants from Table 6.5 and assuming joints fail when 100% crack occurs, life for the joints with the secondary crack was 6521 cycles, while life for the joints without secondary cracks was 9783 cycles—an increase of 50%. Table 6.8 shows changes in life with J integral. For example, for an aged SnPb joint without a secondary crack, the life spent during crack growth from 15.5% to 38.9% is derived from Eq. 6.1 by inserting the J integral, 3.7N/m, and the constants, c=0.0155 and m=1.1.

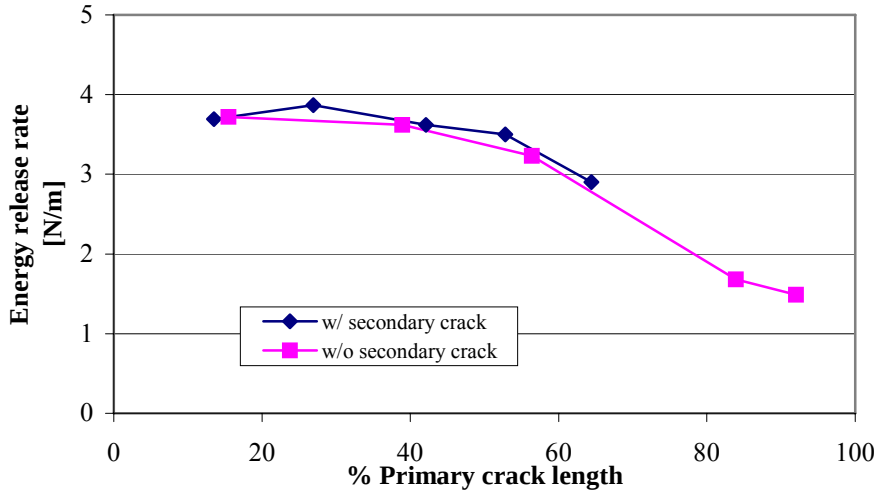

Figure 6.8. ABAQUS-calculated J-integral FEM analysis in aged SnPb joints with and without secondary crack subjected to 0-100°C ATC test cycles

Table 6.8. ABAQUS-calculated J-integral and the life comparison in aged SnPb G13 joints with and without secondary crack subjected to 0-100°C ATC test cycles(nominal diameter: 560 μm-PI). Mean % crack length data from Table 6.1.

	Aged SnPb joint with secondary crack				Aged SnPb joint without secondary crack			
No.	% Crack P-PI	J [N/m]	ΔLife ($crack_{n+1}$ – $crack_n$)	Accum. life	% Crack P-PI	J [N/m]	ΔLife ($crack_{n+1}$ – $crack_n$)	Accum. life
1	15.5	3.7	1993	1993	15.5	3.7	980	980
2	38.9	3.9	1536	3529	26.9	3.6	1239	2219
3	56.4	3.6	2736	6265	42.1	3.2	939	3158
4	83.9	3.5	1654	7919	52.8	1.7	1056	4214
5	92.0	2.9	1864	**9783**	64.4	1.5	2307	**6521**
6	100				85*			

Note: * it was assumed that when the primary crack reached 85%, it merged with the secondary crack to give 100% crack length

If joints with two cracks at the package interface, such as air-cooled SnPb and SnAg joints or aged SnAg joints, are designed to suppress the secondary cracks, life is expected to increase (see Chapter 5 for why secondary crack does not form). This simulation result implies increased joint life can be achieved without secondary cracks—but this conclusion contradicts the experimental results that showed aged solder joints, which have no secondary crack, failed earlier than air-cooled SnPb solder joint which have secondary cracks. However, the primary cause of the earlier failures of aged SnPb solder joint is believed to be due to different microstructure through aging (see Chapter 3 Section 3.3.1).

Effects of boundary conditions

When the fracture mechanics approach is applied to solder joints for life prediction and propagation analysis, constant boundary conditions, which are derived assuming initial conditions of no cracks in the joints, are typically imposed on the joints. J.H. Lau and D.W. Rice [44] applied constant boundary conditions to their FEM solder joint model in flip chip package, and J.H. Lau and C. Chang [25] also used constant boundary conditions for the solder joint in chip scale packages. It seems that applying constant boundary conditions based on the CTE mismatch between die and PWB is an accepted practice for flip-chip and chip-scale packages, since the solder joints lie between the die and PWB. However, for PBGA package, the solder joints lie between the substrate and PWB, and the amount of PWB warping changes as cracks grow, as shown in Figure 6.4. Therefore, the conjecture is that crack propagation analysis results will vary with boundary conditions: constant boundary conditions versus PWB displacements caused by increased cracks.

To study the effects of boundary conditions on crack propagation rates, two different boundary conditions were generated from the global model: with and without cracks. Figure 6.9 and Table 6.9 shows that for aged SnPb joints, the calculated energy release rate, J, is much larger for the case in which actual cracks are embedded than for the case of constant boundary condition based upon a no-crack-assumption. The predicted life using Eq. (6.1) and Table 6.5 gives 9783 cycles using the actual boundary condition versus 63258 cycles under the constant boundary condition assumption.

For life calculation and comparison, the crack growth model in Eq. (6.1) and corresponding constants, c=0.0155 and m=1.1, from Table 6.5 were used. Initial crack sizes of 15.5% were chosen based upon data from Table 6.3, and joints were assumed to fail when 100% crack length occurred.

As shown in Table 6.9, the energy release rate of joints that use boundary conditions without cracks are much smaller than release rates for joints with imposed cracks in the boundary conditions. This is because without cracks the boundary conditions cannot generate enough stress for cracks to propagate in the solder joints as those conditions do not change with increasing crack sizes and, hence, results in smaller energy release rates and life increases unrealistically.

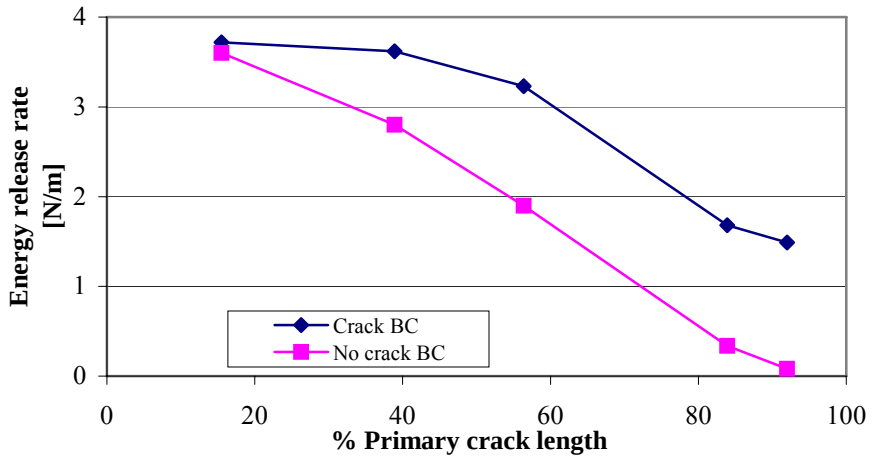

Figure 6.9. ABAQUS-calculated J-integral analysis in aged SnPb G13 joint subjected to 0-100°C ATC test cycles comparing two boundary conditions: no crack and with cracks

Table 6.9. ABAQUS-calculated J-integral and the life comparison in aged SnPb G13 joint between two boundary conditions: no crack and with cracks, subjected to 0-100°C ATC test cycles (nominal diameter: 560 μm-PI). Mean % crack length data from Table 6.1.

	Aged SnPb joint with BC, with cracks				Aged SnPb joint with BC, no cracks			
No.	% Crack P-PI	J [N/m]	ΔLife (crack_n+1 – crack_n)	Accum. life	% Crack P-PI	J [N/m]	ΔLife (crack_n+1 – crack_n)	Accum. life
1	15.5	3.7	1993	1993	15.5	3.6	2066	2066
2	38.9	3.9	1536	3529	38.9	2.8	2037	4103
3	56.4	3.6	2736	6265	56.4	1.9	4904	9007
4	83.9	3.5	1654	7919	83.9	0.34	9587	18594
5	92.0	2.9	1864	**9783**	92.0	0.083	44664	**63258**
6	100				100			

Effects of primary crack at the board interface

The primary cracks at the board interface are the second largest in the joints after the primary cracks at the package interface, but they are not the typical source of package failure [56]. However, multiple cracks in the joint geometry and mixed loading modes can affect each other. Recall that the ratio of primary cracks at the board interface compared to the package interface was larger for SnAg solder joints than SnPb joints. To study the effects of board interface cracks on the package interface, air-cooled SnPb joints with 42% primary crack length at the package interface and 7% and 14% primary crack lengths at the board interface (no secondary cracks on either interface) were simulated to compare energy release rates. The results showed the energy release rates of 3.65 N/m and

3.45 N/m for the joints with 7% and 14% crack at the board interface, respectively. The increase of the primary crack size at the board interface from 7% to 14% decreases the energy release rate of the primary crack at the package interface by 6%, implying that crack growth at board interface may be *slightly* beneficial. A larger primary crack at the board interface appears to increase joint compliance thereby reduces the stress imposed on the primary crack at the package interface.

6.3. SUMMARY

Based upon experimental data:

- Primary and secondary cracks propagated through the package and board interfaces of the joints except at the package interface of aged SnPb joints, where no secondary cracks evolved.
- The crack growth rates at the package interface were larger by ~200% for SnPb and ~100% for SnAg than at the board interface, and the package interface is the location for typical joint failures.
- For SnPb, aged joints had ~50% larger crack growth rates than non-aged SnPb joints, while aged SnAg joints had ~40% smaller crack growth rates than non-aged SnAg joints. SnPb joints had ~100% faster crack growth rates than SnAg joints, implying earlier failure.
- The primary crack growth rate at the package interface decreased as the crack grew. For aged SnPb joints, the crack grew approximately at a constant rate of 10%/K cycles until 8K cycles (84% length), then the rate

decreased to ~3%/K cycles to 13K cycles (98% length) and was nearly zero after 13K cycles.

- While the primary crack at the package interface was the largest crack and the one that ultimately leads to package failure (in combination with the secondary crack), the other cracks are significantly larger in proportion to the primary crack in SnAg solder joints than in SnPb solder joints.
- The ratio of the primary crack lengths at the board to package interfaces were ~50% larger in SnAg solder joints (20~65%) than for SnPb joints (10~37%).
- The ratio of the secondary cracks relative to the primary cracks at the package interface was ~100% larger for air-cooled SnAg solder joints than air-cooled SnPb joints.

Based upon FEM simulations:

- Applying constant no-crack boundary conditions to the crack propagation model significantly overestimated joint life. PWB warping decreased as cracks grew—therefore, the boundary conditions for analyzing crack propagation should reflect these compliance changes.
- The primary crack growth rate at the package interface decreased as the crack grew. Therefore, joint life increased by ~50% if there was no secondary crack to merge with the primary crack.

- A larger primary crack at the board interface appeared to increase joint compliance thereby reduceing the stress imposed on the primary crack at the package interface.
- Shear load was a major cause of crack growth, but the contribution of tensile load increased up to almost 80% of shear load as crack grew. The primary crack at the board interface slightly decreased the growth rate of the primary crack at the package interface.

CHAPTER 7

ATC Life Tests and Life Prediction Modeling

Chapters 3 and 4 focus on the experimental results of microstructrual analysis and joint crack evolution for SnPb and SnAg solder joints exposed to three post-process conditions (aged, air-cooled, quenched), thermally cycled at 0-100°C at UT. Chapters 5 and 6 focus on the experimental results and FEM modeling/ analysis of crack initiation and propagation, respectively, of SnPb and SnAg solder for a subset of the experimental data—joints having the largest cracks in the boundary region of single-dense package layout exposed to 0-100°C ATC test cycles at UT. Chapter 7 presents life-cycle studies for SnPb and SnAg solder joints with 1) four package layouts (single-dense, single-sparse, double-alternating, double-dense), three ATC test protocols (0-100°C, -40-125°C, and -55-125°C) at Motorola test location and 2) single-dense package layout, 0-100°C ATC test, at UT test location. All the knowledge gained from these chapters and the experimental data are used to develop life-cycle prediction models of SnPb and SnAg solder joints. A severity metric, which estimates damage to the solder joints, is proposed to link material properties and parameters associated with package layout and thermal conditions to the time-dependent creep, time-independent plastic deformation, and a time-dependent and geometric effective stress of the solder joint, which is computed from the ATC parameters of temperature limits, dwell-time, and ramp rates, and from the package-on-board

configurations. The life-prediction based on the severity metric is compared with widely-used reliability models using internal and external data for validation.

7.1. EXPERIMENTAL SOLDER JOINT LIFE RESULTS

Experimental solder joint life tests were run at two different locations (UT and Motorola) due to the availability and capabilities of the test equipment. As discussed in Chapter 2, the boards were monitored for joint failure by event detectors. Life-cycle effects of solder type, post-processing, board layout, ATC test protocol, and test location were experimentally determined in this study.

7.1.1. UT Solder Joint Life Tests

Six unslotted boards (each board has 15 packages—single-dense layout) and 18 strips (each strip has three packages) were monitored for life studies at the UT facilities. The UT test parameters were as follows (see Appendix B, Table B-1 for Test Matrix):

- 0-100^{o}C ATC tests
- Single-dense (SD) package layout
- SnPb: aged, air-cooled, and quenched (1 board, 3 strips each)
- SnAg: aged, air-cooled, and quenched (1 board, 3 strips each)

The complete set of life data is presented in Appendix G (Note failure detection Criterion 4 was used to define life for SnAg solder joints).

7.1.1.1. UT Life: SnPb vs. SnAg solder

The mean life for SnPb packages were 10994 (24 packages), 12800 (23 packages), and 12244 cycles (24 packages) for aged, air-cooled and quenched packages, respectively, for the single-dense layout, 0-100^{o}C ATC tests at UT. For SnAg packages, the mean life was 41236 (12 packages), 23252 (11 packages), and 22850 cycles (24 packages) for aged, air-cooled, and quenched packages, respectively, for the same test conditions. Table 7.1 lists the mean life, standard deviation. and cycle number of the first and last package failures. The Student t-test [79] with 95% confidence interval was run on the data and Table 7.2 summarizes the results—for both SnPb and SnAg solders, the mean life for aged packages is statistically different from the air-cooled and quenched packages, but the mean between the air-cooled and quenched packages are not statistically different. The aged packages failed slightly earlier than the non-aged package for SnPb solder, but failed significantly later than the non-aged packages for SnAg solder. Note the aged SnAg joints had resin cracks that reduced solder joint stresses and increased their life (See Section 3.3.3 in Chapter 3).

Table 7.1. Mean and standard deviation of measure cycles-to-package failure: 0-100°C ATC, single-dense, UT cycling

Solder Type	Aging	No. Package	1st Failure Cycle	Last Failure Cycle	Mean Life Cycle (Std)
SnPb	Aged	24	7566	15177	10994 (1657)
	Air	23	9884	15620	12800 (1452)
	Quen.	24	9840	15042	12244 (1432)
SnAg	Aged*	12	29485	48351	41236 (6020)
	Air	11	12487	31989	23252 (6279)
	Quen.	24	14615	31383	22850 (3947)

Table 7.2. Paired student t-test results (95% confidence level): comparing mean life between different post-processing during manufacturing (data from Table 7.1) (bold indicates pairs of data which are statistically significantly different from each other)

	Aged & Air-Cooled	Aged & Quenched	Quench & Air-Cooled
SnPb	**921**	**375**	-328
SnAg	**13682**	**14741**	-3352

Note: bold shows statistically significant

When compared with the life of SnPb solder joints as references, Table 7.3 shows that SnAg solder joints had ~80% longer lives than air-cooled and quenched SnPb joints and over 300% longer life for aged SnPb joints.

Table 7.3. Acceleration factor as a function of post-processing conditions for 0-100°C ATC, single dense, UT cycling

Post Processing	SnPb		SnAg		Ratio $\frac{Life_{SnAg}}{Life_{SnPb}}$
	No. Fails	Mean Life, cycles (STD)	No. Fails	Mean Life, cycles (STD)	
Aged	24	10994 (1657)	12	41236 (6020)	3.75
Air-cooled	23	12800 (1452)	11	23252 (6279)	1.82
Quenched	24	12244 (1432)	24	22850 (3947)	1.87

7.1.1.2. UT Life: Post-Processing

Using air-cooled life as a basis for comparison, Table 7.4 shows that air-cooled and quenched packages for both SnAg and SnPb packages have similar mean life, are within 4% of each other and are not statistically different (see Table 4.4). However, aged SnPb packages failed 14% earlier than non-aged SnPb packages but failed 76% later than non-aged SnAg packages.

Table 7.4. Acceleration factor of aged and quenched packages relative to air-cooled packages for 0-100°C ATC, single-dense, UT cycling

ATC Test		No. Failures	Avg. Life, cycles (STD)	Ratio $Life/Life_{air}$
SnPb	Aged	24	10994 (1657)	0.86
	Air-cooled	23	12800 (1452)	1
	Quenched	24	12244 (1432)	0.96
SnAg	Aged	12	41236 (6020)	1.77
	Air-cooled	11	23252 (6279)	1
	Quenched	24	22850 (3947)	0.98

A Weibull plot [80] in Figure 7.1 shows that the Characteristic Life Cycle (CLC) (typically used in industry) of aged, air-cooled, and quenched packages at

a 63.2% failure rate is 11649, 13376, and 12827 cycles, respectively, for SnPb solder joints, and 43816, 25652, and 24407 cycles, respectively, for SnAg packages. The CLC life for SnAg non-aged packages are almost twice their non-aged SnPb counterparts, and nearly four times for aged SnPb packages. The non-aged SnPb packages have a 1.1-1.15 AF (Acceleration Factor) over the life of aged SnPb packages, and the aged SnAg packages have approximately 1.7 AF over the life of non-aged SnAg packages.

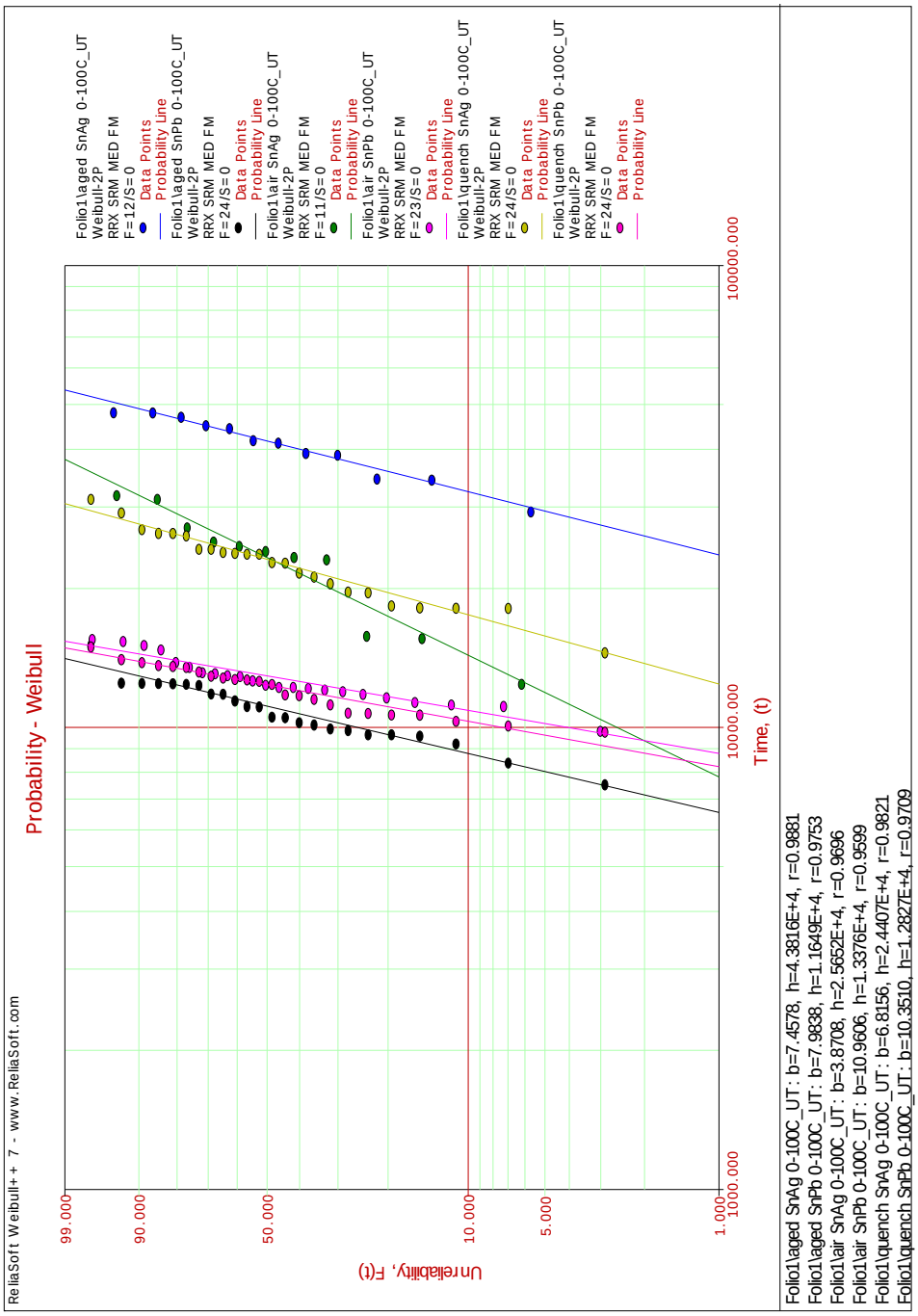

Figure 7.1. Weibull plot for aged, air-cooled, and quenched SnPb and SnAg packages: 0- 100°C ATC, single-dense, UT cycling

7.1.1.3. UT Life: False Failures and Failure Criterion

According to the industry-standard failure criterion of IPC-9701 [53], failure is defined as the first interruption of electrical continuity recorded by an event detector that is confirmed by nine additional interruptions within an additional 10% of the total cycles leading up to the first interruption. Applying this failure criterion to the SnAg packages generated premature false failures that were not confirmed with resistance measurements and destructive dye-penetration crack measurements. As a result, additional failure criteria were proposed and the following-criterion adopted for cycles-to-failure (see Appendix D for more details and comparisons of various proposed criteria).

The failure criterion used to generate the UT data above uses the .dat file. Failure is defined as the cycle of the first event in a data file with nine additional events in that data file, followed by two consecutive data files showing 10 events in the first two cycles of those data files. The rationale for this criterion is that once a package has failed the event detector should indicate failure very quickly in subsequent data files.

7.1.2. Motorola Solder Joint Life Tests

Thirty-six unslotted boards, all with air-cooled post processing, were monitored for life at the Motorola Ed Bluestein facilities. The test parameters were as follows (see Appendix B, Table B.2 for complete Test Matrix)—three

ATC tests, package layouts noted, and air-cooled post processing (number in parentheses denote number of boards) :

0^{o}C-100 ^{o}C ATC test

SnPb: SD (4), SS (3), DD (1), DA (1)

SnAg: SD (3), SS (3), DD (1), DA (1)

-40 ^{o}C -125 ^{o}C ATC test

SnPb: SD (4), SS (3), DD (1), DA (1)

SnAg: SD (3), SS (3), DD (1), DA (1)

-55 ^{o}C-125 ^{o}C ATC test

SnPb: SD (1)

SnAg: SD (1)

The complete set of measured data is given in Appendix H.

7.1.2.1. Motorola: ATC Test Protocols (see Figure 2.7, Chapter 2)

The goal of accelerated cycling tests is to accurately predict package life (in terms of thermal cycles) while minimizing test times. The test results for air-cooled, single-dense boards, and different ATC test conditions, listed in Table 7.5, show that compared to packages exposed to the 0-100^{o}C ATC test, packages exposed to the -55-125°C LLTS (Liquid-to-Liquid Thermal Shock) and the -40-125°C ATC tests had only 0.22 and approximately 0.29 (0.25-0.33) the life of the comparable SnPb bords, respectively.

Table 7.5. Comparison of ATC tests: air-cooled SnPb and SnAg, single-dense, Motorola

ATC Test		No. Failures	Avg. Life, cycles (STD)	Ratio Life/Life$_{0\text{-}100C}$
SnPb	0-100°C	26	12160 (810)	1
	-40-125°C	29	3970 (440)	0.33
	-55-125°C	13	2850 (270)	0.23
SnAg	0-100°C	25	16260 (2500)	1
	-40-125°C	26	4020 (1420)	0.25
	-55-125°C	13	3370 (500)	0.21

As shown in Table 7.6, life results for the -40-125^{o}C and -55-125^{o}C ATC tests are statistically different than the 0-100^{o}C ATC test results for both SnPb and SnAg joints. However, life results for the -55-125^{o}C ATC test are statistically different from the -40-125^{o}C test results for SnPb and SnAg solder joints.

Table 7.6. Paired student t-test results (95% confidence level): comparison of mean life between different ATC test conditions and solders (computed using JMP). (bold indicates pairs of data which are statistically significantly different from each other)

ATC Test and Type of Solder	0-100^{o}C SnPb	-40-125^{o}C SnPb	-55-125^{o}C SnPb	0-100^{o}C SnAg	-40-125^{o}C SnAg	-55-125^{o}C SnAg
0-100^{o}C SnPb	-735	**7480**	**8415**			
-40-125^{o}C SnPb	**7480**	-696	**235**			
-55-125^{o}C SnPb	**8415**	**235**	-1039			
0-100^{o}C SnAg				-749	**9855**	**11983**
-40-125^{o}C SnAg				**9855**	-933	-950
-55-125^{o}C SnAg				**11983**	-950	-1039

Note: bold shows statistically significant

7.1.2.2. Motorola: Package Layout

Data from the four package layouts of air-cooled boards exposed to the 0-100°C and -40-125°C ATC tests are shown in Figure 7.2 and Table 7.7. The mean life of the singe-dense package layout was used as the reference in Table 7.7. The data shows for SnPb solder and:

- -40-125°C ATC test (3970 mean life (cycles) of single-dense layout)

  The mean life for single-sparse and double alternating layouts were only +2/-4% different, respectively, than the reference single-dense case
- 0-100°C ATC test (12160 mean life (cycles) of single-dense layout)

  The mean life for single-sparse and double alternating layouts were -4/-15% different, respectively, than the reference single-dense case
- The mean life of double-dense layouts were only 26% and 32% of the reference single-dense case for 0-100°C and -40-125°C ATC tests, respectively.

The data shows for SnAg solder and:

- 40-125^{o}C ATC test (5462 mean life (cycles) of single-dense layout)

  The mean life for single-sparse and double alternating layouts were only +1/+28% different, respectively, than the reference single-dense case
- 0-100^{o}C ATC test (16260 mean life (cycles) of single-dense layout)

  The mean life for single-sparse and double alternating layouts were -4/-10% different, respectively, than the reference single-dense case

- The mean life of double-dense layouts were only 41% and 28% of the reference single-dense case for 0-100°C and -40-125°C ATC tests, respectively.

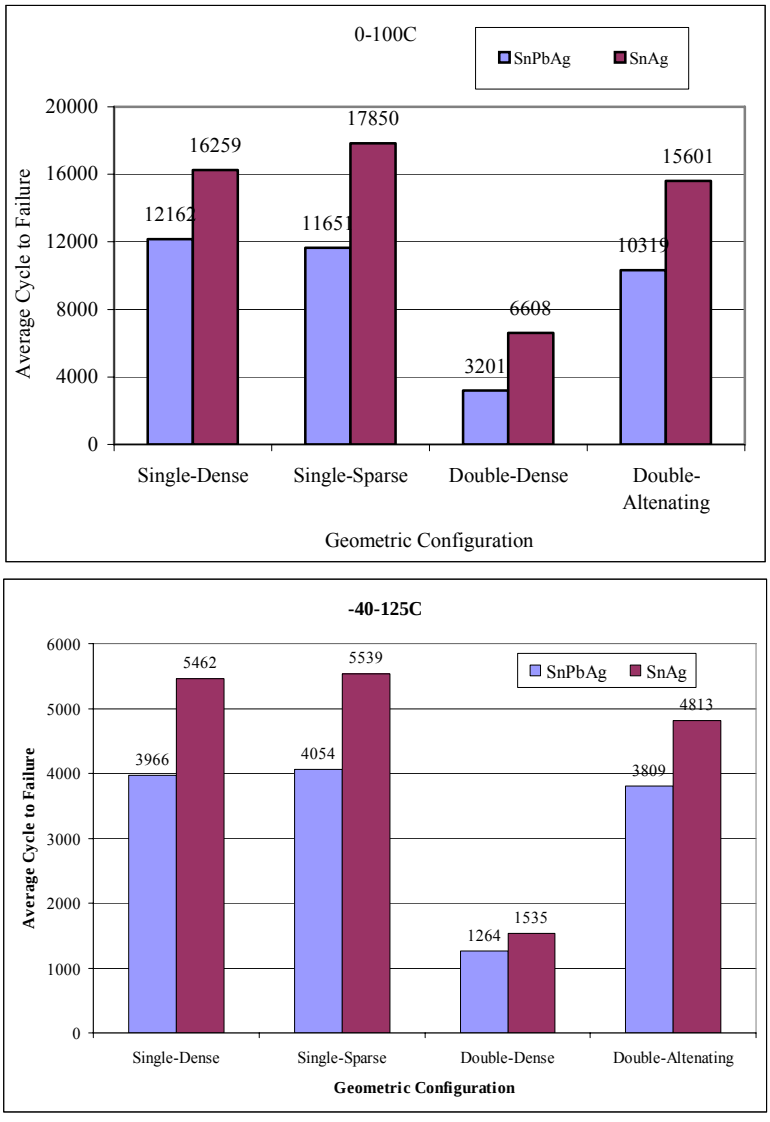

Figure 7.2. Mean life (cycles) of four package layouts, air-cooled, 0-100°C and –40-125°C ATC tests, Motorola. (same as data given in Table 7.7)

Table 7.7. Mean life (cycles) and acceleration factors (single-dense layout used as basis for comparison) of four package layouts, 0-100°C and –40-125°C ATC tests, air-cooled, Motorola

Solder	Geometric Config.	ATC Test, °C	No. Failures	Avg. Life, cycles (STD)	Ratio Life/$Life_{SD}$
SnPb	SD	0-100	26	12160 (810)	1.00
		-40-125	29	3970 (440)	1.00
	SS	0-100	18	11650 (1110)	0.96
		-40-125	18	4050 (430)	1.02
	DA	0-100	13	10320 (880)	0.85
		-40-125	13	3810 (340)	0.96
	DD	0-100	14	3200 (630)	0.26
		-40-125	15	1260 (140)	0.32
SnAg	SD	0-100	25	16260 (2500)	1.00
		-40-125	26	5462 (894)	1.00
	SS	0-100	14	15600 (1680)	0.96
		-40-125	14	5540 (630)	1.01
	DA	0-100	15	17850 (1710)	1.10
		-40-125	11	4810 (1000)	0.88
	DD	0-100	15	6610 (3160)	0.41
		-40-125	15	1540 (770)	0.28

Table 7.8 summarizes the results of running the Student t-test with 95% confidence interval [79]. For both SnPb and SnAg packages and two ATC tests (0-100^{o}C and -40-125^{o}C), the double-dense layouts were statistically different from the other package layouts, as were three other pairs at the 0-100^{o}C ATC test—single-dense and double-alternating SnPb boards (0.85), single-sparse and double-alternating SnPb boards, and single-dense and single-sparse SnAg boards (0.96).

Table 7.8. Paired student t-test comparisons of the mean life of the four package layouts of air-cooled packages and 0-100°C and –40-125°C ATC tests, Motorola (computed using JMP). (bold indicates pairs of data which are statistically significantly different from each other)

Solder	ATC Test and Geometric Conf.		SD	SS	DA	DD
SnPb	0-100°C	SD	-487	-28	**1246**	**8378**
		SS	-28	-585	**693**	**7823**
		DA	1246	693	-689	**6440**
		DD	8378	7823	6440	-664
	-40-125°C	SD	-202	-142	-100	**2456**
		SS	-142	-292	-31	**2524**
		DA	-100	-31	-303	**2252**
		DD	2456	2524	2252	-282
SnAg	0-100°C	SD	-1672	**459**	-1745	**6780**
		SS	459	-2243	-34	**8959**
		DA	-1745	-34	-1672	**6749**
		DD	6780	8959	6749	-2243
	-40-125°C	SD	-464	-477	**46**	**3384**
		SS	-477	-1765	-1155	**2268**
		DA	**46**	-1155	-1991	**1424**
		DD	**3384**	2268	1424	-1705

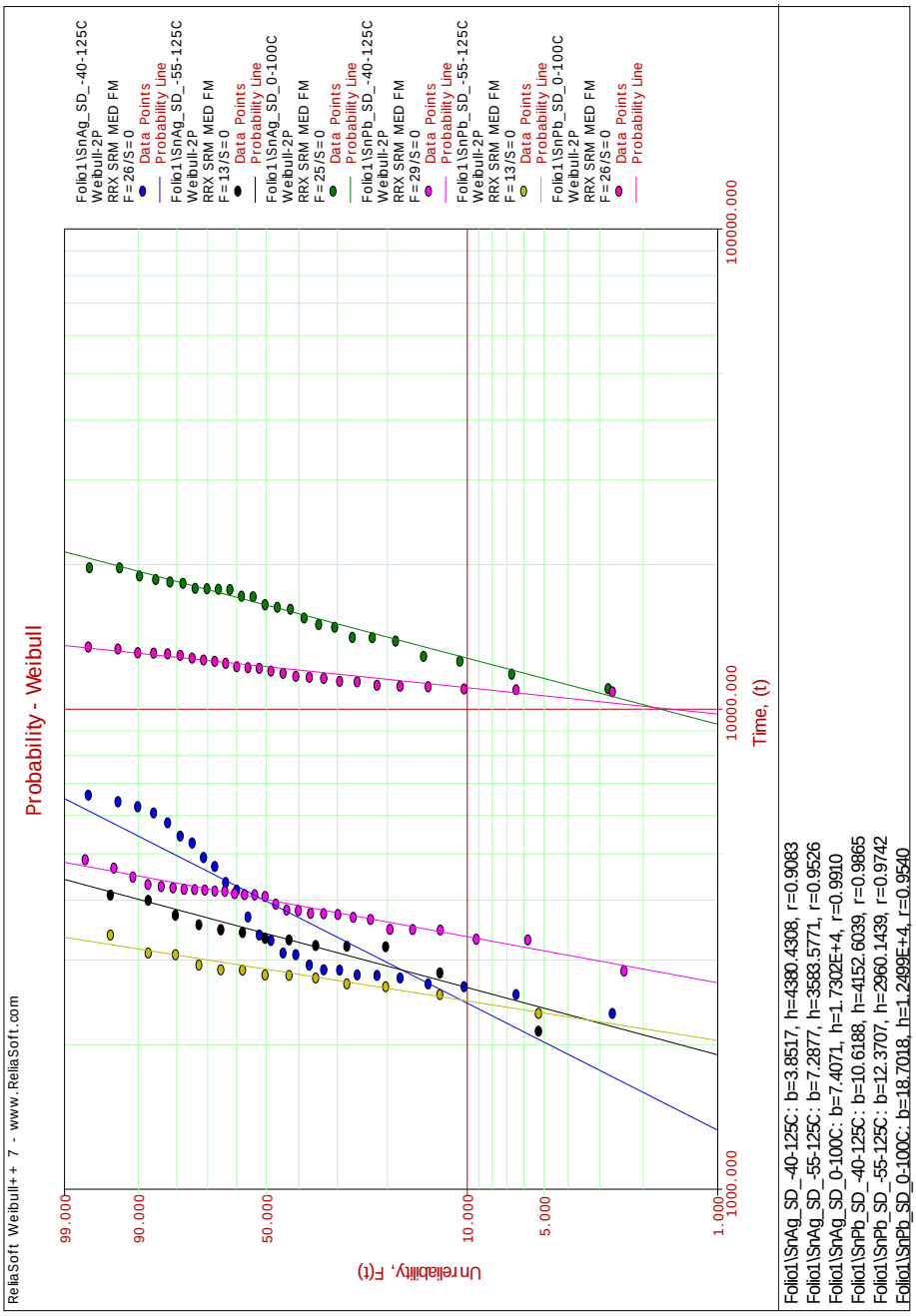

Figure 7.3. Weibull plot for SnPb and SnAg packages: 0-100°C ATC, -40-125°C ATC, and -55-125°C ATC: air-cooled, single-dense, MOT

Figure 7.3 illustrates the Weibull plot for air-cooled, single-dense SnPb and SnAg packages at 0-100^{o}C, -40-125^{o}C, and -55-125^{o}C ATC test conditions. It shows that the Characteristic Life Cycle (CLC) (63.2% failure rate) of SnPb joints are 12499, 4152, and 2960 cycles, respectively, and 17302, 5843, and 3583 cycles, respectively, for SnAg joints. The SnPb joints at -55-125^{o}C ATC have 4.2 and 1.4 AF (Acceleration Factor) over the 0-100^{o}C ATC test. The SnAg joints at -55-125^{o}C ATC have 4.8 and 1.2 AF (Acceleration Factor) over 0-100^{o}C ATC test data.

Figure 7.4 and Figure 7.5 show the Weibull plot for the single-dense, single-sparse, double-dense, and double-alternating SnPb and SnAg packages at 0-100^{o}C ATC and -40-125^{o}C ATC test conditions. Figure 7.4 shows that the characteristic life (63.2% failure rate) of SnPb joints in single-sparse, single-dense, double-alternating, and double-dense package layouts are 12124, 12499, 10686, and 3412 cycles, respectively, at 0-100^{o}C ATC test, and 4236, 4152, 3960, and 1319 cycles, respectively, at -40-125^{o}C ATC test. The SnPb joints for double-dense boards have a 3.1-3.7 AF (Acceleration Factor) over the other three board layouts. Figure 7.5 shows that the characteristic life (63.2% failure rate) of SnAg joints in single-sparse, single-dense, double-alternating, and double-dense boards are 18592, 17302, 16321, and 7310 cycles, respectively, at 0-100^{o}C ATC test, and 5814, 5843, 5236, and 1683 cycles, respectively, at -40-125^{o}C ATC test. The SnAg joints for double-dense boards have a 2.2-3.5 AF (Acceleration Factor) over the other three board layouts.

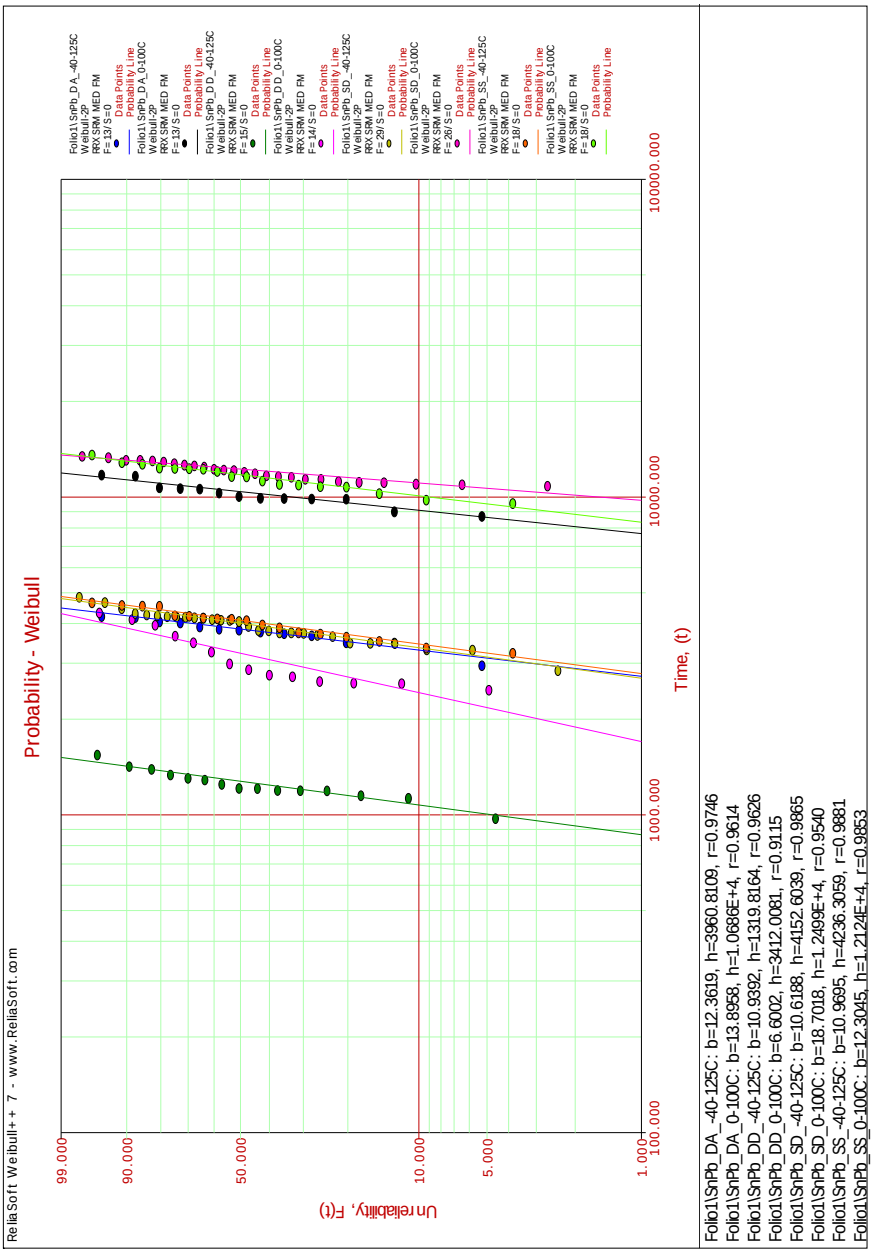

Figure 7.4. Weibull plot for single-dense, single-sparse, double-dense, and double-alternating SnPb packages: air-cooled, 0-100°C ATC and -40-125°C ATC, Motorola

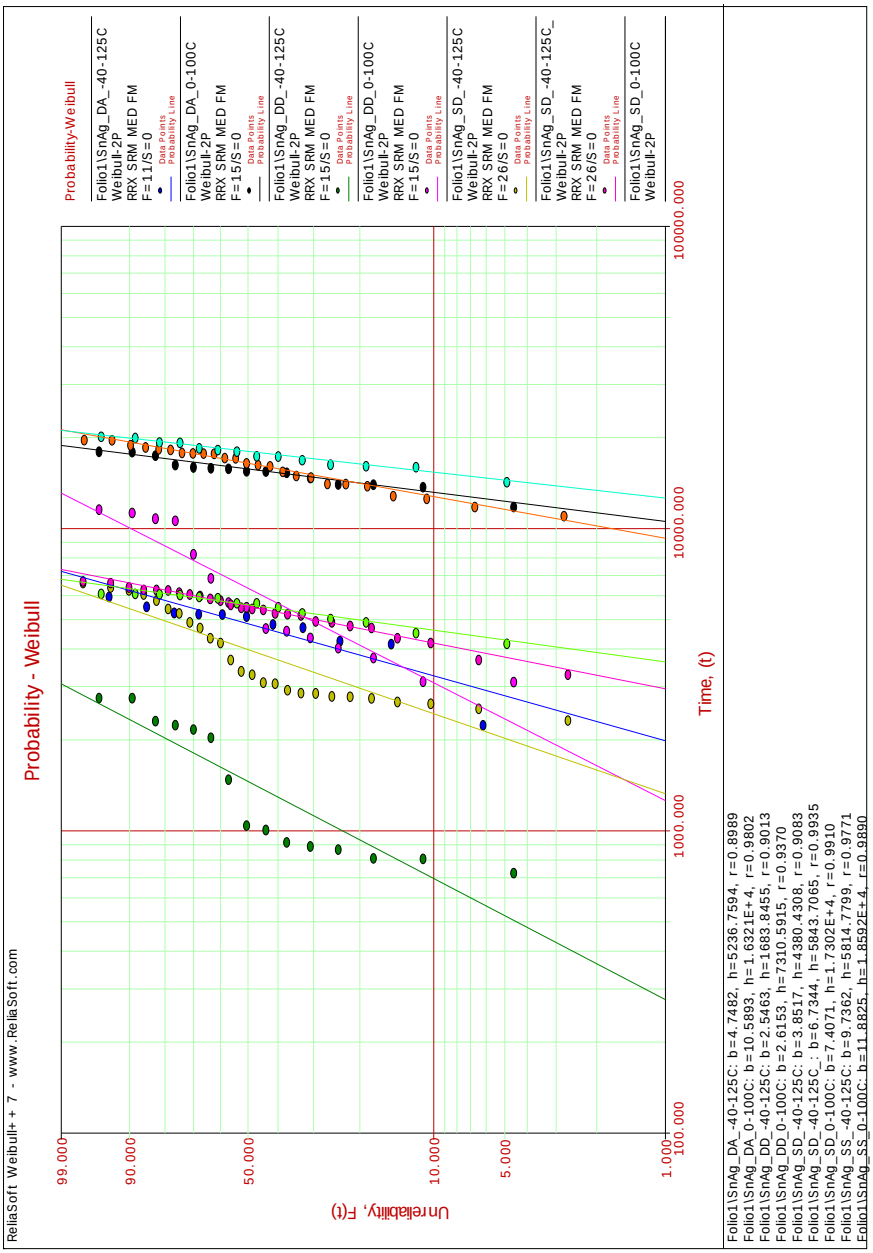

Figure 7.5. Weibull plot for single-dense, single-sparse, double-dense, and double-alternating SnAg packages: air-cooled, 0-100°C ATC and -40-125°C ATC, Motorola

Figures 7.6 and 7.7 focus on SnAg packages, mounted in SD, SS, DA and DD layouts, cycled -40-125^{o}C and 0-100^{o}C, respectively. It is clear from both of these plots that even for SnAg solder joints, the more compliant layouts of SD, SS and DA did not significantly affect the failure process and live. However, they also clearly illustrate that the DD layout and corresponding global stress state substantially affected the SnAg joint failure process.

Figure 7.8 provides a side-to-side comparison of two DD SnAg boards—one cycled at 40-125^{o}C and the other of at 0-100^{o}C. Clearly the failure process is the same, albeit accelerated at the more severe ATC cycle: 40-125^{o}C. The lack of out-of-plane warpage during the thermal cycling of the DD board—and the consequent high interfacial shear stresses at the package interface—means that the stresses experienced by the DD package joints are significantly higher than those experienced by the SS, SD, and DA layouts (refer to Table 7.12).

Further examination of the progressive package failure process (see Table 7.9 for the data) reveals that—like the package solder joints—the packages farthest away from the 'effective' centroid of the remaining unfailed packages experience the greatest globally-imposed shear stresses and become the next most likely packages to fail. For example, in Figure 7.9, the failure sequence in the two DD SnAg boards is illustrated; they are strikingly similar and seemingly repeatable.

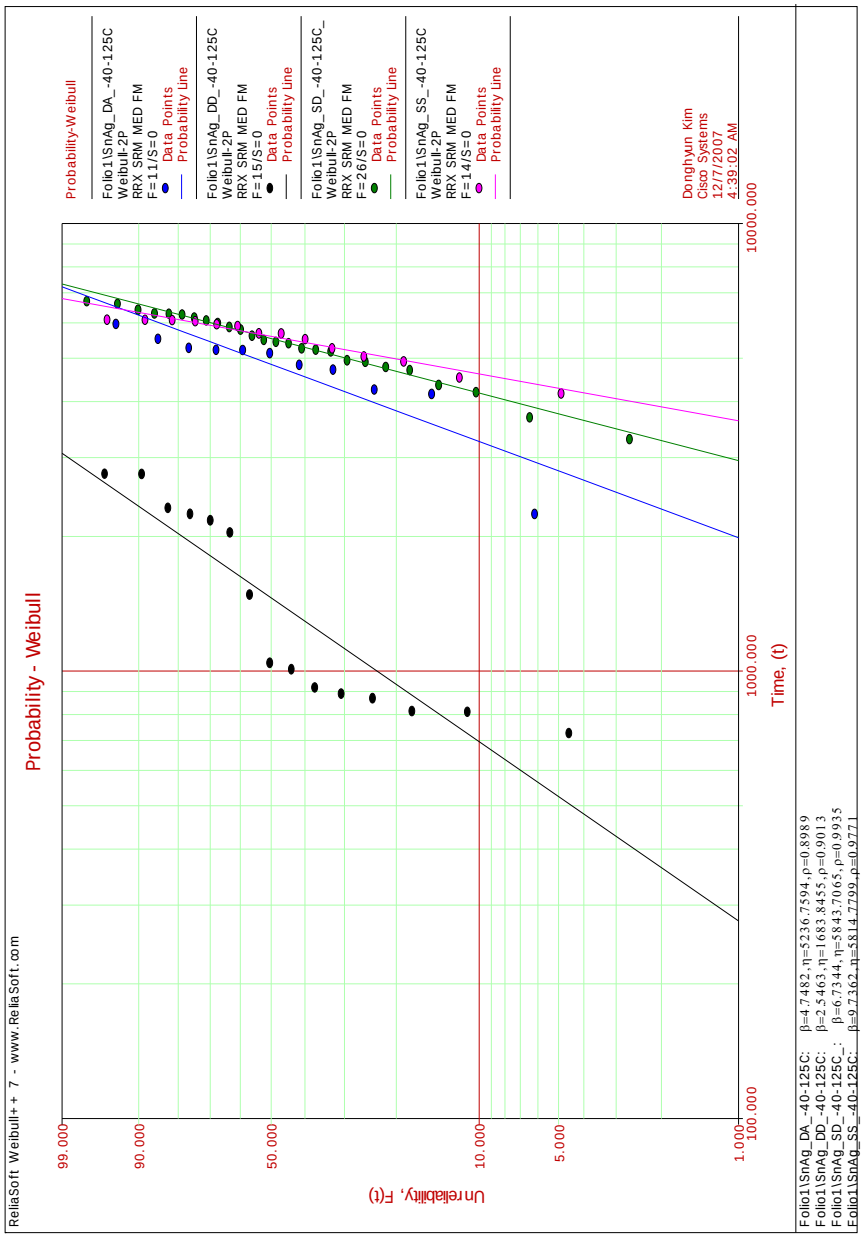

Figure 7.6. Weibull plot for single-dense, single-sparse, double-dense, and double-alternating SnAg packages: air-cooled, -40-125°C ATC, Motorola

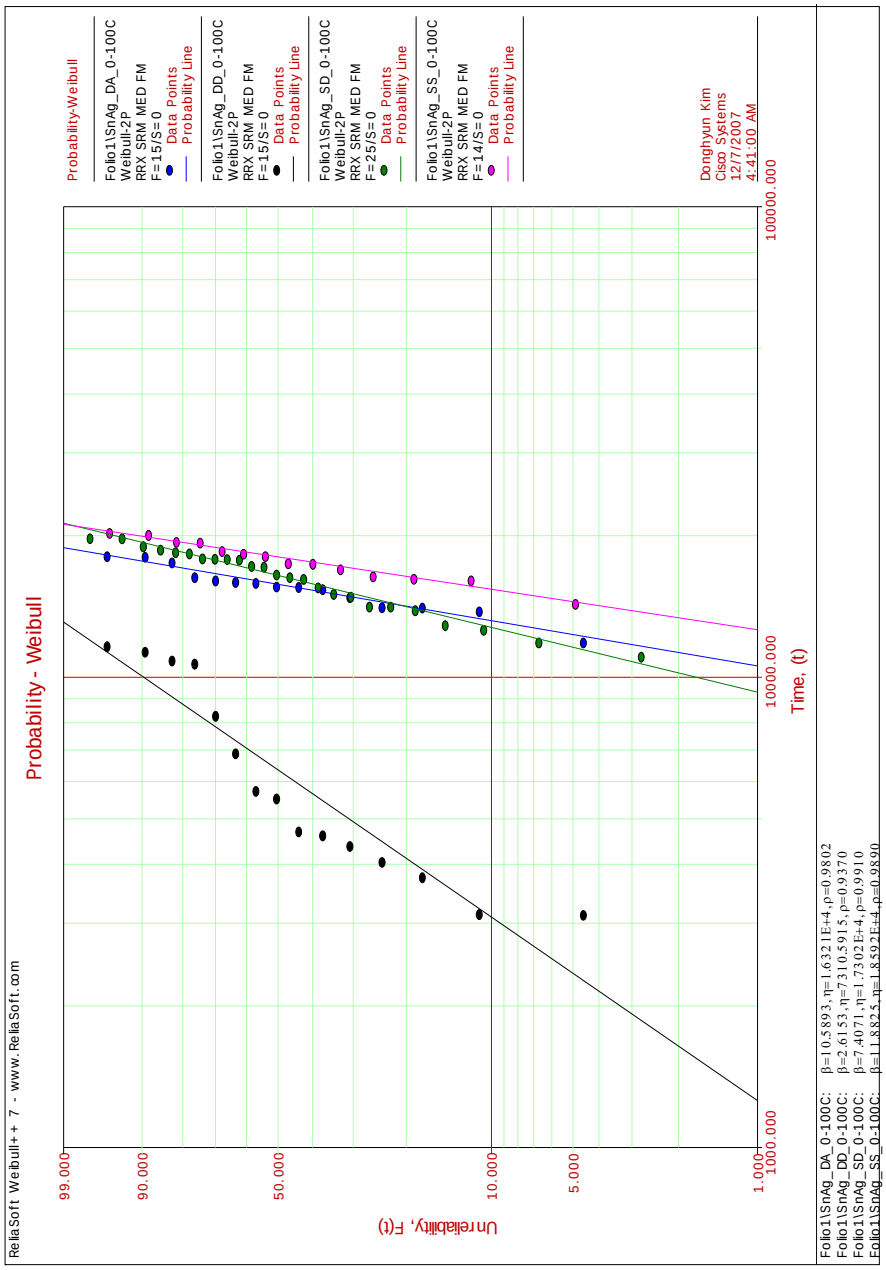

Figure 7.7. Weibull plot for single-dense, single-sparse, double-dense, and double-alternating SnAg packages: air-cooled, 0-100°C ATC, Motorola

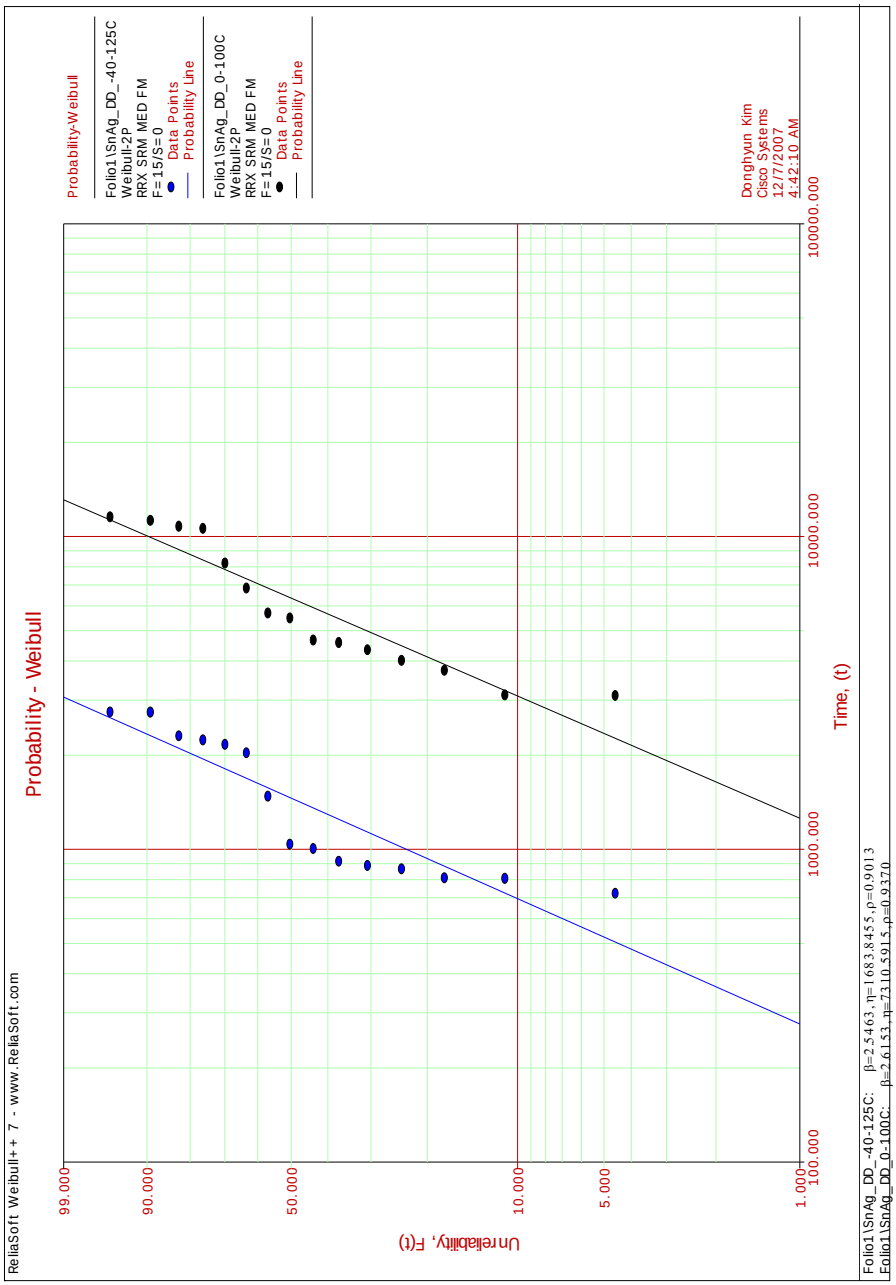

Figure 7.8. Weibull plot for double-dense SnAg packages: air-cooled, 0-100°C ATC and -40-125°C ATC, Motorola

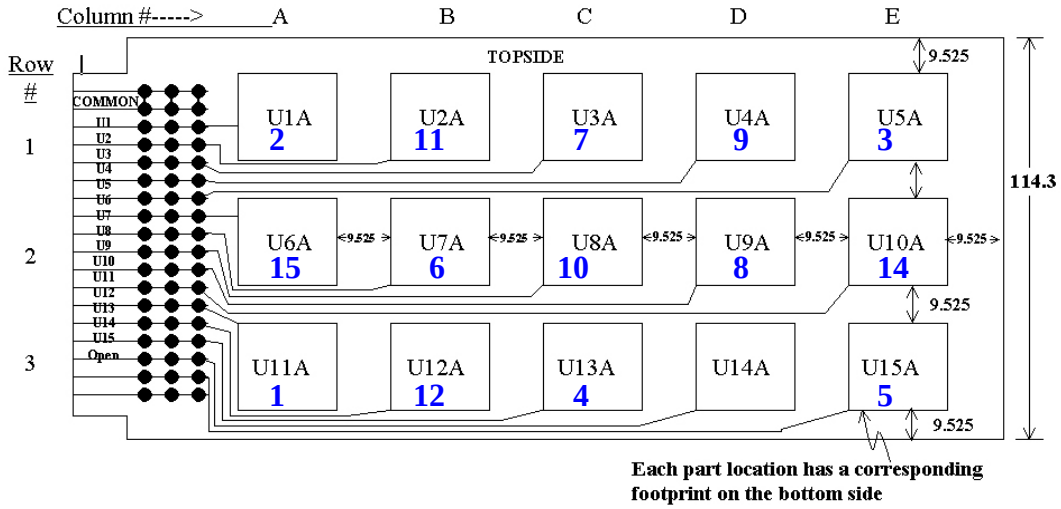

-40-125C ATC

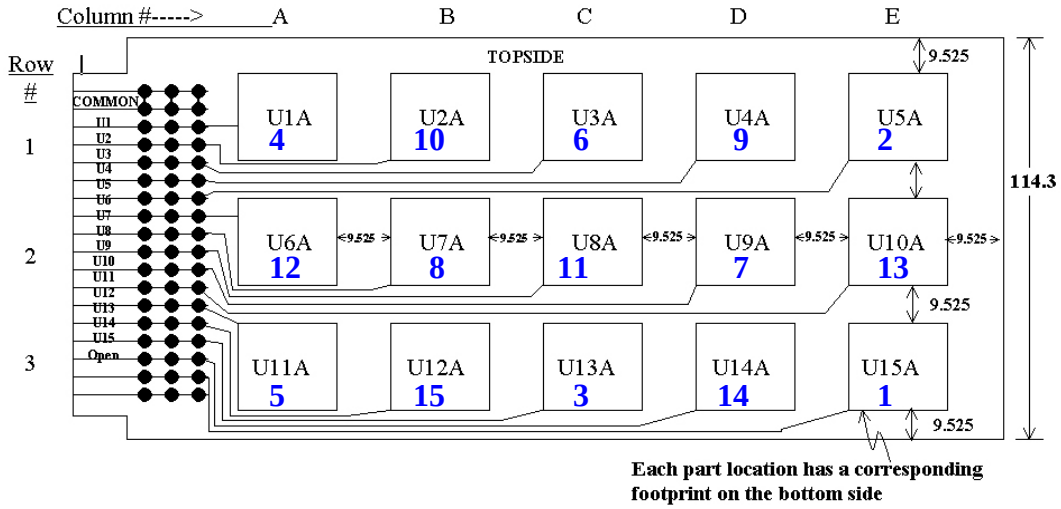

0-100C ATC

Figure 7.9. Failure sequence of SnAg package in double dense (DD) layout: air-cooled, 0-100°C ATC and -40-125°C ATC (see Table 7.9 for data)

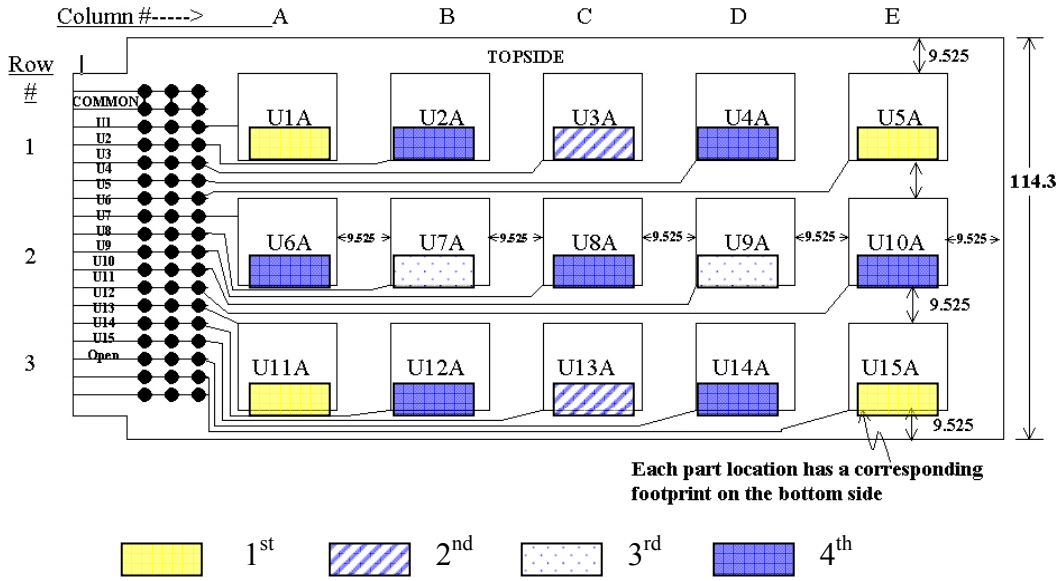

Figure 7.10. Failure sequence of SnAg package groups in double dense (DD) layout: air-cooled, 0-100°C ATC and -40-125°C ATC

The observed trends are shown in Figure 7.10. The first most-likely set of packages to fail are those whose centroid is fartherst from the center of the board (nominally at U8), namely U1, U5, U11 and U15. Once these have failed, the effective centroid splits into two: U7 and U9. From these, the second most-likely set of packages to fail is U3 and U13. The third set is now U7 and U9. The fourth and final set is is U2, U4, U6, U8, U20, U12, U14. Noteably, this fourth set has an alternating pattern, very similar to that of the more compliant DA layout.

It is also interesting to note that for the two DD board data, the Weibull plots appear to have two slopes—one for roughly the first 50% of the failures (when the board compliance is relatively low) and another for the final failures (when the board compliance has increased significantly). In both cases, the final-

failure slope approaches that for the SS, SD, DA data (reference Figures 7.6 and 7.7). Based upon these and other experimental results, it can be concluded that poorl-selected board layouts—particularly configurations which are symmetric about the board's thru-thickness midplane (known as clam-shelling, mirror-shape or back-to-back)—can dramatically reduce package life.

Table 7.9. SnAg Cycle-to-failure and package location in a board: double-dense, air-cooled, 0-100°C ATC and –40-125°C ATC, Motorola

0-100°C	Package location	-40-125°C	Package location
3138	U15A	732	U11A
3150	U5A	817	U1A
3772	U13A	820	U5A
4066	U1A	876	U13A
4396	U11A	897	U15A
4631	U3A	926	U7A
4721	U9A	1017	U3A
5547	U7A	1051	U9A
5759	U4B	1493	U4B
6916	U2B	2056	U8B
8313	U8B	2189	U2B
10732	U6B	2262	U12B
10904	U10B	2331	U14B
11383	U14B	2778	U10B
11687	U12B	2781	U6B

Summarizing, based upon the mean life and paired student t-test results computed in JMP, the double-dense boards had significantly shorter lives for both SnPb (26-32%) and SnAg solder joints (38-41%) compared to the single-dense boards, more severely affecting SnPb joints than SnAg joints. This could be

expected as the symmetry of double-dense boards contrains the board from flexing/warping out-of-plane and, thus, imposes larger stresses on the solder joints. For 0-100^{o}C ATC tests, the double-alternating layout reduces the life of SnPb joints and the single-sparse boards reduce the life of SnAg joints. All other board configurations had no statistical significant effects on life—the spacing of packages was large enough so neighboring packages did not affect each other. These results may guide board layout designs to enhance reliability.

7.1.2.3. Motorola: SnPb vs. SnAg solder

Table 7.10 shows that air-cooled, single-dense package layout, SnAg solder joints had 34%, 1% and 18% longer life than SnPb joints for 0-100^{o}C, -40-125^{o}C, and -55-125^{o}C ATC test conditions, respectively. SnAg joints.

Table 7.10. Mean cycle-life by solder type: single-dense, air-cooled, 0-100°C, –40-125°C, and –55-125°C ATC tests, Motorola

ATC Test	SnPb		SnAg		Ratio
	No. Fails	Avg. Life, cycles (STD)	No. Fails	Avg. Life, cycles (STD)	$\frac{Life_{SnAg}}{Life_{SnPb}}$
0-100°C	26	12160 (810)	25	16260 (2500)	1.34
-40-125°C	29	3970 (440)	26	5462 (894)	1.37
-55-125°C	13	2850 (270)	13	3370 (500)	1.18

7.1.3. Test location: Motorola versus UT

Some test conditions were duplicated at Motorola and UT—specifically, the air-cooled, 0-100^{o}C ATC, single-dense conditions. This section compares

those results. Table 7.11 shows the mean life results from the UT and Motorola tests are within 5% for SnPb solder joints (12800—UT versus 12162 cycles—Motorola), but for SnAg joints, the UT results were 43% longer than those tested at Motorola (23252—UT versus 16259 cycles—Motorola).

Table 7.11. Mean life by test location: air-cooled, 0-100°C ATC, single-dense boards, UT vs Motorola

ATC	Test	No. Failures	Avg. Life, cycles (STD)	Ratio $Life/Life_{Motorola}$
SnPb	UT	23	12800 (1452)	1.05
	Motorola	26	12160 (810)	1.00
SnAg	UT	11	23252 (6279)	1.43
	Motorola	25	16260 (2500)	1.00

There are two possible explanations for the longer life experienced at UT facilities—1) increased aging at UT due to boards being exposed to high temperatures (100^{o}C) resulting from compressor failures and 2) the choice of failure criterion. Note that environmental chambers at Motorola use liquid nitrogen for cooling, while UT chambers use refrigeration compressors.

First, compressor failures—and resulting insufficient cooling—in the UT environmental chamber caused the board assemblies to remain at 100°C (or slightly lower due to conduction losses) rather than 0°C for 88 hours for SnPb boards and 217 hours for SnAg boards (based upon review of temperature profile data)—thereby aging all boards. Y. Miyazawa and T. Ariga [36] studied microstructural and hardness changes for eutectic SnAg solder and found that

aging at 100°C for over 100 hours reduced hardness by about 35% (aged-softening process), which is interpreted to increase ductility and thereby prolong solder joint life. The additional aging did not affect SnPb solder joints as much because cracks in SnPb joints were already greater than 75% when these compressor failures occurred. thereby SnPb data from UT and Motorola are close. However, at the times of compressor failures, the SnAg joints still had small crack areas, so the aging increased their cycle lives.

The second explanation for the difference between UT and Motorola data is the criterion used to detect joint failures. As discussed in Section 7.1.1.3, applying the industry-standard failure criterion resulted in premature false failures (confirmed with resistance measurements and dye penetration studies) for SnAg solder joints.

Table 7.12 shows comparison of life for air-cooled, 0-100°C ATC, single-dense boards cycled at UT using the proposed UT and Industry Standard IPC criteria. Life based on both criteria differed by less than 1% for all SnPb solder joints. However, for aged, air-cooled and quenched SnAg solder joints, life using the IPC failure criterion was 18906, 12677, and 11549 cycles, respectively, versus 41236, 23252, and 22850 cycles using the UT criterion—life based upon the UT criterion was 1.8X to 2.2X larger. Refer to Appendix D for details on the UT criterion.

Table 7.12. Comparison of UT and IPC criteria using UT life data: air-cooled, 0-100°C ATC, single-dense,

ATC Test		No. Failures	Avg. Life, cycles (STD)	Ratio $Life_{Industry}/Life_{UT}$
SnPb	Industry	23	12800 (1453)	1.00
	UT	23	12800 (1452)	1.00
SnAg	Industry	20	11549 (10341)	0.50
	UT	11	23252 (6279)	1.00

7.2. FEM JOINT LIFE AND STRESS ANALYSIS

In this section, two-dimensional FEM models are run to determine stress/strain in the solder joints subjected to different ATC test cycles, post-processing and package layouts and to help to explain the ATC test results for different package-layouts. The simulations demonstrate the effects of grain boundary sliding, dislocation-induced creep strain and joints undergoing plastic deformation.

The following discussions are for those 24 joints located in the boundary region, shown in Chapter 2, Figure 2.2, where the joints exhibited the largest cracks, therefore the highest stresses/strains, of any region.

7.2.1. FEM Model

Two-dimensional plane stress elements were used for the solder joints, and 2-D plane strain elements were used for the packaging materials, substrates, PWB, die, and die attach. See Chapter 5 for detailed descriptions of the FEM models.

7.2.2. FEM Simulations: ATC Test Protocols

Table 7.13 shows the simulation results for the maximum stress and strains at corner joint in boundary region (G7 or G13 or N7 or N13, see Fig 2.2) during one thermal cycle for air-cooled joints, three ATC test protocols, and four package layouts. Using the two-dimensional stress analysis global model, the computed maximum stress, creep strain, and plastic strain were identical for the single-dense, single-sparse, and double alternating board layouts—the double-dense layout had different results. Using the maximum stresses of 21.5MPa for SnPb and 20.6MPa for SnAg from the 0-100°C ATC tests as reference for single-sparse, double-dense and double-alternating (all the same), the stresses increased by 85% and 103% for SnPb and by 16% and 16% for SnAg for the -40-125°C and the -55-125°C ATC tests, respectively. Similarly, creep strain, 0.0077 for SnPb and 0.0048 for SnAg, at the 0-100°C ATC test changed by +58% and –30% for SnPb and by +103% and +58% for SnAg for the -40-125°C and the -55-125°C ATC tests, respectively. The creep strain from the -55-125°C ATC test is smaller in the SnPb case due to the fast transit time between temperatures while the creep strain is larger in the SnAg case due to slower stress relaxation than in SnPb.

For the double-dense cases and using the maximum stresses of 31.2MPa for SnPb and 23.6MPa for SnAg from the 0-100°C ATC test as a reference, the maximum stresses increased by 39% for SnPb and by 2% for SnAg in both the -40-125°C and the -55-125°C ATC tests. Similarly, the creep strain of 0.0212 for SnPb and 0.0261 for SnAg at 0-100^{o}C tests increased by 54% and 12% for SnPb

and by 81% and 44% for SnAg from the -40-125°C and -55-125°C tests, respectively.

Table 7.13. Maximum ABAQUS-calculated stress [MPa], creep strain, and plastic strain for air-cooled corner joint (G7 or G13 or N7 or N13) in the boundary region for two solder types, four package layouts, and three ATC test protocols

Solder	ATC Test and Stress/Strain		SD	SS	DA	DD
SnPb	0-100°C	Stress	21.5	21.5	21.5	31.2
		Creep	.0077	.0077	.0077	.0212
		Plastic	0	0	0	0
	-40-125°C	Stress	39.6	39.6	39.6	43.3
		Creep	.0122	.0122	.0122	.0327
		Plastic	0	0	0	.0025
	-55-125°C	Stress	43.3	43.3	43.3	43.3
		Creep	.0053	.0053	.0053	.0237
		Plastic	.0034	.0034	.0034	.021
SnAg	0-100°C	Stress	20.6	20.6	20.6	23.6
		Creep	.0048	.0048	.0048	.0261
		Plastic	0	0	0	0
	-40-125°C	Stress	24	24	24	24
		Creep	.01	.01	.01	.0472
		Plastic	.0026	.0026	.0026	.0187
	-55-125°C	Stress	24	24	24	24
		Creep	.0076	.0076	.0076	.0377
		Plastic	.0093	.0093	.0093	.048

No plastic deformation occurred for all SnPb and SnAg joints at the 0-100°C ATC tests, and for the SnPb solder joints at the -40-125°C ATC tests, except for the double-dense board layout. For single-dense, single-sparse and double-alternating board layouts, the plastic strains were the same: 0.0034 for SnPb and 0.0093 for SnAg at the -55-125°C ATC tests, and 0.0026 for SnAg at

the -40-125°C ATC tests. For the double-dense board layout, the plastic strains of 0.0025 for SnPb and 0.0187 for SnAg at the -40-125°C ATC tests increased by 740% and 157% at the -55-125°C ATC tests. Here, 22 Mpa and 43 Mpa were used for SnAg and SnPb solder joint as yield stress.

7.2.3. FEM Simulations: Post-Processing

Table 7.14 shows the ABAQUS simulation results for the maximum calculated stress, creep strain and plastic strain at the corner joint in boundary region (G7 or G13 or N7 or N13, see Fig 2.2) during one thermal cycle 0-100°C ATC test protocol for single-dense SnPb joints for three post-process conditions . For aged joints with 9.5mm mean phase size and air-cooled joints with 4.5mm mean phase size (obtained from sectioning measurements [58]), the air-cooled joints have 60% larger grain boundary sliding-induced creep strain than aged joints (0.0077 vs. 0.00479), while the dislocation-induced creep strain in the aged joints is 2.7 times larger than in air-cooled joints (0.00059 vs. 0.00016)—notably the large phase sizes in the aged joints increase resistance to grain boundary sliding, resulting in higher stresses and lower life. There was no plastic deformation in either case.

Table 7.14. Stress and strain in the single-dense SnPb corner joint (G7 or G13 or N7 or N13) in the boundary region due to different post-processing at 0-100°C ATC test protocol

Parameters	SnPb	
	Air-cooled	Aged
Max stress [MPa]	21.5	23.6
Creep strain	0.0077	0.00479
Grain boundary sliding-creep strain	0.00765	0.00427
Dislocation-creep strain	0.00016	0.00059
Plastic strain	0	0

7.2.4. FEM Simulations: Package Layout

Figure 7.11 shows the package assembly deformation at 0°C/100°C for the four package layouts with air-cooled SnPb joints subjected to the 0-100°C ATC test. As expected, the double-dense configuration shows no warping due to the package layout symmetry about the midplane of the PWB, expanding only in the 1-direction; the stresses it impses upon the mounted packages are significantly larger than for the other configurations (see Table 7.12). All the thermal mismatch is focused at the joint's package interface. For the other three layouts, warpage of the PWB reduces the effects of the CTE mismatch on the solder joints and the stresses/strains are dominated by local effects due to the CTE mismatch between die and solder joint—the characteristic lengths of the package locations on the board appear to be small and are not affected by the global effect caused by the interaction between adjacent packages—thereby the stresses and strains for single-dense, single-sparse, and double-alternating are identical within the

computational capabilities of ABAQUS. Recall from Table 7.13 that the creep and plastic strains for the double-dense layout are 4-7 times larger than those of the other layouts. Also, the stresses in the double-dense boards are 45% (SnPb) and 15% (SnAg) larger.

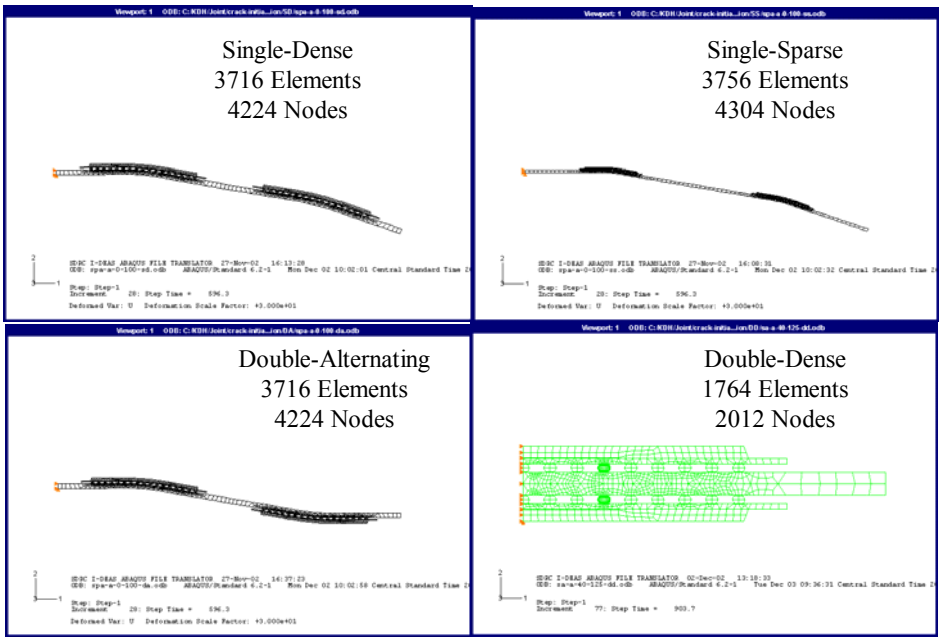

Figure 7.11. Deformation of PWB with four package layouts for air-cooled SnPb 0-100°C ATC test—100°C stress-free temperature. (Note: displacements are scaled-up automatically by ABAQUS for improved visualization)

7.2.5. FEM Simulations: Conclusions

The most important conclusions of these ABAQUS FEM simulations investigating package layouts and ATC test protocols on air-cooled solder joints in the boundary region are:

- Inter-package spacing of the single-dense, single-sparse, and double-alternating package layouts appears to be large compared to the characteristic 'stress-affected' lengths of each package so as not to affect immediately adjacent packages. FEM simulations show maximum stress, creep strain and plastic strain are unaffected by the three package layouts: SS, SD, DA.
- Due to its significantly increased stiffness, the double-dense package layout imposed the highest stresses in the solder by far.
- The -40-125°C and -55-125°C ATC tests caused plastic deformation in SnPb and SnAg solder joints, while no plastic deformation was found in the 0-100°C ATC cycling.

These observations and data are used in the development of the life-prediction models, including the severity metric described in the next section.

7.3. LIFE PREDICTION MODEL: SEVERITY METRIC

A severity metric is proposed in this study to estimate damage to solder joints subjected to thermal cycling that attempts to link material properties and parameters associated with board geometry, manufacturing processing and thermal conditions to the time-dependent creep, time-independent plastic deformation and a time-dependent and geometric effective stress of the solder joint, which is computed from the ATC parameters of temperatures, dwell-time, and ramp rates, and from the package layouts (single-dense and double-dense only). The effects of post-processing are not included in this metric, which

assumes that the board assemblies were processed identically (air-cooled). These links were established from thermal testing and FEM analysis from previous chapters and discussions.

7.3.1. Industry-Standard Life-Prediction Models

Table 7.15. Life-prediction using Coffin-Manson (CM), Engelmaier, and Norris-Landzberg (NL) models and comparison with experimental life data (Motorola)

Solder Type	ATC Tests, °C	Package -Layout	Post-Process Cond	Exp. Mean Life, cycles (STD)	Predicted Life, cycles		
					CM**	Engelm-aier*	NL**
SnPb	0-100	SD	Air	12160 (810)		9190	
SnPb	-40-125	SD	Air	3970 (440)	4466	1942	2617
SnPb	-55-125	SD	Air	2850 (270)	3753	2136	3842
SnPb	0-100	DD	Air	3200 (630)		9190	
SnPb	-40-125	DD	Air	1260 (140)	1175	1942	689

Notes:
*fitting parameter, F, chosen as 1
** Coffin-Manson model and Norris-Landzberg models calculate AF. Therefore, 0-100^{o}C test is used as reference data and the predicted life of -40-125^{o}C or -55-125^{o}C is equal to AF*life (cycle) of 0-100^{o}C ATC
[The raw data, including sample size, can be found in Appendix H].

In Chapter 1, Section 1.4.6, three commonly-used life-prediction models for SnPb solder were reviewed: Coffin-Manson, Engelmaier, and Norris and

Landzberg. Below are the predictions from these models with the Motorola SnPb data for various ATC test protocols and board layouts. It is notable that there are no widely accepted models for SnAg solder joints, so life-prediction comparisons were limited to SnPb joints.

The Coffin-Manson and Norris-Landzberg models calculate acceleration factors (AFs) between two ATC test conditions. Hence, life at 0-100ºC ATC was used as the basis of comparison to predict life at -40-125ºC ATC and at -55-125ºC ATC. For the single-dense package layout, the CM model overestimates life at -40-125ºC ATC and -55-125ºC ATC by 12% and 31%, respectively, and NL model underestimates the life at -40-125ºC ATC by 34% but overestimates at -55-125ºC ATC by 35%. Engelmaier's model underestimates life at the 0-100ºC ATC, -40-125ºC ATC, and -55-125ºC ATC by 24%, 51%, and 25%, respectively. For double-dense board layout, the CM model underestimates life at -40-125ºC ATC by 7%, and the NL model underestimates life by 45%. The Engelmaier model overestimates both the 0-100ºC ATC and -40-125ºC ATC by 187% and 54%, respectively. Of the three life-prediction models, the CM model predicts best followed by the NL, and finally the Engelmaier model predicted life the worst since it did not take the package layout differences into account.

7.3.2. Severity Metric for SnPb Solder Joints

To account for the different damage mechanisms imposed on SnPb joints, the severity metric S includes the effects of grain boundary sliding creep, dislocation creep, and time-independent plastic deformation, represented

respectively by the three terms in Eq. (7.1). The first two terms originate from creep Equation (5.1), and since most creep deformation in the solder joint takes place during temperature ramp up/down, the creep terms are multiplied by the ratio of temperature rise time to cycle time. Note that the plastic deformation term only contributes to the metric when the delta function is positive. When exposed to temperature cycles, the interfacial stress reaches its maximum at the low-temperature dwell, and once it reaches the solder's yield stress, the solder joints remain at yield stress during the low-temperature dwell period. Most creep deformation occurs during the temperature-rise period. To account for these effects, the ratio of rise-time to cycle-time was added to the first two severity creep terms, while the ratio of dwell-time to cycle-time was added to the third plastic term.

$$S = A(\sigma_{eff})^{n2}\left(\frac{2t_{rise}}{t_{cycle}}\right)^{\alpha} + B(\sigma_{eff})^{n3}\left(\frac{2t_{rise}}{t_{cycle}}\right)^{\alpha} + C\log_{10}\left[1+(\tau_r / t_{rise})^{\gamma}\right]\sigma_0(\sigma_0-\sigma_{sys})\delta(\sigma_0-\sigma_{sys})\left(\frac{t_{dwell}}{t_{cycle}}\right)^{\alpha} \quad (7.1)$$

Here A=64, a fitting constant for grain boundary sliding creep; B=2.9 × 10^{-6}, a fitting constant for dislocation creep; C=188, a fitting constant for time-independent plastic deformation; γ=1 and α=1; σ_{eff} (defined later) is an effective stress [MPa]; σ_{sys} is the yield stress=43.3 [MPa] for SnPb joints [9] and =24 [MPa] for SnAg joints [9]—here since the maximum stress occurs at the low temperature dwell, the yield stress is assumed to be constant-i.e. temperature independent; σ_0 is a characteristic thermal stress reflecting the differences in

CTE of the materials as well as the dwell temperature differences associated with the different ATC test protocols [MPa]; n2=2, a stress exponent; n3=7, a stress exponent; and t_{rise}, t_{cycle} and t_{dwell} are the ATC test ramp, cycle, and dwell times [sec]; respectively, and τ_r is a time constant of temperature ramp, which is related to the rate at which the maximum stress relaxes, and defined by

$$\tau_r = \frac{t_{rise}}{\ln \sigma_0} \tag{7.2}$$

$$\sigma_0 = E(\Delta\alpha_{eff})(\Delta T) \tag{7.3}$$

where, E is the elastic modulus of the solder; $\Delta\alpha_{eff}$ is the difference in coefficients of thermal expansion between the die and the PWB; ΔT is temperature difference between the two cycle temperature extremes.

Effective stress

An effective stress is proposed to include the effects of different package layouts and different ATC test parameters. It is defined as

$$\sigma_{eff} = \sigma(\tau)\bar{g}\bar{h} \tag{7.4}$$

Here, $\sigma(\tau)$ represents a time-dependent mean stress for the thermal cycle, $\bar{g}$ is a global geometric effect represented by a ratio of bending stiffness for different package layouts to that of the single-dense case raised to the ratio of the rise time between temperatures to the total cycle time, and $\bar{h}$ is a local geometric effect for different die sizes and solder joint pitches. Note, in this study, only the SD and DD package layouts were studied because FEM analysis showed that the spacing of SD, SS, and DA package layouts were large compared to the characteristic lengths of each package so as not to affect adjacent packages. FEM simulations

show maximum stress, creep strain and plastic strain are not affected by these package layouts. Moreover, life data from Table 7.7 indicated that the life for these three package layouts were for the same ATC test conditions to first order, reasonably close. The experimental data clearly demonstrates that crack growth in solder joints depends on the amount of board warpage, which is a function of modulus and moment of inertia of the package. Therefore, these are defined as

$$\sigma(\tau) = \frac{\int \sigma(t)dt}{t_{cycle}} \tag{7.5}$$

$$\overline{g} = \left[\frac{(1/\rho)_{test}}{(1/\rho)_{ref}}\right]^{\frac{t_{rise}}{t_{cycle}}} = \left[\frac{(EI)_{test}}{(EI)_{ref}}\right]^{\frac{t_{rise}}{t_{cycle}}} \tag{7.6}$$

Here, 'ref' refers to the 357-PBGA test package on a 62mil-thick test board, 'test' refers to the other test package assembly whose life is being predicted, ρ is the radius of curvature of the package assembly, $\rho = \frac{M}{EI}$, E is the effective modulus of the package assembly components, I is the moment of inertia of the package assembly, and EI represents the sum of each component,

$$EI = \sum E_i I_i \tag{7.7}$$

As shown in Figure 7.12, the neutral axis, defined in Eq. (7.7) of the double-dense boards lies at the center of the cross-sectioned area, while the neutral axis of the single-dense board lies in the substrate.

$$\sum E_i \int y_i dA_i = 0 \tag{7.8}$$

Here, y_i represents the distance from the neutral axis to the centroid of each component and A_i represents the unit cross-section area of each component.

To evaluate the time-dependent mean stress, the stress histories shown in Figure 7.13 for three thermal cycles were calculated with the ABAQUS FEM model using the two-dimensional stress analysis global model (see Figure 7.11): all three could be reasonably approximated by:

$$\sigma(t) \approx e^{t/\tau_r} \qquad \text{for } t < t_{rise} \tag{7.9}$$

$$\sigma(t) \approx \sigma(t_{rise}) \qquad \text{for } t_{rise} < t < t_{rise} + t_{dwell} \tag{7.10}$$

$$\sigma(t) \approx \sigma(t_{rise}) e^{\frac{-(t - t_{dwell} - t_{rise})}{\tau_r}} \qquad \text{for } t_{rise} + t_{dwell} < t < t_{rise} + t_{dwell} + t_{rise} \tag{7.11}$$

$$\sigma(t) \approx 0 \qquad \text{for } t_{rise} + t_{dwell} + t_{rise} < t < t_{cycle} \tag{7.12}$$

Here, t_{rise} and t_{dwell} are the ATC test ramp and dwell times [sec]. Then, the integrated form of stress during a cycle period is

$$\int \sigma(t)dt \approx 2\tau_r (e^{t_{rise}/\tau_r} - 1) + t_{dwell} e^{t_{rise}/\tau_r} \tag{7.13}$$

$\bar{h}$ represents a local geometric effect and takes into account the effects of die size and solder join pitch on the effective stress.

$$\bar{h} = \left(\frac{DNP_{test}}{DNP_{ref}} \times \frac{pitch_{test}}{pitch_{ref}} \right)^{\beta} \tag{7.14}$$

Here, β is a fitting constant, chosen as 0.5, and DNP is the distance from neutral point to the solder joint that has the largest strain, which is located under die periphery.

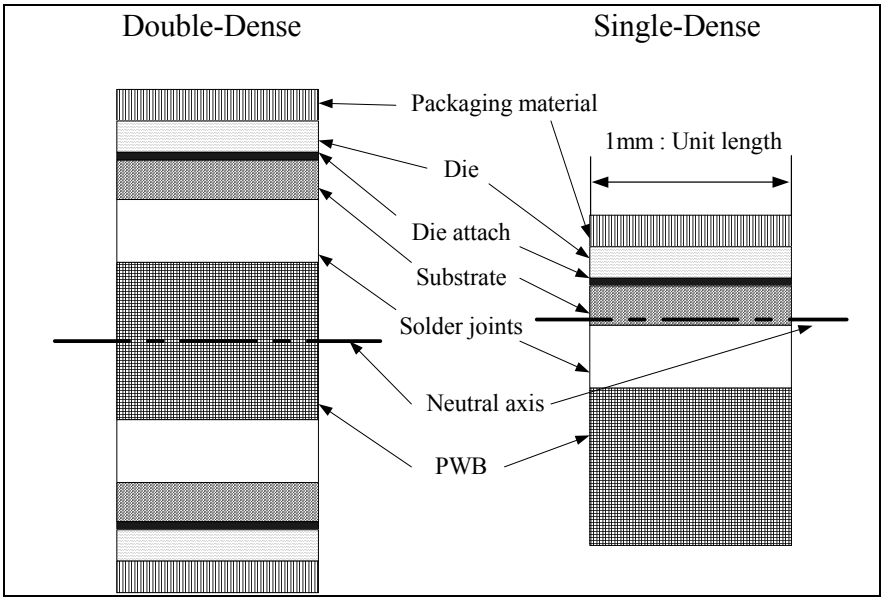

Figure 7.12. Cross-section area and neutral axes of double dense and single-dense geometric configurations

Figure 7.13 shows stress histories from the solder joint G13 during one thermal cycle by FEM analysis. Equations 7.9-7.13 approximate these stress histories during one thermal cycle.

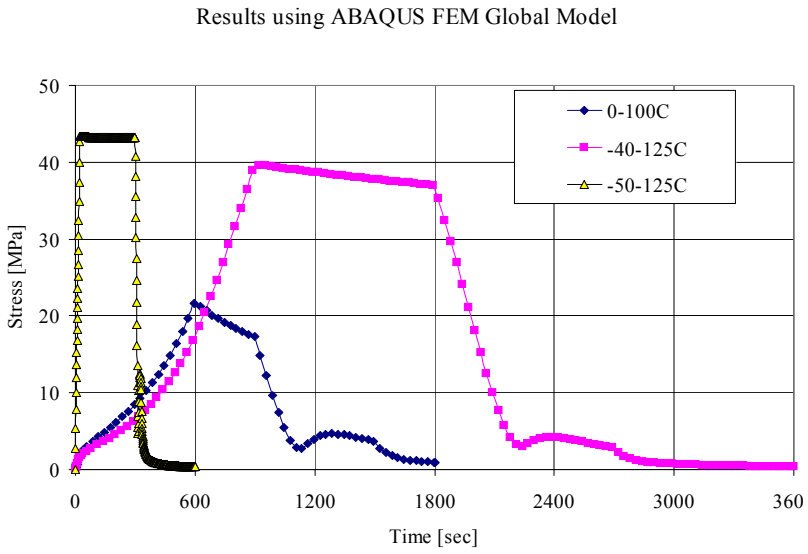

Figure 7.13. Stress histories for three ATC test conditions at corner joint (G7 or G13 or N7 or N13; see Fig 2.2) in the boundary region

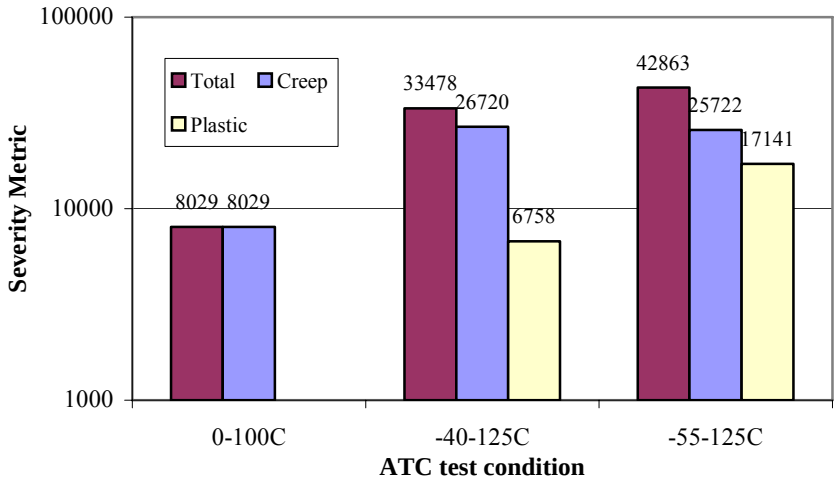

Figure 7.14. Contributions of creep and plastic strains to the severity metric for air-cooled SnPb joints for different ATC test conditions

The fitting constants, A, B, and C in Eq. (7.1), were determined by least-mean-square curve-fitting the severity model into Motorola ATC test results at 0-100^{o}C, -40-125^{o}C, and -55-125^{o}C ATC conditions for single-dense, single-sparse, double-alternating, and double-dense board layouts. Here, single-sparse and double-alternating data were regarded the same as the single-dense board layout because they are not significantly different from the single-dense layout (see Table 7.8 for paired student t-test and Table 7.13 for FEM stress and strain analysis

Appendix H contains the raw life (cycles) used in this model. As the post-processing conditions are not included in the severity model, Motorola data (air-cooled post-processing only) is used to calibrate the severity model. First, A was selected as 64 arbitrarily to initiate the process, then B was selected as 2.9×10^{-6} from the ratio of 48 of grain boundary sliding-induced creep strain to the dislocation-induced creep strain under the 0-100°C test condition. Finally, C was chosen as 188 from the ratio of 1.5 of creep strain to plastic strain under the –55-125°C ATC test condition. Once A, B, and C are chosen as described, any subsequent use of the severity metric does not require a FEM model. The severity metrics and the relative contributions from creep and plastic strains for air-cooled joints for the three ATC test conditions are shown in Fig. 7.14.

Table 7.16 shows values of model parameters used for the life-prediction of air-cooled SnPb solder joints used in deriving the severity metric. Note that $\bar{h}$ has value 1 because the dimensions of the 357-PBGA are used as the reference values (see DNP and pitch). Board stiffness effect $\bar{g}$ has value 1 for the single-

dense case since it is the reference case, and the double-dense case increased the stiffness effect by a factor 1.8. τ_r represents stress relaxation time in the solder joint due to creep: the -55-125ºC ATC test gives much shorter time, 7sec, compared to 214sec and 163sec in the -40-125ºC ATC and 0-100ºC ATC, respectively. Note, the rise times are ~0.5min, 10min, and 15 minutes for the -55ºC to 125ºC, 0-100ºC, and -40-125ºC ATC tests, respectively. The -55-125ºC ATC test has the largest σ_0 (since it has the largest temperature difference, 180ºC), $\sigma(\tau)$ and σ_{eff} compared to the -40-125ºC and 0-100ºC ATC test conditions for the single-dense package layout. However, for the double-dense package layout, σ_{eff} is larger for the -40-125ºC ATC test case than in the -55-125ºC ATC test for single-dense package layout since $\bar{g}$ is 1.8 rather than 1 in the single-dense case.

Table 7.16. Life-prediction model parameters for air-cooled SnPb solder joints used in the severity metric for different ATC test conditions and two package layouts (SD and DD)

ATC Tests, °C	Pkg layout *	τ_r [sec]	σ_0 [MPa]	$\sigma(\tau)$ [MPa]	$\bar{g}$	y_i [mm]	$\bar{h}$	σ_{eff} [MPa]	DNP _ref [mm]	Pitch _ref [mm]	EI _ref [Nmm^2]
0-100	SD	163	39.5	13.6	1	0.09**	1	13.6	5.4	1.27	92215
-40-125	SD	214	66.6	24.5	1	0.09**	1	24.5	5.4	1.27	92215
-55-125	SD	7	73.6	34.8	1	0.09**	1	34.8	5.4	1.27	92215
0-100	DD	163	39.5	13.6	1.8	0***	1	24.4	5.4	1.27	550200
-40-125	DD	214	66.6	24.5	1.8	0***	1	38.1	5.4	1.27	550200

*only SD and DD package layouts studied. Assumes SS, DA, and SD package layout results are similar.
**distance from interface between package and solder joint (see Fig 7.12)
*** on neutral axis (see Fig 7.12)

Table 7.17. Contributions of creep and plastic strains from Equation 7.1 in the severity metric for air-cooled SnPb joints at different ATC test conditions and two package layouts (SD and DD)

Solder Type	ATC Tests, °C	Package-Layout*	Severity_Creep by GBS*	Severity_Creep by DC*	Severity_Creep	Severity_Plastic	Severity_Total
SnPb	0-100	SD	7864	165	8029	0	8029
SnPb	-40-125	SD	19136	7584	26720	6758	33478
SnPb	-55-125	SD	7756	17966	25722	17141	42863
SnPb	0-100	DD	25480	10062	35542	0	35542
SnPb	-40-125	DD	46570	170501	217071	6759	223830

* only SD and DD package layouts studied. Assumes SS, DA, and SD package layout results are similar.

Table 7.17 shows contributions to the severity metric by creep and plastic strains for air-cooled SnPb joints at different ATC test conditions and two package layouts (SD and DD). There is no plastic deformation at the 0-100°C ATC test condition since the stresses do not reach the SnPb yield stress. In the -40-125°C and -55-125°C test conditions, the solder joint exhibits both creep and plastic deformation due to the large temperature changes. As thermal conditions become more severe, the severity metric increases, but its rate decreases—for example between the 0-100^{o}C and -40-125^{o}C tests, total severity increase more than 3X from 8029 to 33478, but between the -40-125^{o}C and -55-125^{o}C tests, the increase is only 28% from 33478 to 42863.

7.3.3. Severity Metric for SnAg Solder Joints

The severity metric for SnAg joints is similar to the one used for SnPb joints but also includes the contributions of time-dependent creep (but no contribution from grain boundary sliding) and time-independent plastic deformation and an effective stress and is given by

$$S = D(\sigma_{eff})^{C_2}\left(\frac{2t_{rise}}{t_{cycle}}\right)^{\alpha} + F\log_{10}\left[1+(\tau_r / t_{rise})^{\gamma}\right]\sigma_0(\sigma_0-\sigma_{sys})\delta(\sigma_0-\sigma_{sys})\left(\frac{t_{dwell}}{t_{cycle}}\right)^{\alpha} \qquad (7.15)$$

The first term in Equation (7.15) originates from the creep Equation (5.17) for SnAg solder joints, and since most creep deformation in the solder joint takes place during temperature ramp up/down, the creep terms are multiplied by the ratio of temperature rise time to cycle time. Here, D=0.002, F=121, γ=1, α=1, C_2=4.75 and σ_{sys} is the yield stress =24 [MPa] for SnAg joints [9]. Since the maximum stress occurs at the low-temperature dwell, the yield stress is assumed to be constant-i.e. temperature independent; σ_0 is a characteristic stress [MPa]. D was selected to give the same value of the severity metric as the case for air-cooled, single-dense SnPb boards at the 0-100°C test condition. That is, the 0-100°C case is used as a normalizing reference. F was chosen as 121, which is the ratio of the plastic strain to creep strain under the –55-125°C ATC test condition because creep and plastic strains accumulate damage in solder joints. Here, –55-125°C was chosen since the condition induces both creep and plastic strains (see Table 7.12).

Figure 7.15 shows the contributions of creep and plastic deformation to the SnAg severity metric for the three test conditions.

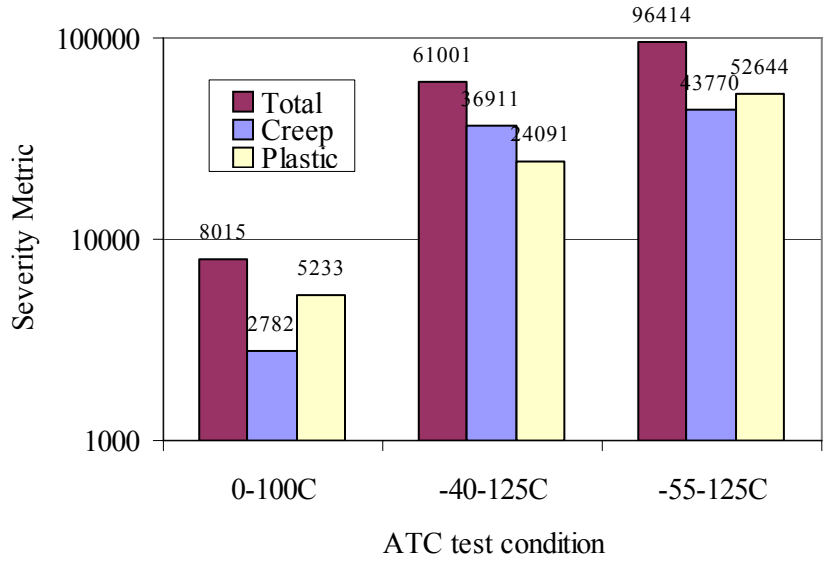

Figure 7.15. Contributions of creep and plastic strains on the severity metric for air-cooled SnAg joints at different ATC test conditions

Table 7.18 shows values of model parameters used for life-prediction of air-cooled SnAg solder joints used in deriving the severity metric. As with the SnPb cases, $\bar{h}$ has value 1 because the dimensions of the 357-PBGA are used as the reference values (see DNP and pitch). Board stiffness effect $\bar{g}$ has value 1 for the single-dense case since it is the reference case, and note that the double-dense package layout increased the stiffness effect by a factor 1.8. τ_r has values of

6sec, 191sec, and 143sec for the -55-125ºC , -40-125ºC, and 0-100ºC ATC tests, respectively.

Table 7.18. Life-prediction model parameters for air-cooled SnAg solder joints used in the severity metric for different ATC test conditions and two package layouts (SD and DD)

ATC Tests, °C	Pkg layout *	τ_r [sec]	σ_0 [MPa]	$\sigma(\tau)$ [MPa]	$\bar{g}$	y_i [mm]	$\bar{h}$	σ_{eff} [MPa]	DNP _ref [mm]	Pitch _ref [mm]	EI _ref [Nmm^2]
0-100	SD	143	66.2	21.4	1	0.07**	1	21.4	5.4	1.27	94374
-40-125	SD	191	110.2	39.2	1	0.07**	1	39.2	5.4	1.27	94374
-55-125	SD	6	121.1	57.0	1	0.07**	1	57.0	5.4	1.27	94374
0-100	DD	143	66.2	21.4	1.8	0***	1	38.9	5.4	1.27	575378
-40-125	DD	191	110.2	39.2	1.8	0***	1	61.5	5.4	1.27	575378

*only SD and DD package layouts studied. Assumes SS, DA, and SD package layout results are similar.
**distance from interface between package and solder joint (see Fig 7.6)
*** on neutral axis (see Fig 7.6)

Table 7.19 shows the relative contributions to the severity metric by creep and plastic strains for air-cooled SnAg joints at different ATC test conditions and two package layouts (SD and DD). In contrast to the SnPb case, there is plastic deformation for the SnAg joints at the 0-100°C ATC test condition. As thermal conditions become more severe from 0-100°C to -40-125°C and -55-125°C, the severity metric increased by 7.6X from 8015 to 61001 and by 12X from 8015 to 96414, respectively. The severity metric increased by 58% going from -40-125°C to -55-125°C.

Table 7.19. Contributions of creep and plastic strains from Equation 7.15 in the severity metric for air-cooled SnAg joints at different ATC test conditions and two package layouts (SD and DD)—no contributions from grain boundary sliding creep and dislocation climb creep

Solder Type	ATC Tests, °C	Package-Layout*	Severity_Creep	Severity_Plastic	Severity_Total
SnAg	0-100	SD	2782	5233	8015
SnAg	-40-125	SD	36910	24091	61001
SnAg	-55-125	SD	43770	52644	96414
SnAg	0-100	DD	47830	5233	53063
SnAg	-40-125	DD	314540	24091	338631

* only SD and DD package layouts studied. Assumes SS, DA, and SD package layout results are similar.

Summary: Severity Parameters

Table 7.20 lists and categorizes the parameters used in the severity metric for SnPb and SnAg joints. The ATC test conditions are known. The known material constants for the solder and other package components are for eutectic SnPb, SnAg and the board materials. The parameters for the geometric configuration are computed from known material properties and geometry. The remaining parameters use properties of the solder and PWB and the temperature profiles from the ATC test conditions to compute σ_o and τ_r. The integrated time-dependent effective stress is a function of other previously computed values.

Table 7.20. Parameters used in the severity metric by category

Category		Parameters
Thermal Cycle	ATC test	t_{rise}, t_{cycle}, t_{dwell}, ΔT
Materials	Solder (SnPb)	A=64, B=2.9×10^{-6}, C=188, n2=2, n3=7, α=1, γ=1, σ_{sys}, E
	Solder (SnAg)	D=0.002, F=121, α=1, γ=1,C_2=4.75, E
	Solder & ATC test	σ_0 (Eq. 7.3), τ_r (Eq. 7.2), σ_{eff} (Eq.7.4)
	Other package components	E_i (Appendix A)
Geometry	Geometric Configuration	$\bar{g}$ (Eq.6), y_i, A_i, I_i, $\bar{h}$

FEM analysis was only needed to generate the form of the stress profiles for the corner joint in the boundary region (joints with largest cracks) for the three ATC test protocols (Figure 7.7). The time responses of the profiles were represented by Equations 7.9-7.12, but ultimately the integrated stress form was approximated by Equation 7.13. Thus FEM was necessary only to get the approximate integrated form of stress. This equation is then used for the three ATC test protocols (or any other protocol—as long as the stress profiles have reasonably similar shape), and no further FEM analysis is required to compute the severity metric. Test data from Motorola was used in determining the constants since MOT data represents a wider range of data in thermal conditions (0-100C, -40-125C, and -55-125C) and package layouts (single-dense, single-sparse, double-alternating, and double-dense).

7.3.4. Life-Prediction Results

The severity metric was designed to reflect the overall damage to the solder joints resulting from differing conditions for various package designs. The severity model was fitted only using Motorola data, so that UT data is independent of the fit. The life prediction models were generated as follows (as fitted to Motorola data):

For SnPb:

$$\log [\text{life (cycles)}] = -0.7037 \times \log [\boldsymbol{S}] + 6.7856 \tag{7.16}$$

For SnAg:

$$\log [\text{life (cycles)}] = -0.6492 \times \log [\boldsymbol{S}] + 6.7563 \tag{7.17}$$

These life predictions are plotted and tabulated with the Motorola and UT data in Figure 7.10 and Table 7.21, respectively. The vertical bars in Figure 7.10 represents two standard deviations of the life data. Instead of discussing the data as a whole, the discussion below breaks down the data into three sub-sections.

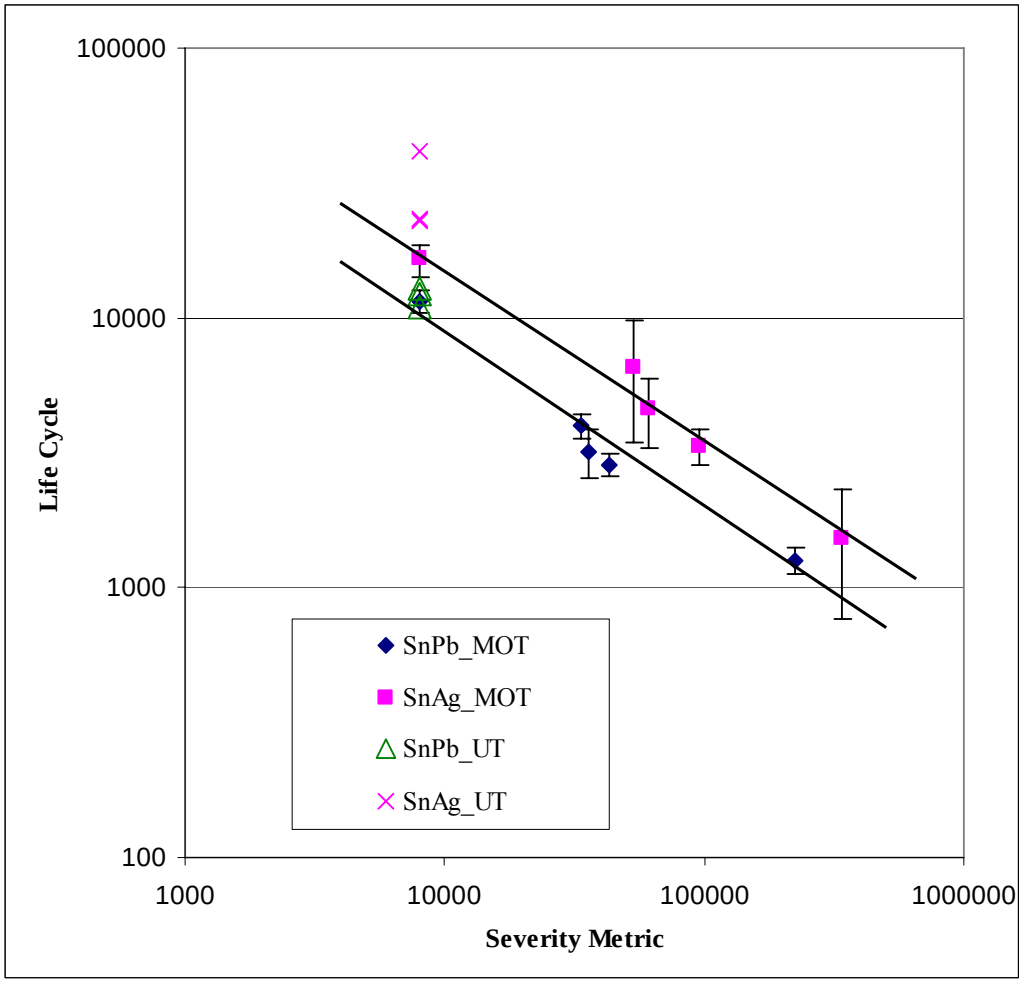

Figure 7.16. Severity metric and life cycles for SnAg and SnPb joints for 24 internal test cases (MOT+UT)

Table 7.21. Life-prediction using severity metric compared with experimental life data (all data, UT and Motorola)

Test Case	Solder Type	ATC Tests, °C	No. Fails	Package -Layout	Post-Process Cond	Severity Metric S	Exp. Mean Life, cycles (STD)	Predicted Life, cycles	% Diff.
1*	SnPb	0-100	24	SD	Aged	8028	10990 (1660)	10912	-1
2*	SnPb	0-100	23	SD	Air	8028	12800 (1450)	10912	-15
3*	SnPb	0-100	24	SD	Quench	8028	12240 (1430)	10912	-11
4	SnPb	0-100	26	SD	Air	8028	12160 (810)	10912	-10
5	SnPb	-40-125	29	SD	Air	33478	3970 (440)	3995	1
6	SnPb	-55-125	13	SD	Air	42863	2850 (270)	3357	18
7	SnPb	0-100	18	SS	Air	8028	11650 (1110)	10912	-6
8	SnPb	-40-125	18	SS	Air	33478	4050 (430)	3995	-1
9	SnPb	0-100	13	DA	Air	8028	10320 (880)	10912	6
10	SnPb	-40-125	13	DA	Air	33478	3810 (340)	3995	5
11	SnPb	0-100	14	DD	Air	35542	3200 (630)	3830	20
12	SnPb	-40-125	15	DD	Air	223830	1260 (140)	1049	-17
13**	SnAg	0-100	12	SD	Aged	NA	41236 (6020)	NA	NA
14*	SnAg	0-100	11	SD	Air	8015	23250 (6280)	16668	-28
15*	SnAg	0-100	24	SD	Quench	8015	22850 (3950)	16668	-27
16	SnAg	0-100	25	SD	Air	8015	16260 (2500)	16668	3
17	SnAg	-40-125	26	SD	Air	61001	5462 (894)	4463	-18
18	SnAg	-55-125	13	SD	Air	96414	3370 (500)	3316	-2
19	SnAg	0-100	15	SS	Air	8015	15600 (1680)	16668	7
20	SnAg	-40-125	14	SS	Air	61001	5540 (630)	4463	-19
21	SnAg	0-100	14	DA	Air	8015	17850	16668	-7

							(1710)		
22	SnAg	-40-125	11	DA	Air	61001	4810 (1000)	4463	-7
23	SnAg	0-100	15	DD	Air	53063	6610 (3160)	4886	-26
24	SnAg	-40-125	15	DD	Air	338631	1540 (770)	1467	-5

Note: *tests run in UT, and others at Motorola
**Data set 13 not used—life data artificially long due to resin cracks (Chapter 3, Section 3.3.3)

7.3.4.1. Life-Prediction Results: Motorola Data

Table 7.22. Life-prediction using severity metric compared with Motorola experimental life data for the specific cases covered by the severity metric

Test Case	Solder Type	ATC Tests, °C	No. Fails	Package -Layout	Post-Process Cond	Severity Metric S	Exp. Mean Life, cycles (STD)	Predicted Life, cycles	% Diff
4	SnPb	0-100	26	SD	Air	8028	12160 (810)	10912	-10
5	SnPb	-40-125	29	SD	Air	33478	5462 (894)	3995	-26
6	SnPb	-55-125	13	SD	Air	42863	2850 (270)	3357	18
11	SnPb	0-100	14	DD	Air	35542	3200 (630)	3830	20
12	SnPb	-40-125	15	DD	Air	223830	1260 (140)	1049	-17
16	SnAg	0-100	25	SD	Air	8015	16260 (2500)	16668	3
17	SnAg	-40-125	26	SD	Air	61001	4020 (1420)	4463	11
18	SnAg	-55-125	13	SD	Air	96414	3370 (500)	3316	-2
23	SnAg	0-100	15	DD	Air	53063	6610 (3160)	4886	-26
24	SnAg	-40-125	15	DD	Air	338631	1540 (770)	1467	-5

First, Table 7.22 focuses only on the life data that the severity metric was specifically developed for: SnPb and SnAg solders, air-cooled post processing, single-dense and double-dense package layouts, and 0-100^{o}C, -40-125 ^{o}C, and -55-125 ^{o}C ATC test protocols. Out of the 10 cases, four have predictions less than 6% different from the mean experimental data, four between 10%-20%, and two cases at 26%. Except for the largest difference (26%) in case 23 (DD, 0-100^{o}C), the predictions are better for SnAg solder than for SnPb solder, which is promising since no industry-standard lead-free life prediction models exist. Otherwise, there does not appear to be trends for which cases the predictions did best.

Except for one case, the life-prediction using the severity metric was much better than the predictions from the industry-standard life prediction models (Table 7.14) applied to the above SnPb test conditions as shown in Table 7.23.

Second, Table 7.23 focuses on the life data that are restricted to air-cooled post-processing but allows for the single-sparse and double-alternating package layouts to be represented by the single-dense case. Not counting the data already presented in Table 7.24, eight additional cases covering SS and DA are shown. In general, the life predictions are much better for these two package-layout cases than for the single-dense and double-dense cases for both SnPb and SnAg solders. The severity metric predicts life with less than 10% difference from the mean experimental life, except for one case.

Table 7.23. Life-prediction using Severity Metric, Coffin-Manson (CM), Engelmaier, and Norris-Landzberg (NL) models and comparison with experimental life data (Motorola) for the specific cases covered by the severity metric

Test Case	Solder Type	ATC Tests, °C	Package -Layout	Post-Process Cond	Exp. Mean Life, cycles (STD)	Predicted Life, cycles			
						Severity	CM **	Engelm -aier*	NL **
4	SnPb	0-100	SD	Air	12160 (810)	10912		9190	
5	SnPb	-40-125	SD	Air	3970 (440)	3995	4466	1942	2617
6	SnPb	-55-125	SD	Air	2850 (270)	3357	3753	2136	3842
11	SnPb	0-100	DD	Air	3200 (630)	3830		9190	
12	SnPb	-40-125	DD	Air	1260 (140)	1049	1175	1942	689

Notes:
See section 1.4.6 for CM, NL and Engelmaier life models and the model parameters. Here, n was chosen as 2 in CM model.
*fitting parameter, F, chosen as 1.
** Coffin-Manson model and Norris-Landzberg models calculate AF. Therefore, 0-100^{o}C test is used as reference data and the predicted life of -40-125^{o}C or -55-125^{o}C is equal to AF*life (cycle) of 0-100^{o}C ATC

Table 7.24. Life-prediction using severity metric compared with Motorola experimental life data assuming the effects of SS and DA are the same as SD package layout

Test Case	Solder Type	ATC Tests, °C	No. Fails	Package -Layout	Post-Process Cond	Severity Metric S	Exp. Mean Life, cycles (STD)	Predicted Life, cycles	% Diff
7	SnPb	0-100	18	SS	Air	8028	11650 (1110)	10912	-6
8	SnPb	-40-125	18	SS	Air	33478	4050 (430)	3995	-1
9	SnPb	0-100	13	DA	Air	8028	10320 (880)	10912	6
10	SnPb	-40-125	13	DA	Air	33478	3810 (340)	3995	5
19	SnAg	0-100	15	SS	Air	8015	15600 (1680)	16668	7
20	SnAg	-40-125	14	SS	Air	61001	5540 (630)	4463	-19
21	SnAg	0-100	14	DA	Air	8015	17850 (1710)	16668	-7
22	SnAg	-40-125	11	DA	Air	61001	4810 (1000)	4463	-7

Except for one case, the life-prediction using the severity metric was much better than the industry-standard life prediction models applied to the above SnPb test conditions with single-sparse and double-alternating package layouts as shown in Table 7.25.

Table 7.25. Life-prediction using Severity Metric, Coffin-Manson (CM), Engelmaier, and Norris-Landzberg (NL) models (Table 7.14) and comparison with experimental life data (Motorola) assuming the effects of SS and DA are the same as SD package layout.

Test Case	Solder Type	ATC Tests, °C	Package -Layout	Post-Process Cond	Exp. Mean Life, cycles (STD)	Predicted Life, cycles			
						Severity	CM**	Engelm-aier*	NL**
7	SnPb	0-100	SS	Air	11650 (1110)	10912		9190	
8	SnPb	-40-125	SS	Air	4050 (430)	3995	4279	1942	2507
9	SnPb	0-100	DA	Air	10320 (880)	10912		9190	
10	SnPb	-40-125	DA	Air	3810 (340)	3995	3791	1942	2221

Notes:
See section 1.4.6 for CM, NL and Engelmaier life models and the model parameters. Here, n was chosen as 2 in CM model.
*fitting parameter, F, chosen as 1
** Coffin-Manson model and Norris-Landzberg models calculate AF. Therefore, 0-100^{o}C test is used as reference data and the predicted life of -40-125^{o}C or -55-125^{o}C is equal to AF*life (cycle) of 0-100^{o}C ATC

7.3.4.2. Life-Prediction Results: UT Data

Third, Table 7.26 focuses on the five cases of experimental life tests done at UT that includes aged and quenched joints. Recall that the severity metric does not include the effects of quenched and aged post-processing at this time, Also since the UT data is only for the single-dense package layout and 0-100^{o}C ATC protocol, the predicted life are the same for the three SnPb cases and the same for the two SnAg cases. The predicted life consistently underestimated the UT experimental life data by less than 15% for SnPb and less than 28% for SnAg.

Recall that the UT life data was always larger than the Motorola data for the same solder, air-cooled, and single-dense cases, but especially for SnAg solder joints.

Table 7.26. Life-prediction using severity metric compared with UT experimental life data

Test Case	Solder Type	ATC Tests, °C	No. Fails	Package -Layout	Post-Process Cond	Severity Metric S	Exp. Mean Life, cycles (STD)	Predicted Life, cycles	% Diff
1*	SnPb	0-100	24	SD	Aged	8028	10990 (1660)	10912	-1
2*	SnPb	0-100	23	SD	Air	8028	12800 (1450)	10912	-15
3*	SnPb	0-100	24	SD	Quench	8028	12240 (1430)	10912	-11
14*	SnAg	0-100	11	SD	Air	8015	23250 (6280)	16668	-28
15*	SnAg	0-100	24	SD	Quench	8015	22850 (3950)	16668	-27

Here, the industry-standard life predictions from Coffin-Manson and Norris-Landzburg are not compared because the data is only for 0-100^{o}C ATC tests and both require reference values. The Engelmaier model was not compared since it consistently did the worst predictions.

7.3.5. Life-Prediction Models applied to External Data

The life-prediction models, Equations 7.15 and 7.16, based upon the severity metric were developed from the 18 life data sets from tests run Motorola. The results were then applied to the six cases of UT test data. In this section, the models were applied to configurations and thermal cycling tests from external sources. Recall that the UT/Motorola conditions were:

357 PBGA

10mm die size

1.27mm pitch

DNP=5.4mm

1.6mm board thickness

ATC test protocols: 0-100ºC (30min cycle), -40-125ºC (1hr cycle), -55-125ºC (20min cycle)

Life-prediction of SnPb solder joints

The seven external SnPb joint data are from Amkor, Motorola and a confidential source. The number of solder joints differed from 256 to 1156, the DNP (distance from neutral point to worst joint under die periphery) from 5.4mm to 13.4mm, the board thickness from 1.6mm to 3.2mm, the joint pitch from 1mm to 1.27mm, some of the ATC tests differed in dwell and ramp times, but the single-dense, air-cooled condition were identical to the UT experimental study. Table 7.27 compares the life-prediction from the severity metric to the external data.

Table 7.27. Comparison of life-prediction based on severity metric with external test data for SnPb solder and different ATC tests (all data for single-dense and air-cooled.)

Test Pkg	Solder Type	ATC Test° C	PWB thick [mm]	DNP [mm]	Severity Metric S	Exp. Life, cycles	Predicted Life, cycles	% Diff
+256 I/O PBGA 1.27mm pitch	SnPb	0-100	1.6	6.3	9456	6194	9725	57
+256 I/O PBGA 1.27mm pitch	SnPb	-40-125	1.6	6.3	42091	3164	3401	-7
++361 I/O PBGA 1.27mm pitch	SnPb	0-100	1.6	5.4	8028	10221	10912	-7
+256 I/O PBGA 1.27mm pitch	SnPb	-55-125*	1.6	6.3	64022	4544	2531	-44
1156 I/O PBGA 1mm pitch	SnPb	0-100**	1.6	13.4	37654	3050	3677	21
1156 I/O PBGA 1mm pitch	SnPb	0-100**	2.3	13.4	61182	2736	2613	-4
1156 I/O PBGA 1mm pitch	SnPb	0-100**	3.2	13.4	130511	1814	1488	-18

Note: + from Amkor, ++ from Motorola, all others from confidential source *2min ramp/ 13min dwell, **10min ramp/ 10min dwell, all other ATC test conditions are identical to UT experimental study

Of the seven external cases, the severity metric predicted life within 7% for three cases, and 18%, 21%, 44% and 57% for the remaining four cases. The metric did very well for the confidential source data even though that data represented the largest differences in physical parameters: pitch—1.0 versus 1.27mm (1156 versus 356 joints), 0-100^{o}C ATC (40- versus 30-minute thermal cycles), PWB thichness (up to 3.2 versus 1.6mm), DNP (13.4 versus 5.4). The

metric did worse on the the three data from Amkor (57%, 7%, and 44%). The only differences in conditions of these three data from UT are the number of joints (although the joint pitch was the same), DNP of 6.3 versus 5.4mm and the -55-125^{o}C ATC test had 3min ramp/13min dwell versus 1min ramp/4min dwell. The change in DNP caused an 8% increase in the effective stress which was insufficient to decrease life as needed to match the data. A note on the -55-125^{o}C ATC test data from Amkor—that cycle has 2min ramp/13min dwells compared to the UT test with 1min ramp/4min dwell. So the Amkor test appears to be less stressful, however, it increases τ_r which allows more time for creep deformation (compare with -55-125^{o}C ATC test data in Table 7.17). This along with a larger DNP causes a lower life prediction than experimental data. The metric did very well in the single data from Motorola.

Tables 7.28 and 7.29 show life prediction model parameters and severity metrics, respectively, for the external data. For example, cases with 1156PBGA had the largest $\bar{h}$ due to the largest DNP (13.4mm versus 5.4mm), and the effective stress increased by 20% and the severity increased by 3X when the board thickness increases from 1.6mm to 3.2mm.

Table 7.28. Life-prediction model parameters applied to air-cooled SnPb solder joints used in the severity metric for the external data

Test Pkg	ATC Tests, °C	Pkg layout*	τ_r [sec]	σ_0 [MPa]	$\sigma(\tau)$ [MPa]	$\bar{g}$	$\bar{h}$	σ_{eff} [MPa]
+256 PBGA	0-100	SD	163	39.5	13.6	1	1.08	14.7
+256 PBGA	-40-125	SD	214	66.6	24.5	1	1.08	26.4
++361 PBGA	0-100	SD	163	39.5	13.6	1	1	13.6
+256 PBGA	-55-125*	SD	28	73.6	34.2	1	1.08	36.9
1156 PBGA	0-100**	SD	163	39.5	19.1	1	1.4	26.8
1156 PBGA	0-100**	SD	163	39.5	19.1	1.12	1.4	30.1
1156 PBGA	0-100**	SD	163	39.5	19.1	1.31	1.4	35.2

Note: + from Amkor, ++ from Motorola, all others from confidential source
*2min ramp/ 13min dwell, **10min ramp/ 10min dwell, all other ATC test conditions are identical to UT experimental study

Table 7.29. Contributions of creep and plastic strains from Equation 7.1 in the severity metric applied to air-cooled SnPb joints for the external data

Test Pkg	ATC Tests, °C	Package-Layout*	Severity_ Creep by GBS*	Severity_ Creep by DC*	Severity _Creep	Severity_ Plastic	Severity Total
*256 PBGA	0-100	SD	9174	282	9174	0	9456
*256 PBGA	-40-125	SD	22326	13007	35333	6758	42091
**361 PBGA	0-100	SD	7864	164	8028	0	8028
*256 PBGA	-55-125	SD	11608	35907	47515	16507	64022
1156 PBGA	0-100**	SD	23068	14586	37654	0	37654
1156 PBGA	0-100**	SD	28937	32245	61182	0	61182
1156 PBGA	0-100**	SD	39588	96569	136157	0	136157

Note: + from Amkor, ++ from Motorola, all others from confidential source
*2min ramp/ 13min dwell, **10min ramp/ 10min dwell, all other ATC test conditions are identical to UT experimental study

Table 7.30 compares the life-prediction from the severity metric and industry-standard models for the external data. Except for one case, the severity metric predicts experimental life more closely than the other three models.

Table 7.30. Comparison of life-prediction based on severity metric with external test data for SnPb solder and different ATC tests (all data for single-dense and air-cooled.)

Test Pkg	Solder Type	ATC Test° C	PWB thick [mm]	DNP [mm]	Exp. Life, cycles	Severity cycles	CM^ cycles	Engel cycles	NL^ cycles
+256 I/O PBGA	SnPb	0-100	1.6	6.3	6194	9725		6235	
+256 I/O PBGA	SnPb	-40-125	1.6	6.3	3164	3401	2275	1335	1333
++361 I/O PBGA	SnPb	0-100	1.6	5.4	10221	10912		9190	
+256 I/O PBGA	SnPb	-55-125*	1.6	6.3	4544	2531	1219	1232	1598
1156 I/O PBGA	SnPb	0-100**	1.6	13.4	3050	3677		751	
1156 I/O PBGA	SnPb	0-100**	2.3	13.4	2736	2613		751	
1156 I/O PBGA	SnPb	0-100**	3.3	13.4	1814	1488		751	

Note: + from Amkor, ++ from Motorola, all others from confidential source
See section 1.4.6 for CM, NL and Engelmaier life models and the model parameters. Here, n was chosen as 2 in CM model.
*2min ramp/ 13min dwell, **10min ramp/ 10min dwell, all other ATC test conditions are identical to UT experimental study
^ Coffin-Manson model and Norris-Landzberg models calculate AF. Therefore, 0-100^{o}C test is used as reference data and the predicted life of -40-125^{o}C or -55-125^{o}C is equal to AF*life (cycle) of 0-100^{o}C ATC

Life-prediction of SnAg solder joints

The single SnAg joint data is from Motorola. The number of solder joints (334) and the DNP (4.5mm) differ, as shown in Table 7.31 but the board thickness, single-dense, air-cooled and ATC tests are identical to the UT experimental study. The metric underpredicts life by 40%.

Table 7.31. Comparison of life-prediction model for SnAg based on severity metric applied to external test data

Test Pkg	Solder Type	ATC Tests, °C	PWB thickness [mm]	DNP [mm]	Severity Metric S	Exp. Life, cycles	Predicted Life, cycles	% Diff
324 PBGA	SnAg	-45-125	1.6	4.5	48029	8690 (b=8.0)	5212	-40

Tables 7.32 and 7.33 list the model parameters and contributions of creep and plastic strains to the severity metric for the single SnAg external test case.

Table 7.32. Life-prediction model parameters for air-cooled SnAg solder joints used in the severity metric applied to external data

Test Pkg	ATC Tests, °C	Pkg layout*	τ_r [sec]	σ_0 [MPa]	$\sigma(\tau)$ [MPa]	$\bar{g}$	$\bar{h}$	σ_{eff} [MPa]
324 PBGA	-45-125	SD	191	110.3	39.2	1	0.91	35.8

Table 7.33. Contributions of creep and plastic strains from Equation 7.1 in the severity metric for air-cooled SnAg joints applied to external data

Test Pkg	ATC Tests, °C	Package-Layout*	Severity_ Creep by GBS*	Severity_ Creep by DC*	Severity _Creep	Severity_ Plastic	SeverityTotal
324 PBGA	-45-125	SD	NA	23939	23939	24090	48029

7.4. CONCLUSIONS

In this chapter FEM modeling and experimental data showed that solder joint life is affected by solder type, post-process condition, package layout, and ATC test conditions. The following summarizes the major findings from the experimental life study, FEM analyses, and life-prediction models.

Experimental Life Study

- Solder type

  Air-cooled SnAg solder joints had longer life than SnPb joints by 34-107%, 18-37%, and 18% under 0-100^{o}C, -40-125^{o}C, and -55-125^{o}C ATC test conditions, respectively

- Post-processing

  Air-cooled and quenched packages for both SnAg and SnPb packages have similar mean life and are within 4% of each other and are not statistically different.

Aged packages failed 14% earlier than non-aged for SnPb solder but lasted 76% longer than non-aged packages for SnAg solder. The aged SnAg joints had PCB resin cracks that reduced solder joint stress thereby increasing life (See section 3.3.3 in chapter 3).

- Package Layout

Double-dense package layout reduced solder joint life significantly, approximately by 70% for SnPb joints and 40% for SnAg joints, compared to the other three configurations.

The single-dense, single-sparse, and double-alternating board layout packages had similar mean life and were within 15% of each other for SnPb packages and within 37% of each other for SnAg packages.

- ATC Protocols

Compared to packages exposed to the 0-100^{o}C ATC test, packages exposed to the -55-125°C LLTS (Liquid-to-Liquid Thermal Shock) and the -40-125°C ATC tests had only 0.22 and approximately 0.29 (0.25-0.33) the life, respectively.

FEM Study

- Solder Type

Creep strain, 0.0077 for SnPb and 0.0048 for SnAg, at the 0-100°C ATC test changed by +58% and –30% for SnPb and by +103% and +58% for SnAg for the -40-125°C and the -55-125°C ATC tests, respectively. The creep strain from the -55-125°C ATC test is smaller in the -40-125°C case for SnPb due to

the fast transit time between temperatures while the creep strain is larger in the SnAg case due to slower stress relaxation.

- Post-processing

Aged SnPb joints with 9.5mm mean phase size resulted in higher stresses and lower life than air-cooled joints with 4.5mm mean phase size. There was no simulation run on SnAg joints for different post-processing conditions since the constitutive equation does not have a microstructural parameter.

- Package Layout

The double-dense configuration shows no warping due to symmetry, and its stresses are larger than for the other configurations (single-dense, single-sparse, and double-alternating). For the other three layouts, the PWB warping reduces the effects of thermal loads on the solder joints and the stresses/strains are dominated by local effects due to the CTE mismatch between die and solder joint—thereby the stresses and strains for single-dense, single-sparse, and double-alternating were identical.

- ATC Protocols

No plastic deformation occurred for all SnPb and SnAg joints at the 0-100°C ATC tests, and for the SnPb solder joints at the -40-125°C ATC tests, except for the double-dense package layout.

For single-dense, single-sparse and double-alternating board layouts, the plastic strains were the same: 0.0034 for SnPb and 0.0093 for SnAg at the -55-125°C ATC tests, and 0.0026 for SnAg at the -40-125°C ATC tests.

For the double-dense board layout, the plastic strains of 0.0025 for SnPb and 0.0187 for SnAg at the -40-125°C ATC tests increased by 740% and 157% at the -55-125°C ATC tests.

Life-Prediction Model based upon the Severity Metric

- Motorola Experimental Data

The Motrola data provided the most extensive test parameter changes: two solder types (SnPb and SnAg), three ATC test protocols (0-100^{o}C, -40-125^{o}C, -55-125^{o}C), four package layouts (SD, SS, DA, DD) but all for air-cooled post processing, so this data set was used for developing the severity metric. For the 18 Motorola cases and compared to experimental life data, the severity metric predicted life with a difference less than 7% for 11 cases, between 10-20% in five cases, and two cases at 26%. The comparison was very good for the double alternating and single-spare package layout cases—these two configurations were not modeled in the severity metric and assumed to be the same as the single-dense cases.

- UT Experimental Data

The severity metric underestimated all five of the UT experimental cases: by less than 10% in one case, between 10-20% in two cases, and between 20-30% in two cases. It should be noted, that the UT life data was higher than the Motorola data for all cases that were identical in experimental parameters. Also note that the UT data was not used in developing the severity metric.

- External Experimental Data

Seven SnPb data cases from external sources were used to test the severity metric. The number of solder joints differed from 256 to 1156, the DNP from 5.4mm to 13.4mm, the board thickness from 1.6mm to 3.2mm, the joint pitch from 1mm to 1.27mm, some of the ATC tests differed in dwell and ramp times, but the single-dense, air-cooled condition were identical to the UT experimental study. Of the seven cases, the severity metric predicted life within 7% for three cases, and 18%, 21%, 44% and 57% for the remaining four cases. The metric did exteremely well for the data that represented the largest differences in physical parameters from the UT parameter values. The severity metric had a 40% difference to the one external SnAg data case.

- Life-Predictions from the Severity Metric and Industry-Standard Models for SnPb solders.

Overall, the severity metric was a better predictor of life than applying the Coffin-Manson, Engelmaeier, and Norris-Lanzberg models.

CHAPTER 8

Conclusions and Recommendations

The major objectives of this research were to develop an integrated, experimentally-verified, life-prediction model that includes material and structural parameters and that is based upon the prototypic packaging system, plastic ball-grid arrays, and to evaluate the reliability of semiconductor packages with SnPb and SnAg solders for different design and testing parameters. To achieve these objectives, this study undertook extensive experimental and analytical studies. The experimental effort focused on the reliability of solder joints in 357-PBGA semiconductor packages with the following parameters:

Solder type: SnPb: 62%Sn36%Pb2%Ag

SnAg: 96.5%Sn3.5%Ag

Post-process heat treatment:

Air-cooled

Quenched to 0^{o}C

Aged at 150 ^{o}C (SnPb) and 160 ^{o}C (SnAg) for 1008 hours

Thermal loading—accelerated thermal cycling (ATC) tests:

0 ^{o}C to 100 ^{o}C, 30-minute cycles

-40 ^{o}C to 125 ^{o}C, 1-hour cycles

-55 ^{o}C to 125 ^{o}C, 10-minute cycles

Package Layouts (package layout on PWB defined in Chapter 2):

Single (sided)-sparse—SS

Single (sided)-dense—SD

Double (sided)-alternating—DA

Double (sided)-dense—DD

Test locations: Motorola and the University of Texas

Solder joint crack growth, microstructure and life were experimentally measured and evaluated, using dye penetration and optical imaging techniques, polishing and optical/SEM images, and electrical continuity and event detection, respectively. In parallel, FEM models were developed and simulated to explain the test results as well as investigating the effects of parameter variations. Based upon the test and FEM results, a life-prediction model was proposed for both SnPb and SnAg solder joint packages.

The following is a summary of major findings presented in the same order as chapters in this dissertation.

8.1. MICROSTRUCTURE STUDY (CHAPTER 3)

SnPb Solder Joints

- Compared to non-aged SnPb joints, aged SnPb solder joints exhibited coarser microstructure so tended to deform more by dislocation than by grain sliding, resulting in earlier failure. Initially, aged SnPb joints showed large lead-rich phases of about 4μm in size in the tin matrix, while the air/quenched joints showed smaller and more uniformly scattered lead-rich phases of 0.6-0.8μm size.

- For aged SnPb joints, a CuNiSn intermetallic layer about 9μm thick formed during aging and early thermal cycling. The tin phase near the joint interface was consumed to form the intermetallic layer, resulting in a long layer of lead-rich phase. No CuNiSn intermetallic layer was observed at the package interface in the air-cooled and quenched SnPb packages until 14K cycles, when a layer 1-2μm thick developed. Intergranular failure was observed in all sectioned quenched, air-cooled and aged SnPb joints--propagating through the interphase boundary between the lead-rich and tin-rich phases. For aged SnPb joints, straight cracks propagated along the layer of lead-rich phase. For air-cooled and quenched SnPb joints the crack path was longer and coarser.

SnAg Solder Joints

- Initially, SnAg solder joint microstructure consisted of primary Sn phase surrounded by Sn-Ag eutectic structures, and the aged joints showed smaller, globular Ag_2Sn particles (effects of long thermal diffusion process), compared to the rod-like Ag_2Sn particles in the non-aged joints.
- At 21K cycles for the 0-100^{o}C ATC test conditions, coarse Ag_2Sn particles were found to reside within or at the grain boundaries for all SnAg joints. Microstructural pictures revealed grain boundaries in the etched air-cooled and quenched SnAg joints, while few, if any, grain boundaries were revealed in aged SnAg joints. Preliminary microstructural observations between aged and non-aged SnAg packages

did not reveal anything substantive to explain the longer life of aged SnAg solders.

- Knoop microhardness measurements showed that aged SnAg joints were slightly softer than the non-aged SnAg joints, but the differences were not significant.
- Laminate cracks were found in the package substrate and test board in aged SnAg joints only. The laminate cracks were probably created by the embrittling effect of the long aging (1008hr at 160^{o}C) on the resins. These cracks, so called pad cratering, were believed to relieve the strain and stress on the aged SnAg solder joints thereby prolonging life in ATC testing.

8.2. CRACK SHAPE/ ORIENTATION/ AREA/ LENGTH STUDY (CHAPTER 4)

- SnPb solder joints had about twice the crack growth rates compared to SnAg joints, reflecting shorter life.
- Air-cooled and quenched solder joints had similar crack growth characteristics, independent of solder type.
- Aged SnAg joints had much smaller growth rates (as much as 50% less) than non-aged SnAg joints.
- Experimental crack orientation angles, measured from the joint center to the centroid of the measured crack areas, had similar trends as the geometric and FEM-estimated angles, but with large standard deviations

and only about half of the angles agreed to within $\pm 15^{o}$ of the other two angle measures.

- Crack shapes were concave in all SnPb and SnAg solder joints except for aged SnPb joints which exhibited straight crack fronts.
- For aged SnPb joints, the % crack length appeared to better predict joint life than % crack area.

8.3. CRACK INITIATION ANALYSIS AND MODELING STUDY (CHAPTER 5)

Based upon experimental data:

- Cracks propagated through the package and board interfaces of joints, and the primary cracks at the package interface showed the largest growth followed by the primary cracks at the board interface.
- There were no secondary cracks observed at the package interface of aged SnPb joints.

Based upon FEM simulations:

- Simulation showed lead phase particles of aged SnPb joints did not grow, while in air-cooled joints they grew from 0.6 μm to 1.3 μm until microcracking occurred. The voids of air-cooled SnPb joints did not nucleate until the lead phase particles became large enough to cause void nucleation. Once voids nucleated, the growth rates increased as void size increased.

- Voids are distributed at the joint interfaces, and no voids nucleated in the other areas.
- Aged SnPb joints had larger cracks because of larger dislocation creep caused by larger phase sizes than air-cooled SnPb joints (4μm versus 0.6-0.8μm)
- Secondary cracks were suppressed at the package interface of aged SnPb joints because compressive stresses prevented voids from nucleating.
- The void nucleation rate of aged SnAg joints was slower than in air-cooled joints due to higher strain to failure, and the time spent for microcracking in aged SnAg joints was 15% longer than in air-cooled SnAg joints.
- The crack initiation life in SnAg joints was approximately 100% longer than in SnPb joints.

8.4. CRACK PROPAGATION ANALYSIS AND MODELING STUDY (CHAPTER 6)

Based upon experimental data:

- Primary and secondary cracks propagated through the package and board interfaces of the joints except at the package interface of aged SnPb joints, where no secondary cracks evolved.
- The crack growth rates at the package interface were larger by ~200% for SnPb and ~100% for SnAg than at the board interface, and the package interface is the location for typical joint failures.
- For SnPb, aged joints had ~50% larger crack growth rates than non-aged SnPb joints, while aged SnAg joints had ~40% smaller crack growth rates

than non-aged SnAg joints. SnPb joints had ~100% faster crack growth rates than SnAg joints, implying earlier failure.

- The primary crack growth rate at the package interface decreased as the crack grew. For aged SnPb joints, the crack grew approximately at a constant rate of 10%/K cycles until 8K cycles (84% length), then the rate decreased to ~3%/K cycles to 13K cycles (98% length) and was nearly zero after 13K cycles.
- While the primary crack at the package interface was the largest crack and the one that ultimately leads to package failure (in combination with the secondary crack), the other cracks are significantly larger in proportion to the primary crack in SnAg solder joints than in SnPb solder joints.
- The ratio of the primary crack lengths at the board to package interfaces were ~50% larger in SnAg solder joints (20~65%) than for SnPb joints (10~37%).
- The ratio of the secondary cracks relative to the primary cracks at the package interface was ~100% larger for air-cooled SnAg solder joints than air-cooled SnPb joints.

Based upon FEM simulations:

- Applying constant no-crack boundary conditions to the crack propagation model significantly overestimated joint life. PWB warping decreased as cracks grew—therefore, the boundary conditions for analyzing crack propagation should reflect these compliance changes.

- The primary crack growth rate at the package interface decreased as the crack grew. Therefore, joint life increased by ~50% if there was no secondary crack to merge with the primary crack.
- A larger primary crack at the board interface appeared to increase joint compliance thereby reduceing the stress imposed on the primary crack at the package interface.
- Shear load was a major cause of crack growth, but the contribution of tensile load increased up to almost 80% of shear load as crack grew. The primary crack at the board interface slightly decreased the growth rate of the primary crack at the package interface.

8.5. LIFE AND LIFE-PREDICTION STUDY (CHAPTER 7)

Based upon experimental data:

- Air-cooled SnAg solder joints had longer life than air-cooled SnPb joints by 34-107%, 18-37%, and 18% under 0-100^{o}C, -40-125^{o}C, and -55-125^{o}C ATC test conditions run at Motorola, respectively.
- Air-cooled and quenched packages had similar mean life and were within 4% of each other and were not statistically different for both solder types. Aged packages failed 14% earlier (at 10994 cycles) than non-aged for SnPb solder but lasted 76% longer (at 41064 cycles) than non-aged packages for SnAg solder. The aged SnAg joints had PCB resin cracks that reduced solder joint stress thereby increasing life.

- Double-dense package layout reduced solder joint life by approximately by 70% for SnPb joints and 40% for SnAg joints, compared to the other three configurations.
- The single-dense, single-sparse, and double-alternating package layouts had similar mean life and were within 15% of each other for SnPb packages and within 37% of each other for SnAg packages.
- Compared to packages exposed to the 0-100^{o}C ATC test, packages exposed to the -55-125°C LLTS (Liquid-to-Liquid Thermal Shock) and the -40-125°C ATC tests had only 0.22 and approximately 0.29 (0.25-0.33) the life, respectively.

Based upon FEM simulations:

- Creep strain at the 0-100°C ATC test increased by +58% and –30% for SnPb and by +103% and +58% for SnAg for the -40-125°C and the -55-125°C ATC tests, respectively. The creep strain from the -55-125°C ATC test was smaller in the -40-125°C case for SnPb due to the fast transit time between temperatures while the creep strain was larger in the SnAg case due to slower stress relaxation.
- Aged SnPb joints with 9.5mm mean phase size resulted in higher stresses and lower life than air-cooled joints with 4.5mm mean phase size. There was no simulation run on SnAg joints for different post-processing conditions since the constitutive equation does not have a microstructural parameter.

- The double-dense configuration showed no warping due to symmetry, and its stresses were larger than for the other package layouts (single-dense, single-sparse, and double-alternating). For the other three package layouts, the PWB warping reduced the effects of thermal loads on the solder joints and the stresses/strains were dominated by local effects due to the CTE mismatch between die and solder joint—thereby the stresses and strains for single-dense, single-sparse, and double-alternating were identical.
- No plastic deformation occurred for all SnPb and SnAg joints at the 0-100°C ATC tests, and for the SnPb solder joints at the -40-125°C ATC tests, except for the double-dense package layout.
- For single-dense, single-sparse and double-alternating board layouts, the plastic strains were the same: 0.0034 for SnPb and 0.0093 for SnAg at the -55-125°C ATC tests, and 0.0026 for SnAg at the -40-125°C ATC tests.
- For the double-dense board layout, the plastic strains of 0.0025 for SnPb and 0.0187 for SnAg at the -40-125°C ATC tests increased by 740% and 157% at the -55-125°C ATC tests.

Life-prediction modeling study

A severity metric was developed to estimate damage to SnPb and SnAg solder joints subjected to thermal cycling and to reflect parameters associated with solder type, package-layouts (SD and DD only), and ATC test protocols. Effects of post-processing were not included in this initial effort.

- Motorola Experimental Data

The Motrola data provided the most extensive test parameter changes: two solder types (SnPb and SnAg), three ATC test protocols (0-100^{o}C, -40-125^{o}C, -55-125^{o}C), four package layouts (SD, SS, DA, DD) but all for air-cooled post processing, so this data set was used for developing the severity metric. For the 18 Motorola cases and compared to experimental life data, the severity metric predicted life with a difference less than 7% for 11 cases, between 10-20% in five cases, and two cases at 26%. The comparison was very good for the double alternating and single-spare package layout cases—these two configurations were not modeled in the severity metric and assumed to be the same as the single-dense cases.

- UT Experimental Data

The severity metric underestimated all five of the UT experimental cases: by less than 10% in one case, between 10-20% in two cases, and between 20-30% in two cases. It should be noted, that the UT life data was higher than the Motorola data for all cases that were identical in experimental parameters. Also note that the UT data was not used in developing the severity metric.

- External Experimental Data

Seven SnPb data cases from external sources were used to test the severity metric. The number of solder joints differed from 256 to 1156, the DNP from 5.4mm to 13.4mm, the board thickness from 1.6mm to 3.3mm, the joint pitch from 1mm to 1.27mm, some of the ATC tests differed in dwell and ramp times, but the single-dense, air-cooled condition were identical to the UT experimental study. Of the seven cases, the severity metric predicted life

within 7% for three cases, and 18%, 21%, 44% and 57% for the remaining four cases. The metric did exteremely well for the data that represented the largest differences in physical parameters from the UT parameter values. The severity metric had a 40% difference to the one external SnAg data case.

- Life-Predictions from the Severity Metric and Industry-Standard Models for SnPb solders.

Overall, the severity metric was a better predictor of life than applying the Coffin-Manson, Engelmaeier, and Norris-Lanzberg models.

8.5. FUTURE WORK

The following are the recommendations for future work.

Life-prediction and the severity metric

The severity metric predicted life very well for the 23 internal (UT and Motorola) and eight external experimental cases. Two experimental parameters were not included in this study: 1) single-sparse and double-alternating package layouts and 2) post-processing. The results presented show that the metric based upon the single-dense case takes care of the single-sparse and double alternating cases well. The severity metric should be expanded to include the effects of aging, as it was shown that air-cooling and quenched yielded similar results. Moreover, the severity metric needs to be tested on more data to determine its effectiveness and robustness. However, the results provided in this work show that the metric

contains many of the properties and processes parameters that determine solder joint life.

Load sharing characteristics of lead-free solders

Observations from crack measurement showed that the boundary region had the largest cracks for both types of solders, but the patterns of crack growth in other regions were different for the two solders. That is, in SnPb solder joints, it was quite clear that regions with the next largest cracks were boundary region, s-outside region, and inner boundary region (see Figure 2.2). For SnAg solder joints, however, the regions with the next largest cracks were not as definitive. It appeared that SnAg joints in other regions were able to share load more uniformly than in SnPb joints, thereby resulting in longer life (see P. K. Bhagavathula's MS Report [72] for detailed experimental findings). This observation should be studied in more detail.

AF modeling of lead-free solder joints

Empirical AF (acceleration factor) models have been developed and been widely used in the electronics industry to predict life of SnPb solder joints, such as the Norris Landzberg model [50]. However, few acceptable AF model exist for lead-free solder joints, partly because the history of lead-free solders is much shorter compared to SnPb solder (~1 decade vs ~5 decades) and because diverse lead-free solder alloys, such as Sn3Ag0.5Cu, Sn1Ag0.5Cu, Sn3.5Ag, etc, are still being proposed and used in the industry. Therefore, ATC test data generation and

collection or AF modeling of lead-free solder joints during ATC test is recommended as future study. The proposed life-prediction using the severity metric is a step in the right direction.

Characterization of dynamic performance of lead-free solder

Electronic products and boards are exposed during assembly and use to various dynamic loads such as bending, shock, drop, or vibration. IPC-JEDEC-9702 [81] specifies a monotonic 4 point bend test methodology for electronics package interconnects, and IPC is also drafting a shock test methodology. Future reliability studies must characterize dynamic bend, shock, and vibration performance for lead-free solder joints in various package types such as PBGA, FCBGA, CBGA and different substrate surface finishes. It may also be worthwhile to study the dynamic characteristics combined with aging.

Early failure of lead-free solder joints

Like our study, industry studies have observed abnormal early failures in lead-free SnAgCu solder joints during ATC testing, but the phenomena are inconsistent. Some studies [82] reported such early failures might be due to different grain orientations between tin grains in the solder joint. However, the exact root-cause of early lead-free solder joint failures is still unknown. iNEMI (International National Electrocnis Manufacturing Initiative) is studying this problem. In addition, experimental life of lead-free solder joints was more scattered—larger standard deviations than SnPb solder joints.

Pad cratering study

Large mechanical stresses occur in the solder joints of BGA (Ball Grid Array) packages assembled on PCB (Printed Circuit Board) when they experiences excessive bending or shock during board assembly or end-use conditions. These stresses induce mechanical cracks which initiate from the edge of the pad and propagate along the PCB fiber bundles, and is called pad cratering. Pad cratering is expected to occur more often in lead-free solder joints than traditional tin-lead joints because of the inherent rigidity of lead-free solder.

PCB material toughness study

Pad cratering can lead to a complete trace fracture in PCBs and result in an open circuit of the entire board. It is worthwhile to investigate the fracture toughness of different PCB materials and develop PCB materials or PCB designs that delay or oppress pad cratering.

APPENDIX A

Material Properties

Table A.1 lists the material properties of eutectic SnPb and SnAg and 62%Sn36%Pb2%Ag solders. The95.5%Sn3.8%Ag0.7%Cu solder properties and the material properties the components of the card assembly used in the FEM analyses are listed in Table A.2. Note: in the FEM analyses the properties of eutectic SnAg were used to model the SnAg solder joints and the properties of 62%Sn36%Pb2%Ag were used to model the SnPb solder joints.

Table A.1. Material properties of SnPb and SnAg solders [9]

Chemical Composition	Elastic Modulus		Yield Strength (0.2 % offset)		Tensile Strength		Relative Elongation (%)		Strength Coefficient		Hard-ening Expo-nent
% by Mass	(ksi)	GPa	(psi)	MPa	(psi)	MPa	Uni-form	Total	(psi)	MPa	
Sn-37Pb	2,273	15.7	3,950	27.2	4,442	30.6	3	48	4,917	33.9	0.033
Sn-2Ag-36Pb	2,617	18.0	6,287	43.3	6,904	47.6	1	31	7,223	49.8	0.011
Sn-3.5Ag	3,793	26.2	3,256	22.5	3,873	26.7	3	24	4,226	29.1	0.026

Note:

Database for Solder Properties with Emphasis on New Lead-free Solders, National Institute of Standards and Technology & Colorado School of Mines, Release 4.0, http://www.boulder.nist.gov/div853/lead%20free/solders.html

Table A.2. Material properties used for FEM stress analysis

Materials	Temp. [K]	Modulus [MPa]	Poisson ratio	CTE [ppm/K]
Die		162717	0.278	2.62
Mold compound	248 298 348 398 423	17443 15789 13513 11721 10686	0.25	15.5
Die attach		4998	0.4	96
Substrate	200 450	E1: 21787, E2: 9514 E3:21787, G: 9790 E1: 11928, E2: 5240 E3: 11928, G: 5377	$\nu_{31}=\nu_{13}$ =0.11 $\nu_{12}=\nu_{32}$ =0.39 ν_{23} =$(E_1/E_3)\nu$ =0.17	$\alpha_1=\alpha_3=16$ $\alpha_2=70$
PWB	200 400	E1: 20477, E2: 8963 E3:20477, G: 9239 E1: 13031, E2: 5722 E3: 13031, G: 5860		
Copper		117000	0.34	16.7
Nickel		220000	0.3	12.3
Ni_3Sn [83]		133300		13.7
Cu_6Sn_5 [84]		85560		16.3
Sn36Pb2Ag [45]	223 323 398	37650 29550 23475	0.35	24.1 26.1 27.9
Sn3.5Ag [77]		52708-61.74×T-0.0587*T^2 [°C]	0.4	21.85+0.02039×T [°C]
Sn3.8Ag0.7Cu * [85]	293-423	45000	0.4	16.7

Note. E1 and E2 represent in-plane Young's modulus of PCB, and E3 represents the out-of-plane Young's modulus.
* solder paste material. The properties were not used for FEM analysis.

APPENDIX B

Longhorn 357-PBGA Test Build Matrix

Appendix B lists the boards, solder type, package layout, post-processing, ATC test protocol and test location for all boards/packages used in this experimental test.

Table B.1. Test board build matrix—University of Texas (UT)

Board Type	Brd #	Parts/ Brd	Board Config	Paste Comp	Sphere Comp	Peak Reflow(C)	Cooling Rate	Aging Type	Cycle Type (C)
Slotted	UT1	15	SD	SnPb	SnPbAg	215	Air	Aged	0 to 100
Slotted	UT2	15	SD	SnPb	SnPbAg	215	Air	Aged	0 to 100
Slotted	UT3	15	SD	SnPb	SnPbAg	215	Air	Aged	0 to 100
Unslotted	UT4	15	SD	SnPb	SnPbAg	215	Air	Aged	0 to 100
Slotted	UT5	15	SD	SnPb	SnPbAg	215	Air	None	0 to 100
Slotted	UT6	15	SD	SnPb	SnPbAg	215	Air	None	0 to 100
Slotted	UT7	15	SD	SnPb	SnPbAg	215	Air	None	0 to 100
Unslotted	UT8	15	SD	SnPb	SnPbAg	215	Air	None	0 to 100
Slotted	UT10	15	SD	SnPb	SnPbAg	215	Quench	None	0 to 100
Slotted	UT11	15	SD	SnPb	SnPbAg	215	Quench	None	0 to 100
Slotted	UT12	15	SD	SnPb	SnPbAg	215	Quench	None	0 to 100
Unslotted	UT13	15	SD	SnPb	SnPbAg	215	Quench	None	0 to 100
Slotted	UT14	15	SD	SnAgCu	SnAg	235	Air	Aged	0 to 100
Slotted	UT15	15	SD	SnAgCu	SnAg	235	Air	Aged	0 to 100
Slotted	UT16	15	SD	SnAgCu	SnAg	235	Air	Aged	0 to 100
Unslotted	UT17	15	SD	SnAgCu	SnAg	235	Air	Aged	0 to 100
Slotted	UT18	15	SD	SnAgCu	SnAg	235	Air	None	0 to 100
Slotted	UT19	15	SD	SnAgCu	SnAg	235	Air	None	0 to 100
Slotted	UT20	15	SD	SnAgCu	SnAg	235	Air	None	0 to 100
Unslotted	UT21	15	SD	SnAgCu	SnAg	235	Air	None	0 to 100
Slotted	UT23	15	SD	SnAgCu	SnAg	235	Quench	None	0 to 100
Slotted	UT24	15	SD	SnAgCu	SnAg	235	Quench	None	0 to 100
Slotted	UT25	15	SD	SnAgCu	SnAg	235	Quench	None	0 to 100
Unslotted	UT26	15	SD	SnAgCu	SnAg	235	Quench	None	0 to 100

NOTE: SD = Single Dense, SS = Single Sparse , DD = Double Dense
DA = Double Alternating (See Section 2.2.1, Chapter 2).

Table B.2. Test board build matrix—Motorola (MOT)

Board Type	Brd #	Parts/ Brd	Board Config	Paste Comp	Sphere Comp	Peak Reflow(C)	Cooling Rate	Aging Type	Cycle Type (C)
Unslotted	MOT1	15	SD	SnPb	SnPbAg	215	Air	None	0 to 100
Unslotted	MOT2	15	SD	SnPb	SnPbAg	215	Air	None	0 to 100
Unslotted	MOT3	15	SD	SnPb	SnPgAg	215	Air	None	-40 to 125
Unslotted	MOT4	15	SD	SnPb	SnPgAg	215	Air	None	-40 to 125
Unslotted	MOT5	15	SD	SnPb	SnPbAg	215	Air	None	-55 to 125
Unslotted	MOT6	15	SD	SnAgCu	SnAg	235	Air	None	0 to 100
Unslotted	MOT7	15	SD	SnAgCu	SnAg	235	Air	None	0 to 100
Unslotted	MOT8	15	SD	SnAgCu	SnAg	235	Air	None	-40 to 125
Unslotted	MOT9	15	SD	SnAgCu	SnAg	235	Air	None	-40 to 125
Unslotted	MOT10	15	SD	SnAgCu	SnAg	235	Air	None	-55 to 125
Unslotted	MOT11	15	SD	SnPb	SnAg	235	Air	None	0 to 100
Unslotted	MOT12	15	SD	SnPb	SnAg	235	Air	None	-40 to 125
Unslotted	MOT13a	15	SD	SnPb	SnAg	215	Air	None	0 to 100
Unslotted	MOT13b	15	SD	SnPb	SnAg	215	Air	None	-40 to 125
Unslotted	MOT14	15	SD	SnAgCu	SnPbAg	235	Air	None	0 to 100
Unslotted	MOT15	15	SD	SnAgCu	SnPbAg	235	Air	None	-40 to 125
Unslotted	MOT16	6	SS	SnPb	SnPbAg	215	Air	None	0 to 100
Unslotted	MOT17	6	SS	SnPb	SnPbAg	215	Air	None	0 to 100
Unslotted	MOT18	6	SS	SnPb	SnPbAg	215	Air	None	0 to 100
Unslotted	MOT19	6	SS	SnAgCu	SnAg	235	Air	None	0 to 100
Unslotted	MOT20	6	SS	SnAgCu	SnAg	235	Air	None	0 to 100
Unslotted	MOT21	6	SS	SnAgCu	SnAg	235	Air	None	0 to 100
Unslotted	MOT22	6	SS	SnPb	SnPgAg	215	Air	None	-40 to 125
Unslotted	MOT23	6	SS	SnPb	SnPgAg	215	Air	None	-40 to 125
Unslotted	MOT24	6	SS	SnPb	SnPgAg	215	Air	None	-40 to 125
Unslotted	MOT25	6	SS	SnAgCu	SnAg	235	Air	None	-40 to 125
Unslotted	MOT26	6	SS	SnAgCu	SnAg	235	Air	None	-40 to 125
Unslotted	MOT27	6	SS	SnAgCu	SnAg	235	Air	None	-40 to 125
Unslotted	MOT28	30	DD	SnPb	SnPbAg	215	Air	None	0 to 100
Unslotted	MOT29	30	DD	SnAgCu	SnAg	235	Air	None	0 to 100
Unslotted	MOT30	30	DD	SnPb	SnPgAg	215	Air	None	-40 to 125
Unslotted	MOT31	30	DD	SnAgCu	SnAg	235	Air	None	-40 to 125
Unslotted	MOT32	15	DA	SnPb	SnPbAg	215	Air	None	0 to 100
Unslotted	MOT33	15	DA	SnAgCu	SnAg	235	Air	None	0 to 100
Unslotted	MOT34	15	DA	SnPb	SnPgAg	215	Air	None	-40 to 125
Unslotted	MOT35	15	DA	SnAgCu	SnAg	235	Air	None	-40 to 125

NOTE: SD = Single Dense, SS = Single Sparse , DD = Double Dense
DA = Double Alternating (See Section 2.2.1, Chapter 2)

Table B.3. Packages and boards used for microstructural sectioning study and dye-penetration crack study

SnPb-Aged									
	Microstructural Sectioning				Dye Penetration				
Read points	Board #	Package			Board#	package			Inspection cycle
1	UT1	U5A	U10A	U15A	UT2	U5A	U10A	U15A	0
2	UT3	U5A	U10A	U15A	UT1	U4A	U9A	U14A	2000
3	UT2	U4A	U9A	U14A	UT3	U4A	U9A	U14A	4000
4	UT1	U3A	U8A	U13A	UT2	U3A	U8A	U13A	6000
5	UT3	U3A	U8A	U13A	UT1	U2A	U7A	U12A	8000
6	UT2	U2A	U7A	U12A	UT3	U2A	U7A	U12A	10000
7	UT1	U1A	U6A	U11A	UT2	U1A	U6A	U11A	13000
8	UT3	U1A	U6A	U11A	UT4	U5A	U10A	U15A	16000

SnPb-Air-coooled									
	Microstructural Sectioning				Dye Penetration				
Read points	Board #	Package			Board#	Package			Inspection cycle
1	UT5	U5A	U10A	U15A	UT6	U5A	U10A	U15A	0
2	UT7	U5A	U10A	U15A	UT5	U4A	U9A	U14A	2000
3	UT6	U4A	U9A	U14A	UT7	U4A	U9A	U14A	4000
4	UT5	U3A	U8A	U13A	UT6	U3A	U8A	U13A	6000
5	UT7	U3A	U8A	U13A	UT5	U2A	U7A	U12A	8000
6	UT6	U2A	U7A	U12A	UT7	U2A	U7A	U12A	10000
7	UT5	U1A	U6A	U11A					14000
					UT6	U1A	U6A	U11A	15000
8	UT7	U1A	U6A	U11A	UT8	U5A	U10A	U15A	16000

SnPb-Quenched									
	Microstructural Sectioning				Dye Penetration				
Read points	Board #	Package			Board#	Package			Inspection cycle
1	UT10	U5A	U10A	U15A	UT11	U5A	U10A	U15A	0
2	UT12	U5A	U10A	U15A	UT10	U4A	U9A	U14A	2000
3	UT11	U4A	U9A	U14A	UT12	U4A	U9A	U14A	4000
4	UT10	U3A	U8A	U13A	UT11	U3A	U8A	U13A	6000
5	UT12	U3A	U8A	U13A	UT10	U2A	U7A	U12A	8000
6	UT11	U2A	U7A	U12A	UT12	U2A	U7A	U12A	10000
7	UT11	U1A	U6A	U11A	UT12	U1A	U6A	U11A	14000
8	UT10	U1A	U6A	U11A	UT13	U5A	U10A	U15A	16000

SnAg-Aged									
	Microstructural Sectioning				Dye Penetration				
Read points	Board #	Package			Board#	Package			Inspection cycle
1	UT14	U5A	U10A	U15A	UT15	U5A	U10A	U15A	0
2	UT16	U5A	U10A	U15A	UT14	U4A	U9A	U14A	3000
3	UT15	U4A	U9A	U14A	UT16	U4A	U9A	U14A	6000
4	UT14	U3A	U8A	U13A	UT14	U2A	U7A	U12A	9000
5	UT16	U3A	U8A	U13A	UT16	U2A	U7A	U12A	12000
6	UT15	U2A	U7A	U12A	UT14	U1A	U6A	U11A	15000
7	UT16	U1A*	U6A	U11A	UT17	U5A	U10A	U15A	18000
8	UT15	U1A^	U6A	U11A	UT17	U4A	U9A	U14A	21000
9	UT17	U2A+	U7A	U12A	UT17	U3A	U8A	U13A	24000
10					UT17	U1A	U6A	U11A	27000

Note: *used for dye-penetration at 18K, ^ used for dye-penetration at 21K, +used for dye-penetration at 24K

SnAg-Air-Cooled									
	Microstructural Sectioning				Dye Penetration				
Read points	Board #	Package			Board#	Package			Inspection cycle
1	UT18	U5A	U10A	U15A	UT19	U5A	U10A	U15A	0
2	UT20	U5A	U10A	U15A	UT18	U4A	U9A	U14A	3000
3	UT19	U4A	U9A	U14A	UT20	U4A	U9A	U14A	6000
4	UT18	U3A	U8A	U13A	UT19	U3A	U8A	U13A	9000
5	UT20	U3A	U8A	U13A	UT18	U2A	U7A	U12A	12000
6	UT19	U2A	U7A	U12A	UT20	U2A	U7A	U12A	15000
7	UT18	U1A	U6A	U11A	UT21	U5A	U10A	U15A	18000
8	UT19	U1A	U6A	U11A	UT21	U4A	U9A	U14A	21000
9	UT20	U1A	U6A	U11A	UT21	U3A	U8A	U13A	24000
10	UT21	U2A	U7A	U12A	UT21	U1A	U6A	U11A	27000

SnAg-Quenched									
	Microstructural Sectioning				Dye Penetration				
Read points	Board #	Package			Board#	Package			Inspection cycle
1	UT23	U5A	U10A	U15A	UT24	U5A	U10A	U15A	0
2	UT25	U5A	U10A	U15A	UT23	U4A	U9A	U14A	3000
3	UT24	U4A	U9A	U14A	UT25	U4A	U9A	U14A	6000
4	UT23	U3A	U8A	U13A	UT24	U3A	U8A	U13A	9000
5	UT25	U3A	U8A	U13A	UT23	U2A	U7A	U12A	12000
6	UT24	U2A	U7A	U12A	UT25	U2A	U7A	U12A	15000
7	UT25 BAD	U5A	U10A	U15A	UT26	U5A	U10A	U15A	18000
8	UT23	U1A	U6A	U11A	UT26	U4A	U9A	U14A	21000
9	UT25 BAD	U1A	U6A	U11A	UT26	U3A	U8A	U13A	24000
10	UT25 BAD	U3A	U8A	U13A	UT26	U2A	U7A	U12A	27000
11	UT25	U1A	U6A	U11A	UT26	U1A	U6A	U11A	30000

APPENDIX C

Crack Area Measurement: Comparison of Experimental Crack Measurements with R. Darveaux's Algorithm Relating Crack Area and Crack Length

C.1. BACKGROUND

Measurements of crack areas in solder joints from dye penetration studies are extremely time-consuming. As noted in Chapter 2 after dye penetration and joint removal from the PWBs, the solder joint attachments on the package- and/or board-sides must be photographed, crack and joint boundaries manually traced, and image-processing software run to compute crack areas. Alternatively, crack length measurements are much faster to obtain using an appropriate crack propagation angle, typically from the vector connecting the centers of the IC package and joints. Crack length measurements can then be used to compute crack areas based upon geometric assumptions.

Darveaux [56] developed an algorithm relating the geometry between crack length and crack area for concave-shaped areas and a propagation angle mentioned in the above paragraph. He measured both primary and secondary crack lengths

The objective of this appendix is to apply Darveaux's algorithm to our test data and to compare his crack area estimates with our measurements of crack

areas and lengths in the boundary region (under the die edges—see Chapter 2) for SnPb and SnAg solder joints.

C.2. DARVEAUX'S ALGORITHM TO COMPUTE CRACK AREA FROM CRACK LENGTH

The assumed geometry of the solder joint crack is shown below [56]:

Let: A_p =primary crack area

A_s =secondary crack area

A_0 =initial solder pad area

a_p =primary crack length

a_s =secondary crack length.

The total crack area A is the sum of primary crack and secondary crack.

$$A = A_p + A_s \tag{C.1}$$

$$A_p = A_0 - A_2 - A_1 \tag{C.2}$$

$$A_s = A_2 - A_1 \tag{C.3}$$

$$A_1 = \frac{r^2}{2}\left(rad\,\theta_1 - \sin\theta_1\right) \tag{C.4}$$

$$\theta_1 = 2\cos^{-1}\left(\frac{a_p + a_s}{2r}\right) \tag{C.5}$$

$$A_2 = \frac{r^2}{2}\left(rad\,\theta_2 - \sin\theta_2\right) \tag{C.6}$$

$$\theta_2 = 2\cos^{-1}\left(1 - \frac{a_s - a_p + 2r}{2r}\right) \tag{C.7}$$

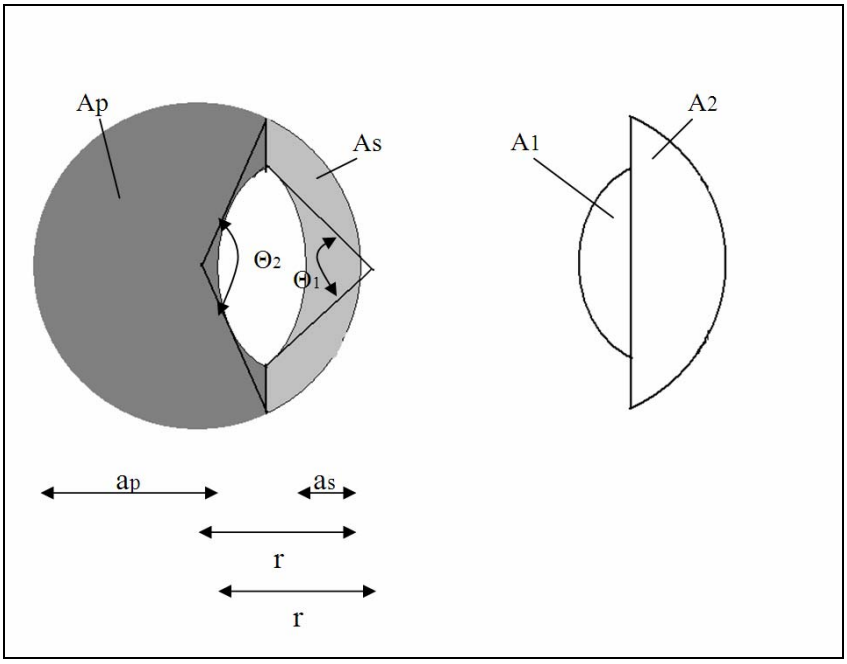

Figure C.1 Model for crack growth [56]

C.3. RESULTS

Table C.1 shows the comparison of measured and estimated (Darveaux algorithm) mean % crack area for aged and air-cooled SnPb solder joints in the boundary region at various cycle times. For the air-cooled case, the estimated and measured areas compare very well and differ by less than 8% area except 4k cycled case, where the % error is 14%. The comparison has the measured areas consistently a little larger than the estimated areas, however, the difference gets smaller at the larger number of cycles. For the aged case, the estimated areas differ much more, up to 17% error than in the air-cooled case. The reason for this larger discrepancy is that the dye penetration study (Chapter 4) showed that the aged SnPb solder joints possessed crack shapes that were not concave; instead the

crack fronts had straight fronts. Note that the measured areas were consistently larger than the estimated areas, but the differences did not become smaller with cycles as they did in the air-cooled cases. Table C.2 shows the comparison of measured and estimated (Darveaux algorithm) mean % crack area for aged and air-cooled SnAg solder joints in the boundary area at various cycle times. For the aged case, the estimated areas compared very well and the difference was upto 6% except 6k cycled case where the % error is 16%. For the air-cooled cases, the differences are 13-18% for 3k to 12k cycled cases, and the estimated areas of the rest cycled cases compare extremely well below 5%.

Table C.1. Comparison of mean % crack area (and standard deviation) using Darveux algorithm (Est) and experimental measured areas in aged and air-cooled SnPb solder joints in the boundary region (nominal joint diameter=560 μm)

	Aged			Air-cooled		
	Measured crack area%	Calculated crack area%	% Error	Measured crack area%	Calculated crack area%	**% Error**
2K	4.7 (4.5)	5.5 (7.1)	17%	7.0 (3.9)	7.4 (5.6)	6%
4K	20.8 (14.0)	23.3 (17.4)	12%	22.2 (8.3)	19.1 (10.3)	-14%
6K	33.8 (19.6)	35.7 (22.9)	6%	35.1 (12.0)	32.4 (14.2)	-8%
8K	51.1 (22.7)	57.9 (25.7)	13%	50.9 (14.9)	47.1 (19.0)	-7%
10K	57.6 (24.0)	64.9 (26.4)	13%	58.3 (13.2)	56.1 (16.1)	-4%
13K	68.0 (21.7)	73.2 (23.3)	8%	73.9 (14.7)	73.6 (17.4)	-0.4%
16K	69.9 (20.2)	75.7 (20.4)	8%	82.0 (12.7)	82.4 (15.8)	0.5%

Note: See Table G.1 in Appendix G for the raw crack length data used to calculate crack area%. The sample size is same as Table 4.5 in Chapter 4.

Table C.2. Comparison of mean % crack area (and standard deviation) using Darveux algorithm (Est) and experimental measured crack areas in aged and air-cooled SnAg solder joints in the boundary region (nominal joint diameter=560 μm)

	Aged			Air-cooled		
No. Cycles	Measured crack area%	Calculated crack area%	**% Error**	Measured crack area%	Calculated crack area%	**% Error**
3K	3.9 (4.7)	3.8 (6.0)	-3%	11.3 (7.4)	8.3 (9.2)	-18%
6K	8.9 (9.1)	7.5 (9.4)	-16%	25.7 (13.5)	23.5 (16.3)	-9%
9K	17.7 (11.3)	17.7 (15.5)	0%	35.0 (13.4)	30.3 (16.4)	-13%
12K	19.2 (14.8)	18.8 (19.0)	-2%	41.0 (18.9)	35.4 (20.1)	-14%
15K	24.1 (14.8)	23.2 (18.1)	-4%	50.5 (16.1)	49.1 (19.0)	-3%
18K	27.4 (15.9)	26.5 (19.6)	-3%	53.6 (15.3)	50.8 (19.4)	-5%
21K	23.7 (14.0)	24.0 (17.4)	1%	50.5 (21.9)	51.7 (23.6)	2%
24K	37.8 (15.0)	35.6 (18.0)	-6%	56.7 (18.6)	59.4 (20.4)	5%
27K				64.8 (12.8)	62.1 (15.9)	-4%

Note: See Table G.2 in Appendix G for the raw crack length data used to calculate crack area%. The sample size is same as Table 4.6 in Chapter 4.

The four plots in Figure C.1 show the comparative data of Tables C.1 and C.2. The estimated values from Darveaux's algorithm compare very well with the measured crack area data, except for the SnPb-aged case, where the crack shape is different from the concave shape assumed by the algorithm.

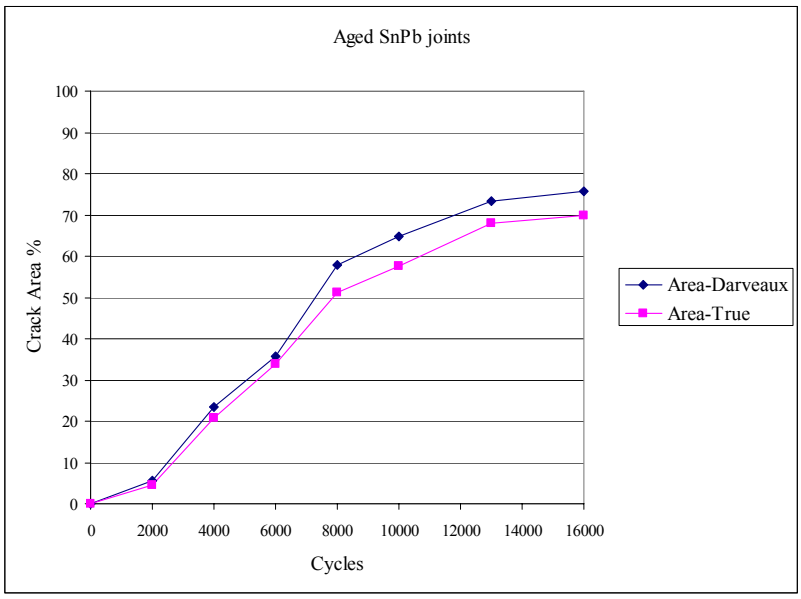
Aged SnPb joints
Crack Area %
100
90
80
70
60
50
40
30
20
10
0
0
2000
4000
6000
8000
10000
12000
14000
16000
Cycles
Area-Darveaux
Area-True

(a)

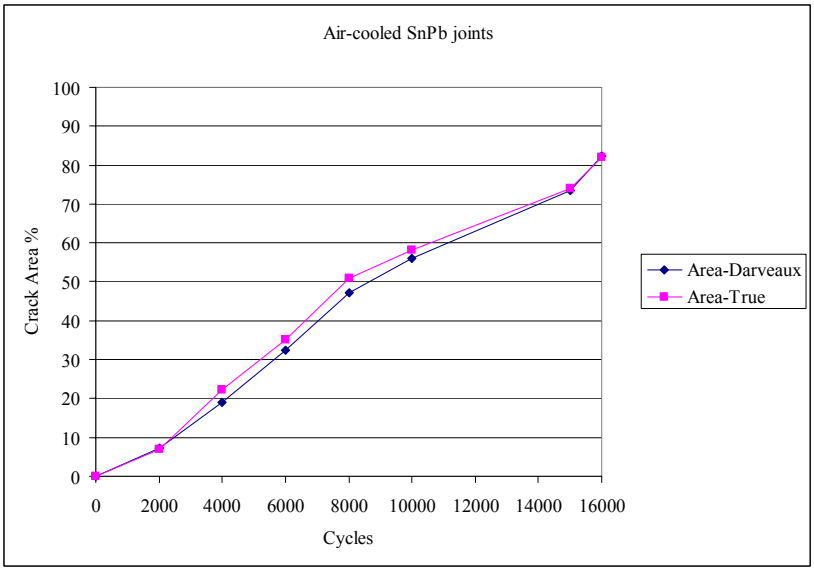
Air-cooled SnPb joints
Crack Area %
100
90
80
70
60
50
40
30
20
10
0
0
2000
4000
6000
8000
10000
12000
14000
16000
Cycles
Area-Darveaux
Area-True

(b)

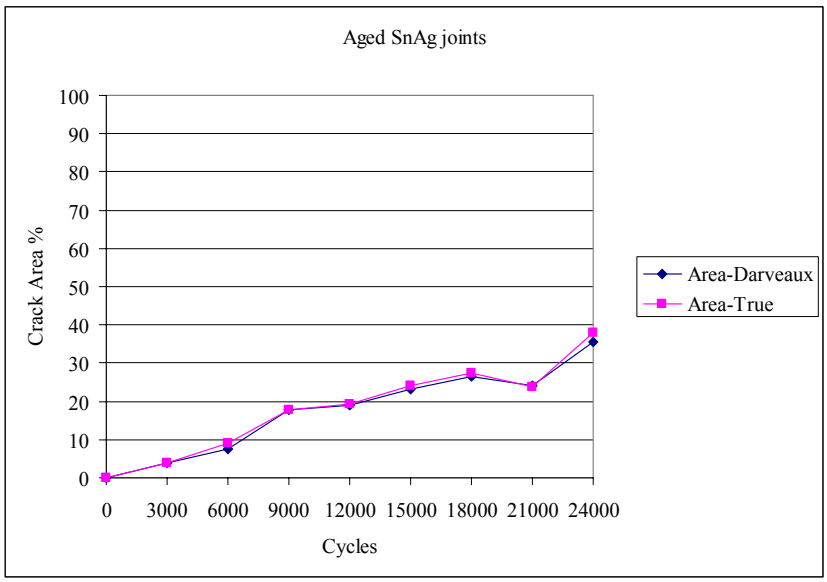

(c)

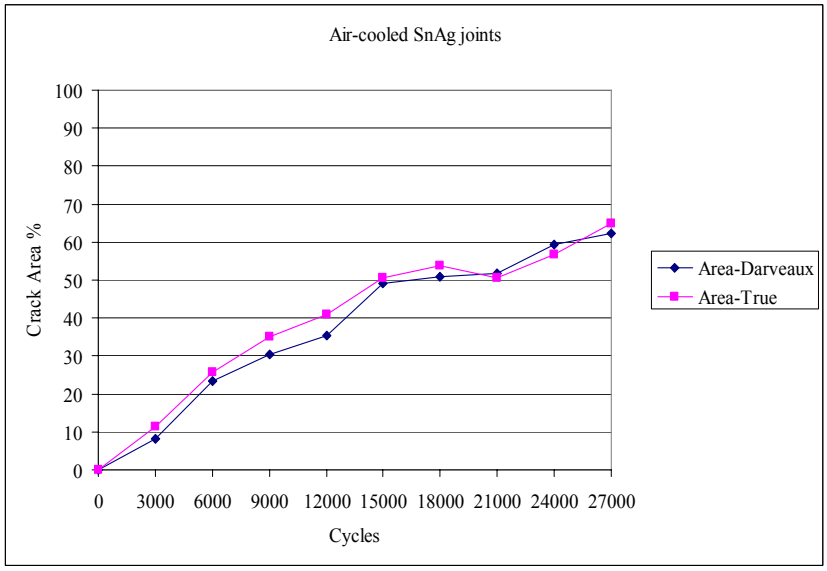

(d)

Figure C.1. Comparisons of means of % crack areas for SnPb and SnAg solder joints in the boundary region using measured data and Darveaux's crack area algorithm (a) SnPb-aged (b) SnPb air-cooled (c) SnAg-aged (d) SnAg air-cooled

C.4. RAW DATA

Crack length data from Tables G.1 and G.2 in Appendix G was used to calculate crack area using Darveaux's equations. Also, the measured crack area data (see Table A in Appendix A in C. Park's MS thesis [51]) was compared with the calculated crack area.

APPENDIX D

False Failures and Alternative Failure Criteria for PBGA Packages with SnAg Solder Joints

Ideally, package failures occurring during accelerated thermal cycling (ATC) testing are detected by the event detector and confirmed with subsequent manual high resistance measurements. For packages with SnPb solder joints, this was the case. However, for packages with SnAg solder joints, early failures detected by the event detector were not confirmed by high resistance values. This appendix describes the failure detection methodology of the event detector and the industry-standard failure criterion, discusses early false failures, proposes and compares alternative failure criteria with data, and discusses the rationale for choosing an alternative failure criterion for packages with SnAg solder joints.

D.1. FAILURE DETECTION METHOD OF THE EVENT DETECTOR

Electrical failure of an electronic package (solder joint failure) during ATC testing is monitored by an event detector, such as the ANATECH [90], which measures the resistances of daisy-chained packages on a printed wiring board. Electrical connectors on the test boards are set into ribbon connectors on a card carrier that connect the carrier to the event detector—every channel of the ribbon cable is associated with a specific package on a test board. The event detector is connected to a computer for data monitoring and storage. The

resistance of a 357-PBGA package is nominally 1.5Ω. The ANATECH event detector checks resistances every 10 seconds (each check is called a poll). An 'event' is detected whenever a resistance measurement exceeds 300Ω (set by user) and the event detector records the cycle number that the event occurred (note does not record the resistance value) in a data file. The data file contains two files: .dat file and .log file. These are described below. Whenever the event detector is reset or stopped, as occurs when repairs are made on the environmental chamber, a new data file and new data are generated—that is, the ANATECH resets and starts monitoring all channels again.

The ANATECH provides the following data using its DATALOG software.

1) Computer screen continuous data update (note data displayed is for current cycle only)—called Schmoo plot. The screen shows the following information:

Datafile Name, Current Cycle, Next Poll

Table showing:

Channel No. of all channels (each line represents 32 channels in four groups of 8 channels)

Hexadecimal number of events detected during the cycle in progress

(if no events have been detected, a dot is displayed)

(when more than 15 events have occurred, an asterisk is displayed)

2) Printout at the end of each data file

Starting Date, Cycle Duration (1800sec), Poll Rate (180/cycle), Data File Name

Table showing:

Channel No having events

No. events in hexadecimal (if none, period shown, if >15, * shown)

Elapsed time (since start of new datafile), Elapsed cycles, No. of next poll

List of all channels with events detected

Name of datafile data is written to.

No. completed cycles

3) .log file

File name

Date and Time started, 30-minute cycles, 180 polls/cycle

Total number of cycles for block

Maximum possible number of events: =180*number of cycles

Table showing

Channel No., Total Events, Cycle No.-1st event, Cycle No.-Last event, % polls

w/ events (ratio of total number of events to the number of polls between the first and last detected events)

EXAMPLE OF .LOG FILE

Data history file: UT31500D.DAT

Total number of tests (cycle-offset blocks) = 1

Date/time: 04-03-2000 10:16:20 Cycle= 30 min, 180 polls/cy.

Test block cycle-offset = 0

Total cycles for block = 130

Maximum possible # of events = 23400

' Ch#	Event Tally	1st-Ev D-Cycle	Last-Ev D-Cycle	% polls w/ Events
7	7	1	120	0.0
8	17	1	120	0.1
28	23400	1	130	100.0
35	1982	1	130	8.5

Discussion of .log file:

Total number of polls=23400 (=180 polls/cy*130cy)

Channel 7 had 1 event starting at cycle 1 and ending at cycle 120 and the events took 0.0% of the possible polls (100*7/[120cy*180poll/cy])

Channel 8 had 17 events starting at cycle 1 and ending at cycle 120 and the events took 0.1% of the possible polls (100*17/21,600)

Channel 28 had 23400 events starting at cycle 1 and ending at cycle 130 and the events took 100% of the possible polls (100*23400/[23400*180])

Channel 35 had 1982 events starting at cycle 1 and ending at cycle 130 and the events took 8.5% of the possible polls (100*1982/23,400)

4) When 10 events (total of 10 polls with resistance measurements exceeding 300Ω) have been detected on a channel, the ANATECH stops recording more events for that channel on the dat. file.

5) .dat file

Starting Date/Time, Cycle=30 min @ 180 polls/cycle

Cycle No., Date, Time, File Name, Cycle=30 min, 180 polls/cy.

Event No., Channel No., and time that event occurred in % of one cycle time.

EXAMPLE OF .DAT FILE

Starting Date/Time: 11-21-2000 21:52:52 Cycle = 30 min. @ 180 polls/cycle

Cycle # 157 11-25-2000 04:22:50 UT315009.DAT Cycle= 30 min, 180 polls/cy.

4:: 231 0.183

6:: 252 0.183

8:: 228 0.183 230 0.183 233 0.183 234 0.183 250 0.183

9:: 251 0.183

10:: 227 0.183

Discussion of UT315009.DAT data file:

At 329.4 seconds (=0.183*1800sec/cycle) into cycle number 157 of datafile UT315009.DAT

Channel 231 recorded its 4^{th} event

Channel 252 recorded its 6^{th} event

Channels 228, 230, 233, 234, and 250 recorded their 8^{th} event

Channel 251 recorded its 9^{th} event

Channel 227 recorded its 10^{th} event

D.2. INDUSTRY-STANDARD FAILURE CRITERION AND FALSE FAILURES

The industry-standard failure criterion (IPC-SM-785) defines failure as "the first interruption of electrical continuity that is confirmed by nine additional interruptions within an additional 10% of the cyclic life" [57]. For example, failure at 5000 cycles occurs if the first event occurred at cycle 5000 and nine additional events occurred with the next 500 cycles. This criterion will be labeled Criterion 1.

Table D.1 shows the life of SnPb and SnAg joints using the industry-standard failure criterion applied to the tests run at UT. Note that the failure cycles of SnAg joints have about 500 – 750% larger standard deviations than SnPb joints. More signficantly, SnAg joints showed early false failure cycles, such as 500-700 cycles, which was inconsistent with measured dye-penetration crack area data and not verified by electrical resistance measurements using an ohm meter. On the other hand, SnPb joints failures were confirmed by crack area data and resistance measurements using an ohm meter. As a consequence of these

false failures for SnAg solder joints, alternative failure criteria are proposed and discussed in the next section.

Table D.1. Life (cycles) of SnPb and SnAg joints using the industry-standard failure detection criterion and UT test data

	Aged			Air-cooled			Quenched		
	N	STD	Mean	N	STD	Mean	N	STD	Mean
SnPb	24	1657	10995	23	1453	12800	24	1653	12118
SnAg	20	12981	18906	20	10341	11549	24	8854	12677

Several other studies have addressed false failures. Y. Oi, et al. [86] increased the failure resistance of the event detector to 1000Ω to minimize the effects of electrical noise. W. Johnson, et al. [87] defined failure as resistance readings of 100Ω, but 10 failures were measured prior to the recording of the failure in the data file to avoid affects of random noise. J. Rathod, et al. [88], defined failure when the resistance of a component-circuitry increased by 10% of its initial resistance and was based upon previous research experiences. Q. Zhang, et al. [89], defined failure as 15 events.

D.3. ALTERNATIVE FAILURE CRITERIA FOR SNAG SOLDER JOINTS

Besides the industry-standard failure criterion (denoted now as Criterion 1) discussed in the previous section, four other criteria were proposed. They are:

Criterion 2: Use the industry-standard failure criterion, but neglect the failure cycle if other packages failed during the same cycle. The failure data showed that several packages had early false failures at the same cycle number. It was thought that the event was triggered by some external interference that affected many channels at the same time. The crack area/length data showed no identical area/length measurements at a given cycle number, so it was assumed that the chances that multiple packages failed at the same life cycle was very small.

Criterion 3: Failure is defined as the cycle of the first event in a data file with nine additional events in that data file, followed by two consecutive data files showing at least 10 events in each. Recall that new data files are generated whenever the event detector is stopped for any reason. The rationale for this criterion is that if a package has failed, then the event detector should indicate failures in subsequent files. Note, however, file sizes vary from 1 cycle to 1800 cycles, with hundreds of cycles in a data file more typical.

Criterion 4: Failure is defined as the cycle of the first event in a data file with nine additional events in that data file, followed by two consecutive data files showing 10 events in the first two cycles of those data files. The rationale for this criterion is that once a package is failed the event detector should indicate failure very quickly in subsequent data files. Criterion 4 is more restrictive that Criterion 3.

Criterion 5: Failure is defined as the cycle of the first event in a data file with nine additional events in that data file if the ratio of total number of events to the number of polls between the first and last detected events (as shown in the .log file) ≥ 10%. Here, the ratio of the total number of events to the number of polls between the first and last detected events can screen out any false events generated by noise effect, because noise-induced false events will produce ratios of only 1-2%. A ratio of 10% was chosen so the false reading due to noise effects can be avoided. However, one possible error is the case when real events occur at the end of cycle and when the ratio does not reach 10%. Then, this criterion will read the next cycle as failure cycle instead of the cycle when the real event started.

The following section applies these criteria to the electrical continuity data generated from the ANATECH event detector.

D.4. FAILURE CRITERIA APPLIED TO ANATECH DATA

The five failure detection criteria were applied to the data from the ANATECH event detection. Table D.2 shows that all failure detection criteria for SnPb packages yield life (cycles) are within less than 1% of each other—implying that SnPb joint failure is very definitive.

Table D.3 shows that the mean life (cycles) and standard deviations of SnAg packages vary significantly for the five failure detection criteria. For example, the life (cycles) of SnAg packages using Criterion 5 is approximately

200% larger than using Criterion 1. As the criterion changes from 1 to 5, the mean of life (cycles) gets larger, and the standard deviations get smaller. Therefore, it is necessary to choose one failure detection criterion to determine the final life (cycles) of SnAg joints. Notice that life for the air-cooled and quenched SnAg joints were similar based upon Criteria 3-5. It appears that the real problem was in aged SnAg where life varied significantly based upon Criteria 3-5.

Table D.2. Mean life (cycles) and standard deviation for five failure detection criteria for SnPb solder joints

Criteria	Aged			Air-cooled			Quenched		
	N	STD	Mean	N	STD	Mean	N	STD	Mean
1	24	1657	10995	23	1453	12800	24	1653	12118
2	24	1657	10995	23	1453	12800	24	1653	12118
3	24	1657	10995	23	1453	12800	24	1432	12244
4	24	1658	11007	23	1470	12811	24	1438	12257
5	24	1657	10994	23	1452	12800	24	1432	12244

Table D.3. Mean life (cycles) and standard deviation for five failure detection criteria for SnAg solder joints

Criteria	Aged			Air-cooled			Quenched		
	N	STD	Mean	N	STD	Mean	N	STD	Mean
1	20	12981	18906	20	10341	11549	24	8854	12677
2	19	9895	23598	18	5982	21066	24	4154	19517
3	11	4081	34430	11	6367	23393	24	3884	22894
4	12	6020	41236	11	6279	23252	24	3947	22850
5	12	6041	41064	11	6279	23252	24	3923	22801

D.5. FAILURE DETECTION CRITERION RESULTS

Due to false failures, Criteria 1 and 2 were not used. As noted above, Criteria 3-5 yielded similar life measurements for air-cooled and quenched SnAg solder joints. Criterion 4 was more restrictive than Criterion 3 and Criterion 5 had possible problems as noted in its description. In this study, failure Criterion 4 was used to derive failure cycles for SnAg. Below are tables showing all criteria applied to the SnAg solder joint thermal tests at UT.

Table D.4. SnAg joint life (cycles) of 0-100^{o}C ATC tests run at UT as monitored with ANATECH event detector—Failure Criteria 1&2

SnAg Failure Criterion 1			SnAg Failure Criterion 2		
Single-dense 0-100C			Single-dense 0-100C		
Aged UT14/UT15/UT16/UT17-SA-AG	Air-cooled UT18/UT19/UT20/UT21-SA-A	Quenched UT23/UT24/UT25/UT26-SA-Q	Aged UT14/UT15/UT16/UT17-SA-AG	Air-cooled UT18/UT19/UT20/UT21-SA-A	Quenched UT23/UT24/UT25/UT26-SA-Q
558	672	19708	11502	13499	19708
717	672	1135	11592	13790	14638
4408	672	1920	13662	23233	14636
4343	14615	15239	13997	23612	15261
12699	23233	15568	13976	14684	15585
11373	23487	15568	13652	14752	18278
13652	1993	15668	13674	25142	15688
4325	1993	15668	9321	25200	15696
589	1993	6268	34560	25200	15596
34560	15249	26473	30040	25178	26473
25343	15249	22845	30059	25236	22845
27220	15249	1993	30052	14766	23487
27222	15249	1993	30054	14844	18235
27222	1993	1993	30047	25477	19911
27222	1993	1993	30084	24833	18453
27222	1999	1993	29705	25365	15306
27050	24833	15249	30042	12489	22959
30042	25365	15249	32886	31895	23487
32886	12487	1993	39465		15132
39465	31989	14016			20621
		21320			21320
		24090			24090
		24640			29349
		21663			21664

Table D.5. SnAg joint life (cycles) of 0-100oC ATC tests run at UT as monitored with ANATECH event detector—Failure Criteria 3& 4

SnAg Failure Criterion 3			SnAg Failure Criterion 4		
Single-dense 0-100C			Single-dense 0-100C		
Aged UT14/UT15/UT16/UT17-SA-AG	Air-cooled UT18/UT19/UT20/UT21-SA-A	Quenched UT23/UT24/UT25/UT26-SA-Q	Aged UT14/UT15/UT16/UT17-SA-AG	Air-cooled UT18/UT19/UT20/UT21-SA-A	Quenched UT23/UT24/UT25/UT26-SA-Q
34560	23233	20297	34560	23233	19708
30026	23875	14615	45327	23487	14615
35460	15670	20294	42045	15670	19775
30030	31943	18348	47259	31383	18249
30034	15867	24201	48351	15867	24477
34745	24815	18364	48323	24207	18277
35462	27248	26157	34745	27248	26491
29485	24833	23990	44641	24833	23990
39460	25365	26165	29485	25365	26165
39462	12487	26473	41527	12487	26473
40008	31989	22845	39107	31989	22845
		23871	39465		23871
		18229			18229
		23871			23871
		18453			18453
		26998			26998
		23871			22923
		23991			24477
		31383			31383
		20621			20621
		21320			21320
		24090			24090
		29348			29348
		21663			21760

Table D.6. SnAg and SnPb joint life (cycles) of 0-100°C ATC tests run at UT as monitored with ANATECH event detector—Failure Criterion 5

SnAg Failure Criterion 5			SnPb Failure Criterion 5		
Single-dense 0-100C			Single-dense 0-100C		
Aged UT14/UT15/UT16/UT17-SA-AG	Air-cooled UT18/UT19/UT20/UT21-SA-A	Quenched UT23/UT24/UT25/UT26-SA-Q	Aged UT1/UT2/UT3/UT4-SPA-AG	Air-cooled UT5/UT6/UT7/UT8-SPA-A	Quenched UT9/UT10/UT11/UT12-SPA-Q
34560	23233	19708	9919	11261	11278
45327	23487	14615	10003	12433	14126
42045	15670	19775	12493	13927	12797
44641	31383	18249	11496	11883	10711
47259	15867	24201	11905	11670	12482
48351	24207	18277	11184	14821	13282
48323	27248	26157	9280	12702	13648
34745	24833	23990	9651	12135	10379
29485	25365	26165	11885	15146	13583
39460	12487	26473	12425	15620	10722
39107	31989	22845	15177	13040	15042
39465		23871	12545	13233	11847
		18229	10607	12045	10820
		23871	10317	12981	9840
		18453	8436	11179	11590
		26998	12562	11407	13715
		22923	9714	N/A	12772
		23991	7566	15454	12669
		31383	11160	13163	10144
		20621	9714	9884	10800
		21320	10199	12300	13921
		24090	12536	12230	12884
		29348	10577	13595	13010
		21663	12521	12300	11803

APPENDIX E

Phase Size of Lead and Cross-sectioned Pictures of SnAg Solder Joints

Table E.1. Phase size (μm) of lead in N7 and G7 SnPb solder joints at different cycles for different post-processing conditions [58]

Cycle	Aged				Air				Quench			
	G7		N7		G7		N7		G7		N7	
	Mea	STD	Mea	STD	Mean	STD	Mean	STD	Mean	STD	Mean	STD
0K	3.55	0.62	4.63	0.68	0.72	0.27	1.15	0.16	0.81	0.18	1.28	0.43
2K	2.74	0.66	4.91	5.72	1.08	0.2	1.16	0.19	0.97	0.2	2.73	0.7
4K	4.15	0.78	7.42	1.22	1.48	0.53	1.13	1.19	1.32	0.41	2.42	0.82
6K	3.26	2.67	4.78	0.89	1.62	0.38	1.30	0.39	2.46	0.67	1.43	0.25
8K	4.58	1.43	3.45	0.35	2.24	0.66	1.36	0.66	2.80	0.72	0.97	0.15
10K	2.97	0.97	2.84	0.93	2.26	0.59	2.62	1.48	2.58	0.28	2.78	0.69
13K	3.48	0.67	5.45	1.41	1.84	0.29	2.61	0.53	3.86	0.61	3.07	0.74
16K	4.29	1.57	3.03	0.52	2.80	0.42	2.22	0.46	4.05	1.87	2.95	1.22

Aged SnAg			
	UT15-U4A-SA-AG-6-G8	UT15-U4A-SA-AG-6-L8	UT15-U4A-SA-AG-6-N8
100X	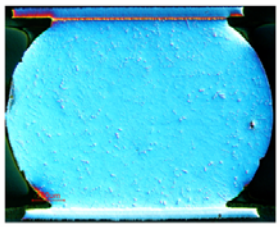	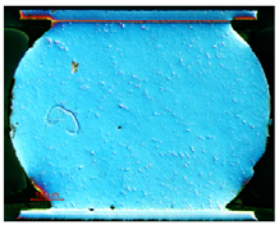	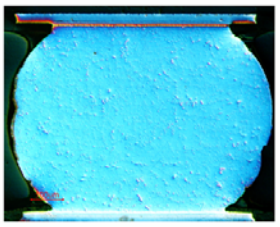
500X-PI-L			
500X-PI-R	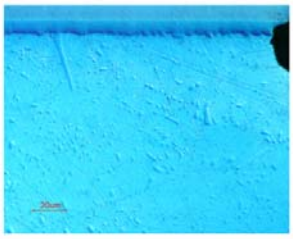		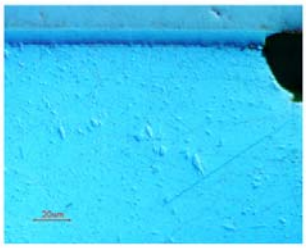
500X-BI-L			

500X-BI-R	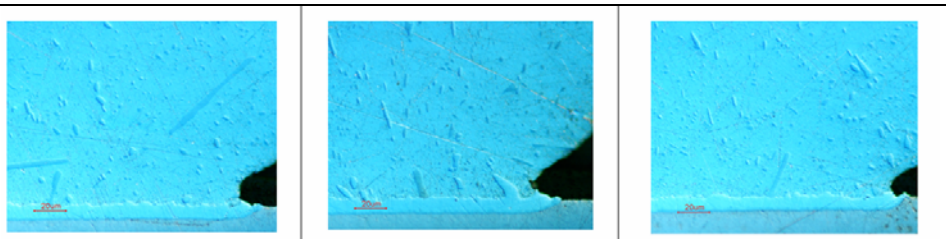
500X-C	

	Air-cooled SnAg		
	UT19-U4A-SA-A-6-G8	UT18-U3A-SA-A-9-G8	UT19-U2A-SA-A-15-G8
100X	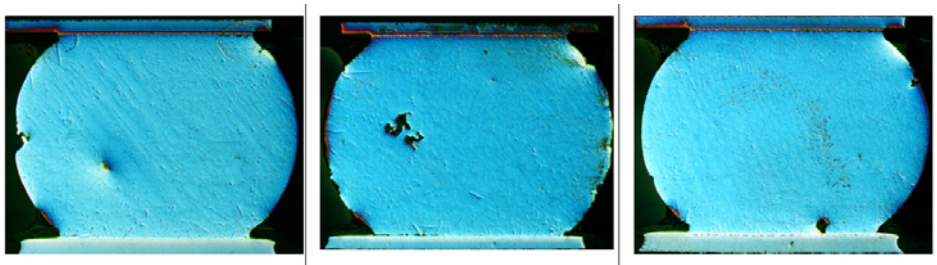		
500X-PI-L			

500X-PI-R	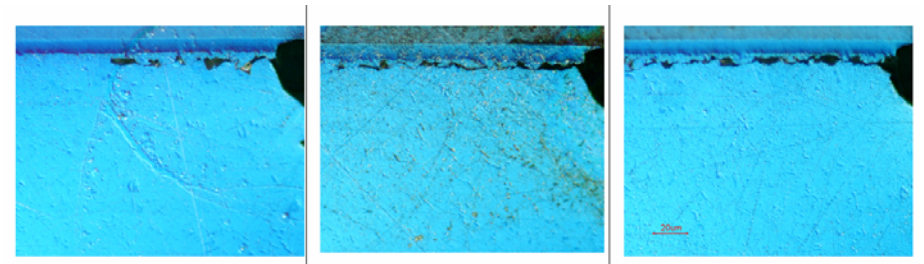
500X-BI-L	
500X-BI-R	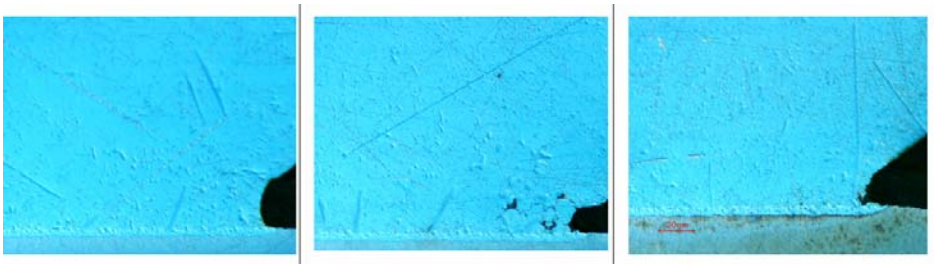
500X-C	

APPENDIX F

Experimentally-measured Crack Orientation Angles

Table F.1. Experimentally-measured crack orientation angles (measured from joint center to the centroid of the crack area) at the package interface

UT3-U14A-SPA-AG-4- / UT3-U9A-SPA-AG-4- / UT3-U4A-SPA-AG-4-PI						UT2-U13A-SPA-AG-6- / UT2-U3A-SPA-AG-6- / UT2-U8A-SPA-AG-6-P-PI					
Joint No.	Crack angle^o	Joint No.	Crack angle^o	Joint No.	Crack angle^o	Joint No.	Crack angle^o	Joint No.	Crack angle^o	Joint No.	Crack angle^o
G10	-45	G10	-33.3	G10	-19.6	G10	-51.9	G10	-70.3	G10	-56.2
G11	44.1	G11	66.7	G11	56.5	G11	-17.7	G11	8.3	G11	32.4
G12		G12	42.9	G12	24.4	G12	70.4	G12	38.4	G12	-47.5
G13	10.2	G13	29.9	G13	2.9	G13	5.5	G13	52.2	G13	56.5
G7	-65.5	G7	-18.8	G7	-33.6	G7	-32	G7	2.3	G7	-22.9
G8	-164.6	G8	-93.6	G8	-161.3	G8	-74	G8	-61.6	G8	-100
G9	-178.1	G9	-36.5	G9	-32.4	G9	-68.6	G9	-22	G9	-56.6
H13	65.4	H13	73.3	H13	-56	H13	36.3	H13	95.1	H13	59.4
H7	-93.5	H7	-3.3	H7	-98.8	H7	-127	H7	-62.4	H7	-93.8
J13	-179.6	J13	91.1	J13	54.2	J13	31.5	J13	83.9	J13	7.6
J7	-101	J7	-128.8	J7	-67.2	J7	-86	J7	-59.1	J7	-107.4
K13	34.1	K13	100.7	K13	-78.9	K13	61.5	K13	75.4	K13	2
K7	-91.6	K7	-110.4	K7	-151.3	K7	-32.7	K7	-109.9	K7	-92.2
L13	95.9	L13	120.3	L13	144.7	L13	169.1	L13	141.3	L13	177
L7	-97.7	L7	-115.9	L7	-151.2	L7	-135.5	L7	-140	L7	-108.8
M13	116.8	M13	132.4	M13	162.4	M13	155.1	M13	130.3	M13	151.2
M7	141.8	M7	-150.6	M7	-116.6	M7	-137	M7	-114.1	M7	-146.3
N10	176.3	N10	164.4	N10	162	N10	175.7	N10	-97.9	N10	158.3
N11	173.3	N11	132.6	N11	152.9	N11	171	N11	-106.8	N11	166.6
N12	105.1	N12	134.9	N12	169.3	N12	145.5	N12	112.7	N12	133.7
N13	169.8	N13	145.1	N13	172	N13	164	N13	163.5	N13	169.5
N7	-175.3	N7	-170.8	N7	-163.9	N7	-166.8	N7	157.9	N7	-170.6
N8	-122.9	N8	-133.8	N8	-119.8	N8	-153.6	N8	-51.7	N8	-148.6
N9	173.8	N9	-134.7	N9	-177.2	N9	-149.8	N9	-130.4	N9	-140.5

UT1-U12A-SPA-AG-8- / UT1-U2A-SPA-AG-8- / UT1-U7A-SPA-AG-8-P-PI						UT3-U12A-SPA-AG-10- / UT3-U2A-SPA-AG-10- / UT3-U7A-SPA-AG-10-PI					
Joint No.	Crack angle°	Joint No.	Crack angle°	Joint No.	Crack angle°	Joint No.	Crack angle°	Joint No.	Crack angle°	Joint No.	Crack angle°
G10	-21.3	G10	-3.6	G10	177.2	G10	-45.1	G10	-52.9	G10	-37.4
G11	-33.2	G11	5.5	G11	-68.6	G11	-1.1	G11	1	G11	42.9
G12	30.2	G12	38.3	G12	70	G12	68	G12	20.5	G12	72.5
G13	3.7	G13	26.9	G13	34.5	G13	66.6	G13	48.5	G13	2.8
G7	-70	G7	-38.8	G7	-32.5	G7	7.3	G7	-56.4	G7	-43.7
G8	-60.2	G8	-88.2	G8	-81.9	G8	-59.8	G8	-38.5	G8	-47.2
G9	-78.5	G9	-2.9	G9	-31.6	G9	-21.9	G9	-38	G9	-24.8
H13	42.2	H13	72.4	H13	44.8	H13	65.3	H13	54.5	H13	64.2
H7	-107	H7	-58.2	H7	-90	H7	-87.2	H7	-69.4	H7	-90.7
J13	105.4	J13	88.5	J7	-70.6	J13	77.5	J13	92	J13	85.6
J7	-94.4	J7	-137.4	K13	70.9	J7	-27.4	J7	-86.6	J7	-71
K13	24.2	K13	91.8	K7	-90.3	K13	50	K13	58.1	K13	39.4
K7	-107.4	K7	-112.1	L13	90.9	K7	-160.2	K7	-114.7	K7	-85.5
L13	111.9	L13	148.6	L7	-113.2	L13	125.3	L13	56.4	L13	58.6
L7	-104.3	L7	-131	M13	102.3	L7	-153.5	L7	-95.6	L7	-117.1
M13	133.1	M13	102.6	M7	-74.5	M13	130.6	M13	137.9	M13	166.5
M7	-84.3	M7	-165.7	N10	-166.7	M7	-162.6	M7	-134.3	M7	-142.3
N10	159.3	N10	165.7	N11	-114.9	N10	171.3	N10	178.8	N10	178.7
N11	131.6	N11	176.5	N12	21.2	N11	133.5	N11	130	N11	171.1
N12	156.4	N12	118.9	N13	157.6	N12	38	N12	103.7	N12	118.8
N13	-164.6	N13	143.7	N7	-173.7	N13	152.4	N13	121.3	N13	144.4
N7	-122.6	N7	-160.4	N8	-107.9	N7	163.5	N7	-155.3	N7	-163.7
N8	-112.1	N8	-134.2	N9	-110	N8	-139.8	N8		N8	-113.1
N9	-137.8	N9	-132.1			N9	-135.8	N9	-109.3	N9	179.2

UT7-U14A-SPA-A-4- / UT7-U4A-SPA-A-4- / UT7-U9A-SPA-A-4-PI						UT6-U13A-SPA-A-6- / UT6-U3A-SPA-A-6- / UT6-U8A-SPA-A-6-PI					
Joint No.	Crack angle°	Joint No.	Crack angle°	Joint No.	Crack angle°	Joint No.	Crack angle°	Joint No.	Crack angle°	Joint No.	Crack angle°
G10	-51.8	G10	26.9	G10	-10.2	G10	-38.2	G10	27.4	G10	-0.7
G11	-11.3	G11	-65	G11	28.6	G11	-49.6	G11	16.7	G11	21.3
G12	91.5	G12	40.9	G12	42.5	G12	49.6	G12	84.7	G12	29.3
G13	63.7	G13	19.8	G13	-6.7	G13	23.2	G13	22.8	G13	23.1
G7	-20.5	G7	-31.9	G7	-39.1	G7	-39.5	G7	-59.4	G7	-33
G8	-25.7	G8	-72.7	G8	-47.4	G8	-43.7	G8	-101.8	G8	-41.3
G9	-0.4	G9	-26	G9	-17.5	G9	-22.2	G9	-38	G9	-4.5
H13	101.7	H13	83.9	H13	30.5	H13	63.5	H13	69.6	H13	51.8
H7	-62.1	H7	-80.6	H7	-61.3	H7	-93.7	H7	-93	H7	-71.5
J13	101.7	J13	105	J13	-172.2	J13	57.4	J13	126.4	J13	75.6
J7	-127.5	J7	-81.5	J7	-113.2	J7	-80.5	J7	-42	J7	-104.5
K13	88.1	K13	80.1	K13	62.4	K13	141.6	K13	129.6	K13	54.7
K7	-137.2	K7	-15.9	K7	-86.2	K7	-133.5	K7	-97	K7	-98.7
L13	88.4	L13	78.8	L13	-167.2	L13	172.3	L13	144.5	L13	134.2
L7	-148.1	L7	-36.2	L7	-108.5	L7	-112	L7	-102.6	L7	-91
M13	118.7	M13	111	M13	161.2	M13	142.2	M13	135.6	M13	129.5
M7	-131.6	M7	-144.7	M7	-128.4	M7	-115.8	M7	-103.1	M7	-142.4
N10	177.2	N10	-170.5	N10	150.8	N10	179.7	N10	176.3	N10	171.2
N11	108	N11	163.5	N11	113	N11	60.2	N11	134.9	N11	153.6
N12	136.6	N12	75.3	N12	105.5	N12	156.7	N12	140.8	N12	131.2
N13	-173	N13	163.9	N13	-147.2	N13	-178.4	N13	146.7	N13	134
N7	-174.5	N7	179	N7	-126.1	N7	-168.8	N7	-154.3	N7	-166.6
N8	-133.8	N8	-157	N8	-112.6	N8	-131.8	N8	-137.3	N8	-125.1
N9	-142.8	N9	-153.8	N9	-170.8	N9	-133.8	N9	172	N9	-163.8

UT5-U12A-SPA-A-8- / UT5-U2A-SPA-A-8- / UT5-U7A-SPA-A-8-PI						UT7-U12A-SPA-A-10- / UT7-U2A-SPA-A-10- / UT7-U7A-SPA-A-10-PI					
Joint No.	Crack angle^{o}	Joint No.	Crack angle^{o}	Joint No.	Crack angle^{o}	Joint No.	Crack angle^{o}	Joint No.	Crack angle^{o}	Joint No.	Crack angle^{o}
G10	-46.1	G10	-0.3	G10	-34.8	G10	16.8	G10	40.5	G10	-24.8
G11	19.7	G11	26.3	G11	-0.9	G11	35.2	G11	-28.9	G11	-39.9
G12	41.4	G12	60.1	G12	10.4	G12	66.7	G12	44.4	G12	9.6
G13	18.8	G13	49.3	G13	11.6	G13	17.2	G13	29.5	G13	19.8
G7	-45.3	G7	-33.4	G7	-34.7	G7	-38.2	G7	-22.7	G7	-18.1
G8	-40.4	G8	-20.1	G8	-83.6	G8	-51.1	G8	-75.4	G8	-40.1
G9	-34.7	G9	-5.1	G9	12.5	G9	27.9	G9	-40.3	G9	11.3
H13	55.4	H13	68	H13	37.1	H13	76.2	H13	56	H13	31.3
H7	-30.1	H7	-99.8	H7	-108.2	H7	-68.1	H7	-49.3	H7	-77.8
J13	55.7	J13	61.2	J13	94.1	J13	88.3	J13	84.4	J13	99.9
J7	-76.1	J7	-69.1	J7	-86.6	J7	-79.3	J7	-87.5	J7	-63.5
K13	132.2	K13	86.9	K13	84.8	K13	79.8	K13	125.8	K13	82.1
K7	-107.3	K7	-79.3	K7	-31.4	K7	-120.4	K7	-114	K7	-89.5
L13	124.7	L13	104.2	L13	136	L13	128.3	L13	169.1	L13	145.9
L7	-105.6	L7	-83.2	L7	-104.9	L7	-129.7	L7	-111.3	L7	-116
M13	112.7	M13	71.9	M13	-165.9	M13	101.8	M13	125.5	M13	113.7
M7	-120	M7	-137.1	M7	-94.3	M7	-134.5	M7	-115.9	M7	-152.1
N10	-174.3	N10	151.3	N10	179.2	N10	149.4	N10	-179.7	N10	-169.2
N11	177.6	N11	157	N11	176.1	N11	124	N11	-156.5	N11	-159.3
N12	143.1	N12	134.8	N12	161.6	N12	137.6	N12	146.2	N12	128.3
N13	176.2	N13	175.1	N13	-167.5	N13	-177.2	N13	170.2	N13	147.6
N7	-126.3	N7	-147	N7	-165.2	N7	-159.6	N7	179.1	N7	-175.1
N8	-115.6	N8	-134.8	N8	-117.4	N8	-113.2	N8	-122.1	N8	-148.5
N9	-161.1	N9	178.5	N9	-146.7	N9	-152	N9	-178.5	N9	178.1

UT12-U14A-SPA-Q-4- / UT12-U4A-SPA-Q-4- / UT12-U9A-SPA-Q-4-PI						UT11-U13A-SPA-Q-6- / UT11-U3A-SPA-Q-6- / UT11-U8A-SPA-Q-6-PI					
Joint No.	Crack angle°	Joint No.	Crack angle°	Joint No.	Crack angle°	Joint No.	Crack angle°	Joint No.	Crack angle°	Joint No.	Crack angle°
G10	-11.6	G10	-19.6	G10	15.4	G10	7.5	H7	-92.7	G10	-57.4
G11	9.1	G11	-34	G11	-4.9	G11	-33.4	H13	51.7	G11	-7.4
G12	12.9	G12	22.4	G12	0.4	G12	27	G9	-28	G12	-4.5
G13	4.4	G13	5.5	G13	-13.3	G13	37.3	G8	-63.8	G13	6.9
G7	-15.8	G9	-30.3	G7	-36.7	G7	-50.5	G7	-29.5	G7	-16
G8	-16.1	H13	89.5	G8	-26.7	G8	-24.4	G13	47.6	G8	-41.1
G9	-37.2	J13	65.9	G9	13.3	G9	-26	G12	51.3	G9	-8.3
H13	56.2	K13	173.5	H13	34.7	H13	48.9	G11	9.5	H13	5.3
H7	-92.6	L13	146.3	H7	-72.7	H7	-78.9	G10	-2.8	H7	-76.2
J13	121.1	M13	149.5	J13	142.5	J13	58.5	N9	-46	J13	123.7
J7	-159.9	N10	-157.6	J7	-87.6	J7	-59.2	N8	-132.9	J7	-101
K13	-158.7	N11	-149.5	K13	-6.9	K13	32	N7	-128.4	K13	-118.5
K7	-85.7	N12	131	K7	-119.1	K7	-88.3	N13	144.5	K7	-102
L13	116.9	N13	172.7	L13	141.6	L13	133.3	N12	93.6	L13	161.4
L7	-78.5	N7	-133.7	L7	-133.2	L7	-38.3	N11	160.3	L7	-91.7
M13	157.8	N9	-153.7	M13	131.2	M13	157.5	N10	155.6	M13	108.3
M7	-117.5			M7	-144.3	M7	-134.6	M7	-107.8	M7	-151.1
N10	118			N10	173	N10	171.8	M13	52.9	N10	-170
N11	19.2			N11	-158.2	N11	-179.7	L7	-136.1	N11	-145.3
N12	88.9			N12	142.9	N12	145.8	L13	134.7	N12	147.8
N13	162.1			N13	-164	N13	149.3	K7	-101	N13	-175.9
N7	-86.4			N7	-164.9	N7	-162.7	K13	89	N7	-161.5
N8	-151.5			N8	-115	N8	-162.4	J7	-75.5	N8	-126.1
N9	117.6			N9	-165.4	N9	-133.8	J13	110.8	N9	-129.4

UT10-U12A-SPA-Q-8- / UT10-U2A-SPA-Q-8- / UT10-U7A-SPA-Q-8-PI						UT12-U12A-SPA-Q-10- / UT12-U2A-SPA-Q-10- / UT12-U7A-SPA-Q-10-PI					
Joint No.	Crack angle°	Joint No.	Crack angle°	Joint No.	Crack angle°	Joint No.	Crack angle°	Joint No.	Crack angle°	Joint No.	Crack angle°
G10	-12.7	G10	-13.1	G10	0.3	G10	-1	G10	-48.1	G10	-42.3
G11	10.8	G11	-3.9	G11	-8.6	G11	34	G11	-38.4	G11	0.5
G12	33.7	G12	34.3	G12	28.2	G12	29.7	G12	1.5	G12	68.1
G13	27.3	G13	26.6	G13	27	G13	23.2	G13	23.6	G13	47.3
G7	-2.9	G7	-53.4	G7	-39.5	G7	-27.2	G7	-52.5	G7	-41.5
G8	-50.9	G8	-48.8	G8	-1.2	G8	-48.2	G8	-72.7	G8	-51.7
G9	-11.2	G9	-47.1	G9	-24	G9	-35.4	G9	-14.1	G9	-19.8
H13	13.7	H13	41.5	H13	53.2	H13	55.8	H13	35	H13	45.5
H7	-69.7	H7	-62.4	H7	-58.2	H7	-62.8	H7	-56.6	H7	-84.7
J13	95.5	J13	56.9	J13	104	J13	50.1	J13	126.5	J13	59.9
J7	-83.5	J7	-65.2	J7	-77.1	J7	-44.6	J7	-86.3	J7	-71.2
K13	70.2	K13	83.3	K13	79.2	K13	98.9	K13	92.6	K13	116.9
K7	-64.4	K7	-107.9	K7	-86.1	K7	-100.5	K7	-98	K7	-76.3
L13	92	L13	112.6	L13	111.2	L13	65.9	L13	175.5	L13	111.2
L7	-104.5	L7	-162.6	L7	-88.1	L7	-102.4	L7	-92.5	L7	-94
M13	156.5	M13	143.1	M13	126.6	M13	93.1	M13	-159.4	M13	149.3
M7	-154.8	M7	-106.3	M7	-120.3	M7	-111	M7	-108.8	M7	-102
N10	-164.5	N10	-154.9	N10	-162.2	N10	-140.3	N10	-161.2	N10	172
N11	103.9	N11	157.3	N11	142.6	N11	-161.2	N11	-165.8	N11	148.6
N12	129.4	N12	127.8	N12	137.9	N12	154.6	N12	180	N12	119.9
N13	-178.7	N13	147.2	N13	-169	N13	171.4	N13	177.2	N13	179.1
N7	-164.4	N7	-146.6	N7	-154.8	N7	-156.4	N7	-138	N7	-119.1
N8	-136.9	N8	-102.5	N8	-130.7	N8	-128.8	N8	-106.2	N8	-101.1
N9	-168.3	N9	-139.9	N9	-138.1	N9	-174	N9	-136.6	N9	-165.6

UT16-U14A-SA-AG-6- / UT16-U4A-SA-AG-6- / UT16-U9A-SA-AG-6-PI						UT14-U12A-SA-AG-9- / UT14-U2A-SA-AG-9- / UT14-U7A-SA-AG-9-PI					
Joint No.	Crack angle°	Joint No.	Crack angle°	Joint No.	Crack angle°	Joint No.	Crack angle°	Joint No.	Crack angle°	Joint No.	Crack angle°
G10		G10	-59.6	G10	-13.4	G10	43.7	G10	5.3	G10	15.8
G11		G11	67	G11	119.4	G11	23.5	G11	14.4	G11	80.5
G12	54.4	G12	57.8	G12	27	G12	22.2	G12	7.3	G12	75.7
G13	-42.3	G13	25.2	G13	-148.7	G13	-4.5	G13	2.5	G13	23.9
G7	-69	G7	-82.1	G7		G7	-29.8	G7	-6.5	G7	12.3
G8	-21.2	G8		G8		G8	-27.4	G8	-61.5	G8	-82.5
G9		G9	-34.4	G9	-27.9	G9	-48.8	G9	-44.5	G9	-7.2
H13	44.3	H13	13.4	H13	7.6	H13	43.7	H13	138.9	H13	106.1
H7		H7		H7	3.7	H7	-138	H7	-117.1	H7	0.7
J13	40.1	J13	118.7	J13	27.4	J13	76.9	J13		J13	92
J7		J7	-114.5	J7	-11.1	J7	-147.4	J7	-95.1	J7	29.7
K13	85	K13	76.9	K13	146.5	K13		K13	123.4	K13	98.7
K7	-160.1	K7	-124	K7	-55.2	K7	-65	K7	31	K7	-5.6
L13	138	L13	-123	L13	-101	L13	116.1	L13	141.3	L13	-79.2
L7		L7	-132.3	L7	-4.6	L7	77.6	L7	-110.7	L7	-106.1
M13	-163.9	M13	-108.1	M13	91.1	M13	91.3	M7	148	M13	146.3
M7	-137.4	M7	-141.4	M7	-74	M7	-159.3	N10	-11.4	M7	-71.8
N10	175	N10	-169.6	N10	12	N10	-171.4	N11	141.6	N10	-176.8
N11	-167.7	N11	131.2	N11	144.8	N11	-10.5	N12	73.4	N11	178.6
N12	64.4	N12	99.9	N12	115.4	N12	53.3	N7	-134.2	N12	116.4
N13	-179.4	N13	168	N13	-179.5	N13	68.2	N8	-91.6	N13	106
N7	-158.6	N7	-147.6	N7	-83.9	N7	-18	N9	-158.6	N7	-147.8
N8		N8	142.2	N8	123.8	N8	-171.9			N8	-113.9
N9		N9		N9	-12.6	N9	39.5			N9	-98.7

UT16-U12A-SA-AG-12- / UT16-U2A-SA-AG-12- / UT16-U7A-SA-AG-12-PI						UT14-U11A-SA-AG-15- / UT14-U1A-SA-AG-15- / UT14-U6A-SA-AG-15-PI					
Joint No.	Crack angle°	Joint No.	Crack angle°	Joint No.	Crack angle°	Joint No.	Crack angle°	Joint No.	Crack angle°	Joint No.	Crack angle°
G10	-13.8	G10	-59.3	G10		G10	58.6	G10	-20.2	G10	42.5
G11	-38.5	G11	-4.5	G11	2.9	G11	-6.5	G11	-162.8	G11	-33.2
G12	1.6	G12		G12	19	G12	46.3	G12	69.7	G12	117
G13	16	G13	42.3	G13	-11.9	G13	49.2	G13	32.4	G13	15.5
G7	178.7	G7	-9.3	G7	-63.6	G7	0	G7	-86.6	G7	-86.8
G8	-46	G8	-9.3	G8		G8	-105.7	G8	-164.9	G8	
G9	-27.8	G9	-66.8	G9	-54.7	G9	-51.8	G9	-74.6	G9	-34.7
H13	129.5	H13	-28.9	H13	147.6	H13	-60.1	H13	132.6	H13	95.9
H7	-97.2	H7	-66.6	H7	10.3	H7	-116	H7	-86.9	H7	23.4
J13	-114.5	J13	76	J13	75.4	J13	91	J13	82.2	J13	61.5
J7		J7	-155.9	J7	84	J7	-97.3	J7	-88.7	J7	-54.3
K13	-104.3	K13	-175.5	K13	14.5	K13	66.6	K13	89.1	K13	-137.5
K7	70.6	K7	75.5	K7		K7	-86.1	K7	-35.8	K7	-155.3
L13	-138.8	L13	157	L13	86.6	L13	89.2	L13	145.9	L13	-100.3
L7	-97.9	L7		L7	151.9	L7	-127.8	L7	-119.2	L7	101.6
M13	149	M13	149	M13	115.4	M13	132.1	M13	132.4	M13	118.5
M7	-145.8	M7	-126.6	M7	147.5	M7	-171	M7	-143.1	M7	-99.1
N10	-14.4	N10	163.4	N10	-83.3	N10	-32.1	N10	-145.6	N10	-165
N11	-40.8	N11		N11	150.3	N11	166.9	N11	-48.3	N11	98.5
N12	111.2	N12	146.1	N12	166.8	N12	120.2	N12	109.4	N12	57.6
N13	105.3	N13	147.4	N13	111.2	N13	173.8	N13	-179.5	N13	91.1
N7		N7	-178	N7	153.6	N7	-173.5	N7	174.4	N7	-110.4
N8	-32.2	N8	-129.5	N8	-92.3	N8	-148.6	N8	-49.4	N8	-113.9
N9	-170.1	N9	-25	N9	162.5	N9	-126.4	N9	69.5	N9	-160.4

UT20-U14A-SA-A-6- / UT20-U4A-SA-A-6- / UT20-U9A-SA-A-6-PI						UT19-U13A-SA-A-9- / UT19-U3A-SA-A-9- / UT19-U8A-SA-A-9-PI					
Joint No.	Crack angle°	Joint No.	Crack angle°	Joint No.	Crack angle°	Joint No.	Crack angle°	Joint No.	Crack angle°	Joint No.	Crack angle°
G10	-35.8	G10	-46.6	G10	-75.4	G10	-15.5	G10	-46.3	G10	-78.5
G11	-27.7	G11	52.7	G11	-72	G11	-43	G11	-27	G11	-39.2
G12	8.2	G12	-2.1	G12		G12	99.3	G12	12.3	G12	-1.2
G13	128.5	G13	-56.5	G13	15.8	G13	-22.3	G13	76	G13	37.8
G7	-25.8	G7	-85.2	G7	-96.1	G7	-79.8	G7	-10.9	G7	-22.1
G8	-43.7	G8	-88.9	G8	-28.9	G8	-46	G8	-70.3	G8	-63.6
G9	-51.3	G9	108.8	G9	-131.6	G9	-37.1	G9	-25.6	G9	-78.3
H13	50.4	H13	71.6	H13	172.5	H13	57.7	H13	53.8	H13	120
H7	-87.1	H7	-12.2	H7	172.9	H7	-98.1	H7	-178.2	H7	-50.9
J13	136.4	J13	99.3	J13	59.8	J13	12.7	J13	105.2	J13	91.7
J7	-83.7	J7	102.1	J7	94.1	J7	-127.8	J7	-74.9	J7	-9.4
K13	-85.1	K13	71.6	K13	38.7	K13	102.1	K13	101.5	K13	115.7
K7	158.6	K7	-101.8	K7	-53.2	K7	-106	K7	-88.2	K7	-56.8
L13	57.4	L13	172.5	L13	-31.7	L13	-17.6	L13	157.3	L13	90
L7	-118.9	L7	-96.7	L7	-81.5	L7	-74.9	L7	-115.8	L7	-104.8
M13	137.6	M13	165.7	M13	146.8	M13	-2.3	M13	111.2	M13	177.7
M7	-14.3	M7	-19.9	M7	124.4	M7	-110.8	M7	-86.1	M7	-117.8
N10	-171.4	N10	37.5	N10	-151.4	N10	162.1	N10	123.3	N10	-146.5
N11	-54.3	N11	-156.8	N11	90.5	N11	145.1	N11	-177.9	N11	-140.4
N12	165.5	N12	-178.4	N12	169.1	N12	117.9	N12	111.1	N12	-163.3
N13	176.4	N13	105.6	N13	177.9	N13	121	N13	-150.9	N13	156.2
N7	157	N7	155.4	N7	-120.3	N7	-149.6	N7	-164.9	N7	-91.9
N8	-143.6	N8	-168.7	N8	-15.5	N8	-108.6	N8	-147.5	N8	-96.5
N9	-54.7	N9	-140.4	N9	176.7	N9	166.3	N9	-30	N9	-112

UT18-U12A-SA-A-12- / UT18-U2A-SA-A-12- / UT18-U7A-SA-A-12-PI						UT20-U12A-SA-A-15- / UT20-U2A-SA-A-15- / UT20-U7A-SA-A-15-PI					
Joint No.	Crack angle°	Joint No.	Crack angle°	Joint No.	Crack angle°	Joint No.	Crack angle°	Joint No.	Crack angle°	Joint No.	Crack angle°
G10	-0.7	G10	12.4	G10	-24.5	G10	-27.2	G10	1.4	G10	-4.4
G11	-6.7	G11	-14.2	G11	29.8	G11	-149.3	G11	-36.3	G11	-70.3
G12	51.5	G12	29	G12	29.3	G12	18.3	G12	25.7	G12	-2.7
G13	87.5	G13	27.8	G13	-9.1	G13	-24.1	G13	35.6	G13	-22.8
G7	-26.9	G7	-75.7	G7	5.8	G7	-61.6	G7	-44	G7	-14
G8	-73.4	G8	-39	G8	-7.7	G8	-74.9	G8	-44.6	G8	-46.8
G9	-58.1	G9	94.5	G9	-64.8	G9	-45.1	G9	-164.9	G9	33.1
H13	49.6	H13	69.3	H13	128.3	H13	148.7	H13	77.5	H13	-14.5
H7	-96.7	H7	-82.5	H7	-60.7	H7	-137.9	H7	-68.2	H7	-80.8
J13	-136.1	J13	123.3	J13	71.6	J13	59.7	J13	-7.8	J13	87.8
J7	-100	J7	89.6	J7	-141.6	J7	-105.5	J7	-25.7	J7	-32.5
K13	-77	K13	95.7	K13	150.5	K13	-96.6	K13	90.5	K13	149.8
K7	-102.1	K7	-112.7	K7	-54.4	K7	-72.9	K7	121.6	K7	-75
L13	120.2	L13	101.4	L13	88.1	L13	23.8	L13	79.8	L13	142.7
L7	-97.7	L7	-178.3	L7	165.6	L7	-101.2	L7	-105.5	L7	73.6
M13	34.1	M13	133.5	M13	172.5	M13	107.5	M13	99	M13	97.3
M7	-110.8	M7	-152.8	M7	-117.6	M7	-90	M7	-144.3	M7	-153.6
N10	-134.4	N10	176.8	N10	-139.5	N10	140.1	N10	-24.3	N10	-139.4
N11	150.2	N11	-177.2	N11	16.4	N11	47.4	N11	131.1	N11	-144
N12	134.2	N12	36.4	N12	108.5	N12	-170.5	N12	96.8	N12	-177.3
N13	-165.4	N13	118.2	N13	87.3	N13	151.9	N13	99.8	N13	-162.8
N7	-112.2	N7	-150.9	N7	-111.3	N7	-126.8	N7	-145.1	N7	-132.9
N8	-135.3	N8	-131.6	N8	-134.4	N8	-135.7	N8	-98.6	N8	-86.3
N9	-152.9	N9	5.2	N9	-136.3	N9	-153.2	N9	-175.1	N9	-163.9

UT25-U14A-SA-Q-6- / UT25-U4A-SA-Q-6- / UT25-U9A-SA-Q-6-PI						UT24-U13A-SA-Q-9- / UT24-U3A-SA-Q-9- / UT24-U8A-SA-Q-9-PI					
Joint No.	Crack angle°	Joint No.	Crack angle°	Joint No.	Crack angle°	Joint No.	Crack angle°	Joint No.	Crack angle°	Joint No.	Crack angle°
G10	7.1	G10	-20.7	G10	26.3	G10	31.3	G10	83.7	G10	-26.9
G11	-7.7	G11	-112.2	G11	47.5	G11	-17.3	G11	-16.2	G11	33.9
G12	-9.3	G12	36.5	G12	-87	G12	22.2	G12	77	G12	61.1
G13	29.7	G13	2.3	G13	0.1	G13	-7.4	G13	1.5	G13	26.4
G7	-43.2	G7	130.1	G7	-101.9	G7	27.7	G7	-48.5	G7	-26.3
G8	-44.1	G8	-62.2	G8	-62.9	G8	-41.4	G8	-25.7	G8	-40.7
G9	11.6	G9		G9	-14.2	G9	11.4	G9	13.9	G9	-66.4
H13	4.6	H13	74.3	H13	151.9	H13	33	H13	130.9	H13	90.9
H7	-44.2	H7	-44.1	H7	-123.8	H7	-84.6	H7	-60.6	H7	-17
J13	141	J13	91.3	J13	94.1	J13	80.6	J13	-31.9	J13	62.7
J7	-72.6	J7	-104.7	J7	-14.6	J7	-71.4	J7	-98.8	J7	-54.9
K13	74.5	K13	120.5	K13	76.4	K13	107.5	K13	173.5	K13	-85.6
K7	-81.5	K7	-63.8	K7	-138.7	K7	-104.8	K7	-133.6	K7	-177
L13	135	L13	165.3	L13	139	L13	152.7	L13	99.3	L13	136.3
L7	-79.5	L7	-147	L7	-160.7	L7	3.3	L7	177.3	L7	-110.1
M13	117.3	M13	125.6	M13	94.9	M13	118.8	M13	137	M13	168.1
M7	-82.1	M7	-36.4	M7	-56.9	M7	-156.5	M7	166.1	M7	-89.8
N10	45.2	N10	39	N10	121	N10	165.3	N10	126.5	N10	-174.4
N11	152.7	N11	167.1	N11	-175.6	N11	154.1	N11	118.6	N11	176.4
N12	92.7	N12	159.7	N12	-129.1	N12	141.3	N12	114.9	N12	176.3
N13	164.4	N13	167.1	N13	170.4	N13	17.1	N13	117.1	N13	155.2
N7	-105.1	N7	-155	N7	-171.6	N7	-70.5	N7	-117.2	N7	-130.7
N8	-93.4	N8	-173.2	N8	156.8	N8	-162.3	N8	-141.3	N8	156.7
N9	156.6	N9	-132.1	N9	-159.7	N9	-149.7	N9	-173.8	N9	-109.5

UT23-U12A-SA-Q-12- / UT23-U2A-SA-Q-12- / UT23-U7A-SA-Q-12-PI						UT25-U12A-SA-Q-15- / UT25-U2A-SA-Q-15- / UT25-U7A-SA-Q-15-PI					
Joint No.	Crack angle°	Joint No.	Crack angle°	Joint No.	Crack angle°	Joint No.	Crack angle°	Joint No.	Crack angle°	Joint No.	Crack angle°
G10	-39	G10	-31.2	G10	-46	G10	98.8	G10	-30.1	G10	24
G11	39.8	G11	-45.5	G11	-21.7	G11	-43.3	G11	85.9	G11	-35.9
G12	10	G12	62.3	G12	-0.6	G12	38.6	G12	79.9	G12	-58.5
G13	-22.1	G13	11.2	G13	138.2	G13	9.8	G13	34.1	G13	-19.5
G7	-45.9	G7	6.8	G7	78.6	G7	-44.2	G7	-18.8	G7	-1.1
G8	-82.6	G8	14.3	G8	-44.3	G8	-33.8	G8	-47	G8	-62.2
G9	-48.3	G9	-40.6	G9	-35.9	G9	-8.7	G9	42	G9	-89.9
H13	48.7	H13	77.7	H13	101.5	H13	19.8	H13	67.2	H13	142.3
H7	-42.5	H7	-32.5	H7	-136.8	H7	-119.4	H7	-37.2	H7	-55.2
J13	111	J13	64	J13	102.5	J13	-48	J13	133.1	J13	50
J7	37.5	J7	172.4	J7	-80.7	J7	-123.3	J7	111.2	J7	-99
K13	84.3	K13	-179.9	K13	-3.4	K13	-176.7	K13	126.2	K13	66.3
K7	177.5	K7	-89.4	K7	-105.1	K7		K7	-81.5	K7	-1.9
L13	150.1	L13	109.8	L13	145.2	L13	69.6	L13	126.5	L13	159
L7	-158.3	L7	-111.6	L7	-20.3	L7	-109.9	L7	-70.1	L7	-50.1
M13	142.8	M13	118.6	M13	110.8	M13	174.3	M13	129.5	M13	124.2
M7	-102.5	M7	-164.6	M7	-100	M7	-139.2	M7	-93.2	M7	-167
N10	-131.8	N10	167.4	N10	178.2	N10	-148.9	N10	176	N10	-118.5
N11	129.9	N11	-108.7	N11	45.4	N11	-45.1	N11	135.8	N11	-13.8
N12	151.4	N12	89.2	N12	128.6	N12	-174.2	N12	62.9	N12	105.2
N13	112.8	N13	127.6	N13	-150	N13	106.5	N13	97.7	N13	126.3
N7	-147.9	N7	46.2	N7	-144	N7	-146.7	N7	-121.7	N7	-121.9
N8	-139.9	N8	151.9	N8	-139.4	N8	-172.2	N8	-120.2	N8	-35.4
N9	178.9	N9	-160.3	N9	-122.4	N9	-150.5	N9	-152.9	N9	-165.9

APPENDIX G

Experimentally-measured % Crack Length

Table G.1. % Crack length data for aged, air-cooled, and quenched SnPb joints in the boundary region at the package interface (nominal joint diameter=560 μm)

SnPb, Aged, 2K, PI

UT1-U14A-SPA-AG-2- / UT1-U4A-SPA-AG-2- / UT1-U9A-SPA-AG-2-PI											
Joint No.	% crack length P	% crack length S	% crack length P+S	Joint No.	% crack length P	% crack length S	% crack length P+S	Joint No	% crack length P	% crack length S	% crack length P+S
G10	0.0	0.0	0.0	G10	0.0	0.0	0.0	G10	0.0	0.0	0.0
G11	0.0	0.0	0.0	G11	0.0	0.0	0.0	G11	0.0	0.0	0.0
G12	0.7	0.0	0.7	G12	2.1	0.0	2.1	G12	3.6	0.0	3.6
G13	**20.0**	**0.0**	**20.0**	G13	7.1	0.0	7.1	G13	5.9	0.0	5.9
G7	4.9	0.0	4.9	G7	3.3	0.0	3.3	G7	6.7	0.0	6.7
G8	0.0	0.0	0.0	G8	1.6	0.0	1.6	G8	4.3	0.0	4.3
G9	6.1	0.0	6.1	G9	5.7	0.0	5.7	G9	0.0	0.0	0.0
H13	0.0	0.0	0.0	H13	0.0	0.0	0.0	H13	5.4	0.0	5.4
H7	1.4	0.0	1.4	H7	8.0	0.0	8.0	H7	2.0	0.0	2.0
J13	6.8	3.3	10.2	J13	1.9	0.0	1.9	**J13**	**12.4**	**0.0**	**12.4**
J7	0.0	0.0	0.0	J7	0.0	0.0	0.0	J7	0.0	0.0	0.0
K13	0.0	0.0	0.0	K13	0.0	0.0	0.0	K7	0.0	0.0	0.0
K7	0.0	0.0	0.0	K7	0.0	0.0	0.0	L13	0.0	0.0	0.0
L13	0.0	0.0	0.0	L13	0.0	2.4	2.4	L7	8.6	0.0	8.6
L7	3.0	0.0	3.0	L7	0.0	0.0	0.0	M13	0.0	0.0	0.0
M13	0.0	0.0	0.0	M13	0.0	0.0	0.0	M7	7.4	0.0	7.4
M7	4.5	0.0	4.5	M7	9.1	0.0	9.1	**N10**	**10.5**	**0.0**	**10.5**
N10	**15.7**	**0.0**	**15.7**	N10	0.0	0.0	0.0	**N11**	**19.2**	**0.0**	**19.2**
N11	2.6	0.0	2.6	N11	0.0	0.0	0.0	N12	0.0	0.0	0.0
N12	**10.5**	**0.0**	**10.5**	N12	0.0	0.0	0.0	N13	9.4	0.0	9.4
N13	6.6	0.0	6.6	**N13**	**22.4**	**0.0**	**22.4**	**N7**	**13.6**	**0.0**	**13.6**
N7	**13.1**	**0.0**	**13.1**	**N7**	**18.5**	**0.0**	**18.5**	N8	7.4	0.0	7.4
N8	0.0	0.0	0.0	N8	0.0	0.0	0.0	N9	4.5	0.0	4.5

N9	4.0	0.0	4.0	N9	0.0	6.7	6.7				

Note: **Bold** represents raw data of Table 6.1, crack length data in the upper standard deviation in the boundary region, 0-100°C ATC, UT.

SnPb, Aged, 4K, PI

UT3-U14A-SPA-AG-4- / UT3-U9A-SPA-AG-4- / UT3-U4A-SPA-AG-4-PI											
Joint No.	% crack length P	% crack length S	% crack length P+S	Joint No.	% crack length P	% crack length S	% crack length P+S	Joint No	% crack length P	% crack length S	% crack length P+S
G10	3.4	8.7	12.1	G10	2.2	0.0	2.2	G10	19.2	0.0	19.2
G11	0.0	0.0	0.0	G11	0.0	0.0	0.0	G11	22.4	0.0	22.4
G12	0.0	0.0	0.0	G12	21.1	0.0	21.1	G12	25.7	0.0	25.7
G13	17.5	0.0	17.5	G13	26.4	0.0	26.4	G13	13.4	0.0	13.4
G7	19.3	0.0	19.3	**G7**	**19.9**	**0.0**	**19.9**	G7	32.7	0.0	32.7
G8	0.0	0.0	0.0	G8	18.5	0.0	18.5	G8	0.0	0.0	0.0
G9	0.0	28.3	28.3	**G9**	**33.4**	**0.0**	**33.4**	**G9**	**56.0**	**0.0**	**56.0**
H13	12.6	0.0	12.6	H13	0.0	0.0	0.0	H13	3.3	0.0	3.3
H7	**39.2**	**0.0**	**39.2**	H7	7.7	0.0	7.7	H7	2.6	0.0	2.6
J13	0.0	0.0	0.0	**J13**	**18.7**	**0.0**	**18.7**	J13	37.0	0.0	37.0
J7	0.0	0.0	0.0	J7	18.0	0.0	18.0	K13	0.0	24.8	24.8
K13	0.0	0.0	0.0	K13	14.5	22.9	37.5	K7	46.7	0.0	46.7
K7	3.9	0.0	3.9	**K7**	**7.0**	**0.0**	**7.0**	L13	0.0	0.0	0.0
L13	**33.2**	**0.0**	**33.2**	L13	3.8	0.0	3.8	L7	25.2	0.0	25.2
L7	2.9	0.0	2.9	L7	9.4	0.0	9.4	M13	12.8	0.0	12.8
M13	6.9	0.0	6.9	M13	14.2	0.0	14.2	M7	14.4	0.0	14.4
M7	2.0	0.0	2.0	M7	6.5	0.0	6.5	**N10**	**20.0**	**0.0**	**20.0**
N10	31.3	0.0	31.3	N10	32.0	0.0	32.0	N11	16.9	0.0	16.9
N11	27.4	0.0	27.4	N11	18.8	0.0	18.8	N12	32.2	0.0	32.2
N12	**40.9**	**2.5**	**43.4**	**N12**	**9.4**	**0.0**	**9.4**	N13	31.2	2.4	33.6
N13	**46.3**	**0.0**	**46.3**	N13	28.2	0.0	28.2	**N7**	**13.0**	**0.0**	**13.0**
N7	21.5	0.0	21.5	N7	43.1	0.0	43.1	N8	34.1	0.0	34.1
N8	21.2	0.0	21.2	**N8**	**30.3**	**0.0**	**30.3**	N9	8.0	0.0	8.0
N9	27.9	0.0	27.9	N9	26.4	2.9	29.3				

Note: **Bold** represents raw data of Table 6.1, crack length data in the upper standard deviation in the boundary region, 0-100°C ATC, UT.

SnPb, Aged, 6K, PI

UT2-U13A-SPA-AG-6- / UT2-U3A-SPA-AG-6- / UT2-U8A-SPA-AG-6-PI											
Joint No.	% crack length P	% crack length S	% crack length P+S	Joint No.	% crack length P	% crack length S	% crack length P+S	Joint No	% crack length P	% crack length S	% crack length P+S
G10	0.0	0.0	0.0	G10	20.8	0.0	20.8	G10	32.5	0.0	32.5
G11	15.3	0.0	15.3	G11	29.6	0.2	29.7	G11	0.0	0.0	0.0
G12	32.9	0.0	32.9	**G12**	**56.1**	**0.0**	**56.1**	G12	17.6	0.0	17.6
G13	**50.7**	**0.0**	**50.7**	G13	38.5	0.0	38.5	G13	12.5	0.0	12.5
G7	22.7	0.0	22.7	G7	36.3	0.0	36.3	**G7**	**67.8**	**0.0**	**67.8**
G8	36.3	0.0	36.3	G8	35.6	0.0	35.6	G8	15.5	0.0	15.5
G9	23.7	0.0	23.7	G9	26.7	0.0	26.7	G9	0.0	0.0	0.0
H13	**54.6**	**0.0**	**54.6**	H13	4.0	0.0	4.0	**H13**	**54.5**	**8.9**	**63.3**
H7	0.0	0.0	0.0	H7	22.5	0.0	22.5	**H7**	**49.9**	**0.0**	**49.9**
J13	**50.3**	**2.1**	**52.4**	J13	34.3	3.5	37.8	J13	45.8	9.4	55.2
J7	**75.3**	**0.0**	**75.3**	**J7**	**61.0**	**6.5**	**67.5**	J7	25.7	0.0	25.7
K13	0.0	0.0	0.0	K13	32.8	0.0	32.8	K13	3.1	0.0	3.1
K7	4.2	0.0	4.2	K7	42.5	17.0	59.5	K7	9.9	10.0	19.9
L13	16.2	0.0	16.2	**L13**	**50.6**	**3.7**	**54.3**	L13	37.8	0.0	37.8
L7	12.0	0.0	12.0	L7	10.2	2.9	13.1	L7	10.2	0.0	10.2
M13	25.6	0.0	25.6	M13	35.4	0.0	35.4	**M13**	**53.8**	**0.0**	**53.8**
M7	8.5	0.0	8.5	M7	31.9	0.0	31.9	M7	29.4	0.0	29.4
N10	15.3	0.0	15.3	N10	5.9	0.0	5.9	N10	23.7	0.0	23.7
N11	31.5	0.0	31.5	N11	0.0	0.0	0.0	N11	17.0	6.7	23.7
N12	41.6	0.0	41.6	**N12**	**51.1**	**0.0**	**51.1**	N12	40.7	0.0	40.7
N13	17.6	0.0	17.6	N7	5.9	0.0	5.9	N13	31.2	0.0	31.2
N7	34.5	0.0	34.5	N8	3.7	0.0	3.7	**N7**	**57.8**	**0.0**	**57.8**
N8	32.8	0.0	32.8	N9	24.9	7.2	32.1	N8	37.4	0.0	37.4
N9	16.0	0.0	16.0					N9	40.8	0.0	40.8

Note: **Bold** represents raw data of Table 6.1, crack length data in the upper standard deviation in the boundary region, 0-100°C ATC, UT.

SnPb, Aged, 8K, PI

UT1-U12A-SPA-AG-8- / UT1-U2A-SPA-AG-8- / UT1-U7A-SPA-AG-8-PI											
Joint No.	% crack length P	% crack length S	% crack length P+S	Joint No.	% crack length P	% crack length S	% crack length P+S	Joint No	% crack length P	% crack length S	% crack length P+S
G10	23.2	0.0	23.2	G10	58.1	0.0	58.1	G10	4.0	3.0	7.0
G11	31.4	0.0	31.4	G11	48.2	0.0	48.2	G11	5.3	0.0	5.3
G12	**78.6**	**0.0**	**78.6**	**G12**	**73.4**	**0.0**	**73.4**	G12	7.3	0.0	7.3
G7	31.7	0.0	31.7	G13	48.7	0.0	48.7	G13	50.2	0.0	50.2
G8	**74.9**	**0.0**	**74.9**	**G7**	**74.9**	**0.0**	**74.9**	G7	56.9	0.0	56.9
G9	**98.9**	**0.0**	**98.9**	G8	15.1	0.0	15.1	G8	46.9	0.0	46.9
H13	57.9	0.0	57.9	G9	61.5	0.0	61.5	G9	29.5	2.6	32.1
H7	59.8	0.0	59.8	H13	51.2	0.0	51.2	H13	40.0	0.0	40.0
J13	61.1	0.0	61.1	H7	52.4	0.0	52.4	**H7**	**99.1**	**0.0**	**99.1**
J7	46.0	0.0	46.0	J13	45.5	11.4	56.9	J7	45.9	0.0	45.9
K13	0.0	23.2	23.2	J7	60.5	0.0	60.5	K13	43.4	0.0	43.4
K7	49.4	0.0	49.4	K13	10.9	0.0	10.9	K7	29.0	0.0	29.0
L13	19.9	0.0	19.9	K7	18.1	0.0	18.1	L13	0.0	0.0	0.0
L7	49.4	0.0	49.4	L13	61.3	25.0	86.3	L7	64.0	0.0	64.0
M13	49.7	0.0	49.7	L7	19.8	0.0	19.8	**M13**	**82.1**	**0.0**	**82.1**
M7	53.9	0.0	53.9	M13	53.8	0.0	53.8	M7	63.8	0.0	63.8
N10	45.2	0.0	45.2	M7	44.7	0.0	44.7	N10	49.3	13.6	62.9
N11	29.4	3.9	33.3	N10	11.4	18.3	29.7	N11	0.0	0.0	0.0
N12	38.1	0.0	38.1	N11	46.1	18.8	64.9	N13	47.0	0.0	47.0
N13	56.5	0.0	56.5	**N12**	**98.1**	**0.0**	**98.1**	N8	53.6	0.0	53.6
N7	44.5	12.2	56.7	N13	67.5	0.0	67.5	N9	54.6	19.2	73.8
N8	**87.8**	**0.0**	**87.8**	**N7**	**71.8**	**0.0**	**71.8**				
N9	13.5	7.1	20.6	N8	44.5	0.0	44.5				
				N9	64.1	23.8	87.9				

Note: **Bold** represents raw data of Table 6.1, crack length data in the upper standard deviation in the boundary region, 0-100°C ATC, UT.

SnPb, Aged, 10K, PI

UT3-U12A-SPA-AG-10- / UT3-U2A-SPA-AG-10- / UT3-U7A-SPA-AG-10-PI											
Joint No.	% crack length P	% crack length S	% crack length P+S	Joint No.	% crack length P	% crack length S	% crack length P+S	Joint No	% crack length P	% crack length S	% crack length P+S
G10	13.9	2.8	16.7	G10	0.0	0.0	0.0	G10	58.7	0.0	58.7
G11	34.0	1.6	35.6	G11	9.7	0.0	9.7	G11	30.4	0.0	30.4
G12	18.5	0.0	18.5	G12	80.8	0.0	80.8	G12	73.0	4.8	77.8
G13	23.2	0.0	23.2	G13	37.8	0.0	37.8	G13	56.1	0.0	56.1
G7	40.1	0.0	40.1	G7	73.3	0.0	73.3	G7	19.8	0.0	19.8
G8	60.5	0.0	60.5	G8	73.4	0.0	73.4	G8	53.4	0.0	53.4
G9	40.8	40.2	81.0	G9	54.6	0.0	54.6	G9	20.2	0.0	20.2
H13	74.9	0.0	74.9	H13	72.8	0.0	72.8	H13	64.2	0.0	64.2
H7	44.8	0.0	44.8	H7	13.6	0.0	13.6	**H7**	**86.1**	**0.0**	**86.1**
J13	70.7	2.0	72.7	J13	38.4	0.0	38.4	J13	64.4	0.0	64.4
J7	17.3	7.6	24.9	J7	70.9	0.0	70.9	J7	32.4	0.0	32.4
K13				K13	71.1	0.0	71.1	K13	21.4	0.0	21.4
K7	42.3	19.5	61.8	K7	22.0	0.0	22.0	K7	33.2	18.4	51.6
L13	49.9	0.0	49.9	L13	46.4	0.0	46.4	L13	0.0	0.0	0.0
L7	41.5	0.0	41.5	**L7**	**81.9**	**0.0**	**81.9**	L7	67.8	0.0	67.8
M13	58.4	0.0	58.4	**M13**	**83.6**	**0.0**	**83.6**	M13	41.0	0.0	41.0
M7	**87.1**	**0.0**	**87.1**	**M7**	**99.6**	**0.0**	**99.6**	M7	72.0	0.0	72.0
N10				N10	55.4	6.4	61.8	**N10**	**82.9**	**0.0**	**82.9**
N11	42.1	8.8	50.9	**N11**	**100.0**	**0.0**	**100.0**	N11	56.0	0.0	56.0
N12	**98.8**	**0.0**	**98.8**	**N12**	**99.3**	**0.0**	**99.3**	**N12**	**90.4**	**0.0**	**90.4**
N13	68.1	0.0	68.1	N13	64.4	0.0	64.4	N13	48.5	0.0	48.5
N7	43.6	0.0	43.6	N7	64.4	0.0	64.4	N7	63.2	0.0	63.2
				N8	**100.0**	**0.0**	**100.0**	**N8**	**94.3**	**1.1**	**95.4**
				N9	53.4	0.0	53.4	N9	63.9	0.0	63.9

Note: **Bold** represents raw data of Table 6.1, crack length data in the upper standard deviation in the boundary region, 0-100°C ATC, UT.

SnPb, Aged, 13K, PI

UT2-U11A-SPA-AG-13- / UT2-U1A-SPA-AG-13- / UT2-U6A-SPA-AG-13-PI											
Joint No.	% crack length P	% crack length S	% crack length P+S	Joint No.	% crack length P	% crack length S	% crack length P+S	Joint No	% crack length P	% crack length S	% crack length P+S
G10	52.8	0.0	52.8	G10	81.5	0.0	81.5	G10	65.4	8.0	73.5
G11	72.3	0.0	72.3	G11	70.9	0.0	70.9	**G11**	**99.0**	**0.0**	**99.0**
G12	0.0	43.2	43.2	G12	46.7	0.0	46.7	**G12**	**98.9**	**0.0**	**98.9**
G13	**99.3**	**0.0**	**99.3**	G13	82.9	0.0	82.9	G13	64.9	0.0	64.9
G7	59.0	0.0	59.0	G7	58.2	0.0	58.2	G7	53.2	0.0	53.2
G8	18.0	0.0	18.0	**G8**	**98.4**	**0.0**	**98.4**	G8	84.1	0.0	84.1
G9	67.7	2.1	69.8	G9	78.6	0.0	78.6	G9	80.8	0.0	80.8
H13	**88.7**	**0.0**	**88.7**	H13	83.9	0.0	83.9	**H13**	**99.1**	**0.0**	**99.1**
H7	41.0	0.0	41.0	H7	75.3	0.0	75.3	H7	65.6	0.0	65.6
J13	54.0	0.0	54.0	**J13**	**98.9**	**0.0**	**98.9**	J13	65.3	0.0	65.3
J7	57.9	0.0	57.9	J7	30.6	0.0	30.6	**J7**	**93.3**	**0.0**	**93.3**
K13	0.0	0.0	0.0	K13	67.8	0.0	67.8	K13	58.6	0.0	58.6
K7	30.9	0.0	30.9	K7	33.0	0.0	33.0	K7	65.9	0.0	65.9
L13	30.0	0.0	30.0	L13	60.4	0.0	60.4	L13	41.4	0.0	41.4
L7	48.3	6.6	54.9	L7	75.5	0.0	75.5	L7	59.3	0.0	59.3
M13	61.8	0.0	61.8	M13	66.8	0.0	66.8	M13	79.1	5.5	84.6
M7	48.8	0.0	48.8	M7	40.7	0.0	40.7	**M7**	**94.7**	**0.0**	**94.7**
N10	42.0	0.0	42.0	N10	25.5	7.4	32.9	N10	79.4	11.4	90.8
N11	59.9	4.2	64.1	**N11**	**99.0**	**0.0**	**99.0**	N11	34.5	0.0	34.5
N12	36.1	0.0	36.1	**N12**	**100.0**	**0.0**	**100.0**	N12	78.6	0.0	78.6
N13	**99.3**	**0.0**	**99.3**	**N13**	**100.0**	**0.0**	**100.0**	N13	86.8	0.0	86.8
N7	82.1	0.0	82.1	N7	36.3	0.0	36.3	N7	65.5	0.0	65.5
N8	77.7	0.0	77.7	N8	20.9	0.0	20.9	N8	31.1	0.0	31.1
N9	76.0	5.8	81.7	N9	42.5	0.0	42.5	N9	41.9	0.0	41.9

Note: **Bold** represents raw data of Table 6.1, crack length data in the upper standard deviation in the boundary region, 0-100°C ATC, UT.

SnPb, Aged, 16K, PI

UT4-U10A-SPA-AG-16- / UT4-U15A-SPA-AG-16- / UT4-U5A-SPA-AG-16-PI											
Joint No.	% crack length P	% crack length S	% crack length P+S	Joint No.	% crack length P	% crack length S	% crack length P+S	Joint No	% crack length P	% crack length S	% crack length P+S
G10	67.0	0.0	67.0	G10	63.3	0.0	63.3	G10	50.3	0.0	50.3
G11	56.7	31.2	87.9	G11	79.5	0.0	79.5	G11	28.6	24.3	52.9
G12	47.5	0.0	47.5	G12	61.8	0.0	61.8	G12	80.5	0.0	80.5
G13	64.4	0.0	64.4	G13	83.3	2.3	85.5	G13	56.5	0.0	56.5
G7	64.1	0.0	64.1	G7	60.2	0.0	60.2	G7	63.5	0.0	63.5
G8	55.4	0.0	55.4	G8	36.3	0.0	36.3	G8	77.4	0.0	77.4
G9	57.9	0.0	57.9	G9	52.8	0.0	52.8	G9	65.7	0.0	65.7
H13	23.9	2.4	26.2	H13	59.7	0.0	59.7	H13	45.2	0.0	45.2
H7	42.7	0.0	42.7	**H7**	**98.9**	**0.0**	**98.9**	H7	50.5	0.0	50.5
J13	49.6	0.0	49.6	J13	78.0	2.3	80.3	J13	38.4	0.0	38.4
J7	**98.9**	**0.0**	**98.9**	J7	67.3	0.0	67.3	J7	74.1	0.0	74.1
K13	77.0	7.5	84.5	K13	37.1	0.0	37.1	K13	38.5	0.0	38.5
K7	17.1	0.0	17.1	K7	72.7	0.0	72.7	K7	84.9	0.0	84.9
L13	**98.8**	**0.0**	**98.8**	**L13**	**99.1**	**0.0**	**99.1**	L13	48.1	7.7	55.8
L7	74.8	0.0	74.8	L7	80.0	14.2	94.2	L7	9.4	0.0	9.4
M13	66.1	0.0	66.1	M13	82.8	2.4	85.2	M13	61.1	0.0	61.1
M7	30.9	0.0	30.9	M7	67.0	0.0	67.0	M7	37.3	0.0	37.3
N10	49.0	0.0	49.0	**N10**	**98.7**	**0.0**	**98.7**	N10	37.0	9.8	46.7
N11	68.2	0.9	69.0	N11	70.6	4.3	75.0	**N11**	**99.0**	**0.0**	**99.0**
N12	**98.9**	**0.0**	**98.9**	**N12**	**99.0**	**0.0**	**99.0**	**N12**	**97.2**	**0.0**	**97.2**
N13	57.6	0.0	57.6	N13	74.8	0.0	74.8	**N13**	**93.8**	**0.0**	**93.8**
N7	80.1	0.0	80.1	**N7**	**99.3**	**0.0**	**99.3**	N7	54.3	0.0	54.3
N8	85.6	0.0	85.6	N8	45.3	0.0	45.3	**N8**	**90.2**	**0.0**	**90.2**
N9	**98.9**	**0.0**	**98.9**	**N9**	**99.0**	**0.0**	**99.0**	N9	50.0	11.5	61.4

Note: **Bold** represents raw data of Table 6.1, crack length data in the upper standard deviation in the boundary region, 0-100°C ATC, UT.

SnPb, Air-Cooled, 2K, PI

UT5-U14A-SPA-A-2- / UT5-U4A-SPA-A-2- / UT5-U9A-SPA-A-2-PI											
Joint No.	% crack length P	% crack length S	% crack length P+S	Joint No.	% crack length P	% crack length S	% crack length P+S	Joint No	% crack length P	% crack length S	% crack length P+S
G10	3.7	0.0	3.7	G10	0.0	0.0	0.0	G10	5.4	3.2	8.6
G11	4.3	0.0	4.3	G11	6.2	3.9	10.1	G11	8.7	0.0	8.7
G13	4.5	2.8	7.3	G12	0.0	0.0	0.0	**G12**	**14.5**	**0.0**	**14.5**
G7	0.0	0.0	0.0	G13	6.0	0.0	6.0	G13	13.8	0.0	13.8
G8	0.0	0.0	0.0	G9	4.1	3.8	7.9	G7	9.4	0.0	9.4
G9	7.0	0.0	7.0	H13	4.6	0.0	4.6	**G8**	**14.3**	**1.6**	**15.9**
H7	6.9	0.0	6.9	J13	0.0	0.0	0.0	G9	0.0	0.0	0.0
J7	2.3	0.0	2.3	J7	8.9	0.0	8.9	H13	7.0	0.0	7.0
K7	0.0	0.0	0.0	K13	0.0	1.9	1.9	H7	12.0	0.0	12.0
L7	4.3	0.0	4.3	K7	0.0	0.0	0.0	J13	0.0	0.0	0.0
M13	3.3	0.0	3.3	**L13**	**11.3**	**3.6**	**14.9**	J7	5.8	0.0	5.8
M7	6.4	0.0	6.4	L7	7.4	0.0	7.4	K13	0.0	3.0	3.0
N10	**14.0**	**2.4**	**16.4**	M7	1.7	0.0	1.7	K7	4.9	3.1	8.0
N11	7.2	0.0	7.2	N10	5.7	0.0	5.7	L13	1.8	0.0	1.8
N7	10.1	0.0	10.1	N11	4.1	0.0	4.1	L7	9.0	0.0	9.0
N8	6.6	0.0	6.6	N12	7.4	0.0	7.4	M13	0.0	0.0	0.0
N9	3.1	0.0	3.1	N13	7.9	0.0	7.9	M7	7.2	0.0	7.2
				N7	4.5	0.0	4.5	N10	4.8	4.4	9.2
				N8	12.0	0.0	12.0	N11	2.7	0.0	2.7
				N9	5.0	0.0	5.0	N12	0.0	10.6	10.6
								N13	0.0	0.0	0.0
								N7	3.0	0.0	3.0
								N8	0.0	0.0	0.0
								N9	5.7	0.9	6.6

Note: **Bold** represents raw data of Table 6.1, crack length data in the upper standard deviation in the boundary region, 0-100°C ATC, UT.

SnPb, Air-Cooled, 4K, PI

UT7-U14A-SPA-A-4- / UT7-U4A-SPA-A-4- / UT7-U9A-SPA-A-4-PI											
Joint No.	% crack length P	% crack length S	% crack length P+S	Joint No.	% crack length P	% crack length S	% crack length P+S	Joint No	% crack length P	% crack length S	% crack length P+S
G10	11.4	0.0	11.4	G10	10.7	0.0	10.7	G10	21.0	1.7	22.7
G11	14.1	2.1	16.2	G11	0.0	0.0	0.0	G11	14.3	3.1	17.4
G12	2.9	0.0	2.9	G12	24.3	0.0	24.3	G12	10.5	1.7	12.2
G13	20.5	0.0	20.5	G13	23.4	0.0	23.4	G13	14.6	0.0	14.6
G7	12.9	0.0	12.9	G7	10.7	0.0	10.7	G7	17.6	0.0	17.6
G8	16.2	0.0	16.2	G8	20.2	0.0	20.2	G8	18.6	0.0	18.6
G9	19.6	1.4	21.0	G9	13.6	0.0	13.6	G9	25.7	0.0	25.7
H13	9.8	2.1	11.9	**H13**	**27.2**	**0.0**	**27.2**	H13	13.9	0.0	13.9
H7	10.8	3.6	14.5	H7	11.9	0.0	11.9	H7	16.7	0.0	16.7
J13	23.1	0.0	23.1	J13	11.9	0.0	11.9	J13	5.9	0.0	5.9
J7	0.0	0.0	0.0	J7	10.0	0.0	10.0	J7	14.3	0.0	14.3
K13	15.2	1.9	17.0	K13	11.2	0.0	11.2	K13	5.2	0.0	5.2
K7	0.0	0.0	0.0	K7	0.8	0.0	0.8	K7	13.1	0.0	13.1
L13	9.7	0.0	9.7	L13	14.9	3.7	18.7	**L13**	**26.7**	**0.0**	**26.7**
L7	3.6	0.0	3.6	L7	0.0	0.0	0.0	**L7**	**27.4**	**1.0**	**28.4**
M13	23.8	0.0	23.8	M13	16.7	3.3	20.0	M13	10.7	0.0	10.7
M7	15.7	0.0	15.7	M7	3.7	0.0	3.7	M7	9.7	0.0	9.7
N10	**24.3**	**4.5**	**28.8**	**N10**	**31.4**	**5.9**	**37.3**	**N10**	**24.8**	**3.6**	**28.4**
N11	10.5	6.4	16.9	N11	13.6	0.0	13.6	N11	17.4	5.2	22.6
N12	22.6	0.0	22.6	N12	4.2	0.0	4.2	N12	17.7	0.0	17.7
N13	10.0	0.0	10.0	N13	13.2	0.0	13.2	N13	4.5	0.0	4.5
N7	20.7	0.0	20.7	N7	21.2	0.0	21.2	N7	2.1	0.0	2.1
N8	18.8	0.0	18.8	N8	16.1	0.0	16.1	N8	25.3	0.0	25.3
N9	20.3	0.0	20.3	N9	10.5	0.0	10.5	N9	18.3	7.9	26.2

Note: **Bold** represents raw data of Table 6.1, crack length data in the upper standard deviation in the boundary region, 0-100°C ATC, UT.

SnPb, Air-Cooled, 6K, PI

UT6-U13A-SPA-A-6- / UT6-U3A-SPA-A-6- / UT6-U8A-SPA-A-6-PI											
Joint No.	% crack length P	% crack length S	% crack length P+S	Joint No.	% crack length P	% crack length S	% crack length P+S	Joint No	% crack length P	% crack length S	% crack length P+S
G10	21.3	17.7	39.0	G10	24.0	17.3	41.3	G10	21.7	5.8	27.5
G11	18.4	3.0	21.3	G11	22.4	0.0	22.4	G11	10.8	0.0	10.8
G12	**42.5**	**0.0**	**42.5**	G12	15.8	4.6	20.4	G12	26.1	0.0	26.1
G13	17.0	3.7	20.6	G13	25.3	0.0	25.3	G13	17.3	2.1	19.4
G7	35.8	0.0	35.8	G7	18.0	0.0	18.0	G7	39.2	2.4	41.7
G8	25.5	0.0	25.5	G8	0.0	0.0	0.0	G8	19.8	0.0	19.8
G9	21.9	4.2	26.1	G9	25.7	0.0	25.7	G9	21.6	0.0	21.6
H13	12.3	0.0	12.3	H13	22.6	0.0	22.6	H13	31.7	2.4	34.2
H7	40.6	0.0	40.6	H7	21.9	0.0	21.9	H7	23.4	0.0	23.4
J13	15.4	0.0	15.4	J13	1.4	0.0	1.4	**J13**	**46.0**	**10.0**	**55.9**
J7	**38.8**	**5.1**	**43.9**	J7	12.3	0.0	12.3	J7	29.7	0.0	29.7
K13	19.6	2.8	22.4	K13	22.1	0.0	22.1	K13	10.3	0.0	10.3
K7	5.8	0.0	5.8	K7	19.0	0.0	19.0	K7	22.0	0.0	22.0
L13	14.5	0.0	14.5	L13	7.5	0.0	7.5	L13	33.2	0.0	33.2
L7	17.1	5.2	22.4	L7	24.3	0.0	24.3	**L7**	**34.6**	**9.1**	**43.7**
M13	7.0	0.0	7.0	M13	25.9	3.4	29.3	**M13**	**46.5**	**6.7**	**53.1**
M7	32.9	0.0	32.9	M7	15.6	0.0	15.6	M7	17.7	0.0	17.7
N10	21.3	5.4	26.8	N10	23.5	0.3	23.8	N10	32.9	1.1	34.0
N11	7.9	11.4	19.2	N11	33.6	0.0	33.6	N11	23.6	7.3	30.9
N12	33.3	0.0	33.3	N12	30.1	0.0	30.1	N12	42.0	0.0	42.0
N13	4.9	0.0	4.9	N13	25.9	0.0	25.9	N13	39.1	0.0	39.1
N7	13.6	0.0	13.6	N7	31.0	0.0	31.0	**N7**	**44.8**	**0.0**	**44.8**
N8	28.3	0.0	28.3	N8	32.4	0.0	32.4	N8	33.2	0.0	33.2
N9	25.7	9.4	35.1	N9	27.0	0.0	27.0	N9	27.8	4.5	32.3

Note: **Bold** represents raw data of Table 6.1, crack length data in the upper standard deviation in the boundary region, 0-100°C ATC, UT.

SnPb, Air-Cooled, 8K, PI

UT5-U12A-SPA-A-8- / UT5-U2A-SPA-A-8- / UT5-U7A-SPA-A-8-PI											
Joint No.	% crack length P	% crack length S	% crack length P+S	Joint No.	% crack length P	% crack length S	% crack length P+S	Joint No	% crack length P	% crack length S	% crack length P+S
G10	13.7	12.0	25.7	G10	21.2	3.3	24.5	G10	24.7	0.0	24.7
G11	35.5	0.0	35.5	G11	31.3	6.5	37.8	G11	35.8	4.4	40.2
G12	36.3	9.7	46.0	G12	28.4	7.6	36.0	G12	49.8	7.2	57.0
G13	43.6	0.0	43.6	G13	32.4	0.0	32.4	G13	26.0	0.0	26.0
G7	19.6	0.0	19.6	G7	34.2	9.5	43.6	G7	45.2	12.3	57.5
G8	25.3	3.3	28.6	G8	33.7	0.0	33.7	G8	48.4	6.3	54.7
G9	31.2	7.3	38.5	**G9**	**53.8**	**14.7**	**68.5**	G9	16.0	1.4	17.4
H13	30.9	0.0	30.9	**H13**	**57.0**	**4.3**	**61.3**	H13	25.6	1.6	27.2
H7	9.0	0.0	9.0	**H7**	**60.2**	**7.0**	**67.3**	H7	15.1	0.0	15.1
J13	30.8	15.4	46.2	J13	37.8	7.4	45.2	J13	36.1	0.0	36.1
J7	23.3	0.0	23.3	J7	39.9	0.0	39.9	J7	27.0	4.9	31.9
K13	17.5	0.0	17.5	**K13**	**41.2**	**31.8**	**73.1**	K13	18.1	3.5	21.6
K7	11.5	0.0	11.5	K7	35.8	6.5	42.3	K7	0.0	0.0	0.0
L13	35.7	0.0	35.7	L13	48.4	0.0	48.4	L13	34.2	2.1	36.3
L7	37.1	3.3	40.4	L7	36.1	16.1	52.2	**L7**	**57.2**	**20.5**	**77.7**
M13	57.6	0.0	57.6	M13	32.3	9.0	41.3	M13	2.1	3.7	5.8
M7	30.4	0.0	30.4	M7	36.3	2.7	39.0	M7	38.1	0.0	38.1
N10	27.4	6.8	34.2	N10	25.9	0.0	25.9	N10	52.0	1.1	53.1
N11	22.6	5.0	27.6	N11	49.3	8.6	57.9	**N11**	**46.7**	**21.6**	**68.2**
N12	25.3	0.0	25.3	**N12**	**53.6**	**5.5**	**59.0**	N12	38.2	13.9	52.1
N13	37.4	3.1	40.6	N13	53.6	3.8	57.4	N13	24.7	0.0	24.7
N7	49.1	0.0	49.1	N7	30.6	0.0	30.6	N7	28.8	0.0	28.8
N8	31.8	0.0	31.8	N8	20.4	0.0	20.4	N8	53.7	0.0	53.7
N9	58.0	0.0	58.0	N9	46.4	9.8	56.2	N9	27.2	0.0	27.2

Note: **Bold** represents raw data of Table 6.1, crack length data in the upper standard deviation in the boundary region, 0-100°C ATC, UT.

SnPb, Air-Cooled, 10K, PI

UT7-U12A-SPA-A-10- / UT7-U2A-SPA-A-10- / UT7-U7A-SPA-A-10-PI											
Joint No.	% crack length P	% crack length S	% crack length P+S	Joint No.	% crack length P	% crack length S	% crack length P+S	Joint No	% crack length P	% crack length S	% crack length P+S
G10	37.0	8.8	45.8	G10	56.2	6.1	62.3	G10	30.4	4.7	35.0
G11	28.1	15.2	43.2	G11	45.0	3.3	48.3	G11	36.4	5.5	41.9
G12	43.1	0.3	43.4	G12	50.9	0.0	50.9	G12	42.6	0.0	42.6
G13	24.8	0.0	24.8	G13	23.9	0.0	23.9	G13	36.8	4.1	40.9
G7	46.0	0.0	46.0	G7	58.9	0.0	58.9	G7	36.1	0.0	36.1
G8	56.0	0.0	56.0	**G8**	**70.5**	**0.0**	**70.5**	G8	44.5	0.0	44.5
G9	42.9	8.3	51.1	G9	49.1	0.0	49.1	G9	35.0	0.0	35.0
H13	52.3	0.0	52.3	H13	36.2	5.4	41.5	H13	34.3	4.8	39.2
H7	50.5	0.0	50.5	H7	41.3	0.0	41.3	H7	43.1	13.1	56.3
J13	**55.6**	**10.3**	**65.9**	J13	18.3	10.9	29.1	J13	23.0	0.0	23.0
J7	36.3	5.2	41.5	J7	51.2	4.1	55.3	J7	10.7	0.0	10.7
K13	3.8	0.0	3.8	K13	42.6	8.4	51.0	K13	28.1	5.9	34.0
K7	19.6	7.6	27.2	K7	38.5	4.3	42.9	K7	39.5	9.5	49.0
L13	51.4	0.0	51.4	L13	37.6	0.0	37.6	L13	38.8	0.0	38.8
L7	27.0	0.0	27.0	L7	57.9	4.7	62.7	**L7**	**59.4**	**10.2**	**69.6**
M13	**74.4**	**9.6**	**84.0**	M13	51.5	0.0	51.5	**M13**	**59.2**	**5.0**	**64.2**
M7	57.3	3.4	60.8	M7	56.3	0.0	56.3	M7	46.8	0.0	46.8
N10	52.0	5.3	57.3	N10	41.4	8.6	50.1	N10	50.0	9.3	59.4
N11	46.8	0.2	47.0	N11	45.8	6.9	52.8	**N11**	**67.5**	**2.6**	**70.1**
N12	42.2	5.0	47.2	N12	49.0	7.6	56.6	N12	29.2	0.0	29.2
N13	54.1	8.0	62.1	N13	45.7	0.0	45.7	N13	15.0	0.0	15.0
N7	52.5	0.0	52.5	N7	42.2	7.9	50.1	N7	40.9	0.0	40.9
N8	45.3	0.0	45.3	N8	56.5	0.0	56.5	N8	30.4	0.0	30.4
N9	44.4	1.2	45.6	N9	54.4	6.3	60.8	N9	45.6	0.0	45.6

Note: **Bold** represents raw data of Table 6.1, crack length data in the upper standard deviation in the boundary region, 0-100°C ATC, UT.

SnPb, Air-Cooled, 15K, PI

UT6-U11A-SPA-A-15- / UT6-U1A-SPA-A-15- / UT6-U6A-SPA-A-15-PI											
Joint No.	% crack length P	% crack length S	% crack length P+S	Joint No.	% crack length P	% crack length S	% crack length P+S	Joint No	% crack length P	% crack length S	% crack length P+S
G10	58.0	6.6	64.7	G10	29.4	10.4	39.8	G10	30.6	13.7	44.3
G11	44.4	8.9	53.3	G11	20.6	6.4	26.9	G11	41.0	9.1	50.1
G12	72.4	3.3	75.8	G12	64.7	2.9	67.6	G12	31.1	3.4	34.5
G13	32.4	0.0	32.4	G13	33.9	4.3	38.3	G13	64.4	14.2	78.6
G7	53.3	0.0	53.3	**G7**	**100.0**	**0.0**	**100.0**	G7	25.8	2.9	28.7
G8	63.9	4.6	68.6	G8	54.0	0.0	54.0	G8	70.4	3.9	74.3
G9	40.2	0.0	40.2	G9	59.3	13.8	73.1	G9	70.4	4.8	75.2
H13	60.5	13.8	74.3	H13	36.2	11.0	47.2	H13	59.6	0.0	59.6
H7	48.4	13.1	61.5	H7	73.5	0.0	73.5	**H7**	**99.1**	**0.0**	**99.1**
J13	43.4	29.9	73.3	J13	11.5	28.1	39.7	J13	35.0	6.2	41.2
J7	59.4	22.0	81.5	J7	55.6	8.8	64.4	J7	48.4	14.6	63.0
K13	29.0	2.1	31.1	K13	55.2	22.0	77.1	K13	52.9	5.4	58.3
K7	47.6	16.1	63.6	K7	74.7	6.4	81.0	K7	57.3	6.9	64.2
L13	53.7	17.6	71.4	L13	51.0	13.6	64.5	L13	58.4	0.0	58.4
L7	67.6	15.1	82.7	L7	52.4	6.5	58.9	L7	47.0	10.2	57.2
M13	52.0	0.0	52.0	M13	52.2	7.1	59.3	M13	19.6	2.7	22.3
M7	64.3	18.1	82.5	M7	71.2	0.0	71.2	M7	75.9	5.0	81.0
N10	59.2	11.3	70.5	N10	53.5	9.0	62.4	N10	54.5	18.3	72.8
N11	87.9	5.1	93.0	N11	63.0	12.4	75.4	N11	46.2	27.4	73.6
N12	30.9	3.7	34.6	N12	57.5	7.0	64.5	**N12**	**69.4**	**18.5**	**87.9**
N13	48.3	10.4	58.7	N13	53.2	17.0	70.2	N13	80.3	0.0	80.3
N7	58.4	9.2	67.6	N7	62.2	0.0	62.2	N7	70.6	8.6	79.1
N8	68.4	10.2	78.6	N8	50.5	0.0	50.5	**N8**	**99.1**	**0.0**	**99.1**
N9	59.1	0.0	59.1	N9	64.3	8.0	72.3	N9	71.2	15.8	87.0

Note: **Bold** represents raw data of Table 6.1, crack length data in the upper standard deviation in the boundary region, 0-100°C ATC, UT.

SnPb, Air-Cooled, 16K, PI

UT8-U10A-SPA-A-16- / UT8-U15A-SPA-A-16- / UT8-U5A-SPA-A-16-PI											
Joint No.	% crack length P	% crack length S	% crack length P+S	Joint No.	% crack length P	% crack length S	% crack length P+S	Joint No	% crack length P	% crack length S	% crack length P+S
G10	41.2	10.7	51.8	G10	56.7	5.0	61.7	G10	46.9	20.9	67.8
G11	59.4	7.2	66.6	**G11**	**99.0**	**0.0**	**99.0**	G11	19.5	8.9	28.4
G12	66.5	10.7	77.1	G12	78.8	15.3	94.0	**G12**	**100.0**	**0.0**	**100.0**
G13	79.9	3.3	83.2	**G13**	**99.3**	**0.0**	**99.3**	G13	64.5	14.4	78.9
G7	50.4	0.0	50.4	G7	65.6	5.5	71.1	G7	62.8	0.0	62.8
G8	83.4	0.0	83.4	**G8**	**99.3**	**0.0**	**99.3**	G8	79.1	0.0	79.1
G9	37.7	0.0	37.7	G9	98.9	0.0	98.9	G9	72.0	12.7	84.8
H13	60.6	6.0	66.6	H13	74.7	3.1	77.8	H13	61.9	3.9	65.9
H7	47.9	0.2	48.0	H7	47.4	5.4	52.8	H7	73.0	10.0	83.1
J13	60.3	7.9	68.2	J13	98.9	0.0	98.9	J13	51.1	33.3	84.4
J7	57.9	0.0	57.9	J7	98.8	0.0	98.8	J7	71.2	6.3	77.5
K13	68.9	14.3	83.2	K13	14.9	73.3	88.2	K13	61.7	6.6	68.3
K7	67.2	0.0	67.2	K7	53.7	11.9	65.5	K7	48.9	0.0	48.9
L13	37.9	17.2	55.1	**L13**	**99.1**	**0.0**	**99.1**	L13	98.9	0.0	98.9
L7	55.8	3.1	58.9	L7	43.9	13.5	57.4	L7	70.3	12.9	83.2
M13	68.4	4.5	72.8	M13	98.9	0.0	98.9	M13	67.2	0.0	67.2
M7	62.7	0.0	62.7	M7	98.9	0.0	98.9	M7	70.9	0.0	70.9
N10	74.7	12.6	87.3	N10	55.9	7.1	63.0	N10	48.1	0.0	48.1
N11	**99.0**	**0.0**	**99.0**	N11	57.7	10.6	68.3	N11	47.9	11.5	59.4
N12	68.5	4.3	72.8	**N12**	**99.1**	**0.0**	**99.1**	N12	73.2	11.5	84.7
N13	28.4	0.0	28.4	N13	63.8	9.3	73.2	N13	98.7	0.0	98.7
N7	69.9	8.3	78.2	N7	54.1	0.0	54.1	N7	46.3	0.0	46.3
N8	61.5	19.5	80.9	N8	67.5	5.5	73.0	**N8**	**100.0**	**0.0**	**100.0**
N9	55.5	17.2	72.7	N9	54.1	0.0	54.1	**N9**	**99.0**	**0.0**	**99.0**

Note: **Bold** represents raw data of Table 6.1, crack length data in the upper standard deviation in the boundary region, 0-100°C ATC, UT.

SnPb, Quenched, 2K, PI

UT10-U14A-SPA-Q-2- / UT10-U4A-SPA-Q-2- / UT10-U9A-SPA-Q-2-PI											
Joint No.	% crack length P	% crack length S	% crack length P+S	Joint No.	% crack length P	% crack length S	% crack length P+S	Joint No	% crack length P	% crack length S	% crack length P+S
G10	8.1	0.0	8.1	G10	5.8	0.0	5.8	G10	9.8	0.0	9.8
G11	7.1	0.0	7.1	G11	8.9	0.0	8.9	G11	2.9	0.0	2.9
G12	11.9	0.0	11.9	G12	3.2	0.0	3.2	G12	9.1	0.0	9.1
G13	7.4	0.0	7.4	G13	4.3	0.0	4.3	G13	10.2	0.0	10.2
G7	8.8	0.0	8.8	G7	1.4	0.0	1.4	G7	4.6	0.0	4.6
G8	5.5	0.0	5.5	G8	7.2	0.0	7.2	G8	10.2	0.0	10.2
G9	3.1	0.0	3.1	G9	3.9	0.0	3.9	G9	4.3	0.0	4.3
H7	3.8	0.0	3.8	H13	3.8	0.0	3.8	H13	11.5	0.0	11.5
J7	4.5	0.0	4.5	H7	0.0	0.0	0.0	H7	3.4	0.0	3.4
K13	5.7	0.0	5.7	J13	0.0	0.0	0.0	J13	0.0	0.0	0.0
K7	0.0	0.0	0.0	J7	3.9	0.0	3.9	J7	8.2	0.0	8.2
L13	8.1	0.0	8.1	K13	0.0	0.0	0.0	K13	0.0	2.1	2.1
L7	0.0	0.0	0.0	K7	7.2	0.0	7.2	K7	2.2	0.0	2.2
M13	10.2	0.0	10.2	L13	0.0	5.7	5.7	L13	11.0	0.0	11.0
M7	0.5	0.0	0.5	L7	5.1	0.0	5.1	L7	5.2	0.0	5.2
N10	0.0	0.0	0.0	M13	1.0	0.0	1.0	M13	0.0	0.0	0.0
N11	0.0	0.0	0.0	M7	0.0	0.0	0.0	M7	0.0	0.0	0.0
N12	0.0	0.0	0.0	N10	4.1	3.3	7.4	N10	0.0	0.0	0.0
N13	3.6	0.0	3.6	N11	5.9	0.0	5.9	N11	2.2	2.9	5.2
N7	0.7	0.0	0.7	N12	8.6	0.0	8.6	N12	5.5	0.0	5.5
N8	0.0	0.0	0.0	N13	0.0	0.0	0.0	N13	11.2	0.0	11.2
N9	0.0	6.7	6.7	N7	7.4	0.0	7.4	N7	0.0	0.0	0.0
				N8	8.9	0.0	8.9	N8	3.8	0.0	3.8
				N9	3.1	0.0	3.1	N9	4.7	3.5	8.1

Note: **Bold** represents raw data of Table 6.1, crack length data in the upper standard deviation in the boundary region, 0-100°C ATC, UT.

SnPb, Quenched, 4K, PI

UT12-U14A-SPA-Q-4- / UT12-U4A-SPA-Q-4- / UT12-U9A-SPA-Q-4-PI											
Joint No.	% crack length P	% crack length S	% crack length P+S	Joint No.	% crack length P	% crack length S	% crack length P+S	Joint No	% crack length P	% crack length S	% crack length P+S
G10	11.4	0.0	11.4	G10	5.5	0.0	5.5	G10	18.7	2.2	20.9
G11	25.3	4.7	29.9	G11	18.0	0.0	18.0	G11	18.2	0.0	18.2
G12	18.3	0.0	18.3	G12	22.8	3.8	26.5	G12	16.3	0.0	16.3
G13	26.5	0.0	26.5	G13	12.5	0.0	12.5	G13	26.8	0.0	26.8
G7	14.9	0.0	14.9	G9	18.5	0.0	18.5	G7	17.1	0.0	17.1
G8	12.1	0.0	12.1	H13	20.8	2.2	23.0	G8	17.8	0.0	17.8
G9	12.8	0.0	12.8	J13	9.0	0.0	9.0	G9	9.5	0.0	9.5
H13	25.8	0.0	25.8	K13	0.0	3.3	3.3	H13	7.3	4.7	11.9
H7	14.2	0.0	14.2	L13	14.6	0.0	14.6	H7	15.9	0.0	15.9
J13	15.9	4.0	19.9	M13	21.6	0.0	21.6	J13	5.5	2.6	8.1
J7	9.7	0.0	9.7	N10	12.8	2.9	15.8	J7	13.7	0.0	13.7
K13	0.0	4.0	4.0	N11	24.3	8.7	33.1	K13	0.0	0.0	0.0
K7	9.5	0.0	9.5	N12	13.2	0.0	13.2	K7	7.3	0.0	7.3
L13	11.4	3.3	14.7	N13	20.0	0.0	20.0	L13	25.9	0.0	25.9
L7	10.2	0.0	10.2	N7	17.0	0.0	17.0	L7	14.9	0.0	14.9
M13	15.0	1.2	16.3	N9	15.4	0.0	15.4	M13	18.5	2.2	20.8
M7	23.2	2.6	25.8					M7	13.5	0.0	13.5
N10	0.0	0.0	0.0					N10	21.1	0.0	21.1
N11	12.5	5.5	18.0					N11	9.2	0.0	9.2
N12	15.6	0.0	15.6					N12	25.4	4.7	30.1
N13	23.0	0.0	23.0					N13	31.3	4.0	35.3
N7	0.0	0.0	0.0					N7	35.6	4.7	40.3
N8	8.8	0.0	8.8					N8	23.4	0.0	23.4
N9	4.3	0.0	4.3					N9	22.0	0.0	22.0

SnPb, Quenched, 6K, PI

UT11-U13A-SPA-Q-6- / UT11-U3A-SPA-Q-6- / UT11-U8A-SPA-Q-6-PI											
Joint No.	% crack length P	% crack length S	% crack length P+S	Joint No.	% crack length P	% crack length S	% crack length P+S	Joint No	% crack length P	% crack length S	% crack length P+S
G10	28.6	8.8	37.5	G10	32.4	5.5	37.9	G10	2.9	0.0	2.9
G11	11.8	7.1	18.9	G11	26.3	0.0	26.3	G11	27.5	3.8	31.3
G12	26.0	0.0	26.0	G12	35.4	0.0	35.4	G12	17.2	0.0	17.2
G13	12.7	3.3	16.0	G13	27.1	0.0	27.1	G13	14.6	0.0	14.6
G7	33.5	0.0	33.5	G7	26.8	0.0	26.8	G7	27.7	3.4	31.1
G8	44.9	0.0	44.9	G8	23.0	0.0	23.0	G8	36.9	0.0	36.9
G9	16.3	0.0	16.3	G9	16.7	0.0	16.7	G9	19.4	0.0	19.4
H13	26.2	1.2	27.4	H13	24.8	0.0	24.8	H13	24.4	2.2	26.6
H7	19.1	0.0	19.1	H7	28.3	0.0	28.3	H7	17.1	0.0	17.1
J13	10.6	7.8	18.4	J13	28.6	7.6	36.1	J13	18.0	4.1	22.2
J7	26.5	10.6	37.1	J7	31.3	0.0	31.3	J7	25.3	5.7	30.9
K13	0.0	13.9	13.9	K13	21.2	0.0	21.2	K13	10.7	5.2	15.8
K7	8.8	15.1	23.9	K7	23.2	0.0	23.2	K7	15.1	0.0	15.1
L13	8.0	0.0	8.0	L13	17.0	4.8	21.9	L13	27.8	3.1	30.9
L7	4.9	9.0	13.9	L7	18.2	0.0	18.2	L7	37.8	2.1	39.9
M13	25.6	4.8	30.4	M13	0.0	0.0	0.0	M13	18.7	0.0	18.7
M7	23.1	0.0	23.1	M7	26.3	0.0	26.3	M7	6.9	0.0	6.9
N10	18.4	0.0	18.4	N10	34.2	9.3	43.5	N10	16.2	3.3	19.5
N11	21.7	9.9	31.6	N11	30.5	5.0	35.4	N11	19.3	0.0	19.3
N12	35.8	0.0	35.8	N12	23.2	6.7	30.0	N12	30.8	4.1	34.9
N13	19.5	0.0	19.5	N13	14.8	0.0	14.8	N13	44.8	0.0	44.8
N7	20.6	0.0	20.6	N7	26.3	6.2	32.5	N7	25.8	7.4	33.2
N8	35.6	0.0	35.6	N8	26.0	0.0	26.0	N8	38.3	1.9	40.2
N9	23.6	0.0	23.6	N9	0.0	2.2	2.2	N9	43.3	4.6	47.9

SnPb, Quenched, 8K, PI

UT10-U12A-SPA-Q-8- / UT10-U2A-SPA-Q-8- / UT10-U7A-SPA-Q-8-PI											
Joint No.	% crack length P	% crack length S	% crack length P+S	Joint No.	% crack length P	% crack length S	% crack length P+S	Joint No	% crack length P	% crack length S	% crack length P+S
G10	33.0	0.0	33.0	G10	26.3	2.4	28.7	G10	22.2	0.0	22.2
G11	49.0	0.0	49.0	G11	21.6	0.0	21.6	G11	39.1	0.0	39.1
G12	44.4	0.0	44.4	G12	10.6	0.0	10.6	G12	51.7	1.9	53.6
G13	24.2	3.3	27.5	G13	22.0	0.0	22.0	G13	14.6	0.0	14.6
G7	36.5	4.3	40.8	G7	39.9	0.0	39.9	G7	32.4	0.0	32.4
G8	36.3	0.0	36.3	G8	37.0	0.0	37.0	G8	28.9	0.0	28.9
G9	25.1	0.0	25.1	G9	27.3	0.0	27.3	G9	34.3	2.6	36.9
H13	30.4	7.6	38.0	H13	42.7	5.1	47.9	H13	44.3	2.1	46.3
H7	52.1	10.7	62.8	H7	36.7	0.0	36.7	H7	52.2	2.4	54.6
J13	26.0	4.6	30.6	J13	28.8	0.0	28.8	J13	22.6	5.0	27.6
J7	31.0	0.0	31.0	J7	34.9	0.0	34.9	J7	43.9	0.0	43.9
K13	24.1	3.4	27.5	K13	35.2	8.8	44.0	K13	27.4	9.5	36.9
K7	13.4	0.0	13.4	K7	45.3	2.7	48.1	K7	36.5	0.0	36.5
L13	45.5	4.7	50.2	L13	38.9	0.0	38.9	L13	15.0	19.3	34.3
L7	18.7	8.3	27.0	L7	13.0	17.2	30.2	L7	29.8	0.0	29.8
M13	26.8	6.2	33.0	M13	39.0	4.2	43.3	M13	39.3	3.3	42.5
M7	21.1	0.0	21.1	M7	43.7	3.2	46.9	M7	31.4	0.0	31.4
N10	27.0	4.1	31.1	N10	25.7	10.6	36.4	N10	43.0	15.5	58.6
N11	30.3	0.0	30.3	N11	61.9	4.3	66.2	N11	36.9	0.0	36.9
N12	55.7	0.0	55.7	N12	46.8	1.2	48.0	N12	42.2	0.0	42.2
N13	38.0	4.8	42.8	N13	42.6	3.9	46.5	N13	43.2	5.7	48.9
N7	41.1	0.0	41.1	N7	44.3	0.0	44.3	N7	36.0	0.0	36.0
N8	37.3	8.1	45.4	N8	42.4	0.0	42.4	N8	46.5	0.0	46.5
N9	27.7	10.0	37.7	N9	44.6	0.0	44.6	N9	34.8	0.0	34.8

SnPb, Quenched, 10K, PI

UT12-U12A-SPA-Q-10- / UT12-U2A-SPA-Q-10- / UT12-U7A-SPA-Q-10-PI											
Joint No.	% crack length P	% crack length S	% crack length P+S	Joint No.	% crack length P	% crack length S	% crack length P+S	Joint No	% crack length P	% crack length S	% crack length P+S
G10	29.0	5.0	34.0	G10	40.3	13.9	54.2	G10	27.5	1.2	28.7
G11	36.1	15.3	51.4	G11	55.2	7.5	62.7	G11	9.7	2.9	12.6
G12	59.5	5.1	64.6	G12	55.5	8.2	63.7	G12	38.4	0.0	38.4
G13	46.2	0.0	46.2	G13	43.2	2.2	45.4	G13	39.8	0.0	39.8
G7	60.5	3.5	64.1	G7	55.0	0.0	55.0	G7	38.9	0.0	38.9
G8	64.7	7.1	71.9	G8	51.2	7.1	58.3	G8	39.4	0.0	39.4
G9	43.7	16.1	59.8	G9	47.6	7.3	54.9	G9	56.8	0.0	56.8
H13	60.6	3.4	64.0	H13	55.8	5.3	61.1	H13	57.4	0.0	57.4
H7	42.8	0.0	42.8	H7	34.8	5.6	40.4	H7	55.2	0.0	55.2
J13	35.1	0.2	35.3	J13	65.0	6.2	71.2	J13	41.5	3.3	44.8
J7	51.7	0.0	51.7	J7	49.7	12.8	62.5	J7	44.5	0.0	44.5
K13	39.5	0.0	39.5	K13	32.2	4.5	36.6	K13	41.9	5.2	47.1
K7	41.1	0.0	41.1	K7	29.0	4.6	33.7	K7	34.4	0.0	34.4
L13	34.0	1.9	35.9	L13	27.5	5.1	32.6	L13	53.6	9.2	62.8
L7	44.4	3.7	48.2	L7	44.3	0.0	44.3	L7	56.6	0.0	56.6
M13	36.5	3.9	40.4	M13	65.9	3.7	69.5	M13	35.1	2.4	37.5
M7	45.1	0.0	45.1	M7	55.6	0.0	55.6	M7	57.2	0.0	57.2
N10	37.7	0.0	37.7	N10	51.7	9.6	61.3	N10	57.9	9.0	66.9
N11	54.2	0.0	54.2	N11	47.7	3.1	50.9	N11	54.3	3.1	57.4
N12	54.7	0.0	54.7	N12	54.9	2.4	57.2	N12	58.1	3.5	61.6
N13	45.1	2.3	47.4	N13	58.7	7.8	66.4	N13	59.5	8.8	68.3
N7	50.1	0.0	50.1	N7	34.1	3.5	37.6	N7	51.9	0.0	51.9
N8	41.6	0.0	41.6	N8	38.8	3.3	42.1	N8	70.1	10.2	80.3
N9	34.0	23.5	57.5	N9	32.3	3.1	35.4	N9	43.8	0.0	43.8

SnPb, Quenched, 12K, PI

UT12-U11A-SPA-Q-14- / UT12-U1A-SPA-Q-14- / UT12-U6A-SPA-Q-14-PI											
Joint No.	% crack length P	% crack length S	% crack length P+S	Joint No.	% crack length P	% crack length S	% crack length P+S	Joint No	% crack length P	% crack length S	% crack length P+S
G10	63.0	1.4	64.5	G10	57.6	4.6	62.2	G10	67.1	9.0	76.1
G11	59.9	4.1	64.0	G11	42.3	12.7	55.0	G11	77.1	2.2	79.4
G12	54.9	0.0	54.9	G12	64.5	0.0	64.5	G12	47.6	0.0	47.6
G13	48.1	0.0	48.1	G13	63.6	11.0	74.6	G13	66.1	0.0	66.1
G7	55.1	0.0	55.1	G7	55.1	5.8	61.0	G7	68.7	2.4	71.1
G8	44.1	0.0	44.1	G8	71.2	0.0	71.2	G8	36.8	0.0	36.8
G9	64.3	0.0	64.3	G9	19.4	6.2	25.7	G9	49.9	0.0	49.9
H13	60.5	9.7	70.1	H13	59.5	10.1	69.7	H13	55.7	3.8	59.5
H7	61.1	11.7	72.8	H7	75.3	7.3	82.6	H7	59.2	4.5	63.7
J13	57.7	3.9	61.6	J13	40.1	16.9	57.0	J13	62.3	0.0	62.3
J7	65.0	0.0	65.0	J7	60.5	13.9	74.3	J7	73.0	0.0	73.0
K13	52.7	4.8	57.5	K13	35.1	7.9	43.0	K13	54.4	3.1	57.5
K7	53.6	0.0	53.6	K7	66.8	6.0	72.8	K7	52.6	0.0	52.6
L13	70.3	0.0	70.3	L13	78.3	1.7	80.0	L13	35.9	0.0	35.9
L7	66.7	0.9	67.6	L7	99.0	0.0	99.0	L7	62.7	7.7	70.4
M13	60.8	0.0	60.8	M13	67.3	17.1	84.4	M13	57.3	13.5	70.8
M7	58.4	9.0	67.4	M7	50.1	0.0	50.1	M7	69.2	0.0	69.2
N10	70.6	8.0	78.6	N10	38.1	5.2	43.3	N10	26.9	15.2	42.1
N11	66.7	11.2	77.9	N11	54.2	20.0	74.2	N11	44.0	11.9	55.9
N12	70.1	3.7	73.8	N12	54.2	0.0	54.2	N12	56.8	7.6	64.4
N13	77.2	2.0	79.2	N13	42.9	9.3	52.2	N13	41.6	0.0	41.6
N7	70.4	20.5	91.0	N7	74.5	4.0	78.5	N7	44.7	4.0	48.6
N8	74.9	2.7	77.5	N8	100.0	0.0	100.0	N8	39.0	0.0	39.0
N9	99.1	0.0	99.1	N9	67.2	3.1	70.3	N9	50.3	4.1	54.5

SnPb, Quenched, 16K, PI

UT13-U10A-SPA-Q-16- / UT13-U15A-SPA-Q-16- / UT13-U5A-SPA-Q-16-PI											
Joint No.	% crack length P	% crack length S	% crack length P+S	Joint No.	% crack length P	% crack length S	% crack length P+S	Joint No	% crack length P	% crack length S	% crack length P+S
G10	35.4	6.4	41.9	G10	47.9	12.9	60.8	G10	62.1	0.0	62.1
G11	43.0	6.2	49.2	G11	62.9	12.7	75.6	G11	55.6	0.0	55.6
G12	34.8	14.6	49.4	G12	80.3	9.1	89.4	G12	67.1	0.0	67.1
G13	48.9	3.9	52.8	G13	47.6	19.3	66.9	G13	59.4	1.7	61.1
G7	51.0	0.0	51.0	G7	58.4	0.0	58.4	G7	50.0	3.9	53.9
G8	60.4	2.9	63.3	G8	78.1	10.3	88.4	G8	76.4	0.0	76.4
G9	37.5	7.5	45.0	G9	58.8	22.1	80.9	G9	72.1	12.0	84.1
H13	63.9	8.3	72.3	H13	98.8	0.0	98.8	H13	47.7	0.0	47.7
H7	74.0	2.3	76.3	H7	72.0	0.0	72.0	H7	64.7	9.8	74.5
J13	41.2	10.1	51.4	J13	70.3	6.5	76.8	J13	62.5	6.3	68.8
J7	64.5	7.8	72.3	J7	17.9	0.0	17.9	J7	61.3	7.2	68.5
K13	54.7	6.7	61.4	K13	74.2	13.2	87.5	K13	98.5	0.0	98.5
K7	56.3	4.5	60.8	K7	57.3	20.4	77.6	K7	48.9	0.0	48.9
L13	58.2	0.0	58.2	L13	99.0	0.0	99.0	L13	98.9	0.0	98.9
L7	53.2	19.3	72.5	L7	58.5	11.6	70.1	L7	77.9	0.0	77.9
M13	77.8	4.8	82.6	M13	74.8	9.3	84.1	M13	100.0	0.0	100.0
M7	71.6	8.2	79.7	M7	70.6	0.5	71.1	M7	98.8	0.0	98.8
N10	66.0	7.6	73.7	N10	69.2	3.2	72.4	N10	37.2	0.0	37.2
N11	99.1	0.0	99.1	N11	98.9	0.0	98.9	N11	58.6	0.0	58.6
N12	99.0	0.0	99.0	N12	98.9	0.0	98.9	N12	72.6	0.0	72.6
N13	98.9	0.0	98.9	N13	99.3	0.0	99.3	N13	50.1	14.5	64.6
N7	65.5	11.1	76.6	N7	99.2	0.0	99.2	N7	66.1	0.0	66.1
N8	48.8	2.4	51.3	N8	99.0	0.0	99.0	N8	46.2	0.0	46.2
N9	38.4	22.4	60.8	N9	98.9	0.0	98.9	N9	55.9	5.1	61.1

Table G.2. % Crack length data for aged, air-cooled, and quenched SnAg joints in the boundary region at the package interface (nominal joint diameter=560 μm)

SnAg, Aged, 3K, PI

UT14-U14A-SA-AG-3- / UT14-U4A-SA-AG-3- / UT14-U9A-SA-AG-3-PI											
Joint No.	% crack length P	% crack length S	% crack length P+S	Joint No.	% crack length P	% crack length S	% crack length P+S	Joint No	% crack length P	% crack length S	% crack length P+S
G10	0.0	0.0	0.0	G10	6.9	0.0	6.9	G10	0.0	3.5	3.5
G11	0.0	0.0	0.0	G11	0.0	0.0	0.0	G11	0.9	0.0	0.9
G12	0.0	0.0	0.0	G12	0.0	0.0	0.0	**G12**	**7.5**	**0.7**	**8.2**
G13	**17.9**	**0.0**	**17.9**	**G13**	**14.9**	**0.0**	**14.9**	G13	0.0	0.0	0.0
G7	5.0	0.0	5.0	G7	1.6	0.0	1.6	G7	0.0	0.0	0.0
G8	0.0	0.0	0.0	G8	0.0	0.0	0.0	G8	0.0	0.0	0.0
G9	0.0	0.0	0.0	**G9**	**9.1**	**0.0**	**9.1**	G9	2.5	0.0	2.5
H13	0.0	0.0	0.0	H13	2.7	0.0	2.7	H13	0.0	0.0	0.0
H7	0.0	2.4	2.4	H7	7.4	0.0	7.4	H7	0.0	0.0	0.0
J13	0.0	0.0	0.0	J13	0.0	0.0	0.0	**J13**	**10.3**	**0.0**	**10.3**
J7	0.0	0.0	0.0	J7	0.0	0.0	0.0	J7	0.0	0.0	0.0
K13	0.0	0.0	0.0	K13	6.7	0.0	6.7	K13	2.6	0.0	2.6
K7	0.0	0.0	0.0	K7	3.1	0.0	3.1	K7	0.0	0.0	0.0
L13	**9.0**	**0.0**	**9.0**	L13	2.1	0.0	2.1	L13	0.0	0.0	0.0
L7	0.0	0.0	0.0	L7	0.0	0.0	0.0	L7	5.4	0.0	5.4
M13	4.5	0.0	4.5	M13	0.0	0.0	0.0	**M13**	**11.0**	**0.0**	**11.0**
M7	0.0	0.0	0.0	M7	0.0	0.0	0.0	**M7**	**10.0**	**0.0**	**10.0**
N10	**15.1**	**3.3**	**18.4**	N10	0.0	0.0	0.0	N10	1.4	0.0	1.4
N11	0.0	5.3	5.3	N11	0.0	0.0	0.0	N11	0.0	0.0	0.0
N12	1.4	0.0	1.4	N12	0.0	0.0	0.0	N12	0.0	0.0	0.0
N13	**16.2**	**0.0**	**16.2**	**N13**	**11.9**	**0.0**	**11.9**	N13	2.1	0.0	2.1
N7	0.0	0.0	0.0	**N7**	**9.4**	**0.0**	**9.4**	N7	0.0	0.0	0.0
N8	0.0	0.0	0.0	N8	0.0	0.0	0.0	N8	0.0	0.0	0.0
N9	0.0	4.3	4.3	N9	0.0	2.2	2.2	N9	0.0	0.0	0.0

Note: **Bold** represents raw data of Table 6.2, crack length data in the upper standard deviation in the boundary region, 0-100°C ATC, UT.

SnAg, Aged, 6K, PI

UT16-U14A-SA-AG-6- / UT16-U4A-SA-AG-6- / UT16-U9A-SA-AG-6-PI											
Joint No.	% crack length P	% crack length S	% crack length P+S	Joint No.	% crack length P	% crack length S	% crack length P+S	Joint No	% crack length P	% crack length S	% crack length P+S
G10	0.0	0.0	0.0	G10	0.0	0.0	0.0	G10	1.9	0.0	1.9
G11	0.0	0.0	0.0	G11	1.1	0.0	1.1	G11	0.0	0.0	0.0
G12	4.1	0.0	4.1	G12	0.0	0.0	0.0	G12	4.5	0.0	4.5
G13	0.0	0.0	0.0	**G13**	**22.8**	**0.0**	**22.8**	G13	0.0	1.2	1.2
G7	**9.1**	**5.2**	**14.3**	G7	3.2	0.0	3.2	G7	0.0	0.0	0.0
G8	**19.7**	**3.0**	**22.7**	G8	0.0	0.0	0.0	G8	0.0	0.0	0.0
G9	0.0	0.0	0.0	G9	3.2	0.0	3.2	**G9**	**14.9**	**5.7**	**20.6**
H13	**22.6**	**1.9**	**24.5**	**H13**	**18.6**	**0.0**	**18.6**	H13	3.4	3.4	6.9
H7	0.0	0.0	0.0	H7	0.0	0.0	0.0	H7	0.0	0.0	0.0
J13	**9.4**	**8.6**	**18.0**	J13	0.9	0.0	0.9	J13	4.3	7.5	11.8
J7	0.0	0.0	0.0	J7	5.3	0.0	5.3	J7	0.0	0.0	0.0
K13	12.1	0.0	12.1	**K13**	**9.8**	**6.8**	**16.6**	K13	2.1	3.8	5.8
K7	0.0	0.0	0.0	K7	1.4	0.0	1.4	K7	0.0	0.0	0.0
L13	12.2	0.0	12.2	L13	0.0	0.0	0.0	L13	6.0	2.1	8.1
L7	0.0	0.0	0.0	L7	0.0	0.0	0.0	L7	0.0	4.5	4.5
M13	6.7	0.0	6.7	M13	0.0	0.0	0.0	**M13**	**21.3**	**0.0**	**21.3**
M7	**13.5**	**0.0**	**13.5**	M7	10.3	0.0	10.3	M7	0.0	0.0	0.0
N10	11.9	0.0	11.9	N10	10.5	0.0	10.5	N10	0.0	2.7	2.7
N11	**19.3**	**0.0**	**19.3**	N11	5.8	0.0	5.8	N11	0.0	0.0	0.0
N12	1.7	0.0	1.7	N12	4.1	0.0	4.1	N12	10.6	0.0	10.6
N13	**17.1**	**0.0**	**17.1**	N13	12.2	0.0	12.2	**N13**	**14.2**	**0.0**	**14.2**
N7	0.0	0.0	0.0	**N7**	**17.9**	**0.0**	**17.9**	N7	4.8	0.0	4.8
N8	0.0	0.0	0.0	N8	0.0	0.0	0.0	N8	0.0	0.0	0.0
N9	0.0	0.0	0.0	N9	0.0	0.0	0.0	N9	0.0	0.0	0.0

Note: **Bold** represents raw data of Table 6.2, crack length data in the upper standard deviation in the boundary region, 0-100°C ATC, UT.

SnAg, Aged, 9K, PI

UT14-U12A-SA-AG-9- / UT14-U2A-SA-AG-9- / UT14-U7A-SA-AG-9-PI											
Joint No.	% crack length P	% crack length S	% crack length P+S	Joint No.	% crack length P	% crack length S	% crack length P+S	Joint No	% crack length P	% crack length S	% crack length P+S
G10	3.5	3.0	6.4	**G10**	**28.3**	**3.1**	**31.4**	G10	14.0	0.0	14.0
G11	**27.4**	**0.0**	**27.4**	G11	3.8	0.0	3.8	G11	4.9	0.0	4.9
G12	**21.8**	**5.4**	**27.2**	G12	18.7	7.0	25.7	G12	20.6	0.0	20.6
G13	**45.5**	**0.0**	**45.5**	G13	16.3	0.0	16.3	**G13**	**42.5**	**4.5**	**47.1**
G7	**38.7**	**0.0**	**38.7**	**G7**	**30.6**	**0.0**	**30.6**	G7	8.2	0.0	8.2
G8	12.7	0.0	12.7	**G8**	**39.5**	**0.0**	**39.5**	G8	16.7	0.0	16.7
G9	2.4	0.0	2.4	G9	15.1	0.0	15.1	G9	16.9	0.0	16.9
H13	**33.1**	**2.8**	**35.9**	H13	0.0	0.0	0.0	H13	19.3	0.0	19.3
H7	0.0	0.0	0.0	H7	5.0	0.0	5.0	H7	5.4	0.0	5.4
J13	4.7	0.0	4.7	J7	23.5	0.0	23.5	**J13**	**26.8**	**0.0**	**26.8**
J7	0.0	0.0	0.0	K13	3.1	0.0	3.1	J7	0.0	0.0	0.0
K13	0.0	0.0	0.0	K7	0.0	0.0	0.0	K13	8.9	0.0	8.9
K7	12.9	0.0	12.9	L13	22.3	0.0	22.3	K7	0.0	0.0	0.0
L13	11.3	0.0	11.3	L7	6.7	0.0	6.7	L13	0.0	0.0	0.0
L7	0.0	13.6	13.6	M7	3.9	0.0	3.9	**L7**	**28.4**	**0.0**	**28.4**
M13	6.1	0.0	6.1	N10	0.0	20.2	20.2	**M13**	**27.6**	**0.0**	**27.6**
M7	3.8	3.1	7.0	**N11**	**30.2**	**0.0**	**30.2**	M7	8.5	0.0	8.5
N10	21.3	0.0	21.3	N7	5.8	0.0	5.8	**N10**	**33.0**	**0.0**	**33.0**
N11	0.0	11.5	11.5	N8	5.0	0.0	5.0	N11	8.2	0.0	8.2
N12	0.0	0.0	0.0	N9	4.5	0.0	4.5	N12	11.5	0.0	11.5
N13	6.1	0.0	6.1					**N13**	**27.4**	**0.0**	**27.4**
N7	0.0	0.0	0.0					N7	9.2	0.0	9.2
N8	17.7	0.0	17.7					N8	12.5	0.0	12.5
N9	0.0	0.0	0.0					N9	3.3	0.0	3.3

Note: **Bold** represents raw data of Table 6.2, crack length data in the upper standard deviation in the boundary region, 0-100°C ATC, UT.

SnAg, Aged, 12K, PI

UT16-U12A-SA-AG-12- / UT16-U2A-SA-AG-12- / UT16-U7A-SA-AG-12-PI											
Joint No.	% crack length P	% crack length S	% crack length P+S	Joint No.	% crack length P	% crack length S	% crack length P+S	Joint No	% crack length P	% crack length S	% crack length P+S
G10	**24.5**	**10.0**	**34.4**	G10	7.2	0.0	7.2	G10	0.0	0.0	0.0
G11	0.0	3.6	3.6	**G11**	**42.0**	**15.0**	**57.0**	G11	24.8	0.0	24.8
G12	0.0	0.0	0.0	**G13**	**32.0**	**5.2**	**37.3**	**G12**	**53.9**	**7.9**	**61.8**
G13	20.1	6.4	26.5	G7	23.3	4.4	27.7	G13	23.4	0.0	23.4
G7	0.0	0.0	0.0	**G8**	**30.2**	**2.7**	**32.9**	G7	10.5	0.0	10.5
G8	24.8	0.0	24.8	G9	8.5	0.0	8.5	G8	0.0	0.0	0.0
G9	**39.6**	**5.5**	**45.1**	H13	6.3	0.0	6.3	**G9**	**33.1**	**0.0**	**33.1**
H13	0.0	0.0	0.0	H7	14.6	0.0	14.6	H13	3.1	0.0	3.1
H7	11.4	0.0	11.4	J13	14.0	0.0	14.0	H7	0.0	0.0	0.0
J13	0.0	1.5	1.5	J7	0.0	0.0	0.0	J13	18.3	0.0	18.3
J7	0.0	0.0	0.0	K13	0.0	0.0	0.0	J7	0.0	12.2	12.2
K13	0.0	8.3	8.3	K7	1.6	8.9	10.5	K13	5.2	0.0	5.2
K7	0.0	3.4	3.4	L13	9.8	0.0	9.8	K7	0.0	0.0	0.0
L13	7.7	9.8	17.6	L7	0.0	0.0	0.0	**L13**	**37.0**	**2.1**	**39.1**
L7	6.9	0.0	6.9	M13	19.7	3.5	23.2	L7	0.0	0.0	0.0
M13	26.9	0.0	26.9	N10	22.8	4.7	27.5	M13	3.8	0.0	3.8
M7	9.6	0.0	9.6	N12	14.4	0.0	14.4	M7	0.0	0.0	0.0
N10	0.0	0.0	0.0	**N13**	**44.6**	**0.0**	**44.6**	N10	7.7	0.0	7.7
N11	0.0	12.0	12.0	N7	19.8	0.0	19.8	N11	4.1	0.0	4.1
N12	**38.4**	**3.9**	**42.4**	**N8**	**42.5**	**9.7**	**52.1**	N12	5.2	0.0	5.2
N13	2.2	0.0	2.2	N9	0.0	16.7	16.7	N13	15.8	0.0	15.8
N7	0.0	0.0	0.0					N7	8.1	0.0	8.1
N8	0.0	0.0	0.0					N8	18.3	0.0	18.3
N9	22.6	0.0	22.6					N9	20.5	6.7	27.2

Note: **Bold** represents raw data of Table 6.2, crack length data in the upper standard deviation in the boundary region, 0-100°C ATC, UT.

SnAg, Aged, 15K, PI

UT14-U11A-SA-AG-15- / UT14-U1A-SA-AG-15- / UT14-U6A-SA-AG-15-PI											
Joint No.	% crack length P	% crack length S	% crack length P+S	Joint No.	% crack length P	% crack length S	% crack length P+S	Joint No	% crack length P	% crack length S	% crack length P+S
G10	3.7	0.0	3.7	**G10**	**35.9**	**0.0**	**35.9**	G10	8.5	1.2	9.7
G11	**44.6**	**0.0**	**44.6**	G11	0.0	21.8	21.8	G11	14.2	0.0	14.2
G12	**36.4**	**0.0**	**36.4**	G12	15.8	0.0	15.8	G12	17.1	0.0	17.1
G13	13.8	0.0	13.8	**G13**	**44.1**	**0.0**	**44.1**	**G13**	**44.3**	**6.9**	**51.2**
G7	10.3	0.0	10.3	G7	15.3	0.0	15.3	G7	14.9	0.0	14.9
G8	6.1	0.0	6.1	G8	0.0	11.7	11.7	G8	0.0	0.0	0.0
G9	22.8	0.0	22.8	**G9**	**34.7**	**5.1**	**39.8**	G9	11.4	0.0	11.4
H13	0.0	0.0	0.0	H13	2.7	0.0	2.7	**H13**	**46.4**	**0.0**	**46.4**
H7	14.1	0.0	14.1	H7	0.0	0.0	0.0	H7	8.0	0.0	8.0
J13	**37.8**	**15.9**	**53.7**	J13	10.5	0.0	10.5	**J13**	**49.0**	**0.0**	**49.0**
J7	19.7	0.0	19.7	J7	7.7	0.0	7.7	J7	17.1	0.0	17.1
K13	8.6	0.0	8.6	**K13**	**31.9**	**21.8**	**53.7**	K13	6.9	12.1	19.0
K7	21.1	0.0	21.1	K7	3.8	0.0	3.8	K7	4.2	0.0	4.2
L13	23.7	2.3	26.0	L13	13.4	9.6	23.0	L7	0.0	6.2	6.2
L7	10.7	0.0	10.7	L7	7.2	0.0	7.2	**M13**	**52.1**	**0.0**	**52.1**
M13	8.0	0.0	8.0	M13	26.8	3.9	30.7	M7	20.6	0.0	20.6
M7	14.3	0.0	14.3	M7	9.1	0.0	9.1	N10	8.0	0.0	8.0
N10	0.0	0.0	0.0	N10	6.9	0.0	6.9	N11	0.0	3.3	3.3
N11	30.2	0.0	30.2	N11	0.0	0.0	0.0	N12	0.0	0.0	0.0
N12	28.2	0.0	28.2	N12	29.3	0.0	29.3	N13	24.6	0.0	24.6
N13	12.5	0.0	12.5	**N13**	**36.2**	**0.0**	**36.2**	N7	16.4	0.0	16.4
N7	16.0	0.0	16.0	N7	14.6	0.0	14.6	N8	25.4	0.0	25.4
N8	22.5	0.0	22.5	N8	8.4	0.0	8.4	N9	9.8	0.0	9.8
N9	**27.9**	**8.3**	**36.2**	N9	4.1	4.3	8.4				

Note: **Bold** represents raw data of Table 6.2, crack length data in the upper standard deviation in the boundary region, 0-100°C ATC, UT.

SnAg, Aged, 18K, 21K, 24K, PI

UT16-U1A-SA-AG-18- / UT15-U1A-SA-AG-21- / UT17-U2A-SA-AG-24-PI											
Joint No.	% crack length P	% crack length S	% crack length P+S	Joint No.	% crack length P	% crack length S	% crack length P+S	Joint No	% crack length P	% crack length S	% crack length P+S
G10	4.9	1.6	6.5	**G10**	**35.5**	**0.0**	**35.5**	G10	0.0	0.0	0.0
G11	32.2	0.0	32.2	G11	0.0	20.2	20.2	G11	0.0	21.9	21.9
G12	36.4	0.0	36.4	G12	10.8	11.5	22.3	G12	5.1	0.0	5.1
G13	15.7	0.0	15.7	G13	9.8	0.0	9.8	G13	41.3	0.0	41.3
G7	**40.0**	**0.0**	**40.0**	G7	31.5	0.0	31.5	G7	23.8	0.0	23.8
G8	7.1	0.0	7.1	G8	0.0	7.4	7.4	G8	0.0	0.0	0.0
G9	4.2	0.0	4.2	G9	0.0	0.0	0.0	G9	16.6	7.3	24.0
H13	0.0	5.9	5.9	H13	18.0	11.5	29.5	H13	28.1	2.3	30.4
H7	0.0	0.0	0.0	H7	18.3	0.0	18.3	H7	36.4	0.0	36.4
J13	15.7	9.4	25.2	J13	17.0	0.0	17.0	J13	26.9	12.1	39.0
J7	0.0	7.7	7.7	J7	8.6	0.0	8.6	J7	37.4	4.4	41.8
K13	6.8	2.1	8.9	K13	0.0	8.7	8.7	**K13**	**21.9**	**31.8**	**53.6**
K7	0.0	0.0	0.0	K7	3.9	0.0	3.9	K7	25.5	0.0	25.5
L13	29.9	0.0	29.9	L13	0.0	18.9	18.9	L13	40.0	0.0	40.0
L7	13.1	0.0	13.1	**L7**	**35.5**	**19.7**	**55.2**	**L7**	**41.6**	**4.5**	**46.2**
M13	**39.8**	**0.0**	**39.8**	**M13**	**42.7**	**0.0**	**42.7**	M13	29.4	3.0	32.4
M7	5.6	0.0	5.6	M7	0.0	8.7	8.7	M7	30.6	0.0	30.6
N10	3.7	16.3	19.9	N10	0.0	0.0	0.0	N10	30.0	0.0	30.0
N12	26.2	0.0	26.2	N11	0.0	13.4	13.4	**N11**	**47.2**	**0.0**	**47.2**
N13	33.0	0.0	33.0	N12	19.0	0.0	19.0	N12	11.4	0.0	11.4
N7	**40.0**	**2.8**	**42.8**	N13	14.7	0.0	14.7	**N13**	**44.0**	**0.0**	**44.0**
N8	33.0	0.0	33.0	N7	8.7	0.0	8.7	N7	26.4	0.0	26.4
N9	**39.5**	**16.6**	**56.1**	**N8**	**42.0**	**0.0**	**42.0**	N8	15.2	0.0	15.2
				N9	25.4	0.0	25.4	N9	10.2	11.5	21.7

Note: **Bold** represents raw data of Table 6.2, crack length data in the upper standard deviation in the boundary region, 0-100°C ATC, UT.

SnAg, Air-Cooled, 3K, PI

UT18-U14A-SA-A-3- / UT18-U4A-SA-A-3- / UT18-U9A-SA-A-3-PI											
Joint No.	% crack length P	% crack length S	% crack length P+S	Joint No.	% crack length P	% crack length S	% crack length P+S	Joint No	% crack length P	% crack length S	% crack length P+S
G10	1.7	0.0	1.7	G10	0.0	0.0	0.0	G10	0.0	0.0	0.0
G11	3.4	4.3	7.7	G11	2.4	0.0	2.4	G11	0.0	0.0	0.0
G12	8.4	3.8	12.2	**G12**	**19.2**	**8.7**	**28.0**	G12	3.4	0.0	3.4
G13	0.0	5.5	5.5	G13	5.5	0.0	5.5	**G13**	**17.6**	**1.4**	**18.9**
G7	0.0	0.0	0.0	G7	11.1	1.0	12.1	G7	0.0	0.0	0.0
G8	10.8	0.0	10.8	G8	8.2	0.0	8.2	G8	1.7	0.0	1.7
G9	7.9	0.0	7.9	G9	8.8	5.3	14.1	G9	4.3	0.0	4.3
H13	2.9	0.0	2.9	H13	6.5	0.0	6.5	H13	10.5	0.0	10.5
H7	1.4	0.0	1.4	H7	0.0	2.9	2.9	**H7**	**13.3**	**7.3**	**20.6**
J13	0.0	0.0	0.0	J13	0.0	0.0	0.0	J13	0.0	6.7	6.7
J7	3.4	0.0	3.4	J7	3.6	0.0	3.6	**J7**	**18.3**	**0.0**	**18.3**
K13	0.0	0.0	0.0	K13	2.1	0.0	2.1	K13	0.0	6.0	6.0
K7	0.0	0.0	0.0	**K7**	**14.9**	**0.0**	**14.9**	K7	0.0	0.0	0.0
L13	0.0	6.5	6.5	L13	0.0	0.0	0.0	L13	0.0	0.0	0.0
L7	10.8	0.0	10.8	L7	3.8	0.0	3.8	L7	0.0	1.9	1.9
M13	2.2	0.0	2.2	**M13**	**28.5**	**0.0**	**28.5**	M13	9.4	0.0	9.4
M7	1.9	1.9	3.8	M7	2.6	0.0	2.6	M7	0.0	0.0	0.0
N10	3.6	0.0	3.6	N10	0.0	0.0	0.0	N10	0.0	11.8	11.8
N11	0.0	8.1	8.1	N11	0.0	3.4	3.4	**N11**	**21.1**	**0.0**	**21.1**
N12	2.9	0.0	2.9	N12	0.0	0.0	0.0	N12	0.0	2.6	2.6
N13	2.2	0.0	2.2	**N13**	**18.7**	**0.0**	**18.7**	**N13**	**25.9**	**0.0**	**25.9**
N7	9.5	0.0	9.5	N7	0.0	0.0	0.0	N7	0.0	1.5	1.5
N8	0.0	0.0	0.0	**N8**	**21.8**	**0.0**	**21.8**	N8	2.6	0.0	2.6
N9	6.7	0.0	6.7	N9	11.2	0.0	11.2	N9	7.5	0.0	7.5

Note: **Bold** represents raw data of Table 6.2, crack length data in the upper standard deviation in the boundary region, 0-100°C ATC, UT.

SnAg, Air-Cooled, 6K, PI

UT20-U14A-SA-A-6- / UT20-U4A-SA-A-6- / UT20-U9A-SA-A-6-PI											
Joint No.	% crack length P	% crack length S	% crack length P+S	Joint No.	% crack length P	% crack length S	% crack length P+S	Joint No	% crack length P	% crack length S	% crack length P+S
G10	**33.2**	**13.5**	**46.7**	G10	4.2	0.0	4.2	G10	1.4	0.0	1.4
G11	**34.0**	**0.0**	**34.0**	G11	2.5	0.0	2.5	G11	0.0	0.0	0.0
G12	24.0	0.0	24.0	G12	25.0	4.7	29.7	G12	0.0	0.0	0.0
G13	9.1	0.0	9.1	G13	0.0	2.6	2.6	G13	26.6	3.8	30.4
G7	24.5	0.0	24.5	G7	8.5	0.0	8.5	G7	8.6	0.0	8.6
G8	13.2	0.0	13.2	G8	16.9	7.7	24.6	G8	19.6	0.0	19.6
G9	19.4	0.0	19.4	G9	0.0	8.9	8.9	H13	10.0	7.5	17.5
H13	17.6	0.0	17.6	**H13**	**34.4**	**14.2**	**48.6**	H7	0.0	0.0	0.0
H7	22.9	5.2	28.1	H7	0.0	0.0	0.0	J13	17.8	0.0	17.8
J13	15.6	0.0	15.6	**J13**	**32.4**	**6.1**	**38.5**	J7	0.0	6.6	6.6
J7	26.9	3.1	30.1	J7	0.0	3.0	3.0	K13	18.7	4.6	23.3
K13	0.0	9.4	9.4	**K13**	**23.0**	**14.3**	**37.3**	K7	16.6	6.7	23.3
K7	0.0	0.0	0.0	K7	29.3	0.0	29.3	L13	0.0	22.9	22.9
L13	10.2	0.0	10.2	L13	17.6	2.6	20.2	L7	27.8	0.0	27.8
L7	30.6	0.0	30.6	L7	27.9	0.0	27.9	**M13**	**25.7**	**8.9**	**34.6**
M13	5.8	0.0	5.8	M13	15.7	0.0	15.7	M7	2.1	0.0	2.1
M7	7.0	9.0	16.0	M7	0.0	2.4	2.4	N10	2.0	0.0	2.0
N10	**35.7**	**19.6**	**55.2**	N10	17.6	12.0	29.6	N11	9.2	0.0	9.2
N11	0.0	9.8	9.8	N11	25.6	5.3	30.9	N12	21.0	0.0	21.0
N12	30.4	1.7	32.2	N13	27.7	3.3	31.0	N13	32.5	0.0	32.5
N13	19.1	9.6	28.7	N7	7.5	0.0	7.5	**N7**	**33.3**	**0.0**	**33.3**
N7	5.9	0.0	5.9	N8	18.6	0.0	18.6	N8	14.0	10.8	24.8
N8	18.2	0.0	18.2	N9	28.6	3.3	31.9	N9	6.5	0.0	6.5
N9	0.0	11.4	11.4								

Note: **Bold** represents raw data of Table 6.2, crack length data in the upper standard deviation in the boundary region, 0-100°C ATC, UT.

SnAg, Air-Cooled, 9K, PI

UT19-U13A-SA-A-9- / UT19-U3A-SA-A-9- / UT19-U8A-SA-A-9-PI											
Joint No.	% crack length P	% crack length S	% crack length P+S	Joint No.	% crack length P	% crack length S	% crack length P+S	Joint No	% crack length P	% crack length S	% crack length P+S
G10	**31.7**	**10.6**	**42.4**	G10	21.3	14.1	35.4	G10	11.5	0.0	11.5
G11	10.9	15.5	26.4	**G11**	**30.6**	**13.6**	**44.1**	G11	18.1	4.6	22.7
G12	14.5	0.0	14.5	G12	19.6	0.0	19.6	G12	18.9	0.0	18.9
G13	8.1	0.0	8.1	G13	16.6	4.5	21.1	G13	17.6	4.8	22.4
G7	28.6	0.0	28.6	G7	5.0	0.0	5.0	G7	9.1	0.0	9.1
G8	29.5	0.0	29.5	G8	24.7	0.0	24.7	G8	22.4	0.0	22.4
G9	11.6	0.2	11.7	**G9**	**26.1**	**14.1**	**40.2**	G9	7.6	0.0	7.6
H13	**43.7**	**9.5**	**53.2**	H13	17.0	7.4	24.4	H13	11.2	1.7	12.9
H7	19.0	2.9	21.9	H7	2.1	7.6	9.6	H7	33.6	0.0	33.6
J13	3.5	0.0	3.5	J13	6.5	0.0	6.5	**J13**	**35.7**	**21.5**	**57.2**
J7	16.8	0.0	16.8	J7	16.0	0.0	16.0	J7	0.0	0.0	0.0
K13	**43.5**	**7.9**	**51.5**	K13	18.4	3.6	22.0	K13	16.2	3.1	19.3
K7	**36.8**	**11.4**	**48.2**	K7	25.4	0.0	25.4	K7	16.5	3.8	20.3
L13	0.0	4.3	4.3	L13	15.8	3.9	19.7	L13	8.6	0.0	8.6
L7	21.4	0.0	21.4	**L7**	**39.3**	**0.0**	**39.3**	L7	32.4	0.0	32.4
M13	3.1	4.0	7.1	M13	20.1	0.0	20.1	M13	20.0	0.0	20.0
M7	35.2	0.0	35.2	M7	31.9	3.1	35.0	**M7**	**38.7**	**0.0**	**38.7**
N10	26.8	0.0	26.8	N10	11.3	11.3	22.6	N10	17.1	0.0	17.1
N11	14.3	0.0	14.3	N11	25.9	0.2	26.1	**N11**	**32.7**	**15.3**	**48.0**
N12	26.3	0.0	26.3	N12	12.7	10.6	23.3	N12	14.6	0.0	14.6
N13	18.1	0.0	18.1	N13	12.5	4.5	17.0	N13	35.3	0.9	36.2
N7	28.3	0.0	28.3	**N7**	**35.4**	**14.4**	**49.8**	N7	13.4	0.0	13.4
N8	**36.3**	**15.7**	**52.0**	**N8**	**46.7**	**0.0**	**46.7**	N8	17.4	0.0	17.4
N9	28.5	1.0	29.5	N9	0.0	10.1	10.1	N9	20.0	5.4	25.3

Note: **Bold** represents raw data of Table 6.2, crack length data in the upper standard deviation in the boundary region, 0-100°C ATC, UT.

SnAg, Air-Cooled, 12K, PI

UT18-U12A-SA-A-12- / UT18-U2A-SA-A-12- / UT18-U7A-SA-A-12-PI											
Joint No.	% crack length P	% crack length S	% crack length P+S	Joint No.	% crack length P	% crack length S	% crack length P+S	Joint No	% crack length P	% crack length S	% crack length P+S
G10	10.9	5.0	15.9	G10	18.9	4.8	23.8	G10	6.9	0.0	6.9
G11	2.8	0.0	2.8	**G11**	**54.1**	**27.0**	**81.1**	G11	24.0	13.0	37.0
G12	18.7	0.0	18.7	**G12**	**45.4**	**3.3**	**48.7**	G12	27.3	6.4	33.7
G13	14.7	5.7	20.4	G13	30.8	1.5	32.4	G13	9.3	9.8	19.0
G7	**37.1**	**9.7**	**46.8**	G7	14.4	0.0	14.4	G7	18.9	0.0	18.9
G8	12.3	0.0	12.3	G8	3.8	0.0	3.8	G8	0.0	4.6	4.6
G9	10.4	0.0	10.4	G9	5.7	7.1	12.7	G9	25.2	0.0	25.2
H13	33.2	8.3	41.5	**H13**	**45.3**	**15.8**	**61.1**	H13	21.7	2.6	24.3
H7	40.8	0.0	40.8	H7	36.5	4.6	41.1	H7	32.7	4.7	37.3
J13	0.0	0.0	0.0	J13	22.9	5.0	27.9	J13	22.8	0.0	22.8
J7	28.0	0.0	28.0	J7	0.0	3.6	3.6	J7	4.3	0.0	4.3
K13	0.0	19.2	19.2	K13	42.4	0.0	42.4	K13	2.9	5.0	7.9
K7	2.9	4.3	7.3	K7	26.2	4.0	30.1	K7	34.2	4.0	38.2
L13	**46.5**	**1.4**	**47.9**	**L13**	**33.1**	**14.3**	**47.4**	L13	15.2	0.0	15.2
L7	39.1	0.0	39.1	L7	0.0	0.0	0.0	L7	11.1	15.4	26.4
M13	15.7	12.1	27.8	**M13**	**42.9**	**7.9**	**50.8**	M13	3.3	5.5	8.8
M7	**31.8**	**19.0**	**50.8**	M7	19.7	0.0	19.7	M7	23.8	5.7	29.5
N10	33.5	10.7	44.2	N10	21.5	0.0	21.5	N10	9.3	1.2	10.5
N11	**46.5**	**13.8**	**60.3**	N11	35.6	1.5	37.2	N11	0.0	24.9	24.9
N12	22.6	0.0	22.6	N12	7.9	17.7	25.6	N12	40.9	0.0	40.9
N13	**51.0**	**9.7**	**60.6**	N13	25.8	1.5	27.4	N13	25.4	0.0	25.4
N7	40.8	0.0	40.8	N7	29.4	0.0	29.4	N7	43.4	0.0	43.4
N8	26.3	0.0	26.3	N8	23.8	5.5	29.3	N8	40.5	0.0	40.5
N9	40.3	3.8	44.1	N9	3.6	18.2	21.8	**N9**	**38.9**	**19.6**	**58.6**

Note: **Bold** represents raw data of Table 6.2, crack length data in the upper standard deviation in the boundary region, 0-100°C ATC, UT.

SnAg, Air-Cooled, 15K, PI

UT20-U12A-SA-A-15- / UT20-U2A-SA-A-15- / UT20-U7A-SA-A-15-PI											
Joint No.	% crack length P	% crack length S	% crack length P+S	Joint No.	% crack length P	% crack length S	% crack length P+S	Joint No	% crack length P	% crack length S	% crack length P+S
G10	19.4	0.0	19.4	G10	38.4	1.2	39.7	G10	35.3	17.5	52.8
G11	6.6	17.7	24.3	G11	25.6	6.7	32.3	G11	16.6	12.6	29.2
G12	**50.4**	**11.4**	**61.8**	**G12**	**40.2**	**22.8**	**63.0**	**G12**	**40.2**	**17.3**	**57.5**
G13	22.0	6.1	28.1	G13	54.2	2.8	57.0	G7	35.5	0.0	35.5
G7	28.6	0.0	28.6	G7	35.1	11.1	46.2	G8	42.2	9.7	51.9
G8	27.8	0.0	27.8	G8	40.6	15.5	56.0	G9	19.3	5.0	24.3
G9	21.9	0.0	21.9	G9	1.6	18.8	20.4	H13	34.9	4.1	38.9
H13	20.0	16.8	36.8	**H13**	**49.8**	**17.1**	**66.9**	H7	50.2	0.0	50.2
H7	16.1	7.7	23.8	H7	49.8	0.0	49.8	J13	23.6	3.8	27.4
J13	30.4	1.4	31.8	J13	13.0	17.3	30.4	J7	23.4	0.0	23.4
J7	39.6	0.0	39.6	J7	27.1	0.0	27.1	K13	22.7	4.5	27.3
K13	0.0	2.6	2.6	**K13**	**38.3**	**22.7**	**61.0**	K7	13.8	35.5	49.3
K7	34.1	0.0	34.1	K7	1.7	15.6	17.3	L13	33.3	0.0	33.3
L13	6.2	5.9	12.1	**L13**	**43.7**	**18.1**	**61.8**	L7	13.3	27.3	40.6
L7	26.7	0.0	26.7	L7	22.0	14.4	36.5	M13	35.5	19.2	54.7
M13	50.3	5.0	55.4	**M13**	**59.3**	**7.3**	**66.6**	M7	23.4	0.0	23.4
M7	25.4	6.5	31.9	M7	43.3	5.4	48.8	**N10**	**37.5**	**24.5**	**62.0**
N10	16.9	2.1	19.0	N10	14.1	15.1	29.2	N11	43.8	3.2	47.1
N11	0.0	18.1	18.1	N11	24.1	7.7	31.8	**N12**	**67.6**	**4.3**	**71.9**
N12	29.8	5.8	35.6	N12	14.4	3.3	17.8	**N13**	**58.7**	**5.8**	**64.5**
N13	**58.2**	**0.0**	**58.2**	**N13**	**57.7**	**0.0**	**57.7**	N7	31.3	0.0	31.3
N7	39.6	7.4	47.0	N7	39.9	8.9	48.8	N8	18.0	7.0	25.0
N8	34.3	14.4	48.6	**N8**	**72.4**	**1.9**	**74.3**	N9	43.7	0.0	43.7
N9	**44.6**	**19.0**	**63.6**	**N9**	**49.1**	**15.0**	**64.2**				

Note: **Bold** represents raw data of Table 6.2, crack length data in the upper standard deviation in the boundary region, 0-100°C ATC, UT.

SnAg, Air-Cooled, 18K, 21K, 24K, PI

UT18-U1A-SA-A-18- / UT19-U1A-SA-A-21- / UT20-U1A-SA-A-24-PI											
Joint No.	% crack length P	% crack length S	% crack length P+S	Joint No.	% crack length P	% crack length S	% crack length P+S	Joint No	% crack length P	% crack length S	% crack length P+S
G10	2.4	20.1	22.6	G10	6.5	22.5	29.0	G10	39.0	4.2	43.2
G11	18.8	21.0	39.8	G11	41.8	9.9	51.8	G11	45.1	0.0	45.1
G12	25.3	14.3	39.6	G12	46.6	0.0	46.6	G12	58.2	5.1	63.3
G13	12.9	13.3	26.2	G13	54.2	2.1	56.2	G13	33.0	20.5	53.5
G7	10.0	3.4	13.4	G7	19.4	2.9	22.3	G7	45.8	10.8	56.6
G8	32.7	0.3	33.1	G8	1.4	0.0	1.4	G8	42.1	0.0	42.1
G9	18.8	12.9	31.7	G9	3.8	20.2	24.0	G9	48.1	5.6	53.7
H13	15.7	2.4	18.1	H13	56.6	2.2	58.8	**H13**	**99.0**	**0.0**	**99.0**
H7	45.8	7.9	53.7	H7	16.9	21.9	38.7	H7	20.8	9.4	30.2
J13	**54.6**	**25.0**	**79.6**	J13	7.7	25.8	33.6	J13	11.9	1.6	13.5
J7	24.3	4.1	28.4	J7	0.0	0.0	0.0	J7	33.9	3.3	37.2
K13	9.6	3.3	12.9	**K13**	**56.3**	**28.4**	**84.7**	K13	0.0	36.8	36.8
K7	19.8	18.1	37.9	K7	17.4	23.2	40.6	K7	10.7	7.5	18.2
L13	43.2	0.0	43.2	L13	40.0	0.0	40.0	L13	19.4	24.1	43.5
L7	39.1	3.4	42.5	L7	10.9	20.2	31.0	L7	32.3	0.0	32.3
M13	53.0	2.1	55.0	**M13**	**72.7**	**0.0**	**72.7**	**M13**	**59.8**	**20.1**	**79.9**
M7	**45.1**	**22.5**	**67.6**	M7	35.8	16.0	51.8	M7	51.4	1.4	52.9
N10	23.1	17.0	40.1	**N10**	**43.4**	**20.3**	**63.7**	N10	8.7	41.3	50.0
N11	42.5	4.8	47.3	N11	50.1	2.8	52.9	N11	22.7	13.1	35.9
N12	**47.2**	**16.4**	**63.6**	**N12**	**61.3**	**3.6**	**64.9**	N12	46.7	0.0	46.7
N13	53.3	0.0	53.3	**N13**	**59.2**	**4.8**	**64.1**	N13	38.4	28.8	67.1
N7	**64.9**	**0.0**	**64.9**	N7	19.5	3.8	23.3	N7	60.7	4.1	64.8
N8	40.0	5.7	45.6	N8	29.6	3.1	32.7	**N8**	**49.2**	**39.3**	**88.4**
N9	20.6	24.0	44.6	N9	45.3	2.1	47.4	N9	45.6	5.8	51.4

Note: **Bold** represents raw data of Table 6.2, crack length data in the upper standard deviation in the boundary region, 0-100°C ATC, UT.

SnAg, Air-Cooled, 27K, PI

UT21-U2A-SA-A-27-PI											
Joint No.	% crack length P	% crack length S	% crack length P+S	Joint No.	% crack length P	% crack length S	% crack length P+S	Joint No	% crack length P	% crack length S	% crack length P+S
G10	42.1	3.2	45.3								
G11	47.7	14.4	62.1								
G12	34.4	29.6	64.0								
G13	48.3	0.0	48.3								
G7	20.7	6.3	27.0								
G8	44.4	0.0	44.4								
G9	32.1	6.5	38.6								
H13	**57.0**	**22.3**	**79.3**								
H7	36.0	2.3	38.2								
J13	33.0	32.4	65.4								
J7	38.8	0.0	38.8								
K13	0.0	34.5	34.5								
K7	34.3	0.0	34.3								
L13	53.3	0.0	53.3								
L7	35.8	0.0	35.8								
M13	**64.2**	**7.5**	**71.7**								
M7	49.5	9.3	58.8								
N10	**62.6**	**4.8**	**67.3**								
N11	57.4	6.8	64.2								
N12	48.8	0.0	48.8								
N13	25.1	14.4	39.5								
N7	64.8	0.0	64.8								
N8	26.9	19.1	46.0								
N9	**59.4**	**17.1**	**76.5**								

Note: **Bold** represents raw data of Table 6.2, crack length data in the upper standard deviation in the boundary region, 0-100°C ATC, UT.

SnAg, Quenched, 3K, PI

UT23-U14A-SA-Q-3- / UT23-U4A-SA-Q-3- / UT23-U9A-SA-Q-3-PI											
Joint No.	% crack length P	% crack length S	% crack length P+S	Joint No.	% crack length P	% crack length S	% crack length P+S	Joint No	% crack length P	% crack length S	% crack length P+S
G10	3.3	0.0	3.3	G10	11.6	8.0	19.5	G10	0.0	0.0	0.0
G11	17.4	1.6	18.9	G11	4.2	0.0	4.2	G11	5.5	0.0	5.5
G12	31.3	0.0	31.3	G12	10.9	0.0	10.9	G12	4.5	0.0	4.5
G13	0.0	0.0	0.0	G13	12.8	8.1	20.9	G13	0.0	0.0	0.0
G7	1.4	0.0	1.4	G7	6.9	0.0	6.9	G7	0.0	3.4	3.4
G8	5.7	0.0	5.7	G8	1.5	3.6	5.2	G8	26.3	0.0	26.3
G9	6.5	0.0	6.5	G9	18.1	0.0	18.1	G9	0.0	0.0	0.0
H13	5.2	0.0	5.2	H13	0.0	0.0	0.0	H13	14.5	3.6	18.1
H7	0.7	0.0	0.7	H7	3.8	0.0	3.8	H7	10.5	0.0	10.5
J13	0.9	5.0	5.9	J13	9.7	0.0	9.7	J13	0.0	2.2	2.2
J7	3.4	0.0	3.4	J7	21.4	6.4	27.8	J7	14.8	0.0	14.8
K13	0.0	0.0	0.0	K13	0.0	0.0	0.0	K13	0.0	0.0	0.0
K7	0.0	0.0	0.0	K7	0.0	0.0	0.0	K7	0.0	0.0	0.0
L13	0.0	0.0	0.0	L13	5.0	0.0	5.0	L13	18.3	0.0	18.3
L7	6.7	0.0	6.7	L7	0.0	0.0	0.0	L7	0.0	0.0	0.0
M13	9.1	0.0	9.1	M13	10.4	0.0	10.4	M13	9.6	0.0	9.6
M7	5.5	0.0	5.5	M7	8.3	0.0	8.3	M7	10.7	0.0	10.7
N10	2.6	0.0	2.6	N10	0.0	2.6	2.6	N10	6.9	2.9	9.8
N11	0.0	0.0	0.0	N11	5.7	0.0	5.7	N11	0.0	13.3	13.3
N13	6.2	0.9	7.1	N12	6.6	0.0	6.6	N12	0.0	4.0	4.0
N7	0.0	0.0	0.0	N13	14.2	0.0	14.2	N13	0.0	0.0	0.0
N8	1.9	0.0	1.9	N7	0.0	0.0	0.0	N7	0.0	3.3	3.3
N9	0.0	0.0	0.0	N8	2.2	0.0	2.2	N8	9.2	0.0	9.2
				N9	4.7	0.0	4.7	N9	0.0	0.0	0.0

SnAg, Quenched, 6K, PI

UT25-U14A-SA-Q-6- / UT25-U4A-SA-Q-6- / UT25-U9A-SA-Q-6-PI											
Joint No.	% crack length P	% crack length S	% crack length P+S	Joint No.	% crack length P	% crack length S	% crack length P+S	Joint No	% crack length P	% crack length S	% crack length P+S
G10	10.5	5.3	15.8	G10	15.7	0.0	15.7	G10	3.6	0.0	3.6
G11	20.5	3.6	24.1	G11	0.0	8.4	8.4	G11	11.4	0.0	11.4
G13	27.2	9.3	36.5	G12	19.8	0.0	19.8	G12	0.0	0.5	0.5
G7	25.0	0.0	25.0	G13	17.4	0.0	17.4	G13	11.5	15.8	27.4
G8	9.6	5.0	14.6	G7	8.4	6.2	14.6	G7	5.3	0.0	5.3
G9	25.7	5.0	30.7	G8	18.1	0.0	18.1	G8	27.0	5.5	32.5
H13	1.7	0.0	1.7	G9	0.0	0.0	0.0	G9	10.0	0.0	10.0
H7	9.3	0.0	9.3	H13	6.5	0.0	6.5	H13	13.8	4.1	17.9
J13	0.0	0.0	0.0	H7	11.7	0.0	11.7	H7	11.9	0.0	11.9
J7	23.8	0.0	23.8	J13	18.8	0.0	18.8	J13	20.1	4.3	24.5
K13	15.3	9.8	25.1	J7	23.4	7.1	30.5	J7	2.1	0.0	2.1
K7	32.4	0.0	32.4	K13	18.3	1.4	19.6	K13	19.7	6.4	26.1
L13	27.1	11.3	38.3	K7	9.3	0.0	9.3	K7	12.0	0.0	12.0
L7	18.4	0.0	18.4	L13	7.1	0.0	7.1	L13	28.6	0.0	28.6
M13	43.4	0.0	43.4	L7	13.8	0.0	13.8	L7	5.0	0.0	5.0
M7	24.3	0.0	24.3	M13	29.3	0.0	29.3	M13	15.7	4.1	19.8
N10	20.1	15.2	35.3	M7	5.9	2.1	7.9	M7	6.4	0.0	6.4
N12	15.7	6.5	22.2	N10	0.0	10.2	10.2	N10	4.8	0.0	4.8
N13	6.0	0.0	6.0	N11	13.9	12.0	26.0	N11	25.7	17.0	42.7
N7	30.5	0.0	30.5	N12	32.4	2.8	35.1	N12	7.7	4.6	12.4
N8	2.4	0.0	2.4	N13	37.5	0.0	37.5	N13	52.7	3.3	56.0
N9	18.1	0.0	18.1	N7	5.0	0.0	5.0	N7	11.2	0.0	11.2
				N8	10.0	0.0	10.0	N8	9.6	0.0	9.6
				N9	14.6	0.0	14.6	N9	17.6	0.0	17.6

SnAg, Quenched, 9K, PI

UT24-U13A-SA-Q-9- / UT24-U3A-SA-Q-9- / UT24-U8A-SA-Q-9-PI											
Joint No.	% crack length P	% crack length S	% crack length P+S	Joint No.	% crack length P	% crack length S	% crack length P+S	Joint No	% crack length P	% crack length S	% crack length P+S
G10	0.0	0.5	0.5	G10	14.2	7.4	21.6	G10	33.5	19.2	52.7
G11	8.3	2.8	11.0	G11	21.6	10.6	32.3	G11	52.0	10.2	62.2
G12	44.8	15.2	59.9	G12	21.1	9.6	30.7	G12	49.4	1.7	51.1
G13	27.6	14.5	42.0	G13	19.7	0.0	19.7	G13	35.6	7.3	42.8
G7	14.6	10.7	25.3	G7	27.3	3.8	31.1	G7	45.3	2.2	47.5
G8	20.3	0.0	20.3	G8	32.8	7.6	40.3	G8	16.4	0.0	16.4
G9	34.6	4.6	39.3	G9	4.8	7.9	12.7	G9	0.5	2.4	2.9
H13	8.1	0.0	8.1	H13	16.5	5.0	21.5	H13	3.8	0.0	3.8
H7	8.1	0.0	8.1	H7	41.0	0.0	41.0	H7	0.0	0.0	0.0
J13	29.8	0.0	29.8	J13	0.0	4.8	4.8	J13	21.8	0.0	21.8
J7	14.6	0.0	14.6	J7	33.9	0.0	33.9	J7	14.2	0.0	14.2
K13	30.8	1.4	32.2	K13	4.3	0.0	4.3	K13	31.3	14.9	46.1
K7	15.2	4.3	19.5	K7	26.6	10.8	37.4	K7	4.1	0.0	4.1
L13	21.5	3.1	24.6	L13	39.8	6.9	46.7	L13	42.5	27.7	70.3
L7	0.0	2.8	2.8	L7	10.3	10.6	20.9	L7	27.0	5.5	32.6
M13	45.6	7.6	53.2	M13	18.0	0.0	18.0	M13	27.4	14.1	41.5
M7	29.6	9.8	39.4	M7	14.2	0.0	14.2	M7	29.8	0.0	29.8
N10	5.2	0.0	5.2	N10	23.0	3.6	26.6	N10	9.0	0.0	9.0
N11	32.5	16.7	49.3	N11	12.9	0.0	12.9	N11	30.2	9.7	39.9
N12	24.3	3.4	27.7	N12	31.6	9.6	41.2	N12	21.7	0.0	21.7
N13	0.0	0.0	0.0	N13	45.0	0.0	45.0	N13	44.4	7.4	51.8
N7	5.5	0.0	5.5	N7	24.7	0.0	24.7	N7	37.0	0.0	37.0
N8	22.7	0.0	22.7	N8	12.5	0.0	12.5	N8	16.9	4.8	21.7
N9	41.2	8.1	49.3	N9	56.5	22.8	79.3	N9	14.8	0.0	14.8

SnAg, Quenched, 12K, PI

UT23-U12A-SA-Q-12- / UT23-U2A-SA-Q-12- / UT23-U7A-SA-Q-12-PI											
Joint No.	% crack length P	% crack length S	% crack length P+S	Joint No.	% crack length P	% crack length S	% crack length P+S	Joint No	% crack length P	% crack length S	% crack length P+S
G10	32.1	0.0	32.1	G10	18.4	2.9	21.3	G10	48.9	12.1	61.1
G11	38.1	9.6	47.7	G11	11.0	2.7	13.7	G11	49.8	11.9	61.7
G12	52.1	17.8	70.0	G12	6.9	0.0	6.9	G12	50.5	20.3	70.8
G13	14.1	0.0	14.1	G13	21.3	2.6	23.9	G13	0.0	7.9	7.9
G7	29.5	0.0	29.5	G7	28.2	5.3	33.5	G7	4.5	4.5	9.0
G8	11.8	0.0	11.8	G8	21.8	0.0	21.8	G8	60.3	0.0	60.3
G9	23.8	5.0	28.8	G9	10.6	0.0	10.6	G9	53.7	18.6	72.3
H13	46.3	7.9	54.2	H13	29.9	14.8	44.6	H13	19.3	8.4	27.7
H7	32.5	0.0	32.5	H7	21.1	0.0	21.1	H7	7.2	0.0	7.2
J13	36.0	0.0	36.0	J13	10.7	0.0	10.7	J13	18.4	0.0	18.4
J7	7.2	18.1	25.3	J7	0.0	16.7	16.7	J7	11.5	4.6	16.2
K13	31.3	15.7	47.0	K13	5.7	8.4	14.1	K13	4.6	5.5	10.2
K7	0.0	2.9	2.9	K7	28.0	0.0	28.0	K7	44.1	0.0	44.1
L13	54.8	21.4	76.1	L13	39.0	9.3	48.4	L13	43.6	15.2	58.7
L7	21.9	0.0	21.9	L7	40.2	0.0	40.2	L7	12.6	11.5	24.1
M13	48.9	25.7	74.6	M13	26.6	0.0	26.6	M13	12.7	1.0	13.8
M7	48.4	0.0	48.4	M7	16.6	0.0	16.6	M7	26.2	0.0	26.2
N10	20.8	5.5	26.3	N10	36.1	21.8	57.9	N10	28.6	11.7	40.3
N11	50.3	8.1	58.4	N11	36.7	27.1	63.9	N11	8.6	0.0	8.6
N12	28.2	6.5	34.8	N12	0.0	0.0	0.0	N12	34.4	4.1	38.6
N13	25.7	0.0	25.7	N13	49.1	14.6	63.7	N13	39.4	8.4	47.9
N7	43.4	0.0	43.4	N7	1.5	4.3	5.8	N7	41.0	12.2	53.2
N8	49.4	0.0	49.4	N8	25.7	2.4	28.1	N8	42.0	0.0	42.0
N9	43.4	0.0	43.4	N9	25.7	1.9	27.6	N9	25.7	0.0	25.7

SnAg, Quenched, 15K, PI

UT25-U12A-SA-Q-15- / UT25-U2A-SA-Q-15- / UT25-U7A-SA-Q-15-PI											
Joint No.	% crack length P	% crack length S	% crack length P+S	Joint No.	% crack length P	% crack length S	% crack length P+S	Joint No	% crack length P	% crack length S	% crack length P+S
G10	0.0	2.9	2.9	G10	34.7	7.9	42.6	G10	11.9	0.0	11.9
G11	53.4	16.7	70.1	G11	0.0	0.0	0.0	G11	17.4	4.1	21.5
G12	33.1	8.3	41.3	G12	30.0	5.2	35.2	G12	16.2	8.1	24.3
G13	50.6	0.0	50.6	G13	40.7	0.0	40.7	G13	46.3	3.4	49.8
G7	66.6	2.9	69.6	G7	45.5	10.0	55.4	G7	42.0	0.0	42.0
G8	48.0	0.0	48.0	G8	44.6	0.0	44.6	G8	38.4	0.0	38.4
G9	29.8	0.0	29.8	G9	16.4	7.6	23.9	G9	15.2	6.7	21.9
H13	42.5	4.8	47.4	H13	38.2	0.0	38.2	H13	19.3	10.3	29.6
H7	0.0	7.7	7.7	H7	47.0	13.3	60.3	H7	14.5	0.0	14.5
J13	10.2	0.0	10.2	J13	15.5	7.2	22.7	J13	27.9	0.0	27.9
J7	20.1	0.0	20.1	J7	24.6	32.3	56.9	J7	35.6	0.0	35.6
K13	7.4	0.0	7.4	K13	0.0	0.0	0.0	K13	49.6	6.7	56.3
L13	5.9	2.8	8.6	K7	39.1	16.2	55.2	K7	6.2	7.9	14.1
L7	30.7	0.0	30.7	L13	36.3	14.3	50.6	L13	43.1	16.7	59.8
M13	45.1	0.0	45.1	L7	10.7	0.0	10.7	L7	13.4	0.0	13.4
M7	38.2	16.2	54.4	M13	27.4	0.0	27.4	M13	40.0	0.0	40.0
N10	9.5	0.0	9.5	M7	42.3	4.5	46.8	M7	2.1	0.0	2.1
N11	0.0	26.7	26.7	N10	35.3	5.5	40.8	N10	19.6	2.9	22.6
N12	29.6	0.0	29.6	N11	33.6	0.0	33.6	N11	0.0	10.5	10.5
N13	25.7	4.5	30.1	N12	21.3	26.2	47.4	N12	58.6	10.5	69.1
N7	29.6	0.0	29.6	N13	5.5	0.0	5.5	N13	49.1	0.0	49.1
N8	27.2	0.0	27.2	N7	38.6	0.0	38.6	N7	6.7	0.0	6.7
N9	9.2	0.2	9.4	N8	49.1	7.9	57.0	N8	14.1	6.4	20.5
				N9	44.4	2.2	46.6	N9	40.8	14.3	55.1

SnAg, Quenched, 18K, 21K, 24K, PI

UT25BAD-U5A-SA-Q-18- / UT23-U1A-SA-Q-21- / UT25BAD-U1A-SA-Q-24-PI											
Joint No.	% crack length P	% crack length S	% crack length P+S	Joint No.	% crack length P	% crack length S	% crack length P+S	Joint No	% crack length P	% crack length S	% crack length P+S
G10	21.8	15.6	37.4	G10	34.3	18.6	52.9	G10	30.9	5.3	36.3
G11	43.7	8.1	51.8	G11	69.2	10.7	79.9	G11	58.9	17.5	76.5
G12	49.5	3.6	53.1	G12	57.3	22.0	79.4	G12	44.8	4.5	49.3
G13	20.7	0.0	20.7	G13	36.9	10.0	46.8	G13	32.8	11.2	44.0
G7	36.4	0.0	36.4	G7	62.3	2.6	64.9	G7	58.4	16.5	74.9
G8	19.2	15.3	34.5	G8	41.2	11.4	52.5	G8	59.5	6.0	65.5
G9	1.9	4.1	6.0	G9	10.8	16.2	27.0	G9	40.9	0.0	40.9
H13	50.8	4.3	55.0	H13	34.4	0.0	34.4	H13	30.9	0.0	30.9
H7	32.2	0.0	32.2	H7	51.1	25.7	76.8	H7	57.7	0.0	57.7
J13	38.8	0.0	38.8	J13	40.6	10.9	51.5	J13	38.6	0.0	38.6
J7	9.4	0.0	9.4	J7	46.7	0.0	46.7	J7	56.4	6.5	62.9
K13	45.3	27.9	73.2	K13	36.9	5.0	41.8	K13	45.5	22.9	68.4
K7	7.7	0.0	7.7	K7	42.5	1.9	44.4	K7	53.4	0.0	53.4
L13	42.2	19.2	61.4	L13	45.5	5.9	51.3	L13	34.4	9.5	43.8
L7	49.6	0.0	49.6	L7	42.5	9.3	51.8	L7	1.7	22.3	24.1
M13	36.5	7.5	44.1	M13	46.8	0.0	46.8	M13	66.2	14.7	80.9
M7	34.6	0.0	34.6	M7	41.3	11.5	52.9	M7	56.5	31.4	88.0
N10	48.2	3.9	52.1	N10	37.9	33.4	71.3	N10	48.1	24.2	72.3
N11	10.5	39.4	49.9	N11	5.9	27.6	33.4	N11	61.9	9.1	71.0
N12	43.2	0.0	43.2	N12	25.1	14.1	39.3	N12	83.9	4.5	88.3
N13	39.8	14.9	54.7	N13	39.9	3.1	43.0	N13	46.9	14.5	61.4
N7	41.3	15.9	57.3	N7	46.5	16.0	62.5	N7	56.9	19.6	76.4
N8	50.3	23.1	73.4	N8	53.9	2.6	56.5	N8	33.0	16.2	49.1
N9	49.2	0.0	49.2	N9	44.8	7.9	52.7	N9	42.1	0.0	42.1

SnAg, Quenched, 27K, 30K, PI

UT25BAD-U3A-SA-Q-27- / UT25-U1A-SA-Q-30-PI											
Joint No.	% crack length P	% crack length S	% crack length P+S	Joint No.	% crack length P	% crack length S	% crack length P+S	Joint No	% crack length P	% crack length S	% crack length P+S
G10	42.3	32.5	74.8	G10	49.8	9.8	59.6				
G11	39.7	37.5	77.2	G11	67.0	20.3	87.3				
G12	69.8	6.0	75.8	G12	58.8	0.0	58.8				
G7	60.5	0.2	60.7	G13	99.3	0.0	99.3				
G8	56.8	14.4	71.2	G7	68.4	6.9	75.3				
G9	56.1	5.5	61.6	G8	71.9	17.8	89.7				
H13	62.6	2.7	65.3	G9	55.3	26.8	82.1				
H7	62.4	0.0	62.4	H13	94.8	0.0	94.8				
J13	34.1	6.0	40.1	H7	50.2	0.0	50.2				
J7	20.6	11.0	31.5	J13	98.7	0.0	98.7				
K13	29.0	0.0	29.0	J7	72.1	11.6	83.7				
K7	15.1	12.5	27.6	K13	62.4	15.0	77.5				
L13	2.1	22.1	24.2	K7	66.2	19.7	85.9				
L7	62.6	0.0	62.6	L13	52.1	27.7	79.7				
M13	73.8	16.2	90.0	L7	71.1	1.5	72.7				
M7	66.2	7.5	73.7	M13	78.4	2.1	80.4				
N10	25.2	8.2	33.4	M7	41.2	24.2	65.5				
N11	63.7	8.8	72.6	N10	19.8	19.2	39.0				
N12	62.0	15.7	77.7	N11	36.8	2.4	39.2				
N13	33.3	29.3	62.6	N12	27.8	9.2	37.0				
N7	42.5	4.1	46.6	N13	1.9	2.2	4.1				
N8	69.8	0.0	69.8	N7	53.3	0.0	53.3				
N9	48.5	15.8	64.3	N8	52.6	9.1	61.7				
G10	42.3	32.5	74.8	N9	53.6	0.0	53.6				

Table G.3. % Crack length data for aged, air-cooled, and quenched SnPb joints in the boundary region at the board interface (nominal joint diameter=584 μm)

SnPb, Aged, 2K, BI

UT1-U14A-SPA-AG-2- / UT1-U4A-SPA-AG-2- / UT1-U9A-SPA-AG-2-BI											
Joint No.	% crack length P	% crack length S	% crack length P+S	Joint No.	% crack length P	% crack length S	% crack length P+S	Joint No	% crack length P	% crack length S	% crack length P+S
G10	0.0	0.0	0.0	G10	0.0	0.0	0.0	G10	6.5	0.0	6.5
G11	0.0	0.0	0.0	G11	0.0	0.0	0.0	G11	3.9	0.0	3.9
G12	0.0	0.0	0.0	G12	0.0	0.0	0.0	G12	7.0	0.0	7.0
G13	**0.0**	**0.0**	**0.0**	G13	0.0	0.0	0.0	G13	0.0	0.0	0.0
G7	5.5	0.0	5.5	G7	9.6	0.0	9.6	G7	3.3	0.0	3.3
H13	3.4	0.0	3.4	G8	0.0	0.0	0.0	G8	3.6	0.0	3.6
H7	2.6	0.0	2.6	G9	0.0	0.0	0.0	G9	8.9	0.0	8.9
J13	3.6	0.0	3.6	H13	0.0	0.0	0.0	H13	0.0	0.0	0.0
K13	4.6	0.0	4.6	J13	2.6	3.1	5.7	H7	0.0	0.0	0.0
K7	0.0	0.0	0.0	J7	4.4	0.0	4.4	**J13**	**2.9**	**0.0**	**2.9**
L13	14.7	0.0	14.7	K13	0.0	0.0	0.0	J7	0.0	0.0	0.0
M13	8.9	0.0	8.9	K7	3.0	0.0	3.0	K13	0.0	0.0	0.0
N10	**3.6**	**0.0**	**3.6**	L13	0.0	0.0	0.0	K7	0.0	0.0	0.0
N11	6.3	0.0	6.3	L7	5.7	0.0	5.7	L13	2.9	0.0	2.9
N12	**14.4**	**0.0**	**14.4**	M13	4.5	7.7	12.2	L7	0.0	0.0	0.0
N13	13.4	0.0	13.4	M7	11.0	0.0	11.0	M13	3.4	0.0	3.4
N7	**2.2**	**0.0**	**2.2**	N10	0.0	0.0	0.0	M7	0.0	0.0	0.0
N8	7.9	0.0	7.9	N11	0.0	0.0	0.0	**N10**	**0.0**	**0.0**	**0.0**
N9	6.3	0.0	6.3	N12	2.8	0.0	2.8	**N11**	**0.0**	**0.0**	**0.0**
				N13	**5.6**	**0.0**	**5.6**	N12	0.0	0.0	0.0
				N7	**0.0**	**0.0**	**0.0**	N13	2.1	0.0	2.1
				N8	0.0	0.0	0.0	**N7**	**0.0**	**3.4**	**3.4**
				N9	0.0	0.0	0.0	N8	0.0	0.0	0.0
								N9	0.0	0.0	0.0

Note: **Bold** represents raw data of Table 6.1, crack length data in the upper standard deviation in the boundary region, 0-100°C ATC, UT.

SnPb, Aged, 4K, BI

UT3-U14A-SPA-AG-4- / UT3-U4A-SPA-AG-4- / UT3-U9A-SPA-AG-4-BI											
Joint No.	% crack length P	% crack length S	% crack length P+S	Joint No.	% crack length P	% crack length S	% crack length P+S	Joint No	% crack length P	% crack length S	% crack length P+S
G10	11.8	0.0	11.8	G10	5.9	0.0	5.9	G10	0.0	0.0	0.0
G11	0.0	0.0	0.0	G11	12.0	0.0	12.0	G11	2.2	0.0	2.2
G12	5.9	5.0	10.9	G12	21.2	0.0	21.2	G12	28.3	0.0	28.3
G13	0.0	0.0	0.0	G13	17.4	0.0	17.4	G13	23.3	0.0	23.3
G7	0.0	0.0	0.0	G7	30.1	0.0	30.1	**G7**	**7.1**	**0.0**	**7.1**
G8	0.0	0.0	0.0	G8	27.3	3.3	30.6	G8	0.0	0.0	0.0
G9	0.0	13.3	13.3	**G9**	**34.7**	**0.0**	**34.7**	**G9**	**1.2**	**0.0**	**1.2**
H13	5.0	8.3	13.4	H13	0.0	0.0	0.0	H13	20.2	0.0	20.2
H7	**25.0**	**0.0**	**25.0**	H7	20.6	0.0	20.6	H7	8.4	4.8	13.2
J13	1.6	0.0	1.6	J13	0.0	0.0	0.0	**J13**	**6.2**	**0.0**	**6.2**
J7	9.8	0.0	9.8	J7	18.6	0.0	18.6	J7	19.2	0.0	19.2
K7	13.6	0.0	13.6	K13	0.0	9.1	9.1	K13	0.0	0.0	0.0
L13	**3.9**	**0.0**	**3.9**	K7	4.7	0.0	4.7	**K7**	**4.6**	**0.0**	**4.6**
L7	3.5	0.0	3.5	L13	0.0	0.0	0.0	L13	5.3	0.0	5.3
M13	8.2	0.0	8.2	L7	0.0	0.0	0.0	L7	13.7	0.0	13.7
M7	15.1	0.0	15.1	M13	17.2	0.0	17.2	M13	0.0	12.3	12.3
N10	0.0	0.0	0.0	M7	9.1	0.0	9.1	M7	2.7	0.0	2.7
N11	8.8	0.0	8.8	**N10**	**0.0**	**0.0**	**0.0**	N10	0.0	0.0	0.0
N12	**5.7**	**11.8**	**17.6**	N11	0.0	5.4	5.4	N11	6.9	0.0	6.9
N13	**0.9**	**0.0**	**0.9**	N12	0.0	4.4	4.4	**N12**	**16.4**	**0.0**	**16.4**
N7	4.3	0.0	4.3	N13	0.0	0.0	0.0	N13	13.4	0.0	13.4
N8	11.4	0.0	11.4	**N7**	**0.0**	**0.0**	**0.0**	N7	16.3	0.0	16.3
N9	0.0	0.0	0.0	N8	0.0	0.0	0.0	**N8**	**0.0**	**0.0**	**0.0**
				N9	0.0	0.0	0.0	N9	0.0	0.0	0.0

Note: **Bold** represents raw data of Table 6.1, crack length data in the upper standard deviation in the boundary region, 0-100°C ATC, UT.

SnPb, Aged, 6K, BI

UT2-U13A-SPA-AG-6- / UT2-U3A-SPA-AG-6- / UT2-U8A-SPA-AG-6-BI											
Joint No.	% crack length P	% crack length S	% crack length P+S	Joint No.	% crack length P	% crack length S	% crack length P+S	Joint No	% crack length P	% crack length S	% crack length P+S
G10	0.0	0.0	0.0	G10	0.0	0.0	0.0	G10	16.8	0.0	16.8
G11	0.0	0.0	0.0	G11	0.0	0.0	0.0	G11	27.1	14.8	41.9
G12	31.5	0.0	31.5	**G12**	**0.0**	**0.0**	**0.0**	G12	25.8	5.6	31.3
G13	**3.5**	**0.0**	**3.5**	G13	0.0	0.0	0.0	G13	23.3	0.0	23.3
G7	15.3	12.9	28.2	G7	2.6	5.6	8.3	**G7**	**21.8**	**0.0**	**21.8**
G8	9.6	0.0	9.6	G8	0.0	0.0	0.0	G8	21.9	0.0	21.9
G9	8.6	0.0	8.6	G9	0.0	0.0	0.0	G9	35.8	3.4	39.2
H13	**26.8**	**0.0**	**26.8**	H13	3.7	0.0	3.7	**H13**	**20.2**	**0.0**	**20.2**
H7	27.5	0.0	27.5	H7	33.8	0.0	33.8	**H7**	**14.2**	**8.9**	**23.1**
J13	**16.4**	**0.0**	**16.4**	J13	0.0	3.0	3.0	J13	18.3	0.0	18.3
J7	**7.0**	**14.0**	**21.1**	**J7**	**8.8**	**0.0**	**8.8**	J7	15.0	0.0	15.0
K13	14.7	0.0	14.7	K13	0.0	0.0	0.0	K13	21.4	0.0	21.4
K7	0.0	0.0	0.0	K7	0.0	0.0	0.0	K7	0.0	2.1	2.1
L13	33.1	0.0	33.1	**L13**	**0.0**	**4.6**	**4.6**	L13	14.6	0.0	14.6
L7	46.3	6.0	52.3	L7	10.9	0.0	10.9	L7	0.0	9.4	9.4
M13	12.5	0.0	12.5	M13	0.0	0.0	0.0	**M13**	**30.6**	**0.0**	**30.6**
M7	0.0	4.0	4.0	M7	5.1	3.5	8.6	M7	20.2	0.0	20.2
N10	23.0	8.7	31.6	N10	12.2	5.6	17.8	N10	0.0	0.0	0.0
N11	38.4	0.0	38.4	N11	29.6	0.0	29.6	N11	0.0	0.0	0.0
N12	57.4	0.0	57.4	**N12**	**26.4**	**0.0**	**26.4**	N12	0.0	0.0	0.0
N13	40.0	0.0	40.0	N13	41.7	0.4	42.1	N13	5.0	0.0	5.0
N7	10.3	0.0	10.3	N7	12.3	0.0	12.3	**N7**	**0.0**	**4.6**	**4.6**
N8	40.1	2.6	42.7	N8	26.6	2.8	29.4	N8	0.0	0.0	0.0
N9	30.8	0.0	30.8	N9	22.7	2.1	24.8	N9	0.0	0.0	0.0

Note: **Bold** represents raw data of Table 6.1, crack length data in the upper standard deviation in the boundary region, 0-100°C ATC, UT.

SnPb, Aged, 8K, BI

UT1-U12A-SPA-AG-8- / UT1-U2A-SPA-AG-8- / UT1-U7A-SPA-AG-8-BI											
Joint No.	% crack length P	% crack length S	% crack length P+S	Joint No.	% crack length P	% crack length S	% crack length P+S	Joint No	% crack length P	% crack length S	% crack length P+S
G10	0.0	0.0	0.0	G10	0.0	0.0	0.0	G10	10.8	0.0	10.8
G11	22.9	0.0	22.9	G11	28.2	0.0	28.2	G11	7.4	2.9	10.4
G12	**14.4**	**0.0**	**14.4**	**G12**	**21.6**	**9.6**	**31.2**	G12	25.9	7.5	33.3
G13	26.2	0.0	26.2	G13	24.7	0.0	24.7	G13	9.2	2.4	11.6
G7	33.4	0.0	33.4	**G7**	**22.6**	**0.0**	**22.6**	G7	26.4	9.4	35.8
G8	**44.4**	**0.0**	**44.4**	G8	19.2	0.0	19.2	G8	19.5	0.0	19.5
G9	**8.4**	**0.0**	**8.4**	G9	0.0	0.0	0.0	G9	19.5	0.0	19.5
H13	21.4	3.1	24.5	H13	7.0	0.0	7.0	H13	6.9	0.0	6.9
H7	18.2	0.0	18.2	H7	30.5	0.0	30.5	**H7**	**8.3**	**0.0**	**8.3**
J13	29.1	19.2	48.3	J13	40.6	15.5	56.1	J13	13.2	0.0	13.2
J7	25.3	0.0	25.3	J7	32.6	0.0	32.6	J7	27.2	0.0	27.2
K13	5.8	3.6	9.4	K13	11.3	0.0	11.3	K13	16.3	0.0	16.3
K7	8.4	0.0	8.4	K7	35.4	0.0	35.4	K7	15.4	0.0	15.4
L13	22.4	13.5	36.0	L13	30.0	0.0	30.0	L13	26.4	6.7	33.1
L7	22.7	0.0	22.7	L7	32.4	2.3	34.6	L7	15.9	3.8	19.7
M13	5.5	4.6	10.1	M13	30.7	0.0	30.7	**M13**	**23.8**	**0.0**	**23.8**
M7	17.6	0.0	17.6	M7	46.7	0.0	46.7	M7	33.6	0.0	33.6
N10	0.0	0.0	0.0	N10	0.0	0.0	0.0	N10	0.0	0.0	0.0
N11	0.0	0.0	0.0	N11	5.7	0.0	5.7	N11	22.6	20.2	42.8
N12	24.5	0.0	24.5	**N12**	**23.7**	**0.0**	**23.7**	N12	3.9	0.0	3.9
N13	5.0	0.0	5.0	N13	27.9	0.0	27.9	N13	0.0	7.5	7.5
N7	26.5	0.0	26.5	**N7**	**31.9**	**0.0**	**31.9**	N7	8.9	0.0	8.9
N8	**27.3**	**0.0**	**27.3**	N8	20.7	0.0	20.7	N8	5.7	5.3	11.0
N9	20.9	0.0	20.9	N9	0.0	0.0	0.0	N9	2.6	0.0	2.6

Note: **Bold** represents raw data of Table 6.1, crack length data in the upper standard deviation in the boundary region, 0-100°C ATC, UT.

SnPb, Aged, 10K, BI

UT3-U12A-SPA-AG-10- / UT3-U2A-SPA-AG-10- / UT3-U7A-SPA-AG-10-BI											
Joint No.	% crack length P	% crack length S	% crack length P+S	Joint No.	% crack length P	% crack length S	% crack length P+S	Joint No	% crack length P	% crack length S	% crack length P+S
G10	0.0	3.8	3.8	G10	13.6	4.5	18.1	G10	0.5	0.0	0.5
G11	0.0	0.0	0.0	G11	18.1	9.6	27.7	G11	48.8	0.0	48.8
G12	20.9	0.0	20.9	G13	17.6	0.0	17.6	G12	55.0	0.0	55.0
G13	9.9	0.0	9.9	G7	29.6	7.1	36.8	G13	40.8	0.0	40.8
G7	13.3	0.0	13.3	G8	25.4	0.0	25.4	G7	48.3	0.0	48.3
G8	9.9	0.0	9.9	G9	31.2	0.0	31.2	G8	23.8	0.0	23.8
G9	6.0	4.9	10.9	H13	25.4	0.0	25.4	G9	32.9	0.0	32.9
H13	3.7	0.0	3.7	H7	31.9	0.0	31.9	H13	35.5	0.0	35.5
H7	34.9	0.0	34.9	J13	17.1	0.0	17.1	**H7**	**9.9**	**0.0**	**9.9**
J13	4.5	0.0	4.5	J7	35.0	0.0	35.0	J13	48.8	4.6	53.4
J7	24.0	0.0	24.0	K13	0.0	0.0	0.0	J7	29.6	0.0	29.6
K13	0.0	0.0	0.0	K7	46.0	16.5	62.5	K13	37.3	0.0	37.3
K7	31.5	0.0	31.5	L13	0.0	0.0	0.0	K7	19.5	0.0	19.5
L13	0.0	0.0	0.0	**L7**	**25.6**	**7.3**	**32.9**	L13	85.5	0.0	85.5
L7	48.5	0.0	48.5	**M13**	**5.2**	**0.0**	**5.2**	L7	20.0	0.0	20.0
M13	2.6	0.0	2.6	**M7**	**13.8**	**0.0**	**13.8**	M13	38.4	15.8	54.1
M7	**32.4**	**0.0**	**32.4**	N10	0.0	0.0	0.0	M7	5.7	0.0	5.7
N10	0.0	0.0	0.0	**N11**	**0.0**	**5.1**	**5.1**	**N10**	**0.0**	**0.0**	**0.0**
N11	11.0	11.0	21.9	**N12**	**5.6**	**0.0**	**5.6**	N11	12.0	0.0	12.0
N12	**0.2**	**7.2**	**7.4**	N13	0.5	0.0	0.5	**N12**	**65.1**	**0.0**	**65.1**
N13	3.0	4.0	7.0	N7	3.3	0.0	3.3	N13	57.0	0.0	57.0
N7	20.6	0.0	20.6	**N8**	**15.2**	**0.0**	**15.2**	N7	11.3	0.0	11.3
N8	29.0	0.0	29.0	N9	0.0	0.0	0.0	**N8**	**20.0**	**0.0**	**20.0**
N9	18.5	6.7	25.2					N9	16.7	0.0	16.7

Note: **Bold** represents raw data of Table 6.1, crack length data in the upper standard deviation in the boundary region, 0-100°C ATC, UT.

SnPb, Aged, 13K, BI

UT2-U11A-SPA-AG-13- / UT2-U1A-SPA-AG-13- / UT2-U6A-SPA-AG-13-BI											
Joint No.	% crack length P	% crack length S	% crack length P+S	Joint No.	% crack length P	% crack length S	% crack length P+S	Joint No	% crack length P	% crack length S	% crack length P+S
G10	0.0	0.0	0.0	G10	0.0	0.0	0.0	**G11**	**8.6**	**0.0**	**8.6**
G11	55.7	0.0	55.7	G11	31.5	0.0	31.5	**G12**	**3.7**	**0.0**	**3.7**
G12	50.7	0.0	50.7	G12	54.5	0.0	54.5	G13	17.5	12.2	29.7
G13	**14.5**	**0.0**	**14.5**	G13	56.8	0.0	56.8	G7	10.1	0.0	10.1
G7	41.5	0.0	41.5	G7	6.2	0.0	6.2	G8	20.0	0.0	20.0
G8	41.0	0.0	41.0	**G8**	**8.0**	**0.0**	**8.0**	G9	6.3	0.0	6.3
G9	7.5	0.0	7.5	G9	0.0	0.0	0.0	**H13**	**24.7**	**0.0**	**24.7**
H13	**21.7**	**0.0**	**21.7**	H13	13.6	6.5	20.2	H7	28.2	0.0	28.2
H7	19.6	0.0	19.6	H7	23.2	0.0	23.2	J13	14.2	15.8	30.0
J13	34.9	2.8	37.7	**J13**	**0.0**	**0.0**	**0.0**	**J7**	**6.7**	**0.0**	**6.7**
J7	34.3	17.8	52.1	J7	36.1	0.0	36.1	K13	20.3	4.2	24.4
K13	31.3	0.0	31.3	K13	0.0	0.0	0.0	K7	35.9	0.0	35.9
K7	0.0	2.8	2.8	K7	0.0	0.0	0.0	L13	53.0	0.0	53.0
L13	70.7	0.0	70.7	L13	2.5	4.8	7.2	L7	25.6	0.0	25.6
L7	0.0	9.4	9.4	L7	35.5	0.0	35.5	M13	50.3	0.0	50.3
M13	31.3	0.0	31.3	M13	5.3	4.2	9.5	**M7**	**21.8**	**0.2**	**22.0**
M7	25.0	6.8	31.8	M7	24.6	0.0	24.6	N10	6.3	5.8	12.1
N10	0.0	0.0	0.0	N10	0.0	0.0	0.0	N11	26.8	20.6	47.4
N11	0.0	0.0	0.0	**N11**	**0.0**	**0.0**	**0.0**	N12	34.7	0.0	34.7
N12	79.5	0.0	79.5	**N12**	**33.6**	**0.0**	**33.6**	N13	55.5	0.0	55.5
N13	**29.4**	**0.0**	**29.4**	**N13**	**0.0**	**0.0**	**0.0**	N7	37.3	19.4	56.7
N7	0.0	0.0	0.0	N7	40.9	0.0	40.9	N8	36.3	15.7	52.0
N8	22.9	0.0	22.9	N8	42.3	0.0	42.3	N9	0.0	0.0	0.0
N9	4.5	0.0	4.5	N9	16.4	0.5	17.0				

Note: **Bold** represents raw data of Table 6.1, crack length data in the upper standard deviation in the boundary region, 0-100°C ATC, UT.

SnPb, Aged, 16K, BI

UT4-U10A-SPA-AG-16- / UT4-U15A-SPA-AG-16- / UT4-U5A-SPA-AG-16-BI											
Joint No.	% crack length P	% crack length S	% crack length P+S	Joint No.	% crack length P	% crack length S	% crack length P+S	Joint No	% crack length P	% crack length S	% crack length P+S
G10	35.6	0.0	35.6	G10	67.4	0.0	67.4	G10	0.0	0.0	0.0
G11	41.2	3.5	44.6	G11	0.0	0.0	0.0	G11	37.7	20.2	57.8
G12	53.6	0.0	53.6	G12	58.9	0.0	58.9	G12	11.5	22.1	33.6
G13	39.3	0.0	39.3	G13	74.2	0.0	74.2	G13	13.3	0.0	13.3
G7	39.3	0.0	39.3	G7	25.2	0.0	25.2	G7	16.6	0.0	16.6
G8	45.3	0.0	45.3	G8	60.5	0.0	60.5	G8	11.8	1.8	13.6
G9	61.8	0.0	61.8	G9	67.2	0.0	67.2	G9	16.1	0.0	16.1
H13	21.9	0.0	21.9	H13	11.2	0.0	11.2	H13	57.3	0.0	57.3
H7	51.4	35.3	86.8	**H7**	**8.4**	**0.0**	**8.4**	H7	32.7	0.0	32.7
J13	66.1	0.0	66.1	J13	35.2	0.0	35.2	J13	29.0	0.0	29.0
J7	**26.1**	**0.0**	**26.1**	J7	53.1	0.0	53.1	J7	10.6	0.0	10.6
K13	15.0	0.0	15.0	K13	81.7	0.0	81.7	K13	22.5	0.0	22.5
K7	47.3	24.1	71.4	K7	0.0	0.0	0.0	K7	0.0	2.7	2.7
L13	**98.6**	**0.0**	**98.6**	L13	41.9	0.0	41.9	L13	70.7	0.0	70.7
L7	8.4	12.2	20.5	M13	57.1	0.0	57.1	L7	0.0	68.9	68.9
M13	44.1	0.0	44.1	M7	61.5	0.0	61.5	M13	63.5	0.0	63.5
M7	73.3	2.6	75.9	**N10**	**0.0**	**0.0**	**0.0**	M7	23.0	1.6	24.6
N10	0.0	2.6	2.6	N11	0.0	0.0	0.0	N10	0.0	33.6	33.6
N11	0.0	9.1	9.1	**N12**	**39.0**	**0.0**	**39.0**	**N11**	**3.7**	**20.0**	**23.7**
N12	**3.7**	**0.0**	**3.7**	N13	50.7	0.0	50.7	N7	21.4	3.0	24.4
N13	0.0	0.0	0.0	**N7**	**0.0**	**0.0**	**0.0**	**N8**	**20.7**	**0.0**	**20.7**
N7	4.7	19.3	24.0	N8	52.3	0.0	52.3	N9	10.4	4.1	14.5
N8	31.3	0.0	31.3	**N9**	**9.8**	**0.0**	**9.8**				
N9	**9.1**	**0.0**	**9.1**								

Note: **Bold** represents raw data of Table 6.1, crack length data in the upper standard deviation in the boundary region, 0-100°C ATC, UT.

SnPb, Air-Cooled, 2K, BI

UT5-U14A-SPA-A-2- / UT5-U4A-SPA-A-2- / UT5-U9A-SPA-A-2-BI											
Joint No.	% crack length P	% crack length S	% crack length P+S	Joint No.	% crack length P	% crack length S	% crack length P+S	Joint No	% crack length P	% crack length S	% crack length P+S
G8	10.6	0.0	10.6	G8	6.9	0.0	6.9	G10	5.2	0.0	5.2
K7	0.0	0.0	0.0	H7	2.3	0.0	2.3	**G8**	**1.4**	**0.0**	**1.4**
L7	0.0	6.0	6.0	L7	0.0	2.5	2.5	G9	0.0	0.0	0.0
M7	0.0	0.0	0.0	N7	0.0	0.0	0.0	J13	0.0	0.0	0.0
								K13	0.0	0.0	0.0

Note: **Bold** represents raw data of Table 6.1, crack length data in the upper standard deviation in the boundary region, 0-100°C ATC, UT.

SnPb, Air-Cooled, 4K, BI

UT7-U14A-SPA-A-4- / UT7-U4A-SPA-A-4- / UT7-U9A-SPA-A-4-BI											
Joint No.	% crack length P	% crack length S	% crack length P+S	Joint No.	% crack length P	% crack length S	% crack length P+S	Joint No	% crack length P	% crack length S	% crack length P+S
G10	2.8	0.0	2.8	G10	0.0	0.0	0.0	G10	4.7	0.0	4.7
G13	20.7	0.0	20.7	G11	1.8	0.0	1.8	G11	10.9	0.0	10.9
H7	11.6	0.0	11.6	G12	12.7	0.0	12.7	G12	18.1	0.0	18.1
J7	3.8	0.0	3.8	G13	10.6	0.0	10.6	G13	14.0	0.0	14.0
N10	17.2	0.0	17.2	G7	12.7	0.0	12.7	G7	7.8	0.0	7.8
N11	13.1	3.1	16.3	G8	6.2	2.5	8.6	H13	5.1	0.0	5.1
N12	6.6	0.3	7.0	G9	7.1	0.0	7.1	H7	7.2	0.0	7.2
N8	22.2	0.0	22.2	**H13**	**6.2**	**0.0**	**6.2**	J13	14.4	0.0	14.4
				H7	10.9	0.0	10.9	K13	2.6	1.0	3.7
				J13	0.0	1.1	1.1	**L13**	**9.5**	**0.0**	**9.5**
				J7	8.1	0.0	8.1	**L7**	**6.6**	**0.0**	**6.6**
				K13	0.0	0.0	0.0	M13	23.5	0.0	23.5
				K7	8.3	0.0	8.3	M7	12.0	0.0	12.0
				L13	7.1	0.0	7.1	N11	6.8	0.0	6.8
				L7	11.6	0.0	11.6	N12	6.0	2.1	8.1
				M13	1.6	3.2	4.8	N13	3.0	1.7	4.7
				M7	4.2	0.0	4.2	N8	9.8	0.0	9.8
				N10	**13.7**	**0.0**	**13.7**				
				N11	9.8	1.5	11.3				
				N12	12.5	4.1	16.6				
				N13	6.4	0.0	6.4				
				N7	14.3	0.0	14.3				
				N8	25.2	0.0	25.2				
				N9	15.1	0.0	15.1				

Note: **Bold** represents raw data of Table 6.1, crack length data in the upper standard deviation in the boundary region, 0-100°C ATC, UT.

SnPb, Air-Cooled, 6K, BI

UT6-U13A-SPA-A-6- / UT6-U3A-SPA-A-6- / UT6-U8A-SPA-A-6-BI											
Joint No.	% crack length P	% crack length S	% crack length P+S	Joint No.	% crack length P	% crack length S	% crack length P+S	Joint No	% crack length P	% crack length S	% crack length P+S
G10	5.6	1.4	7.0	G10	11.5	5.6	17.1	G10	38.5	4.7	43.2
G11	6.4	0.0	6.4	G11	31.0	17.1	48.1	G11	33.9	1.6	35.5
G12	**19.4**	**0.0**	**19.4**	G12	28.8	4.1	32.8	G12	40.9	1.6	42.5
G13	14.0	0.0	14.0	G13	34.6	3.2	37.8	G13	29.7	2.6	32.4
G7	16.8	3.5	20.3	G7	21.5	6.7	28.2	G7	31.4	0.0	31.4
G8	6.6	0.0	6.6	G8	22.4	5.6	28.1	G8	34.7	2.4	37.2
G9	18.4	1.2	19.6	G9	31.2	6.9	38.1	G9	42.1	5.4	47.5
H13	33.6	0.0	33.6	H13	33.3	0.0	33.3	H13	11.2	1.8	13.0
H7	27.9	0.0	27.9	H7	39.2	0.0	39.2	H7	2.7	4.4	7.1
J13	22.6	2.6	25.2	J13	27.5	0.0	27.5	**J13**	**42.6**	**1.9**	**44.5**
J7	**41.5**	**9.6**	**51.1**	J7	21.7	0.0	21.7	J7	23.1	0.0	23.1
K13	24.1	0.0	24.1	K13	36.9	0.0	36.9	K13	16.4	0.0	16.4
K7	11.3	0.0	11.3	K7	22.4	13.1	35.5	K7	9.6	6.1	15.7
L13	21.5	0.0	21.5	L13	19.8	0.0	19.8	L13	2.1	0.0	2.1
L7	22.9	0.0	22.9	L7	21.9	5.8	27.7	**L7**	**18.1**	**0.0**	**18.1**
M13	29.5	5.3	34.7	M13	84.7	19.9	104.6	**M13**	**44.9**	**0.0**	**44.9**
M7	19.0	3.3	22.3	M7	46.4	3.7	50.1	M7	40.0	3.9	43.9
N10	12.0	0.0	12.0	N10	4.1	10.6	14.6	N10	6.3	0.3	6.6
N11	18.8	1.4	20.2	N11	0.0	13.4	13.4	N11	4.9	0.0	4.9
N12	19.6	3.0	22.6	N12	19.9	0.0	19.9	N12	16.8	0.0	16.8
N13	20.9	14.5	35.3	N13	13.2	2.8	16.0	N13	27.7	3.5	31.2
N7	45.2	4.5	49.7	N7	30.9	1.9	32.8	**N7**	**7.3**	**0.0**	**7.3**
N8	36.7	0.0	36.7	N8	19.2	0.0	19.2	N8	17.7	0.0	17.7
N9	28.2	1.4	29.6	N9	22.2	0.0	22.2	N9	18.5	5.9	24.4

Note: **Bold** represents raw data of Table 6.1, crack length data in the upper standard deviation in the boundary region, 0-100°C ATC, UT.

SnPb, Air-Cooled, 8K, BI

UT5-U12A-SPA-A-8- / UT5-U2A-SPA-A-8- / UT5-U7A-SPA-A-8-BI											
Joint No.	% crack length P	% crack length S	% crack length P+S	Joint No.	% crack length P	% crack length S	% crack length P+S	Joint No	% crack length P	% crack length S	% crack length P+S
G10	0.0	1.8	1.8	G10	16.1	5.1	21.2	G10	0.0	2.3	2.3
G11	31.6	0.0	31.6	G11	29.5	0.0	29.5	G11	0.0	0.0	0.0
G12	33.7	0.0	33.7	G12	27.6	6.4	33.9	G12	7.0	4.1	11.1
G13	11.6	0.0	11.6	G7	21.6	3.0	24.6	G13	24.1	3.4	27.5
G7	26.1	15.8	41.9	G8	12.6	0.0	12.6	G7	0.0	5.4	5.4
G9	30.8	1.6	32.4	**G9**	**26.5**	**0.0**	**26.5**	G8	3.7	2.7	6.4
H13	17.1	0.0	17.1	**H13**	**11.8**	**0.0**	**11.8**	G9	7.0	0.0	7.0
H7	32.1	2.7	34.8	**H7**	**26.7**	**6.2**	**32.9**	H13	32.1	4.1	36.2
J13	20.9	0.0	20.9	J13	25.1	0.0	25.1	H7	26.4	6.2	32.6
J7	41.4	0.0	41.4	J7	13.8	2.8	16.6	J13	28.9	0.0	28.9
K13	15.8	0.0	15.8	K13	18.7	0.0	18.7	J7	10.9	0.0	10.9
K7	34.6	0.0	34.6	K7	20.9	2.7	23.5	K13	10.8	3.0	13.8
L13	33.8	0.0	33.8	L13	11.3	0.0	11.3	K7	0.0	0.0	0.0
L7	26.2	6.4	32.6	L7	25.3	2.8	28.1	L13	33.7	3.4	37.1
M13	41.1	0.0	41.1	M13	14.1	0.0	14.1	**L7**	**0.0**	**0.0**	**0.0**
M7	42.1	0.0	42.1	M7	27.6	7.6	35.2	M13	5.8	12.4	18.2
N10	0.0	0.0	0.0	N10	22.6	14.1	36.8	M7	25.9	3.7	29.6
N11	12.8	18.5	31.4	**N11**	**20.7**	**3.9**	**24.6**	N10	0.0	0.0	0.0
N12	33.5	11.1	44.6	**N12**	**13.4**	**14.5**	**27.9**	N11	0.0	0.0	0.0
N13	21.9	5.4	27.3	N13	15.7	7.1	22.8	N12	11.1	1.8	12.8
N7	38.7	8.0	46.7	N7	37.5	0.0	37.5	N13	49.8	4.3	54.0
N8	22.3	0.0	22.3	N8	47.6	12.9	60.5	N7	8.0	2.5	10.4
N9	22.8	0.0	22.8	N9	23.0	23.0	46.0	N8	15.5	3.2	18.7
								N9	26.0	0.0	26.0

Note: **Bold** represents raw data of Table 6.1, crack length data in the upper standard deviation in the boundary region, 0-100°C ATC, UT.

SnPb, Air-Cooled, 10K, BI

UT7-U12A-SPA-A-10- / UT7-U2A-SPA-A-10- / UT7-U7A-SPA-A-10-BI											
Joint No.	% crack length P	% crack length S	% crack length P+S	Joint No.	% crack length P	% crack length S	% crack length P+S	Joint No	% crack length P	% crack length S	% crack length P+S
G10	10.3	5.4	15.7	G10	0.0	0.0	0.0	G10	22.1	0.9	23.0
G11	23.0	14.7	37.7	G11	11.3	0.0	11.3	G11	23.5	0.0	23.5
G12	46.9	26.9	73.8	G12	24.9	0.0	24.9	G12	39.5	0.0	39.5
G13	39.0	0.4	39.4	G13	27.2	5.6	32.8	G13	17.5	1.2	18.7
G7	16.4	4.6	21.0	G7	27.5	3.0	30.5	G7	43.3	0.0	43.3
G8	11.1	2.7	13.8	**G8**	**17.5**	**0.0**	**17.5**	G8	35.8	0.0	35.8
G9	7.1	2.0	9.1	G9	10.2	3.0	13.2	G9	45.1	20.3	65.5
H13	52.4	2.5	54.9	H13	53.1	9.4	62.5	H13	4.5	0.0	4.5
H7	12.1	4.6	16.8	H7	19.1	0.0	19.1	H7	17.8	0.0	17.8
J13	13.1	0.0	13.1	J13	42.7	13.8	56.4	J13	19.2	2.2	21.4
J7	0.0	6.2	6.2	J7	13.8	0.0	13.8	J7	34.8	19.8	54.6
K13	36.3	2.5	38.8	K13	13.8	6.0	19.8	K13	23.5	0.0	23.5
K7	0.0	12.4	12.4	K7	18.0	0.0	18.0	K7	0.0	9.0	9.0
L13	25.0	6.2	31.2	L13	24.2	3.2	27.4	L13	10.0	7.8	17.8
L7	24.6	29.7	54.3	**L7**	**21.9**	**0.0**	**21.9**	L7	0.0	11.2	11.2
M13	**31.9**	**0.0**	**31.9**	M13	14.1	6.0	20.1	**M13**	**25.5**	**0.0**	**25.5**
M7	10.9	0.0	10.9	M7	25.4	8.5	33.9	M7	20.8	0.0	20.8
N10	19.8	0.0	19.8	N10	23.8	0.0	23.8	N10	8.3	0.0	8.3
N11	30.7	11.9	42.6	N11	53.3	0.0	53.3	N12	8.7	0.0	8.7
N12	57.8	13.1	70.9	N12	47.5	7.4	54.9	N13	11.6	0.0	11.6
N13	28.6	0.0	28.6	N13	37.6	0.0	37.6	N7	23.0	3.0	26.0
N7	26.2	0.0	26.2	N7	44.8	0.0	44.8	N8	34.2	0.0	34.2
N8	40.8	0.0	40.8	N8	44.3	9.5	53.8	N9	32.8	0.0	32.8
N9	41.2	0.0	41.2	N9	50.3	0.0	50.3				

Note: **Bold** represents raw data of Table 6.1, crack length data in the upper standard deviation in the boundary region, 0-100°C ATC, UT.

SnPb, Air-Cooled, 15K, BI

UT6-U11A-SPA-A-15- / UT6-U1A-SPA-A-15- / UT6-U6A-SPA-A-15-BI											
Joint No.	% crack length P	% crack length S	% crack length P+S	Joint No.	% crack length P	% crack length S	% crack length P+S	Joint No	% crack length P	% crack length S	% crack length P+S
G10	3.4	8.0	11.4	G10	20.9	0.0	20.9	G10	28.4	0.0	28.4
G11	18.2	5.7	23.9	G11	42.8	11.6	54.4	G11	25.3	6.1	31.4
G12	21.0	7.5	28.5	G12	32.6	0.0	32.6	G12	63.9	4.5	68.3
G13	48.7	11.2	59.9	G13	99.1	0.0	99.1	G13	47.4	0.0	47.4
G7	32.9	0.0	32.9	**G7**	**13.3**	**1.2**	**14.6**	G7	63.5	7.0	70.5
G8	14.8	0.0	14.8	G8	38.3	2.8	41.1	G8	47.1	9.9	57.0
G9	7.2	1.6	8.8	G9	38.6	0.0	38.6	G9	37.7	13.1	50.8
H13	44.4	5.4	49.8	H13	99.0	0.0	99.0	H13	25.9	0.0	25.9
H7	41.0	0.0	41.0	H7	80.0	6.3	86.3	**H7**	**38.2**	**5.4**	**43.5**
J13	5.0	0.0	5.0	J13	65.3	10.0	75.3	J13	59.6	1.8	61.4
J7	44.2	0.0	44.2	J7	89.1	2.6	91.8	J7	45.7	4.6	50.3
K13	28.0	12.4	40.4	K13	33.5	24.6	58.1	K13	19.8	0.0	19.8
K7	35.5	3.9	39.4	K7	22.5	3.7	26.1	K7	30.7	6.8	37.5
L13	57.2	8.5	65.7	L13	53.5	3.5	57.0	L13	16.6	0.0	16.6
L7	32.4	0.0	32.4	L7	40.0	0.0	40.0	L7	26.0	0.0	26.0
M13	60.0	19.3	79.3	M13	66.7	11.8	78.4	M13	68.1	7.4	75.6
M7	20.9	0.0	20.9	M7	35.2	7.5	42.8	M7	33.1	0.0	33.1
N10	34.3	0.0	34.3	N10	12.5	20.9	33.3	N10	5.6	0.0	5.6
N11	24.4	0.0	24.4	N11	23.3	0.0	23.3	N11	28.4	0.0	28.4
N12	57.3	2.7	59.9	N12	22.1	11.4	33.5	N12	7.6	0.0	7.6
N13	66.2	0.0	66.2	N13	3.5	3.7	7.2	N13	5.2	0.0	5.2
N7	49.8	0.0	49.8	N7	30.4	23.5	53.9	N7	34.8	4.8	39.6
N8	28.7	0.0	28.7	**N8**	**47.5**	**12.5**	**60.0**	N8	17.5	0.0	17.5
N9	35.1	0.0	35.1	N9	34.2	0.0	34.2	N9	22.7	0.0	22.7

Note: **Bold** represents raw data of Table 6.1, crack length data in the upper standard deviation in the boundary region, 0-100°C ATC, UT.

SnPb, Air-Cooled, 16K, BI

UT8-U10A-SPA-A-16- / UT8-U15A-SPA-A-16- / UT8-U5A-SPA-A-16-BI											
Joint No.	% crack length P	% crack length S	% crack length P+S	Joint No.	% crack length P	% crack length S	% crack length P+S	Joint No	% crack length P	% crack length S	% crack length P+S
G10	36.1	2.2	38.2	G10	37.3	4.6	41.9	G10	36.9	4.5	41.4
G11	37.5	1.4	39.0	**G11**	**15.8**	**3.1**	**18.8**	G11	53.2	0.0	53.2
G12	40.4	0.0	40.4	G12	53.4	2.9	56.3	**G12**	**2.3**	**0.0**	**2.3**
G13	50.0	0.0	50.0	**G13**	**20.7**	**2.9**	**23.6**	G13	47.3	0.0	47.3
G7	61.3	7.9	69.2	G7	11.4	9.6	21.0	G7	63.5	12.2	75.6
G8	49.3	8.6	57.9	**G8**	**45.5**	**14.3**	**59.8**	G8	68.1	3.6	71.6
G9	26.6	3.7	30.3	G9	0.0	13.9	13.9	G9	76.3	10.0	86.4
H13	59.3	0.0	59.3	H13	49.6	7.5	57.2	H13	43.7	0.0	43.7
H7	48.5	8.4	57.0	H7	53.7	0.0	53.7	H7	41.2	3.2	44.4
J13	35.9	0.0	35.9	J13	31.1	0.0	31.1	J13	49.3	1.8	51.1
J7	59.0	2.7	61.7	J7	0.0	0.0	0.0	J7	58.2	0.0	58.2
K13	27.0	0.0	27.0	K13	35.4	4.1	39.5	K13	39.6	6.5	46.1
K7	35.6	0.0	35.6	K7	4.2	0.0	4.2	K7	46.2	5.2	51.4
L13	38.5	0.0	38.5	**L13**	**45.7**	**0.0**	**45.7**	L13	56.6	4.8	61.4
L7	71.0	5.6	76.6	L7	26.1	0.0	26.1	L7	53.4	14.0	67.4
M13	55.8	2.1	58.0	M13	40.8	0.0	40.8	M13	63.4	3.9	67.4
M7	46.9	8.4	55.4	M7	3.0	0.0	3.0	M7	35.7	7.6	43.4
N10	44.8	12.6	57.3	N10	40.4	8.3	48.7	N10	52.1	2.5	54.7
N11	**50.7**	**8.7**	**59.4**	N11	60.6	10.6	71.2	N11	68.8	4.3	73.1
N12	56.6	3.2	59.9	**N12**	**53.3**	**7.0**	**60.3**	N12	59.7	0.0	59.7
N13	64.2	0.0	64.2	N13	49.4	0.4	49.8	N13	46.4	0.7	47.1
N7	57.3	0.0	57.3	N7	40.3	6.1	46.4	N7	50.9	6.3	57.2
N8	67.0	12.8	79.8	N8	47.3	11.1	58.3	**N8**	**54.6**	**7.9**	**62.5**
N9	46.9	10.0	56.9	N9	50.9	2.7	53.6	**N9**	**60.9**	**1.8**	**62.7**

Note: **Bold** represents raw data of Table 6.1, crack length data in the upper standard deviation in the boundary region, 0-100°C ATC, UT.

SnPb, Quenched, 2K, BI

UT10-U14A-SPA-Q-2- / UT10-U4A-SPA-Q-2- / UT10-U9A-SPA-Q-2-BI											
Joint No.	% crack length P	% crack length S	% crack length P+S	Joint No.	% crack length P	% crack length S	% crack length P+S	Joint No	% crack length P	% crack length S	% crack length P+S
G10	0.0	0.0	0.0					L13	0.0	0.0	0.0
G13	0.0	0.0	0.0					M13	4.2	0.0	4.2
G8	0.0	0.0	0.0								
H13	0.0	0.0	0.0								
J13	7.5	0.0	7.5								
J7	8.8	0.0	8.8								
K13	3.3	0.0	3.3								
K7	0.0	0.0	0.0								

SnPb, Quenched, 4K, BI

UT12-U14A-SPA-Q-4- / UT12-U4A-SPA-Q-4- / UT12-U9A-SPA-Q-4-BI											
Joint No.	% crack length P	% crack length S	% crack length P+S	Joint No.	% crack length P	% crack length S	% crack length P+S	Joint No	% crack length P	% crack length S	% crack length P+S
G10	15.8	5.3	21.1	G7	10.2	6.5	16.6	G12	3.1	0.0	3.1
G13	13.0	0.0	13.0	G8	11.5	0.0	11.5	G8	3.6	0.0	3.6
G8	13.1	0.0	13.1	H7	13.4	0.0	13.4	K7	0.0	0.0	0.0
J7	6.6	1.9	8.6	J7	14.7	4.6	19.4	L13	4.2	0.0	4.2
K7	8.4	0.0	8.4	K7	15.1	0.0	15.1	L7	6.2	0.0	6.2
N10	10.9	0.5	11.5	L7	16.3	3.6	19.9	M13	5.8	0.0	5.8
N12	3.6	0.0	3.6	M7	16.1	8.7	24.8	M7	3.3	0.0	3.3
N8	3.3	0.0	3.3	N7	17.8	0.0	17.8	N12	0.0	0.0	0.0
				N8	18.5	5.1	23.5	N7	0.0	0.0	0.0
								N8	1.9	0.0	1.9

SnPb, Quenched, 6K, BI

UT11-U13A-SPA-Q-6- / UT11-U3A-SPA-Q-6- / UT11-U8A-SPA-Q-6-BI											
Joint No.	% crack length P	% crack length S	% crack length P+S	Joint No.	% crack length P	% crack length S	% crack length P+S	Joint No	% crack length P	% crack length S	% crack length P+S
G12	7.8	0.0	7.8	G11	13.2	0.0	13.2	G10	0.0	0.0	0.0
G13	11.3	7.9	19.1	G12	7.4	0.0	7.4	G11	26.3	0.0	26.3
G7	20.0	0.0	20.0	G13	3.8	6.4	10.2	G12	27.7	0.0	27.7
G8	11.9	0.0	11.9	G8	21.2	0.0	21.2	G13	37.8	3.2	41.0
G9	8.1	0.0	8.1	H13	23.6	0.0	23.6	G7	21.3	0.0	21.3
H13	30.2	0.0	30.2	H7	29.2	0.0	29.2	G8	14.8	1.8	16.6
H7	0.0	20.4	20.4	J13	19.2	12.4	31.5	G9	32.3	0.0	32.3
J13	18.8	19.5	38.4	J7	22.1	0.0	22.1	H13	6.9	0.0	6.9
J7	17.6	0.0	17.6	K13	21.6	10.1	31.7	J13	0.0	0.0	0.0
K13	18.1	5.7	23.8	L13	16.8	1.6	18.3	K13	0.0	1.1	1.1
L13	19.1	7.7	26.8	L7	27.3	0.0	27.3	K7	13.4	2.5	15.9
L7	28.5	0.0	28.5	M13	21.2	13.1	34.3	L13	0.0	0.0	0.0
M13	0.0	0.0	0.0	M7	24.0	1.7	25.7	L7	7.5	0.0	7.5
M7	0.0	13.1	13.1	N11	26.5	0.0	26.5	M13	7.5	0.0	7.5
N12	26.1	2.1	28.2	N12	25.1	5.2	30.3	M7	57.4	0.0	57.4
N13	31.7	0.0	31.7	N13	31.2	3.4	34.6	N11	0.0	0.0	0.0
N7	28.2	0.0	28.2	N7	32.2	0.0	32.2	N12	4.3	0.0	4.3
N8	38.9	0.0	38.9	N8	26.2	3.1	29.3	N13	15.8	0.0	15.8
				N9	16.2	6.0	22.2	N8	0.0	0.0	0.0
								N9	0.0	2.5	2.5

SnPb, Quenched, 8K, BI

UT10-U12A-SPA-Q-8- / UT10-U2A-SPA-Q-8- / UT10-U7A-SPA-Q-8-BI											
Joint No.	% crack length P	% crack length S	% crack length P+S	Joint No.	% crack length P	% crack length S	% crack length P+S	Joint No	% crack length P	% crack length S	% crack length P+S
G10	13.4	0.0	13.4	G10	17.9	5.1	23.0	G10	28.9	2.6	31.5
G11	15.0	0.0	15.0	G11	18.2	12.6	30.9	G11	40.5	0.0	40.5
G12	0.0	0.0	0.0	G12	13.6	0.0	13.6	G12	34.4	0.0	34.4
G13	14.7	0.0	14.7	G13	7.5	1.8	9.3	G13	36.8	0.0	36.8
G7	43.5	4.1	47.6	G7	24.7	0.0	24.7	G7	33.6	0.0	33.6
G8	33.8	0.4	34.2	G8	29.6	0.7	30.3	G8	39.4	0.0	39.4
G9	35.7	0.0	35.7	G9	20.7	1.6	22.3	G9	39.8	4.6	44.4
H13	0.0	0.0	0.0	H13	0.0	0.0	0.0	H13	13.0	0.0	13.0
H7	3.4	6.0	9.4	H7	16.7	3.5	20.2	H7	11.5	0.0	11.5
J13	13.8	0.0	13.8	J13	10.9	0.0	10.9	J13	26.1	2.6	28.7
J7	5.2	3.3	8.6	J7	21.2	3.9	25.1	J7	29.3	0.0	29.3
K13	11.6	7.9	19.6	K13	18.8	11.9	30.7	K13	12.5	2.1	14.6
K7	0.0	0.0	0.0	K7	20.2	13.0	33.1	K7	24.7	0.0	24.7
L13	17.9	0.0	17.9	L13	9.1	0.0	9.1	L13	8.1	0.0	8.1
L7	34.9	17.3	52.1	L7	20.9	7.0	27.9	L7	55.4	1.6	57.0
M13	31.4	5.1	36.5	M13	33.1	0.0	33.1	M13	47.0	4.4	51.4
M7	22.4	0.0	22.4	M7	27.5	0.0	27.5	M7	28.4	0.0	28.4
N12	4.1	0.0	4.1	N10	16.8	0.0	16.8	N10	5.5	0.0	5.5
N13	0.0	0.0	0.0	N11	26.0	4.6	30.5	N11	18.0	0.0	18.0
N7	0.0	0.0	0.0	N12	16.0	0.0	16.0	N12	16.7	0.0	16.7
N8	0.0	0.0	0.0	N13	9.3	11.4	20.7	N13	20.3	4.1	24.3
N9	2.5	0.0	2.5	N7	15.1	0.0	15.1	N7	7.2	0.0	7.2
				N8	21.2	4.2	25.4	N8	15.0	0.0	15.0
				N9	12.1	0.0	12.1	N9	10.3	0.0	10.3

SnPb, Quenched, 10K, BI

UT12-U12A-SPA-Q-10- / UT12-U2A-SPA-Q-10- / UT12-U7A-SPA-Q-10-BI											
Joint No.	% crack length P	% crack length S	% crack length P+S	Joint No.	% crack length P	% crack length S	% crack length P+S	Joint No	% crack length P	% crack length S	% crack length P+S
G10	6.6	2.1	8.8	G10	5.9	3.8	9.8	G10	22.9	0.0	22.9
G11	9.2	0.0	9.2	G11	8.2	0.0	8.2	G11	44.4	7.6	52.0
G12	25.7	0.0	25.7	G12	6.7	0.0	6.7	G12	33.4	0.0	33.4
G13	37.9	0.0	37.9	G13	26.5	0.0	26.5	G13	42.3	2.5	44.7
G7	4.8	0.0	4.8	G7	9.4	0.0	9.4	G7	47.4	2.0	49.4
G8	8.1	0.0	8.1	G8	18.0	0.0	18.0	G8	32.9	10.2	43.2
G9	12.2	0.0	12.2	G9	21.2	0.0	21.2	G9	34.5	0.0	34.5
H13	25.4	0.0	25.4	H13	31.9	0.0	31.9	H13	28.3	0.0	28.3
H7	45.5	4.1	49.5	H7	43.5	0.0	43.5	H7	32.9	0.0	32.9
J13	35.6	0.0	35.6	J13	45.2	0.0	45.2	J13	45.5	0.0	45.5
J7	24.1	6.9	31.1	J7	15.6	4.8	20.4	J7	37.6	10.8	48.5
K13	29.3	0.0	29.3	K13	31.9	7.5	39.4	K13	15.4	0.0	15.4
K7	9.1	0.0	9.1	K7	20.9	0.0	20.9	K7	44.2	0.0	44.2
L13	34.4	0.0	34.4	L13	63.1	5.4	68.5	L13	17.8	0.4	18.1
L7	27.7	0.0	27.7	L7	35.3	0.0	35.3	L7	27.5	8.0	35.5
M13	44.6	0.0	44.6	M13	38.0	3.5	41.5	M13	49.0	0.0	49.0
M7	16.0	0.0	16.0	M7	25.9	0.0	25.9	M7	35.9	0.0	35.9
N10	25.9	0.0	25.9	N10	35.7	0.0	35.7	N10	0.0	0.0	0.0
N11	27.7	5.9	33.6	N11	34.5	7.8	42.3	N11	22.6	0.0	22.6
N12	27.6	0.0	27.6	N12	49.7	0.0	49.7	N12	24.2	0.0	24.2
N13	18.6	0.0	18.6	N13	37.1	6.6	43.7	N13	24.3	8.6	32.9
N7	24.0	0.0	24.0	N7	45.1	8.9	54.0	N7	25.0	0.0	25.0
N8	33.2	0.0	33.2	N8	45.3	5.6	50.8	N8	28.3	2.0	30.2
N9	33.1	19.2	52.4	N9	34.6	1.7	36.4	N9	13.0	0.0	13.0

SnPb, Quenched, 14K, BI

UT12-U11A-SPA-Q-14- / UT12-U1A-SPA-Q-14- / UT12-U6A-SPA-Q-14-BI											
Joint No.	% crack length P	% crack length S	% crack length P+S	Joint No.	% crack length P	% crack length S	% crack length P+S	Joint No	% crack length P	% crack length S	% crack length P+S
G10	3.8	8.1	11.8	G10	18.3	5.9	24.2	G10	6.4	1.4	7.8
G11	34.3	2.0	36.2	G11	24.9	17.4	42.3	G11	0.0	0.0	0.0
G12	43.5	0.0	43.5	G12	43.8	0.0	43.8	G12	42.8	3.6	46.3
G13	22.9	0.0	22.9	G13	31.8	0.0	31.8	G13	43.5	0.0	43.5
G7	33.7	0.0	33.7	G7	42.2	0.2	42.3	G7	31.1	0.0	31.1
G8	44.6	0.0	44.6	G8	38.3	0.0	38.3	G8	22.9	0.0	22.9
G9	12.4	0.0	12.4	G9	43.9	4.2	48.0	G9	13.1	2.0	15.1
H13	19.9	0.0	19.9	H13	11.1	0.0	11.1	H13	38.2	0.0	38.2
H7	25.7	0.0	25.7	H7	40.0	0.0	40.0	H7	22.7	1.6	24.3
J13	37.0	0.0	37.0	J13	28.9	14.4	43.2	J13	30.2	13.5	43.7
J7	38.7	0.0	38.7	J7	50.8	0.0	50.8	J7	38.9	0.0	38.9
K13	19.2	0.0	19.2	K13	4.6	0.0	4.6	K13	20.2	0.0	20.2
K7	33.0	0.0	33.0	K7	22.9	3.1	26.0	K7	33.5	0.0	33.5
L13	48.3	0.0	48.3	L13	9.9	0.0	9.9	L13	59.5	15.8	75.3
L7	39.6	0.0	39.6	L7	44.3	2.8	47.1	L7	40.9	0.0	40.9
M13	38.9	0.9	39.8	M13	24.2	0.0	24.2	M13	51.0	0.0	51.0
M7	33.7	0.0	33.7	M7	31.3	0.0	31.3	M7	21.0	0.0	21.0
N10	12.2	0.0	12.2	N10	6.1	4.3	10.4	N10	30.7	4.8	35.4
N11	29.7	3.7	33.4	N11	15.7	2.8	18.5	N11	27.5	14.9	42.4
N12	46.3	4.6	51.0	N12	36.6	0.0	36.6	N12	39.1	0.0	39.1
N13	39.1	0.0	39.1	N13	20.0	0.0	20.0	N13	45.3	0.0	45.3
N7	32.0	0.0	32.0	N7	44.0	0.0	44.0	N7	28.2	4.6	32.8
N8	29.5	0.0	29.5	N8	12.7	1.4	14.1	N8	64.6	0.0	64.6
N9	7.2	0.0	7.2	N9	5.2	3.7	8.9	N9	29.5	5.7	35.2

SnPb, Quenched, 16K, BI

UT13-U10A-SPA-Q-16- / UT13-U15A-SPA-Q-16- / UT13-U5A-SPA-Q-16-BI											
Joint No.	% crack length P	% crack length S	% crack length P+S	Joint No.	% crack length P	% crack length S	% crack length P+S	Joint No	% crack length P	% crack length S	% crack length P+S
G10	30.1	8.6	38.7	G10	42.9	4.7	47.6	G10	15.7	4.6	20.2
G11	44.4	8.0	52.4	G11	33.0	11.1	44.0	G12	17.0	0.0	17.0
G12	59.9	17.8	77.7	G12	62.1	0.0	62.1	G13	24.1	0.0	24.1
G13	31.7	0.0	31.7	G13	63.3	0.0	63.3	G7	46.6	0.0	46.6
G7	37.4	4.7	42.1	G7	41.3	7.6	48.9	G8	39.8	0.0	39.8
G8	27.5	11.0	38.5	G8	40.0	4.6	44.6	H13	61.4	10.9	72.3
G9	37.7	0.0	37.7	G9	31.5	8.2	39.7	J13	19.5	5.3	24.8
H13	53.2	0.0	53.2	H13	31.8	0.0	31.8	J7	15.3	0.0	15.3
H7	48.9	0.0	48.9	H7	24.5	0.0	24.5	K7	24.2	0.0	24.2
J13	41.5	0.0	41.5	J13	53.3	0.0	53.3	L13	18.0	7.2	25.2
J7	19.6	17.6	37.1	J7	62.0	3.8	65.8	L7	47.4	3.2	50.6
K13	28.1	5.3	33.3	K13	46.2	8.6	54.8	N10	48.0	10.2	58.2
K7	40.0	13.6	53.6	K7	4.9	6.8	11.7	N11	35.7	2.6	38.3
L13	30.9	17.5	48.4	L13	33.1	0.0	33.1	N12	50.2	18.4	68.6
L7	34.9	14.0	48.9	L7	75.7	10.5	86.2	N13	98.6	0.0	98.6
M13	59.9	0.0	59.9	M13	67.6	8.2	75.7	N7	53.4	0.0	53.4
M7	52.7	0.0	52.7	M7	35.6	0.0	35.6	N8	62.6	27.7	90.3
N10	25.3	0.0	25.3	N10	7.0	0.0	7.0	N9	45.3	11.7	57.1
N11	35.5	24.8	60.3	N11	28.0	0.0	28.0				
N12	33.2	0.0	33.2	N12	18.6	0.0	18.6				
N13	31.4	5.4	36.7	N13	29.3	0.0	29.3				
N7	8.7	3.6	12.3	N7	0.0	0.0	0.0				
N8	25.4	38.8	64.1	N8	3.6	0.0	3.6				
N9	98.8	0.0	98.8	N9	14.5	0.0	14.5				

Table G.4. % Crack length data for aged, air-cooled, and quenched SnAg joints in the boundary region at the board interface (nominal joint diameter=584 μm)

SnAg, Aged, 3K, BI

UT14-U14A-SA-AG-3- / UT14-U4A-SA-AG-3- / UT14-U9A-SA-AG-3-BI											
Joint No.	% crack length P	% crack length S	% crack length P+S	Joint No.	% crack length P	% crack length S	% crack length P+S	Joint No	% crack length P	% crack length S	% crack length P+S
G10	0.0	0.0	0.0	G10	0.0	0.0	0.0	G10	0.0	0.0	0.0
G11	0.0	0.0	0.0	G11	0.0	0.0	0.0	G11	0.0	0.0	0.0
G12	0.0	0.0	0.0	G12	0.0	0.0	0.0	**G12**	**0.0**	**3.5**	**3.5**
G13	**4.1**	**0.0**	**4.1**	**G13**	**0.0**	**0.0**	**0.0**	G13	0.0	3.9	3.9
G7	3.2	0.0	3.2	G7	2.1	0.0	2.1	G7	0.0	0.0	0.0
G8	0.0	0.0	0.0	G8	1.6	0.0	1.6	G8	0.0	0.0	0.0
G9	0.0	0.0	0.0	**G9**	**1.6**	**0.0**	**1.6**	G9	0.0	0.0	0.0
H13	0.0	1.8	1.8	H13	0.0	0.0	0.0	H13	3.3	0.0	3.3
H7	0.0	0.0	0.0	H7	0.0	0.0	0.0	H7	5.3	0.0	5.3
J13	2.8	0.0	2.8	J13	0.0	3.5	3.5	**J13**	**1.8**	**0.0**	**1.8**
J7	6.2	0.0	6.2	J7	6.0	0.0	6.0	J7	0.0	0.0	0.0
K13	0.0	0.0	0.0	K13				K13	0.0	0.0	0.0
K7	0.0	0.0	0.0	K7	0.0	0.0	0.0	K7	4.2	0.0	4.2
L13	**3.3**	**0.0**	**3.3**	L13				L13	9.0	0.0	9.0
L7	0.0	0.0	0.0	L7	0.0	0.0	0.0	L7	6.3	0.0	6.3
M13	0.0	0.0	0.0	M13	0.0	5.1	5.1	**M13**	**16.8**	**0.0**	**16.8**
M7	0.0	0.0	0.0	M7	0.0	0.0	0.0	**M7**	**0.2**	**0.0**	**0.2**
N11	0.0	0.0	0.0	N10	0.0	0.0	0.0	N10	0.0	6.5	6.5
N12	5.1	0.0	5.1	N11	0.0	0.0	0.0	N11	0.0	0.0	0.0
N13	**6.7**	**0.0**	**6.7**	N12	3.4	0.0	3.4	N12	0.0	0.0	0.0
N7	0.0	0.0	0.0	**N13**	**8.5**	**0.0**	**8.5**	N9	0.0	3.6	3.6
N8	0.0	0.0	0.0	N7	6.0	0.0	6.0				
N9	0.0	0.0	0.0	N9	0.0	0.0	0.0				

Note: **Bold** represents raw data of Table 6.2, crack length data in the upper standard deviation in the boundary region, 0-100°C ATC, UT.

SnAg, Aged, 6K, BI

UT16-U14A-SA-AG-6- / UT16-U4A-SA-AG-6- / UT16-U9A-SA-AG-6-BI											
Joint No.	% crack length P	% crack length S	% crack length P+S	Joint No.	% crack length P	% crack length S	% crack length P+S	Joint No	% crack length P	% crack length S	% crack length P+S
G10	2.8	0.0	2.8	G10	1.0	0.0	1.0	G10	10.9	0.0	10.9
G11	0.0	3.4	3.4	G11	8.9	0.0	8.9	G11	0.0	0.0	0.0
G12	17.4	0.0	17.4	G12	5.3	8.1	13.4	G12	12.0	0.0	12.0
G13	0.0	0.0	0.0	**G13**	**3.7**	**5.9**	**9.6**	G13	3.5	0.0	3.5
G7	**4.4**	**0.0**	**4.4**	**G7**	**0.0**	**0.0**	**0.0**	G7	5.6	0.0	5.6
G8	**17.6**	**0.0**	**17.6**	G8	0.0	1.8	1.8	G8	0.0	0.0	0.0
G9	2.6	3.3	5.9	G9	0.0	0.0	0.0	**G9**	**0.0**	**0.0**	**0.0**
H13	**6.9**	**0.0**	**6.9**	H13	1.0	0.0	1.0	H13	4.6	0.0	4.6
H7	0.0	0.0	0.0	H7	0.0	0.0	0.0	H7	0.0	0.0	0.0
J13	**6.9**	**0.0**	**6.9**	J13	0.0	0.0	0.0	J13	10.0	0.0	10.0
J7	0.0	0.0	0.0	J7	0.0	0.0	0.0	J7	0.0	0.0	0.0
K13	5.6	0.0	5.6	**K13**	**0.0**	**0.0**	**0.0**	K13	4.4	0.0	4.4
K7	0.0	1.2	1.2	K7	0.0	0.0	0.0	K7	0.0	0.0	0.0
L13	3.7	0.0	3.7	L13	0.0	0.0	0.0	L13	0.0	0.0	0.0
L7	0.0	0.0	0.0	L7	0.0	0.0	0.0	L7	0.0	1.9	1.9
M13	0.0	0.0	0.0	M13	3.3	0.0	3.3	**M13**	**5.1**	**0.0**	**5.1**
M7	**22.0**	**0.0**	**22.0**	M7	1.8	0.0	1.8	M7	0.0	0.0	0.0
N10	0.0	0.0	0.0	N11	0.0	0.0	0.0	N10	0.0	0.0	0.0
N11	**0.0**	**0.0**	**0.0**	N12	0.0	3.3	3.3	N11	0.0	0.0	0.0
N12	0.0	0.0	0.0	N13	0.0	0.0	0.0	N12	15.7	0.0	15.7
N13	**0.0**	**0.0**	**0.0**	**N7**	**5.4**	**0.0**	**5.4**	**N13**	**2.3**	**0.0**	**2.3**
N7	0.0	0.0	0.0	N8	2.3	0.0	2.3	N7	0.0	0.0	0.0
N8	0.0	0.0	0.0	N9	0.0	15.5	15.5	N8	0.0	0.0	0.0
N9	0.0	0.0	0.0					N9	0.0	0.0	0.0

Note: **Bold** represents raw data of Table 6.2, crack length data in the upper standard deviation in the boundary region, 0-100°C ATC, UT.

SnAg, Aged, 9K, BI

UT14-U12A-SA-AG-9- / UT14-U2A-SA-AG-9- / UT14-U7A-SA-AG-9-BI											
Joint No.	% crack length P	% crack length S	% crack length P+S	Joint No.	% crack length P	% crack length S	% crack length P+S	Joint No	% crack length P	% crack length S	% crack length P+S
G10	14.4	0.0	14.4	**G10**	**14.6**	**0.0**	**14.6**	G10	0.0	0.0	0.0
G11	**15.0**	**0.0**	**15.0**	G11	19.5	0.0	19.5	G11	0.0	0.0	0.0
G12	**24.3**	**3.9**	**28.2**	G12	16.1	0.0	16.1	G12	3.0	0.0	3.0
G7	**19.4**	**0.0**	**19.4**	G13	12.0	0.0	12.0	**G13**	**0.0**	**0.0**	**0.0**
G8	20.8	0.0	20.8	**G7**	**21.9**	**0.0**	**21.9**	G7	0.0	0.0	0.0
G9	3.5	0.0	3.5	**G8**	**31.5**	**0.0**	**31.5**	G9	0.0	0.0	0.0
H13	**7.8**	**0.0**	**7.8**	G9	26.2	0.0	26.2	H13	5.3	0.0	5.3
H7	0.0	0.0	0.0	H13	0.0	4.1	4.1	H7	12.3	0.0	12.3
J13	2.8	0.0	2.8	H7	0.0	5.4	5.4	J13	5.1	6.2	11.3
J7	4.2	0.0	4.2	J13	3.5	9.9	13.4	J7	0.0	4.5	4.5
K7	8.0	0.0	8.0	J7	22.3	0.0	22.3	K13	0.0	0.0	0.0
L13	2.1	0.0	2.1	K13	1.1	0.0	1.1	K7	0.0	0.0	0.0
L7	4.9	7.2	12.2	K7	0.0	3.0	3.0	L13	7.3	0.0	7.3
M13	0.0	0.0	0.0	L13	26.7	4.2	31.0	**L7**	**19.2**	**0.0**	**19.2**
M7	3.0	3.2	6.2	L7	6.9	7.4	14.3	**M13**	**0.0**	**0.0**	**0.0**
N10	0.0	0.0	0.0	M13	14.4	20.7	35.1	M7	4.4	0.0	4.4
N11	0.0	0.0	0.0	M7	7.7	0.0	7.7	**N10**	**26.1**	**0.0**	**26.1**
N12	0.0	0.0	0.0	N10	0.0	0.0	0.0	N11	26.1	0.0	26.1
N13	0.0	0.0	0.0	**N11**	**4.4**	**0.0**	**4.4**	N12	21.7	0.0	21.7
N7	0.0	0.0	0.0	N12	0.0	0.0	0.0	**N13**	**19.6**	**0.0**	**19.6**
N8	4.8	0.0	4.8	N13	12.4	0.0	12.4	N7	18.5	0.0	18.5
N9	0.0	0.0	0.0	N7	0.0	0.0	0.0	N8	30.2	0.0	30.2
				N8	0.0	0.0	0.0				
				N9	0.0	0.0	0.0				

Note: **Bold** represents raw data of Table 6.2, crack length data in the upper standard deviation in the boundary region, 0-100°C ATC, UT.

SnAg, Aged, 12K, BI

UT16-U12A-SA-AG-12- / UT16-U2A-SA-AG-12- / UT16-U7A-SA-AG-12-BI											
Joint No.	% crack length P	% crack length S	% crack length P+S	Joint No.	% crack length P	% crack length S	% crack length P+S	Joint No	% crack length P	% crack length S	% crack length P+S
G10	14.0	0.0	14.0	G10	0.0	0.0	0.0	G10	0.0	0.0	0.0
G11	12.3	7.2	19.6	G12	13.5	9.2	22.7	G11	36.8	0.0	36.8
G12	6.4	2.5	8.9	**G13**	**20.4**	**0.0**	**20.4**	**G12**	**32.6**	**0.0**	**32.6**
G13	14.6	8.9	23.4	G7	0.0	9.5	9.5	G13	25.2	0.0	25.2
G7	0.0	22.7	22.7	**G8**	**12.5**	**0.0**	**12.5**	G7	30.2	0.0	30.2
G8	6.2	15.1	21.3	G9	0.0	2.6	2.6	G8	5.9	0.0	5.9
G9	**11.8**	**9.5**	**21.3**	H13	23.3	0.0	23.3	**G9**	**20.8**	**0.0**	**20.8**
H13	9.0	0.0	9.0	H7	30.7	0.0	30.7	H13	0.0	0.0	0.0
H7	37.7	0.0	37.7	J13	16.4	0.0	16.4	H7	0.0	0.0	0.0
J13	20.6	0.0	20.6	J7	0.0	8.8	8.8	J13	22.9	0.0	22.9
J7	3.2	0.0	3.2	K13	7.2	0.0	7.2	J7	0.0	2.1	2.1
K13	19.9	12.3	32.1	K7	0.0	0.0	0.0	K13	0.0	0.0	0.0
K7	17.1	2.1	19.2	L13	2.1	0.0	2.1	K7	0.0	0.0	0.0
L13	12.0	0.2	12.2	L7	0.0	1.6	1.6	**L13**	**0.0**	**0.0**	**0.0**
L7	11.6	0.0	11.6	M13	23.8	9.6	33.4	L7	12.7	5.8	18.5
M13	34.0	0.0	34.0	M7	32.1	0.0	32.1	M13	9.8	0.0	9.8
M7	8.3	0.0	8.3	N10	11.6	0.0	11.6	M7	10.0	0.0	10.0
N10	0.0	0.0	0.0	N12	8.5	0.0	8.5	N10	10.1	0.0	10.1
N11	0.0	14.1	14.1	**N13**	**16.6**	**3.2**	**19.7**	N11	0.0	0.0	0.0
N12	**17.6**	**6.0**	**23.6**	N7	4.2	0.0	4.2	N12	0.0	0.0	0.0
N13	1.8	24.5	26.3	**N8**	**20.8**	**3.0**	**23.8**	N13	0.7	0.0	0.7
N7	0.0	10.4	10.4	N9	0.0	15.3	15.3	N7	0.0	1.8	1.8
N8	0.0	6.0	6.0					N8	0.0	0.0	0.0
N9	0.0	0.0	0.0					N9	0.0	0.0	0.0

Note: **Bold** represents raw data of Table 6.2, crack length data in the upper standard deviation in the boundary region, 0-100°C ATC, UT.

SnAg, Aged, 15K, BI

UT14-U11A-SA-AG-15- / UT14-U1A-SA-AG-15- / UT14-U6A-SA-AG-15-BI											
Joint No.	% crack length P	% crack length S	% crack length P+S	Joint No.	% crack length P	% crack length S	% crack length P+S	Joint No	% crack length P	% crack length S	% crack length P+S
G10	0.0	0.0	0.0	**G10**	**0.0**	**0.0**	**0.0**	G10	13.9	0.0	13.9
G11	**2.8**	**0.0**	**2.8**	G11	0.0	14.0	14.0	G11	18.6	0.0	18.6
G12	**21.3**	**0.0**	**21.3**	G12	0.0	0.0	0.0	G12	20.8	4.6	25.4
G13	0.0	3.2	3.2	**G13**	**21.8**	**4.4**	**26.3**	**G13**	**36.8**	**0.0**	**36.8**
G7	0.0	0.0	0.0	G7	0.0	0.0	0.0	G7	6.0	0.0	6.0
G9	15.5	0.0	15.5	G8	0.0	0.0	0.0	G8	0.0	5.3	5.3
H13	0.0	2.5	2.5	**G9**	**0.0**	**0.0**	**0.0**	G9	15.0	19.6	34.5
H7	0.0	0.0	0.0	H13	4.4	0.0	4.4	**H13**	**8.3**	**0.0**	**8.3**
J13	**0.0**	**9.9**	**9.9**	H7	5.7	0.0	5.7	H7	0.0	0.0	0.0
J7	4.4	2.3	6.7	J7	0.0	0.0	0.0	**J13**	**29.1**	**0.0**	**29.1**
K13	3.2	2.1	5.3	**K13**	**1.6**	**20.6**	**22.2**	J7	29.1	0.0	29.1
K7	0.0	0.0	0.0	K7	5.5	0.0	5.5	K13	1.4	20.1	21.5
L13	21.1	0.0	21.1	L13	31.4	5.0	36.4	K7	0.0	0.0	0.0
L7	0.0	0.0	0.0	L7	16.5	0.0	16.5	L13	4.3	6.6	10.8
M13	0.0	3.0	3.0	M13	34.5	1.2	35.8	L7	0.0	7.6	7.6
M7	0.0	0.0	0.0	M7	0.0	0.0	0.0	**M13**	**43.5**	**0.0**	**43.5**
N11	9.0	0.0	9.0	N10	10.3	0.0	10.3	M7	22.7	0.0	22.7
N12	22.6	0.0	22.6	N11	4.4	2.8	7.3	N11	0.0	0.0	0.0
N13	2.1	2.1	4.2	N12	43.1	0.0	43.1	N12	0.0	46.2	46.2
N7	0.0	0.0	0.0	N13	38.7	0.0	38.7	N13	0.0	21.7	21.7
N8	10.8	0.0	10.8	N7	4.9	0.0	4.9	N7	9.6	0.0	9.6
N9	**2.1**	**2.3**	**4.4**	N8	3.5	0.0	3.5	N8	19.4	0.0	19.4
				N9	12.1	0.0	12.1				

Note: **Bold** represents raw data of Table 6.2, crack length data in the upper standard deviation in the boundary region, 0-100°C ATC, UT.

SnAg, Aged, 18K, 21K, 24K, BI

UT16-U1A-SA-AG-18- / UT15-U1A-SA-AG-21- / UT17-U2A-SA-AG-24-BI											
Joint No.	% crack length P	% crack length S	% crack length P+S	Joint No.	% crack length P	% crack length S	% crack length P+S	Joint No	% crack length P	% crack length S	% crack length P+S
G10	0.0	2.8	2.8	**G10**	**4.9**	**0.0**	**4.9**				
G11	35.8	0.0	35.8	G11	0.0	6.2	6.2				
G12	38.6	0.0	38.6	G12	13.4	11.6	25.0				
G13	12.7	0.0	12.7	G13	0.0	13.4	13.4				
G7	**37.9**	**0.0**	**37.9**	G7	33.1	0.0	33.1				
G8	13.2	0.0	13.2	G8	0.0	0.0	0.0				
G9	12.7	0.0	12.7	H13	15.2	3.9	19.0				
H13	26.5	2.1	28.6	H7	40.2	0.0	40.2				
H7	1.4	3.7	5.1	J13	15.4	0.0	15.4				
J13	2.3	0.0	2.3	J7	0.0	0.0	0.0				
J7	0.0	0.0	0.0	K13	0.0	0.0	0.0				
K13	2.6	6.5	9.2	K7	0.0	0.0	0.0				
K7	0.0	0.0	0.0	L13	0.0	0.0	0.0				
L13	8.6	0.0	8.6	**L7**	**17.6**	**17.1**	**34.7**				
L7	0.0	0.0	0.0	**M13**	**17.2**	**0.0**	**17.2**				
M13	**0.0**	**0.0**	**0.0**	M7	0.0	19.9	19.9				
M7	0.0	0.0	0.0	N10	0.0	2.5	2.5				
N10	0.0	11.1	11.1	N12	21.0	0.0	21.0				
N11	7.1	0.0	7.1	N13	0.0	23.4	23.4				
N12	34.0	0.0	34.0	N7	22.9	0.0	22.9				
N13	16.0	0.0	16.0	**N8**	**38.1**	**0.0**	**38.1**				
N7	**18.3**	**0.0**	**18.3**	N9	23.6	0.0	23.6				
N8	0.0	0.0	0.0								
N9	**2.5**	**5.0**	**7.5**								

Note: **Bold** represents raw data of Table 6.2, crack length data in the upper standard deviation in the boundary region, 0-100°C ATC, UT.

SnAg, Air-Cooled, 3K, BI

UT18-U14A-SA-A-3- / UT18-U4A-SA-A-3- / UT18-U9A-SA-A-3-BI											
Joint No.	% crack length P	% crack length S	% crack length P+S	Joint No.	% crack length P	% crack length S	% crack length P+S	Joint No	% crack length P	% crack length S	% crack length P+S
G10	0.0	0.0	0.0	G10	2.8	0.0	2.8	G10	2.3	0.0	2.3
G12	4.4	0.0	4.4	G11	3.9	0.0	3.9	G11	0.0	0.0	0.0
G13	1.2	0.0	1.2	**G12**	**12.3**	**4.9**	**17.2**	G12	19.9	0.0	19.9
G7	4.8	0.0	4.8	G13	3.0	0.0	3.0	**G13**	**30.6**	**0.0**	**30.6**
G8	24.0	0.0	24.0	G7	5.1	0.0	5.1	G7	2.6	0.0	2.6
G9	0.0	0.0	0.0	G8	10.2	0.0	10.2	G8	2.5	1.4	3.9
H7	0.0	4.3	4.3	G9	9.0	0.0	9.0	G9	5.8	0.0	5.8
J13	1.8	0.0	1.8	H13	7.4	0.0	7.4	H13	9.7	0.0	9.7
J7	2.1	0.0	2.1	H7	6.3	3.2	9.5	H7	0.0	8.1	8.1
K13	0.9	0.0	0.9	J13	1.9	0.0	1.9	J13	6.5	0.0	6.5
K7	0.0	0.0	0.0	J7	1.9	0.0	1.9	**J7**	**19.0**	**3.7**	**22.7**
L13	3.8	9.2	13.1	K13	3.0	0.0	3.0	K13	0.0	0.0	0.0
L7	10.9	0.0	10.9	**K7**	**19.0**	**0.0**	**19.0**	K7	0.0	0.0	0.0
M7	0.0	0.0	0.0	L13	3.2	0.0	3.2	L13	0.0	0.0	0.0
N10	2.4	0.0	2.4	L7	0.0	0.0	0.0	L7	0.0	5.3	5.3
N11	3.7	0.0	3.7	**M13**	**10.5**	**0.0**	**10.5**	M13	10.5	0.0	10.5
N12	4.4	0.0	4.4	M7	0.0	3.3	3.3	M7	0.0	0.0	0.0
N7	8.4	0.0	8.4	N10	2.1	2.1	4.2	**N11**	**3.3**	**0.0**	**3.3**
N8	1.6	0.0	1.6	N11	0.0	0.0	0.0	**N13**	**13.9**	**0.0**	**13.9**
N9	1.7	0.0	1.7	N12	1.6	0.0	1.6	N7	0.0	2.5	2.5
				N13	**2.6**	**0.0**	**2.6**	N8	0.0	0.0	0.0
				N7	0.0	4.2	4.2	N9	2.6	0.0	2.6
				N8	**6.7**	**0.0**	**6.7**				
				N9	10.5	0.0	10.5				

Note: **Bold** represents raw data of Table 6.2, crack length data in the upper standard deviation in the boundary region, 0-100°C ATC, UT.

SnAg, Air-Cooled, 6K, BI

UT20-U14A-SA-A-6- / UT20-U4A-SA-A-6- / UT20-U9A-SA-A-6-BI											
Joint No.	% crack length P	% crack length S	% crack length P+S	Joint No.	% crack length P	% crack length S	% crack length P+S	Joint No	% crack length P	% crack length S	% crack length P+S
G10	**9.2**	**13.9**	**23.2**	G10	12.5	1.0	13.6	G10	2.8	0.0	2.8
G11	**16.2**	**0.0**	**16.2**	G11	13.8	0.0	13.8	G11	0.0	9.2	9.2
G12	13.4	0.0	13.4	G12	12.7	4.2	16.9	G12	4.4	0.0	4.4
G13	2.6	0.0	2.6	G13	6.6	0.0	6.6	G13	16.9	0.0	16.9
G7	12.2	0.0	12.2	G7	12.0	1.4	13.4	G7	16.2	2.4	18.6
G8	5.2	0.0	5.2	G8	9.8	0.0	9.8	G8	31.7	0.7	32.4
G9	8.5	0.0	8.5	G9	7.7	9.8	17.4	G9	0.0	7.5	7.5
H13	17.8	0.0	17.8	**H13**	**9.9**	**14.1**	**24.0**	H13	8.4	4.2	12.5
H7	11.3	3.1	14.5	H7	0.0	5.2	5.2	H7	3.5	16.9	20.4
J13	3.5	0.0	3.5	**J13**	**28.8**	**4.9**	**33.6**	J13	30.1	0.0	30.1
J7	7.8	5.9	13.8	J7	3.7	0.0	3.7	J7	8.9	11.7	20.6
K13	0.0	5.2	5.2	**K13**	**12.4**	**6.3**	**18.6**	K13	14.6	0.0	14.6
K7	0.0	0.0	0.0	K7	11.2	5.2	16.4	K7	2.3	3.8	6.1
L13	1.2	0.0	1.2	L13	5.9	0.0	5.9	L13	2.4	14.6	17.1
L7	22.7	0.0	22.7	L7	27.5	2.4	30.0	L7	36.1	8.7	44.8
M13	4.4	9.4	13.8	M13	24.9	0.0	24.9	**M13**	**17.4**	**7.5**	**24.9**
M7	2.3	2.6	4.9	M7	8.0	1.9	9.9	M7	11.0	3.1	14.1
N10	**5.4**	**19.7**	**25.1**	N10	6.4	13.2	19.7	N10	0.0	0.0	0.0
N11	0.0	10.1	10.1	N11	8.0	0.0	8.0	N11	3.1	0.0	3.1
N12	28.1	0.0	28.1	N12	0.0	0.0	0.0	N12	8.7	0.0	8.7
N13	12.4	9.2	21.6	N13	1.7	3.7	5.4	N13	13.4	0.0	13.4
N7	10.8	0.0	10.8	N7	3.7	0.0	3.7	**N7**	**32.8**	**0.0**	**32.8**
N8	23.3	0.0	23.3	N8	0.0	8.5	8.5	N8	0.5	2.6	3.1
N9	2.3	4.9	7.1	N9	15.3	0.0	15.3	N9	15.2	0.0	15.2

Note: **Bold** represents raw data of Table 6.2, crack length data in the upper standard deviation in the boundary region, 0-100°C ATC, UT.

SnAg, Air-Cooled, 9K, BI

UT19-U13A-SA-A-9- / UT19-U3A-SA-A-9- / UT19-U8A-SA-A-9-BI											
Joint No.	% crack length P	% crack length S	% crack length P+S	Joint No.	% crack length P	% crack length S	% crack length P+S	Joint No	% crack length P	% crack length S	% crack length P+S
G10	**28.4**	**0.0**	**28.4**	G10	13.1	22.9	36.0	G10	0.0	0.0	0.0
G11	20.6	20.9	41.5	**G11**	**28.9**	**18.6**	**47.5**	G11	10.5	0.0	10.5
G12	28.9	0.0	28.9	G12	35.8	0.0	35.8	G12	17.0	0.0	17.0
G13	13.3	0.0	13.3	G13	17.9	8.3	26.2	G13	10.7	0.0	10.7
G7	17.6	0.0	17.6	G7	5.7	3.3	9.0	G7	7.2	0.0	7.2
G8	42.7	0.0	42.7	G8	27.2	0.0	27.2	G8	20.6	0.0	20.6
G9	20.0	7.3	27.3	**G9**	**33.2**	**16.1**	**49.3**	G9	1.2	0.0	1.2
H13	**13.5**	**17.9**	**31.4**	H13	6.0	22.3	28.4	H13	7.4	5.4	12.8
H7	11.5	0.0	11.5	H7	3.1	3.0	6.1	H7	21.8	12.3	34.1
J13	21.5	0.0	21.5	J13	18.8	2.4	21.3	**J13**	**21.4**	**12.5**	**33.9**
J7	9.8	0.0	9.8	J7	28.0	2.8	30.9	J7	10.5	0.0	10.5
K13	**29.8**	**1.8**	**31.6**	K13	31.9	0.0	31.9	K13	8.8	0.0	8.8
K7	**6.4**	**9.9**	**16.3**	K7	25.5	0.0	25.5	K7	18.6	0.0	18.6
L13	0.0	15.4	15.4	L13	8.5	27.0	35.5	L13	10.9	0.0	10.9
L7	14.9	0.0	14.9	**L7**	**31.4**	**0.0**	**31.4**	L7	27.6	0.0	27.6
M13	27.3	4.6	31.9	M13	28.7	0.0	28.7	M13	0.0	0.0	0.0
M7	14.9	5.0	19.9	M7	20.4	0.2	20.6	**M7**	**23.6**	**0.0**	**23.6**
N10	5.9	0.0	5.9	N11	2.0	0.0	2.0	N10	0.0	0.0	0.0
N11	0.0	0.0	0.0	N12	0.0	5.1	5.1	**N11**	**24.1**	**10.4**	**34.5**
N12	4.6	0.0	4.6	N13	0.0	22.8	22.8	N12	11.8	4.0	15.8
N13	0.0	0.0	0.0	**N7**	**7.6**	**2.8**	**10.5**	N13	34.5	0.0	34.5
N7	24.5	1.6	26.1	**N8**	**25.0**	**0.0**	**25.0**	N7	11.1	0.0	11.1
N8	12.9	18.6	31.6	N9	0.0	12.1	12.1	**N8**	**19.0**	**0.0**	**19.0**
N9	6.9	6.6	13.5					N9	22.3	0.0	22.3

Note: **Bold** represents raw data of Table 6.2, crack length data in the upper standard deviation in the boundary region, 0-100°C ATC, UT.

SnAg, Air-Cooled, 12K, BI

UT18-U12A-SA-A-12- / UT18-U2A-SA-A-12- / UT18-U7A-SA-A-12-BI											
Joint No.	% crack length P	% crack length S	% crack length P+S	Joint No.	% crack length P	% crack length S	% crack length P+S	Joint No	% crack length P	% crack length S	% crack length P+S
G10	27.7	0.0	27.7	G10	10.1	3.4	13.5	G10	22.5	6.2	28.7
G11	13.1	8.5	21.6	**G11**	**6.9**	**17.9**	**24.8**	G11	23.9	10.5	34.4
G12	29.4	0.0	29.4	**G12**	**25.5**	**0.0**	**25.5**	G12	27.1	0.0	27.1
G13	16.0	6.4	22.3	G13	1.4	0.0	1.4	G13	23.2	16.1	39.4
G7	**35.3**	**18.4**	**53.7**	G7	0.0	0.0	0.0	G7	18.3	0.0	18.3
G8	22.7	0.0	22.7	G8	0.0	4.1	4.1	G8	19.2	17.4	36.5
G9	8.5	5.5	14.0	G9	3.7	9.9	13.7	G9	30.1	0.0	30.1
H13	8.9	7.3	16.1	**H13**	**32.6**	**13.5**	**46.1**	H13	19.2	0.0	19.2
H7	10.1	0.0	10.1	H7	33.0	1.4	34.4	H7	20.7	12.2	33.0
J13	3.5	5.7	9.2	J13	16.8	21.1	38.0	J13	38.1	0.0	38.1
J7	6.0	0.0	6.0	J7	0.0	15.6	15.6	J7	19.2	0.0	19.2
K13	14.4	1.1	15.4	K13	9.9	6.0	16.0	K13	18.4	0.0	18.4
K7	7.8	19.0	26.8	K7	0.0	0.0	0.0	K7	27.8	0.0	27.8
L13	**26.6**	**0.0**	**26.6**	**L13**	**18.8**	**3.7**	**22.5**	L13	20.4	11.0	31.4
L7	26.4	0.0	26.4	L7	32.6	13.3	45.9	L7	14.5	30.7	45.2
M13	2.1	0.0	2.1	**M13**	**16.8**	**9.8**	**26.6**	M13	31.2	30.7	61.9
M7	**24.8**	**21.3**	**46.1**	M7	6.4	4.8	11.2	M7	18.6	0.0	18.6
N10	0.4	0.0	0.4	N10	16.5	0.0	16.5	N10	0.0	0.0	0.0
N11	20.6	5.1	25.7	N11	18.8	0.0	18.8	N11	2.7	18.6	21.3
N12	0.0	0.0	0.0	N12	6.9	29.4	36.4	N12	37.6	0.0	37.6
N13	**17.4**	**7.3**	**24.7**	N13	17.2	20.7	38.0	N13	15.1	0.0	15.1
N7	4.3	5.5	9.8	N7	40.6	0.0	40.6	N7	26.2	0.0	26.2
N8	0.0	3.4	3.4	N8	23.1	14.0	37.1	N8	25.7	0.0	25.7
N9	6.6	9.8	16.3	N9	22.2	20.9	43.1	**N9**	**19.9**	**10.3**	**30.1**

Note: **Bold** represents raw data of Table 6.2, crack length data in the upper standard deviation in the boundary region, 0-100°C ATC, UT.

SnAg, Air-Cooled, 15K, BI

UT20-U12A-SA-A-15- / UT20-U2A-SA-A-15- / UT20-U7A-SA-A-15-BI											
Joint No.	% crack length P	% crack length S	% crack length P+S	Joint No.	% crack length P	% crack length S	% crack length P+S	Joint No	% crack length P	% crack length S	% crack length P+S
G10	12.4	1.9	14.3	G10	21.4	3.3	24.7	G10	35.9	7.7	43.6
G11	20.0	0.0	20.0	G11	13.8	3.7	17.4	G11	17.8	11.0	28.8
G12	**29.6**	**18.1**	**47.7**	G12	25.1	24.6	49.7	**G12**	**28.6**	**22.7**	**51.2**
G13	13.9	6.8	20.7	G13	41.8	0.0	41.8	G13	31.0	28.6	59.6
G7	23.7	11.5	35.2	G7	20.2	24.6	44.8	G7	38.0	8.9	46.9
G8	20.0	0.0	20.0	G8	17.9	25.3	43.2	G8	36.1	0.0	36.1
G9	17.6	0.0	17.6	G9	22.7	29.1	51.8	G9	22.0	0.0	22.0
H13	19.0	16.6	35.5	**H13**	**31.7**	**17.9**	**49.7**	H13	12.9	20.0	32.9
H7	4.7	10.5	15.3	H7	42.2	3.5	45.7	H7	38.0	4.4	42.3
J13	29.0	0.0	29.0	J13	6.3	3.1	9.4	J13	43.6	0.0	43.6
J7	39.6	4.2	43.7	J7	31.5	0.0	31.5	J7	37.5	3.0	40.4
K13	0.0	0.0	0.0	**K13**	**24.0**	**11.3**	**35.4**	K13	26.7	0.0	26.7
K7	21.4	7.8	29.3	K7	7.1	8.7	15.9	K7	12.5	3.1	15.7
L13	6.3	9.1	15.3	L13	24.7	11.3	36.1	L13	35.5	0.0	35.5
L7	8.8	0.0	8.8	L7	11.2	31.7	42.9	L7	18.6	29.3	47.9
M13	28.8	0.0	28.8	**M13**	**28.2**	**15.5**	**43.7**	M13	23.9	4.4	28.2
M7	11.2	14.5	25.6	M7	45.0	9.9	54.9	M7	34.5	3.8	38.3
N10	0.0	7.3	7.3	N10	19.7	0.0	19.7	**N10**	**17.1**	**6.1**	**23.2**
N11	9.4	9.2	18.6	N11	26.8	0.0	26.8	N11	23.2	5.1	28.2
N12	11.0	5.8	16.7	N12	16.0	16.9	32.9	**N12**	**39.4**	**2.8**	**42.2**
N13	**36.5**	**0.0**	**36.5**	**N13**	**20.0**	**0.0**	**20.0**	**N13**	**21.6**	**4.5**	**26.1**
N7	25.8	12.4	38.2	N7	21.3	12.9	34.2	N7	20.6	0.0	20.6
N8	17.6	0.0	17.6	**N8**	**13.9**	**0.0**	**13.9**	N8	0.0	7.7	7.7
N9	**6.3**	**4.0**	**10.3**	**N9**	**11.2**	**0.0**	**11.2**	N9	20.7	0.0	20.7

Note: **Bold** represents raw data of Table 6.2, crack length data in the upper standard deviation in the boundary region, 0-100°C ATC, UT.

SnAg, Air-Cooled, 18K, 21K, 24K, BI

UT18-U1A-SA-A-18- / UT19-U1A-SA-A-21- / UT20-U1A-SA-A-24-PI											
Joint No.	% crack length P	% crack length S	% crack length P+S	Joint No.	% crack length P	% crack length S	% crack length P+S	Joint No	% crack length P	% crack length S	% crack length P+S
G10	0.0	0.0	0.0	G10	23.1	30.7	53.8	G10	38.0	3.0	41.0
G11	27.2	1.1	28.2	G11	14.6	0.0	14.6	G11	61.8	0.0	61.8
G12	31.4	0.0	31.4	G12	27.7	0.0	27.7	G12	58.8	18.7	77.5
G13	15.5	4.4	19.9	G13	19.2	0.0	19.2	G13	38.1	20.4	58.5
G7	24.0	0.0	24.0	G7	28.0	0.0	28.0	G7	30.5	0.0	30.5
G8	16.2	0.0	16.2	G8	21.5	35.9	57.4	G8	43.3	0.0	43.3
G9	11.4	5.1	16.5	G9	19.4	25.0	44.4	G9	39.8	2.6	42.5
H13	8.2	2.7	10.9	H13	31.9	0.0	31.9	**H13**	**15.5**	**0.0**	**15.5**
H7	21.3	10.1	31.4	H7	18.3	11.3	29.6	H7	18.3	10.6	28.9
J13	**27.0**	**21.1**	**48.1**	J13	15.4	20.4	35.9	J13	98.8	0.0	98.8
J7	33.7	14.4	48.1	J7	1.4	18.3	19.7	J7	39.2	0.0	39.2
K13	12.6	5.5	18.1	**K13**	**32.3**	**12.8**	**45.1**	K13	37.7	0.0	37.7
K7	14.6	21.0	35.5	K7	11.0	26.5	37.5	K7	10.7	1.8	12.5
L13	23.6	0.0	23.6	L13	29.7	0.0	29.7	L13	18.0	44.0	62.0
L7	37.6	0.0	37.6	L7	9.5	18.5	28.0	L7	14.6	0.0	14.6
M13	42.6	0.0	42.6	**M13**	**42.8**	**0.0**	**42.8**	**M13**	**23.6**	**0.0**	**23.6**
M7	**24.0**	**18.8**	**42.8**	M7	44.4	14.0	58.4	M7	8.5	1.2	9.7
N10	0.0	8.2	8.2	**N10**	**30.7**	**10.7**	**41.4**	N10	9.0	6.7	15.7
N11	52.4	5.5	57.9	N11	13.3	0.0	13.3	N11	5.5	3.7	9.2
N12	**31.8**	**21.1**	**52.9**	**N12**	**21.7**	**2.3**	**24.0**	N12	15.5	0.0	15.5
N13	44.6	0.0	44.6	**N13**	**9.8**	**0.0**	**9.8**	N13	0.0	14.3	14.3
N7	**14.7**	**0.0**	**14.7**	N7	10.6	24.0	34.5	N7	10.2	0.0	10.2
N8	9.3	0.0	9.3	N8	20.8	0.0	20.8	**N8**	**2.6**	**3.3**	**6.0**
N9	0.0	4.7	4.7	N9	33.6	0.0	33.6	N9	2.8	1.4	4.2

Note: **Bold** represents raw data of Table 6.2, crack length data in the upper standard deviation in the boundary region, 0-100°C ATC, UT.

SnAg, Air-Cooled, 27K, BI

UT21-U2A-SA-A-27-BI											
Joint No.	% crack length P	% crack length S	% crack length P+S	Joint No.	% crack length P	% crack length S	% crack length P+S	Joint No	% crack length P	% crack length S	% crack length P+S
G10	39.6	0.0	39.6								
G11	38.6	26.3	64.9								
G12	28.5	20.8	49.2								
G13	17.0	0.7	17.8								
G7	11.0	0.0	11.0								
G8	26.3	4.3	30.6								
G9	23.4	1.8	25.2								
H13	**29.0**	**16.3**	**45.3**								
H7	42.6	14.0	56.6								
J13	8.8	2.1	10.9								
J7	41.7	0.0	41.7								
K13	7.3	0.0	7.3								
K7	14.6	0.0	14.6								
L13	18.0	0.0	18.0								
L7	47.9	0.0	47.9								
M13	**19.4**	**6.9**	**26.3**								
M7	37.5	12.6	50.1								
N10	**27.7**	**14.5**	**42.2**								
N11	26.4	0.0	26.4								
N12	36.4	0.0	36.4								
N13	16.8	30.7	47.4								
N7	40.9	0.0	40.9								
N8	34.8	19.5	54.3								
N9	**41.7**	**35.4**	**77.1**								

Note: **Bold** represents raw data of Table 6.2, crack length data in the upper standard deviation in the boundary region, 0-100°C ATC, UT.

SnAg, Quenched, 3K, BI

UT23-U14A-SA-Q-3- / UT23-U4A-SA-Q-3- / UT23-U9A-SA-Q-3-BI											
Joint No.	% crack length P	% crack length S	% crack length P+S	Joint No.	% crack length P	% crack length S	% crack length P+S	Joint No	% crack length P	% crack length S	% crack length P+S
G10	0.0	0.0	0.0	G10	6.9	0.0	6.9	G10	0.0	0.0	0.0
G11	2.5	0.0	2.5	G11	0.0	0.0	0.0	G11	3.5	0.0	3.5
G12	4.9	0.0	4.9	G12	0.0	0.0	0.0	G12	1.6	0.0	1.6
G13	0.0	0.0	0.0	G13	2.1	0.0	2.1	G13	2.1	2.3	4.4
G7	0.0	0.0	0.0	G7	14.2	0.0	14.2	G7	0.0	9.3	9.3
G8	1.9	0.0	1.9	G8	6.2	3.2	9.4	G8	3.6	0.0	3.6
G9	0.0	0.0	0.0	G9	10.6	0.0	10.6	G9	0.0	0.0	0.0
H13	5.3	0.0	5.3	H13	7.9	0.0	7.9	H13	8.8	0.9	9.6
H7	0.0	0.0	0.0	H7	2.8	2.8	5.6	H7	2.0	0.0	2.0
J13	0.0	5.6	5.6	J13	1.2	0.0	1.2	J13	0.0	0.0	0.0
J7	13.4	0.0	13.4	J7	4.9	3.9	8.8	J7	6.7	0.0	6.7
K13	0.0	0.0	0.0	K13	6.0	0.0	6.0	K13	0.0	0.0	0.0
K7	0.0	0.0	0.0	K7	0.0	0.0	0.0	K7	0.0	1.8	1.8
L13	2.7	2.8	5.5	L13	10.5	0.0	10.5	L13	8.9	0.0	8.9
L7	8.7	0.0	8.7	L7	1.1	2.6	3.7	L7	0.0	0.0	0.0
M13	2.5	0.0	2.5	M13	3.4	0.0	3.4	M13	9.5	0.0	9.5
M7	3.0	0.0	3.0	M7	0.0	0.0	0.0	M7	3.8	0.0	3.8
N10	7.6	0.0	7.6	N10	0.0	2.4	2.4	N10	1.1	0.0	1.1
N11	4.5	0.0	4.5	N11	3.2	0.0	3.2	N11	0.0	6.9	6.9
N12	16.1	0.0	16.1	N12	15.8	0.0	15.8	N12	0.0	2.3	2.3
N13	10.7	0.0	10.7	N13	8.6	0.0	8.6	N13	0.0	2.7	2.7
N7	0.0	0.0	0.0	N7	5.1	0.0	5.1	N7	0.0	0.0	0.0
N8	2.5	0.0	2.5	N8	6.3	0.0	6.3	N8	5.6	0.0	5.6
N9	0.0	0.0	0.0	N9	12.9	0.0	12.9	N9	0.0	2.7	2.7

SnAg, Quenched, 6K, BI

UT25-U14A-SA-Q-6- / UT25-U4A-SA-Q-6- / UT25-U9A-SA-Q-6-BI											
Joint No.	% crack length P	% crack length S	% crack length P+S	Joint No.	% crack length P	% crack length S	% crack length P+S	Joint No	% crack length P	% crack length S	% crack length P+S
G10	0.0	0.0	0.0	G10	12.6	1.9	14.5	G10	5.1	0.0	5.1
G11	3.7	0.0	3.7	G11	0.0	7.9	7.9	G11	8.3	0.0	8.3
G12	3.7	0.0	3.7	G12	14.6	0.0	14.6	G12	8.7	8.2	17.0
G13	7.5	1.6	9.1	G13	14.4	0.0	14.4	G13	15.4	13.3	28.8
G7	11.3	3.5	14.8	G7	6.7	7.2	13.9	G7	8.2	4.0	12.2
G8	0.0	12.1	12.1	G8	12.6	0.0	12.6	G8	5.5	9.7	15.2
G9	3.0	0.0	3.0	G9	0.0	0.0	0.0	G9	15.2	0.0	15.2
H13	7.3	0.0	7.3	H13	0.7	0.0	0.7	H13	5.3	4.2	9.5
H7	26.6	0.0	26.6	H7	3.0	0.0	3.0	H7	5.8	0.0	5.8
J13	1.4	0.0	1.4	J13	19.2	0.0	19.2	J13	22.6	0.0	22.6
J7	26.7	6.5	33.2	J7	8.8	0.0	8.8	J7	10.6	0.0	10.6
K13	18.4	0.0	18.4	K13	11.5	0.0	11.5	K13	22.6	0.0	22.6
K7	26.2	0.0	26.2	K7	0.0	0.0	0.0	K7	10.8	0.0	10.8
L13	18.8	0.0	18.8	L13	18.2	0.0	18.2	L13	4.2	0.0	4.2
L7	11.8	0.0	11.8	L7	8.6	0.0	8.6	L7	4.6	0.0	4.6
M13	23.0	0.0	23.0	M13	18.7	0.0	18.7	M13	10.8	0.0	10.8
M7	18.8	0.0	18.8	M7	0.0	0.0	0.0	M7	5.4	0.0	5.4
N10	0.0	0.9	0.9	N10	3.9	0.0	3.9	N10	0.0	0.0	0.0
N11	12.5	0.0	12.5	N11	0.0	0.0	0.0	N11	0.9	14.8	15.7
N12	5.8	0.0	5.8	N12	2.1	0.0	2.1	N12	0.0	4.4	4.4
N13	6.6	2.1	8.7	N13	32.0	0.0	32.0	N13	9.4	2.0	11.4
N7	22.4	0.0	22.4	N7	0.0	0.0	0.0	N7	0.0	0.0	0.0
N8	1.6	0.0	1.6	N8	0.0	0.0	0.0	N8	2.5	0.0	2.5
N9	6.6	0.0	6.6	N9	1.6	0.0	1.6	N9	11.0	0.0	11.0

SnAg, Quenched, 9K, BI

UT24-U13A-SA-Q-9- / UT24-U3A-SA-Q-9- / UT24-U8A-SA-Q-9-BI											
Joint No.	% crack length P	% crack length S	% crack length P+S	Joint No.	% crack length P	% crack length S	% crack length P+S	Joint No	% crack length P	% crack length S	% crack length P+S
G10	0.0	0.0	0.0	G10	0.0	4.9	4.9	G10	14.9	12.6	27.5
G11	7.5	1.7	9.3	G11	41.7	3.3	45.0	G11	29.3	4.6	33.9
G12	18.8	15.3	34.1	G12	25.1	4.6	29.6	G12	40.5	0.0	40.5
G13	11.5	21.4	32.9	G13	34.0	0.0	34.0	G13	15.6	0.0	15.6
G7	6.1	14.7	20.9	G7	37.4	0.0	37.4	G7	28.1	5.6	33.7
G8	27.4	0.0	27.4	G8	16.5	14.8	31.3	G8	8.6	0.0	8.6
G9	25.7	0.0	25.7	G9	0.0	10.0	10.0	G9	0.0	0.0	0.0
H13	14.5	0.0	14.5	H13	0.4	11.3	11.6	H13	0.0	0.0	0.0
H7	17.7	0.0	17.7	H7	19.9	0.0	19.9	H7	0.0	0.0	0.0
J13	21.9	0.0	21.9	J13	13.2	20.6	33.8	J13	13.2	0.0	13.2
J7	17.9	4.6	22.5	J7	26.2	0.0	26.2	J7	8.6	0.0	8.6
K13	26.2	0.0	26.2	K13	0.7	0.0	0.7	K13	2.3	12.4	14.7
K7	21.5	0.0	21.5	K7	20.4	0.0	20.4	K7	0.0	0.0	0.0
L13	31.9	0.0	31.9	L13	36.8	16.0	52.8	L13	18.0	7.7	25.7
L7	5.4	15.5	20.9	L7	12.3	6.5	18.8	L7	7.3	4.4	11.7
M13	30.0	0.0	30.0	M13	44.6	0.0	44.6	M13	8.0	0.0	8.0
M7	13.9	3.7	17.5	M7	22.5	0.0	22.5	M7	8.0	0.0	8.0
N10	0.0	0.0	0.0	N10	3.5	0.0	3.5	N10	32.1	0.0	32.1
N11	14.9	0.0	14.9	N11	7.5	0.0	7.5	N11	10.3	1.2	11.5
N12	15.5	0.0	15.5	N12	21.5	20.1	41.6	N12	43.8	0.0	43.8
N13	6.4	7.5	13.9	N13	27.9	0.0	27.9	N13	27.8	0.0	27.8
N7	20.9	2.6	23.5	N7	13.2	0.0	13.2	N7	36.5	0.0	36.5
N8	37.7	0.0	37.7	N8	0.0	0.0	0.0	N8	2.3	0.0	2.3
N9	30.7	4.6	35.3	N9	1.9	0.0	1.9	N9	5.2	0.0	5.2

SnAg, Quenched, 12K, BI

UT23-U12A-SA-Q-12- / UT23-U2A-SA-Q-12- / UT23-U7A-SA-Q-12-BI											
Joint No.	% crack length P	% crack length S	% crack length P+S	Joint No.	% crack length P	% crack length S	% crack length P+S	Joint No	% crack length P	% crack length S	% crack length P+S
G10	30.0	2.7	32.6	G10	9.1	12.7	21.8	G10	16.3	0.0	16.3
G11	39.3	0.0	39.3	G11	0.0	3.2	3.2	G11	22.2	2.3	24.5
G12	28.1	11.0	39.1	G12	4.6	0.0	4.6	G12	13.3	26.3	39.7
G13	14.0	0.0	14.0	G13	6.1	3.8	10.0	G13	19.4	23.4	42.8
G7	52.5	3.2	55.7	G7	8.9	0.0	8.9	G7	24.7	26.3	51.1
G8	3.4	2.5	5.8	G8	18.8	0.0	18.8	G8	32.1	0.0	32.1
G9	59.8	0.2	60.0	G9	11.0	0.0	11.0	G9	30.2	0.0	30.2
H13	9.6	2.8	12.4	H13	25.4	0.0	25.4	H13	18.5	0.0	18.5
H7	10.6	0.0	10.6	H7	14.3	0.0	14.3	H7	23.3	3.4	26.6
J13	5.6	0.0	5.6	J13	10.2	0.0	10.2	J13	32.0	0.0	32.0
J7	0.0	4.3	4.3	J7	0.0	10.1	10.1	J7	27.6	1.4	29.0
K13	9.9	3.9	13.8	K13	0.0	0.0	0.0	K13	13.9	5.0	19.0
K7	5.1	3.0	8.2	K7	21.9	1.4	23.3	K7	34.2	0.0	34.2
L13	11.5	22.3	33.8	L13	28.5	7.7	36.2	L13	23.6	4.8	28.4
L7	15.1	0.0	15.1	L7	45.7	0.0	45.7	L7	27.7	13.3	41.1
M13	39.0	24.0	63.0	M13	36.0	0.0	36.0	M13	21.5	7.1	28.5
M7	20.1	15.1	35.1	M7	36.2	0.0	36.2	M7	12.5	0.0	12.5
N10	4.4	0.0	4.4	N10	0.0	5.8	5.8	N10	5.8	15.3	21.2
N11	21.2	0.0	21.2	N11	13.3	0.0	13.3	N11	18.1	2.1	20.2
N12	4.4	15.3	19.6	N12	0.0	0.0	0.0	N12	27.9	0.0	27.9
N13	10.2	0.0	10.2	N13	20.0	18.2	38.2	N13	14.0	0.0	14.0
N7	23.2	0.0	23.2	N7	0.0	4.5	4.5	N7	33.3	9.6	43.0
N8	7.9	0.0	7.9	N8	0.0	0.0	0.0	N8	33.3	0.0	33.3
N9	9.0	0.0	9.0	N9	8.1	0.0	8.1	N9	15.6	0.0	15.6

SnAg, Quenched, 15K, BI

UT25-U12A-SA-Q-15- / UT25-U2A-SA-Q-15- / UT25-U7A-SA-Q-15-BI											
Joint No.	% crack length P	% crack length S	% crack length P+S	Joint No.	% crack length P	% crack length S	% crack length P+S	Joint No	% crack length P	% crack length S	% crack length P+S
G10	3.1	1.6	4.7	G10	48.4	0.0	48.4	G10	11.8	0.0	11.8
G11	5.8	0.0	5.8	G11	18.5	1.7	20.2	G11	4.4	0.0	4.4
G12	0.0	4.4	4.4	G12	19.2	4.9	24.0	G12	12.5	2.7	15.1
G13	23.7	2.6	26.3	G13	41.1	6.1	47.2	G13	24.2	0.0	24.2
G7	3.5	0.0	3.5	G7	26.8	21.4	48.3	G7	5.2	0.0	5.2
G8	20.1	3.0	23.1	G8	31.7	15.0	46.7	G8	10.8	0.0	10.8
G9	14.1	0.0	14.1	G9	15.9	0.0	15.9	G9	8.4	3.0	11.3
H13	16.7	0.0	16.7	H13	31.2	0.0	31.2	H13	16.0	12.2	28.2
H7	3.0	9.9	12.9	H7	19.2	1.0	20.2	H7	43.7	0.0	43.7
J13	17.0	5.0	22.0	J13	9.6	0.0	9.6	J13	0.0	3.1	3.1
J7	22.3	0.0	22.3	J7	26.8	0.0	26.8	J7	39.6	0.0	39.6
K13	10.1	3.5	13.6	K13	0.0	5.1	5.1	K13	21.6	0.0	21.6
K7	0.0	0.0	0.0	K7	21.1	6.3	27.4	K7	10.5	9.9	20.4
L13	35.5	0.0	35.5	L13	16.0	15.5	31.5	L13	30.1	31.7	61.9
L7	19.5	0.0	19.5	L7	23.9	0.0	23.9	L7	17.8	0.0	17.8
M13	27.2	0.0	27.2	M13	15.3	0.0	15.3	M13	14.6	0.0	14.6
M7	12.7	8.9	21.6	M7	17.9	3.8	21.8	M7	1.9	5.2	7.1
N10	12.4	0.0	12.4	N11	12.5	0.0	12.5	N10	20.6	0.0	20.6
N11	2.4	11.2	13.6	N12	3.3	0.0	3.3	N11	24.1	33.6	57.8
N12	17.1	0.0	17.1	N13	0.0	4.0	4.0	N12	37.1	0.0	37.1
N13	14.9	0.0	14.9	N7	21.6	0.0	21.6	N13	15.3	0.0	15.3
N7	35.0	0.0	35.0	N8	12.9	4.9	17.8	N7	9.6	0.0	9.6
N8	19.9	0.0	19.9	N9	25.3	3.8	29.1	N8	19.3	25.3	44.6
N9	0.0	0.0	0.0					N9	36.4	2.6	39.0

SnAg, Quenched, 18K, 21K, 24K, BI

UT25BAD-U5A-SA-Q-18- / UT23-U1A-SA-Q-21- / UT25BAD-U1A-SA-Q-24-BI											
Joint No.	% crack length P	% crack length S	% crack length P+S	Joint No.	% crack length P	% crack length S	% crack length P+S	Joint No	% crack length P	% crack length S	% crack length P+S
G10	4.0	4.4	8.4	G10	3.4	0.0	3.4	G10	0.0	2.3	2.3
G11	35.3	9.0	44.3	G11	27.7	4.5	32.2	G11	32.7	13.1	45.8
G12	43.6	2.5	46.1	G12	25.0	18.3	43.2	G12	26.5	4.5	31.0
G13	24.6	0.0	24.6	G13	28.4	0.0	28.4	G13	35.9	0.0	35.9
G7	36.8	0.0	36.8	G7	34.0	4.7	38.7	G7	39.5	3.8	43.3
G8	10.1	8.4	18.5	G8	25.0	0.0	25.0	G8	49.5	2.1	51.7
G9	19.7	12.6	32.3	G9	5.1	25.7	30.8	G9	60.0	0.0	60.0
H13	44.9	0.0	44.9	H13	31.7	0.0	31.7	H13	23.3	7.1	30.5
H7	3.8	0.0	3.8	H7	37.8	7.2	45.0	H7	41.1	0.0	41.1
J13	21.9	0.0	21.9	J13	32.4	5.4	37.8	J13	25.5	0.0	25.5
J7	26.9	0.0	26.9	J7	45.4	0.0	45.4	J7	21.2	0.0	21.2
K13	32.0	17.6	49.5	K13	24.1	0.0	24.1	K13	36.7	7.5	44.2
K7	3.1	0.0	3.1	K7	20.8	0.0	20.8	K7	33.8	0.0	33.8
L13	15.4	22.4	37.9	L13	40.4	0.0	40.4	L13	41.0	40.8	81.8
L7	41.7	0.0	41.7	L7	30.2	3.6	33.7	L7	14.5	4.8	19.4
M13	43.3	0.0	43.3	M13	20.8	1.6	22.4	M13	33.3	27.1	60.4
M7	27.6	0.0	27.6	M7	1.6	0.0	1.6	M7	21.6	6.8	28.3
N10	18.9	3.7	22.6	N10	24.8	17.4	42.2	N10	29.7	11.8	41.5
N11	6.6	11.7	18.3	N11	12.1	14.3	26.4	N11	36.0	0.0	36.0
N12	19.9	0.0	19.9	N12	15.0	13.6	28.6	N12	40.3	0.0	40.3
N13	1.8	13.5	15.3	N13	25.1	1.6	26.8	N13	29.9	21.4	51.3
N7	17.6	22.3	39.9	N7	33.5	12.1	45.6	N7	45.1	18.3	63.4
N9	27.6	3.2	30.9	N8	31.2	0.0	31.2	N8	60.2	0.0	60.2
				N9	27.3	13.9	41.3	N9	64.5	0.0	64.5

SnAg, Quenched, 27K, 30K, BI

UT25BAD-U3A-SA-Q-27- / UT25-U1A-SA-Q-30-BI											
Joint No.	% crack length P	% crack length S	% crack length P+S	Joint No.	% crack length P	% crack length S	% crack length P+S	Joint No	% crack length P	% crack length S	% crack length P+S
G10	28.5	30.0	58.5	G10	4.6	4.8	9.4				
G11	9.3	16.3	25.7	G11	21.0	0.0	21.0				
G12	20.3	8.0	28.3	G12	3.0	0.0	3.0				
G13	55.1	20.8	75.9	G13	5.2	0.0	5.2				
G7	31.2	3.2	34.5	G7	25.3	0.0	25.3				
G8	23.5	0.2	23.7	G8	24.2	18.5	42.7				
G9	31.2	10.0	41.1	G9	11.0	13.4	24.4				
H13	44.2	7.5	51.7	H13	28.1	0.0	28.1				
H7	55.9	8.4	64.3	H7	57.7	0.0	57.7				
J13	56.3	0.0	56.3	J13	8.9	0.0	8.9				
J7	19.6	2.8	22.4	J7	40.8	1.8	42.6				
K13	24.8	2.9	27.7	K13	11.8	4.3	16.0				
K7	3.9	0.2	4.1	K7	11.2	0.0	11.2				
L13	8.3	25.8	34.1	L13	52.2	7.8	60.0				
L7	14.0	0.0	14.0	L7	34.9	17.5	52.4				
M13	49.7	17.8	67.5	M13	46.5	6.7	53.2				
M7	46.7	0.0	46.7	M7	0.0	27.8	27.8				
N10	27.3	22.8	50.1	N10	10.2	15.3	25.5				
N11	38.8	0.0	38.8	N11	43.1	0.0	43.1				
N12	35.5	30.2	65.7	N12	44.5	0.0	44.5				
N13	48.8	33.8	82.6	N13	99.2	0.0	99.2				
N7	15.3	0.0	15.3	N7	50.8	2.1	52.9				
N8	40.0	6.3	46.3	N8	44.2	0.0	44.2				
N9	27.4	25.3	52.7	N9	40.8	9.4	50.2				

APPENDIX H

Experimental MOT Life Data

Table H.1. Experimental MOT life data of air-cooled SnPb joint

SnPb-Air-cooled SPA-A								
Single-dense			Single-sparse		Double-dense		Double-altenating	
0-100C MOT1 MOT2	-40-125C MOT3 MOT4	-50-125C MOT5	0-100C MOT16 MOT17 MOT18	-40-125C MOT22 MOT23 MOT24	0-100C MOT28	-40-125C MOT30	0-100C MOT32	-40-125C MOT34
10939	3954	2341	11056	4581	2892	1223	11759	3512
11725	3780	2774	12434	3779	2616	982	9996	4055
12284	4301	3127	11013	3549	3989	1138	9937	3940
11785	4159	2880	10886	4278	2653	1300	8785	4217
11097	3492	2816	9875	3383	3513	1160	11836	3797
11239	4699	2886	12411	4170	2622	1221	9086	3698
13564	3831	2562	13709	3657	4156	1203	9962	3847
11954	3841	3408	12169	4182	2746	1315	10741	4086
12737	2869	3101	10351	3255	4367	1558	10705	3753
13432	3777	2697	12344	4610	2778	1433	10016	3877
13194	3341	2952	9635	4688	3284	1202	10393	2975
11496	3709	2659	11339	4203	3017	1205	10796	3509
12866	4271	2808	12802	4583	3689	1260	10129	4248
11295	4100		12958	4128	2493	1349		
12664	4234		12449	3745		1404		
11208	4133		11721	4001				
11480	4139		10863	4254				
12545	4500		11704	3919				
13024	3330							
12240	3761							
11664	3674							

13122	4204							
13175	4887							
12346	4230							
11044	3501							
12086	4342							
	4211							
	3503							
	4245							

Table H.2. Experimental MOT life data of air-cooled SnAg joint

SnAg-Air-cooled SA-A								
Single-dense			Single-sparse		Double-dense		Double-altenating	
0-100C MOT6 MOT7	-40-125C MOT8 MOT9	-50-125C MOT10	0-100C MOT19 MOT20 MOT21	-40-125C MOT25 MOT26 MOT27	0-100C MOT29	-40-125C MOT31	0-100C MOT33	-40-125C MOT35
17937	3320	3451	14386	5301	3138	897	16391	4288
19816	3714	3356	20155	4953	11383	2331	15650	4753
18751	4230	3499	17028	6095	3772	876	18162	6011
17864	4387	3331	18379	4202	11687	2262	14119	4189
16251	4738	3580	19419	5080	4396	732	18113	5570
18409	4812	3242	16145	6000	10904	2778	11907	2260
12674	4945	4131	19478	5727	4721	1051	15622	5173
19074	4984	3748	18620	6139	8313	2056	17617	5260
15582	5217	4025	17540	5722	5547	926	15938	5316
15097	5265	2842	18177	4561	10732	2781	16134	5256
14198	5301	2149	17500	5946	3150	820	14147	4871
14187	5441	3223	16266	5557	5759	1493	13872	
14900	5478	3230	20355	6143	4631	1017	14864	
16609	5533		16455	6126	6916	2189	16015	
17977	5658				4066	817	15464	
17259	5841							
12959	5918							

17308	6040							
11905	6119							
11104	6209							
18530	6309							
17902	6330							
16397	6345							
13948	6460							
19832	6667							
	6759							

Bibliography

1. J. H. Lau and Y. H. Pao, Solder Joint Reliability of BGA, CSP, Flip Chip, and Fine Pitch SMT Assemblies, McGraw Hill, 1997.
2. http://www.amkor.com/products/ProductFamilies.cfm, Accessed in November 25, 2004.
3. L. T. Yeh, "Review of Heat Transfer Technologies in Electronic Equipment", Journal of Electronic Packaging, Vol. 117, pp. 333-339, December 1995.
4. W. Engelmaier, "Solder Joints In Electronics: Design For Reliability", Design and Reliability of Solders and Solder Interconnections, The Minerals, Metals & Materials Society, pp. 9-19, 1997.
5. B. Wong and D.E. Helling, "A Mechanistic Model for Solder Joint Failure Prediction Under Thermal Cycling", Journal of Electronic Packaging, Vol. 112, pp. 104-109, June 1990.
6. B. Wong and D.E. Helling, "Applying a Physics-of-failure Model to Predicting Surface of Mount Solder Joint Reliability", Quality and Reliability Engineering International, Vol. 7, No. 5, pp. 403-410, Sep-Oct, 1991.
7. iNEMI Roadmap of Lead-Free Assembly in North America, JISSO/PROTEC Forum, November 19-20, 2002.
8. C. Kanchanomai, Y. Miyashita, and Y. Mutoh, "Strain-rate Effects on Low Cycle Fatigue Mechanism of Eutectic Sn-Pb solder", International Journal of Fatigue 24, pp. 987-993, 2002.
9. http://www.boulder.nist.gov/div853/lead%20free/props01.html, Accessed in March, 2003.

10. J. Glazer, “Microstructure and Mechanical Properties of Pb-Free Solder Alloys for Low-Cost Electronic Assembly: A Review”, Journal of Electronic Materials, Vol. 23, No. 8, pp. 693-700, 1994.
11. Lead-Free Solder Project Final Report, National Center for Manufacturing Sciences, Report 0401RE96, August 1997.
12. The European Parliament and the Council of the European Union, “Directive 2002/96/EC on Waste Electrical and Electronic Equipment (WEEE)”, Official Journal of the European Union, pp. L37/24-38, February 13, 2003.
13. The European Parliament and the Council of the European Union, “Directive 2002/95/EC on the Restriction of the Use of Certain Hazardous Substances (RoHS) in Electrical and Electronic Equipment (EEE)”, Official Journal of the European Union, pp. L37/19-23, February 13, 2003.
14. T. Takemoto and M. Takahashi, “Tensile Test for Estimation of Thermal Fatigue Properties of Solder Alloys”, Journal of Materials Science, Vol. 32, No. 15, pp. 4077-4084, Aug 1, 1997.
15. J. Glazer, “Microstructure and Mechanical Properties of Pb-Free Solder Alloys for Low-Cost Electronic Assembly: A Review”, Journal of Electronic Materials, Vol. 23, No. 8, pp. 693-700, 1994.
16. A. Schubert, R. Dudek, H. Walter, E. Jung, A. Gollhardt, B. Michel, and H. Reichl, “Reliability Assessment of Flip-Chip Assemblies with Lead-free Solder Joints”, Proc. Electronic Components and Technology Conf., pp. 1246-1255, 2002.
17. D. Kim and P. Elenius, “Deformation and Crack Growth Characteristics of SnAgCu vs 63Sn/Pb Solder Joints on a WLP in Thermal Cycle Testing”, Proc. Electronic Components and Technology Conf., pp. 681-686, 2001.

18. D. Grivas, K. L. Murty, and J. W. Morris, Jr., “Deformation of Pb-Sn Eutectic Alloys at Relatively High Strain Rates”, Acta Metallurgica, Vol. 27, pp. 731-737, 1979.
19. S. Ahat, L.Du, M. Sheng, L. Luo, W. Kempe, and J. Freytag, “Effetcts of Aging on the Microstructure and Shear Strength of SnPbAg/Ni-P/Cu and SnAg/Ni-P/Cu Solder Joints”, Journal of Electronic Materials, Vol. 29, No. 9, pp. 1105-1109, 2000.
20. S. Choi, K. N. Subramanian, J. P. Lucas, and T. R .Bieler, “Thermo-mechanical Fatigue Behaior of Sn-Ag Solder Joint”, Journal of Electronic Materials, Vol. 29, No. 10, pp. 1249-1257, 2000.
21. W. A. Logsdon, P.K. Liaw, and M.A. Burke, “Fracture Behavior of 63Sn-37Pb,” Engineering Fracture Mechanics, Vol. 36, No. 2, pp. 183-218, 1990.
22. Z. Guo and H. Conrad, “Computer Modeling of Isothermal Low-cycle Fatigue of Pb-Sn Solder Joints,” Proc. Electronics Components and Technology Conf., pp. 831-838, 1993.
23. Z. Guo and H. Conrad, “Fatigue Crack Growth Rate in 63Sn37Pb Solder Joints,” Journal of Electronic Packaging, Vol. 115, pp. 159-164, June 1993.
24. R. Darveaux, “Solder Joint Fatigue Life Model”, Design and Reliability of Solders and Solder Interconnections”, The Minerals, Metals & Materials Society, pp. 213-218, 1997.
25. J. Lau and C. Chang, “Solder Joint Crack Propagation Analysis of Wafer-Level Chip Scale Package on Printed Circuit Board Assemblies,” Proc. Electronic Components and Technology Conf., pp. 1360-1368, 2000.
26. R. Satoh, K. Arakawa, M. Harada, and K. Matsui, “Thermal Fatigue Life of Pb-Sn Alloy Interconnections”, IEEE Trans on Components, Packaging and Manufacturing Technology, Vol. 14, No. 1, pp. 224-232, March 1991.

27. J. M. Hu, “An Empirical Crack Propagation Model And Its Applications For Solder Joints,” Journal of Electronic Packaging, Vol. 118, pp. 104-107, June 1996.
28. A. Syed, “Reliability of Lead-Free Solder connections for Area-Array Packages”, IPC SMENA APEX Conf., pp. 1-8, 2001.
29. M. Farooq, C. Goldsmith, R. Jackson, and G. Martin, “Lead-Free Ceramic Ball Grid Array: Thermomechanical Fatigue Reliability”, Journal of Electronin Materials, Vol. 32, No. 12, pp. 1421-1425, 2003.
30. A. Mawer and K. Levis, “Automotive PBGA Assembly and Board-Level Reliability with Lead-Free versus Lead-Tin Interconnect”, Journal of SMT, pp. 9-16, January 2001.
31. J. Gleason, C. Reynolds, J. Bath, M. Kelly, K. Lyjak, and P. Roubaud, “Pb-Free Assembly, Rework, and Reliability analysis of IPC Class 2 Assemblies”, Proc. Electronic Components and Technology Conf., pp. 960-969, 2005.
32. D.R. Frear, W.B. Jones, and K.R. Kinsman, Solder Mechanics, TMS, Sata Fe, New Mexico, 1990.
33. Z. Mei and J. W. Morris, Jr., “Fatigue Lives On 60Sn/40Pb Solder Joints Made With Different Cooling Rates,” Journal of Electronic Packaging, Vol. 114, pp. 104-108, June 1992.
34. M. C. Shine and L. R. Fox, “Fatigue of Solder Joints In Surface Mount Devices,” Low Cycle Fatigue, ASTM STP 942, pp. 588-610, 1988.
35. John H.L. Pang, K.H. Tan, X. Shi, and Z. Wang, “Thermal Cycling Aging Effects on Solder Joint Properties”, IPACK’01, pp. 1171-1175, July 2001.
36. Y. Miyazawa and T. Ariga, “Microstructural Change and Hardness of Lead Free Solder Alloys”, Proc. 1999 Environmentally Conscious Design and Inverse Manufacturing, pp 16 –619, February 1999.

37. R. Katchmar, E. Goulet, and J. Laliberte, “Factors Influencing Fatigue Life of Area-Array Solder Joints”, International Symposium on Microelectronics, pp. 551-556, 1996.
38. M. Logterman, D. Newton, S. Priore, J. Riebling, M. Smedley, S. Teng, and J. Xue, “Long term Reliability of 0.8mm pitch BGA Packages Double-Side Mounted on a Thin Printed Circuit Board”, Conf. of Surface Mount Technology Association, pp. 238-245, 2003.
39. R. Ghaffarian, “CSP Reliability for Single- and Double-Sided Assemblies”, magazine ChipScale Review, Nov-Dec 1999.
40. E. Ahn, T. Cho, J. Shim, H. Moon, J. Lyu, K. Choi, S. Kang, and S. Oh, “Reliability of Flip Chip BGA Package on Organic Substrate”, Proc. Electronic Components and Technology Conf., pp. 1215-1220, 2000.
41. S. H. Ju, B.I. Sandor, and M.E. Plesha, “Life prediction of Solder Joints by Damage and Fracture Mechanics”, Journal of Electronic packaging, Vol.118, pp. 193-200, 1996.
42. T. Pan, “Critical Accumulated Strain Energy (Case) Failure Criterion for Thermal Cycling Fatigue of Solder Joints,” Journal of Electronic Packaging, Vol.116, pp. 163-170, Septemer 1994.
43. P. T. Vianco, S. N. Burchett, M. K. Neilsen, J. A. Rejent, D. R. Frear, “Coarsening of the Sn-Pb Solder Microstructure in Constitutive Model-Based Predictions of Solder Joint Thermal Mechanical Fatigue, Journal of Electronic Materials, Vol. 28, No. 11, pp. 1290-1298, November 1999.
44. J. H. Lau and D. W. Rice, “Thermal Fatigue Life Prediction of Flip Chip Solder Joints by Fracture Mechanics Method”, Advances in Electronic Packaging ASME, pp. 385-392, 1992.
45. J. Lau and S.-W.R. Lee, “Modeling and Analysis of 96.5Sn-3.5Ag Lead-Free Solder Joints of Wafer Level Chip Scale Package on Buildup

Microvia Printed Circuit Board", IEEE Trans. on Electronics Packaging Manufacturing, Vol. 25, No. 1, pp. 51-58, January 2002.

46. R.M.V. Pidaparti and X. Song, "Fatigue Crack Propagation Life Analysis of Solder Joints under Thermal Cyclic Loading," Theoretical and Applied Fracture Mechanics 24, pp. 157-164, 1996.
47. C. A. Harper, Electronic Packaging & Interconnection Handbook, McGraw Hill, 1997.
48. V. Gektin, A. Bar-Cohen and J. Ames, "Coffin-Manson Fatigue Model of Underfilled Flip-Chips", IEEE Transactions on Components, Packaging, and Manufacturing Technology, Vol. 20, pp. 317-326, September 1997.
49. W. Engelmaier, "Solder Joint Reliability - Part3: Comparing Different Solder Fatigue Models", Global SMT & Packaging, pp. 35-37, 2002.
50. K. Norris and A. Landzberg, "Reliability of Controlled Collapse Interconnections", IBM Journal of Research and Development, pp. 266-271, May 1969.
51. C. Park, Crack Area Analysis of SnPb and SnAg Solder Joints in Plastic Ball Grid Array Packages under Accelerated Thermal Testing, M.S. Thesis, Engineering, University of Texas at Austin, 2002.
52. A. Mawer, Motorola report on 357 PBGA Longhorn Test Board, July 1999.
53. IPC-9701, Performance Test Methods and Qualification Requirements for Surface Mount Solder Attachments, January 2002.
54. JESD22-A106B, Thermal Shock, Revision of JESD22-A106A, JEDEC Solid State Technology Association, June 2004.
55. Scion Image, Scion Image for Windows, Scion Corporation, Frederick, MD, 2000.
56. R. Darveaux, "Crack Initiation and Growth in Surface Mount Solder Joints", Proc. Int Symp Microelectronics, pp. 86-97, 1993.

57. IPC-SM-785, Guidelines for Accelerated Reliability Testing of Surface Mount Solder Attachments, November 1992.
58. P. K. Bhagavathula, Reliability Analysis of SnPb and SnAg Solder Joints in Plastic Ball Grid Array Packages Subjected to Thermal Loads, M.S. Report, Engineering, University of Texas at Austin, 2003.
59. M. C. Smith, Alloy Series in Physical Metallurgy, New York, 1956.
60. W. Horace, The Knoop Microhardness Tester as a Mineralogical Tool, Mineralogical Society of America, Vol. 30, pp. 583-595, 1945.
61. K. L. Murty, "Deformation Mechanisms in Sn-Based Solder Materials", Proc. InterPack, pp. 1221-1231, 1997.
62. P. L. Hacke, A. F. Sprecher, and H. Conrad, "Microstructure Coarsening During Thermo-Mechanical Fatigue Of Pb-Sn Solder Joints", Journal of Electronic Materials, Vol. 26, No. 7, pp. 774-782, 1997.
63. M. A. Clark and T. H. Alden, "Deformation Enhanced Grain Growth in a Superplastic Sn-1% Bi Alloy", Acta Metallurgica, Vol. 21, pp. 774-782, 1973.
64. K. Tu, J. W. Mayer, and L. C. Feldman, Electronic Thin Film Science For Electrical Engineers And Materials Scientists, Macmillan Publishing Company, New York, 1992.
65. W. Desorbo, Bull. Amer. Phys. Soc. (Series II), Vol. 4, pp. 149, 1959.
66. A. Needleman and J. R. Rice, "Plastic Creep Flow Effects in the Diffusive Cavitation of Grain Boundaries", Acta Metallurgica, Vol. 28, pp. 1315-1332, 1980.
67. A. H. Chokshi and A. K. Mukherjee, "An Analysis Of Cavity Nucleation In Superplasticity", Acta Metallurgica, Vol. 37, No. 11, pp. 3007-3017, 1989.
68. R.L. Coble, Journal of Appl. Phys., 34, pp. 1679, 1963.

69. R. Raj and M. F. Ashby, “Intergranular Fracture at Elevated Temperature”, Acta Metallurgica, Vol. 23, pp. 653-666, 1975.
70. D. S. Wilkinson and C. H. Caceres, “Mechanism of Plastic Void Growth During Superplastic Flow”, Materials Science and Technology, Vol. 2, pp. 1086-1092, November 1986.
71. S. Wiese, A. Schubert, H. Walter, R. Dudek, F. Feustel, E. Meusel, and B. Michel, “Constitutive Behavior of Lead-free Solders vs. Lead-containing Solders-Experiments on Bulk Specimens and Flip-Chip Joints”, Proc. Electronic Components and Technology Conf., pp. 890-902, 2001.
72. A. W. Gibson, S. L. Choi, K. N. Subramanian, and T. R. Bieler, “Issues Regarding Microstructural Coarsening Due To Aging of Eutectic Tin-Silver Solder”, The Minerals, Metals & Materials Society, pp. 97-103, 1997.
73. C. Herring, Journal of Appl. Phys., 21, pp. 437, 1950.
74. A.S. Argon, “Intergranular Cavitation in Creeping Alloys”, Scripta Metallurgica, Vol. 17, pp. 5-12, 1983.
75. H. Riedel, Fracture at High Temperatures, Spring-Verlag, 1987.
76. ABAQUS / Standard user’s Manual Version 6.2.1, Hibbitt, Karlsson & Sorensen, Inc., RI, USA.
77. V. Raman and T.C. Reiley, “Cavitation and Cracking in As-cast and Superplastic Pb-Sn Eutectic during in High-Temperature Fatigue”, Journal of Mater. Sci. Lett., Vol. 6, pp. 549-551, 1987.
78. T. L. Anderson, Fracture Mechanics Fundamentals and Applications, CRC Press, 1995.
79. J. Wesley Barnes, Statistical Analysis for Engineers and Scientists, McGraw Hill, 1994.
80. Weibull++7 User’s Guide Version 7, ReliaSoft Corporation, AZ, USA.

81. IPC/ JEDEC 9702, Monotonic Bend Charaterization of Board-Level Interconnects, June 2004.
82. T. R. Bieler and H. Jiang, "Influence of Sn Grain and Orientation on the Thermomechanical Response and Reliability of Pb-free Solder Joints, Proc. Electronic Components and Technology Conf., pp. 1462-1467, 2006.
83. D. R. Frear, S. N. Burchett, H. S. Morgan, and J. H. Lau, The Mechanics of Solder Alloy Interconnects, Van Nostrand Reinhold, New York, 1994.
84. W. K. Jones, Y. Liu, M. A. Zampino, G. Gonzalez and M. Shah, "A Study on Mechanical Properites of Eutectic and Solid Solution Pb-Sn-Ag Solders from –200°C to 150°C", The Minerals, Metals & Materials Society, pp. 85-96, 1997.
85. J. Hwang, Environment-friendly Electronics: Lead-free Technology, Electrochemical Publications, pp. 233, 2001.
86. Y. Qi, A. R. Zbrzezny, M. Agia, R. Lam, "Accelerated Thermal Fatigue of Lead-Free Solder Joints as a Function of Reflow Cooling Rate", Journal of Electronic Materials, December 2004.
87. W. Johnson, V. Wang, and M. Palmer, "Thermal Cycle Reliability of Solder Joints to Alternate Plating Finishes", Circuit World, Vol. 25, No. 2, 1999.
88. J. Rathod, D. Santos, P. Chouta, A. Rae, J. Belmonte, " A Realiability Comparison of Different Pb-Free Alloys and Surface Finishes in SMT Assembly", Proc. APEX Conf., pp. S20-2-1 – S20-2-6, Anaheim, CA, February 2004.
89. Q. Zhang, A. Dasgupta, D. Nelson, and H. Pallavicini, "Systematic Study on Thermo-Mechanical Durability of Pb-Free Assemblies: Experiments and FE Analysis", Journal of Electronic Packaging, Vol. 127, pp. 415-429, December 2005.

90. ANATECH [TM], Operators Manual, Analysis Tech, Wakefield, MA, March 1998.

VITA

Dong Hyun Kim was born in Seoul, Korea on March 7, 1968, the son of Suk-Ki Kim and Young-Hwa Chung. After completing his work at Yoido High School, Seoul, Korea in 1987, he entered The Hanyang University, Seoul, Korea in 1987. He received the degree of Bachelor of Science from The Hanyang University in 1992. Then, he entered The Korean Advanced Institute of Sicence and Technology, and he received the degree of Master of Scicence in 1994. During the following years he was employed as a research engineer at Daewoo Heavy Industrial Corp. In August, 1996, he entered The Graduate School at The University of Texas at Austin. In September, 2003, he joined Cisco Systems, Inc., as a manufacturing engineer.

Permanent Address: SIBUM APT 12-85 YOIDO-DONG
YOUNGDEUNGPO-GU, SEOUL
150-010 KOREA (R.O.K)

This thesis was typed by the author.